RESEARCH ARTICLE

The ant abdomen: The skeletomuscular and soft tissue anatomy of *Amblyopone australis* workers (Hymenoptera: Formicidae)

Ziv E. Lieberman[1] | Johan Billen[2] | Thomas van de Kamp[3,4] |
Brendon E. Boudinot[5]

[1]Department of Entomology and Nematology, University of California, Davis, Davis, California, USA

[2]Department of Biology, Division of Ecology, Evolution & Diversity Conservation, Zoological Institute, University of Leuven, Leuven, Belgium

[3]Institute for Photon Science and Synchrotron Radiation (IPS), Karlsruhe Institute of Technology (KIT), Eggenstein-Leopoldshafen, Germany

[4]Laboratory for Applications of Synchrotron Radiation (LAS), Karlsruhe Institute of Technology (KIT), Karlsruhe, Germany

[5]Friedrich-Schiller-Universität Jena, Institut für Zoologie und Evolutionsforschung, Entomologie Gruppe, Jena, Germany

Correspondence
Brendon E. Boudinot, Friedrich-Schiller-Universität Jena, Institut für Zoologie und Evolutionsforschung, Entomologie Gruppe, Erbertstraße 1, 07743 Jena, Germany.
Email: boudinotb@gmail.com

Abstract

Recent studies of insect anatomy evince a trend towards a comprehensive and integrative investigation of individual traits and their evolutionary relationships. The abdomen of ants, however, remains critically understudied. To address this shortcoming, we describe the abdominal anatomy of *Amblyopone australis* Erichson, using a multimodal approach combining manual dissection, histology, and micro-computed tomography. We focus on skeletomusculature, but additionally describe the metapleural and metasomal exocrine glands, and the morphology of the circulatory, digestive, reproductive, and nervous systems. We describe the muscles of the dorsal vessel and the ducts of the venom and Dufour's gland, and characterize the visceral anal musculature. Through comparison with other major ant lineages, apoid wasps, and other hymenopteran outgroups, we provide a first approximation of the complete abdominal skeletomuscular groundplan in Formicidae, with a nomenclatural schema generally applicable to the hexapod abdomen. All skeletal muscles were identifiable with their homologs, while we observe potential apomorphies in the pregenital skeleton and the sting musculature. Specifically, we propose the eighth coxocoxal muscle as an ant synapomorphy; we consider possible transformation series contributing to the distribution of states of the sternal apodemes in ants, Hymenoptera, and Hexapoda; and we address the possibly synapomorphic loss of the seventh sternal–eighth gonapophyseal muscles in the vespiform Aculeata. We homologize the ovipositor muscles across Hymenoptera, and summarize demonstrated and hypothetical muscle functions across the abdomen. We also give a new interpretation of the proximal processes of gonapophyses VIII and the ventromedial processes of gonocoxites IX, and make nomenclatural suggestions in the context of evolutionary anatomy and ontology. Finally, we discuss the utility of techniques applied and emphasize the value of primary anatomical research.

1 | INTRODUCTION

The hymenopteran abdomen is a complex tagma that shows a great diversity of form and function. Unique to the order, the first sternite is lost and the first abdominal tergite is fused with the metapostnotum (Beutel et al., 2014). In the Apocrita, which contains the majority of hymenopteran diversity (Aguiar et al., 2013), the first abdominal tergum is completely fused with the metathorax, forming the propodeum. The propodeum is integrated with the other thoracic segments, forming a functional tagma, the mesosoma, which flexibly articulates with and is discrete from the rest of the abdomen, or metasoma. In ants, the anterior metasomal segments have undergone further characteristic modification: in addition to the apocritan constriction between mesosoma and metasoma (the "wasp waist"), another constriction occurs between at least metasomal segments I and II, and between metasomal segments II and III in some lineages (the "ant waist" or petiole and postpetiole; Bolton, 2003; Gauld & Bolton, 1988). Other apomorphies of the anterior metasoma include the gain of a subpetiolar process and the prora of the third abdominal segment (Boudinot et al., 2020, 2022b). The flexibility and maneuverability of the metasoma is facilitated by the anterior abdominal skeletomusculature and has important consequences for the functions of the terminal abdominal segments, including the sting in females and genital capsule in males. The sting itself is an evolutionarily plastic organ, derived from the ovipositor, which has acquired diverse functions including prey paralysis, defense against predators and competitors, and dissemination of pheromones, and which is reduced or absent in various lineages (Hölldobler & Wilson, 1990; Oeser, 1961). The "vespiform" Aculeata, that is, all aculeates to the exclusion of the traditional chrysidoid families, are defined in part by complete internalization of abdominal tergum VIII in females (Boudinot et al., 2022b; Brothers, 1975; Brothers & Carpenter, 1993; Carpenter, 1986; Oeser, 1961; Rasnitsyn, 1988; Ronquist et al., 1999). Examples of derived abdominal functions in ants include mechanical attachment in social carrying (Möglich & Hölldobler, 1974) and self-assembled structures during nest construction (Hölldobler & Wilson, 1990) and predation (Peeters & De Greef, 2015); "reversed" phragmosis, that is, nest entrance plugging with the gaster (Brown, 1967; Poldi, 1963); and prey manipulation (Masuko, 2020). The abdomen also contains the visceral and genital segments, thus there are additional, less externally apparent functions in, for example, metabolism, distribution, excretion, and reproduction (Snodgrass, 1935a). The combination of physiological, anatomical, and behavioral-ecological functions of the abdomen, which are often emergent from multitrait phenotypic syndromes, indicate the need for study that is both anatomical in scale and holistic in approach. That is, we must understand the individual anatomical components of the abdomen as discernable phenotypic products of genetically specified developmental programs, or

characters. We must also investigate how these programs are expressed and constrained in a "landscape" of phylogenetic, functional, and selective relationships, or the *character states* in their proximal and ultimate context.

In general, the study of insect morphology is transforming toward highly detailed, holistic investigation potentiated by advanced imaging technologies, often coupled with analysis of incisive molecular data sets or their results (Blanke et al., 2017; Jałoszyński et al., 2020; Wipfler et al., 2019). With respect to the cranium, mesosoma, and limbs, ant anatomy specifically has experienced a recent renaissance in descriptive and comparative research. Three-dimensional imaging technologies such as microcomputed tomography (micro-CT) and confocal laser microscopy provide new opportunities for data exploration and presentation alongside traditional techniques such as histological sectioning, light microscopy, and scanning electron microscopy (SEM) (head: Boudinot et al., 2021; Habenstein et al., 2020; Khalife et al., 2018; Richter et al., 2019, 2020, 2021; mesosoma: Aibekova et al., 2022; Liu et al., 2019). This shift in scope and resolution provides unprecedented opportunities for interrogating morphological diversity, adaptation, and biomechanics in comparative and phylogenetic contexts. The abdomen of ants, however, has received incomplete treatment, with nearly all prior studies restricted to the anterior metasoma (Hashimoto, 1996; Short, 1959), or the sting (Daly, 1955; Kugler, 1978, 1979, 1992, 1997), due to their clear functional and evolutionary significance. While the entire abdomen has occasionally been described in detail (Bolton 1990a, 1990c, 1990b; Keller, 2011), the focus has largely been on external characters, with the exception of Callahan et al. (1959), Pavan & Ronchetti (1955), and the remarkable and pioneering microtomy of Janet (1902). Consequently, the pregenital skeletomusculature of the ant abdomen is mostly uncharacterized. Because the middle pregenital segments are apparently less specialized in function and form than the waist and genitalia, they provide evidence for inferring the abdominal groundplan of ants. Fortunately, significant focus has been given to the entire abdomen of certain apoid wasps, particularly *Apis*, providing useful comparative data (Snodgrass, 1910, 1933, 1935c, 1942, 1956; Youssef, 1968).

Here, we employ a multimodal approach to characterize the abdominal skeletomusculature and exocrine glands of the worker *Amblyopone australis* Erichson (Hymenoptera: Formicidae: Amblyoponinae), using manual dissection, SEM, histology, and synchrotron micro-CT. *Amblyopone* was chosen as it has been historically considered to be a socially and morphologically "primitive" group (though see Section 4.3; Brown, 1954; Traniello 1978, 1982; Wheeler, 1927; Wilson, 1971), and because its abdominal anatomy has been treated in part (Eisner, 1957; Hashimoto, 1996; Hermann & H., 1969; Kugler, 1979). We present hypotheses for general and serial homologies of muscles within ants and Aculeata, provide a muscular nomenclature applicable across the Hexapoda, and

summarize hypotheses for muscle function; we briefly describe the morphology of the circulatory, digestive, reproductive, and nervous systems; and we identify foci for future and discuss the value of fundamental research in the context of digital anatomy.

2 | MATERIALS AND METHODS

2.1 | Material examined

A full list of specimens examined, including destructive dissections, and deposition information is provided in Table S1. Specimens of *A. australis* used are given here.

- Scanned specimen: One worker, CASENT0753222; AUS, ACT: Booroomba Rocks, 9 km SW Tharwa Village, 35°34′S 149°00′ E ± 1 min, 1200 m, 13.i.1999, P.S. Ward, PSW13797.
- Dissected specimens: Four workers; CASENT0866523, CASENT 0866524, CASENT0866525, CASENT 0866526; AUS, WA, 4 km E Walpole, 150 m, 34°59′S 116°47′E, 8.xii.1985, P.S. Ward #8134.
- Histological specimens: Five workers, AUS, NSW, Nelligen, West Nelligen Creek Bridge, J. Billen, and R. W. Taylor.

All figures depict *A. australis* workers.

2.2 | Dissection

Specimens stored in 75%–95% ethanol were initially disarticulated in a petri dish of 75% ethanol on a surface of Blu Tack putty under a Leica MZ125 stereomicroscope. Larger sclerites were easily removed using forceps (5-SA, Rubis) that were sharpened with a wetted diamond whetstone. A minuten pin (Ento Sphinx, S.R.O) held in a pin vise (BioQuip) was used for finer structures, sometimes with the tip bent into a hook using forceps. The undissected parts of the specimens were point-mounted, labeled, and deposited as vouchers in the Bohart Museum of Entomology, University of California, Davis (UCDC).

2.3 | SEM

Dissected specimens examined via photomicroscopy were subsequently repurposed for SEM. Smaller sclerites were dissected out in a drop of glycerol on a glass slide, then washed in 25% ethanol and dehydrated through a graded ethanol series (50%, 75%, 95%, and 99%) for approximately 5 min at each step. For imaging, dehydrated specimens were affixed to a paper point with a droplet of hide glue, applied with the tip of a minuten pin. A Hitachi TM4000 Tabletop Microscope low-vacuum SEM was used with an accelerating voltage of 15 kV and the backscattered electron (BSE) detector (Hitachi High-Tech Corp.). In BSE imaging, brightness is positively correlated with average atomic number; it is suboptimal

for resolving surface topography, but see Section 4.9 for justification (Egerton, 2005).

2.4 | Photomicrography

Photomicrographs were acquired as focus stacks of approximately 25–40 images using a 3.1-megapixel Leica DMC2900 camera affixed to a Leica MZ16A stereomicroscope via a Leica 0.5x video objective (part #10450528), using the Leica Application Suite software (v.4.13.0) for automated z-stepping (Leica Microsystems). Image stacks were combined into full-focus montages and manually retouched using Helicon Focus (Helicon Soft. Ltd.). Additional photomicrographs were obtained from AntWeb (Version 8.64.2, California Academy of Science) and are attributed in figure captions.

2.5 | Histology

The posterior part of the abdomen and the metathorax were cut off by making a transverse cut between the third and fourth abdominal segments, and fixed for 12 h in cold 2% glutaraldehyde in a buffer of 0.05 mol l^{-1} Na-cacodylate and 0.15 mol l^{-1} saccharose. Tissues were postfixed in 2% osmium tetroxide in the same buffer, dehydrated in a graded acetone series and embedded in Araldite. Serial semithin sections with a thickness of 1 μm were made with a Leica EM UC6 microtome (longitudinal for four workers, transverse for one worker). These were stained with methylene blue and thionine, and observed under an Olympus BX-51 microscope. Section photographs were taken at 10 μm intervals.

2.6 | Micro-CT

The synchrotron microtomographic scan was performed at the imaging cluster of the Karlsruhe Institute of Technology (KIT) light source using a parallel polychromatic X-ray beam produced by a 1.5 T bending magnet. The beam was spectrally filtered by 0.7 mm aluminum with a spectrum peak at about 15 keV. We employed a fast indirect detector system, consisting of a 12 μm LSO:Tb scintillator (Cecilia et al., 2011), and a diffraction limited optical microscope (Optique Peter, Lentilly, France; Douissard et al., 2012) coupled with a 12 bit pco.dimax high speed camera with 2016 × 2016 pixels (dos Santos Rolo et al., 2014). We took 3000 projections at 70 fps and an optical magnification of 5X, resulting in an effective pixel size of 2.44 μm. The control system concert (Vogelgesang et al., 2016) was used for automated data acquisition and online reconstruction of tomographic slices for data quality assurance. Online and final data processing including tomographic reconstruction were done by the UFO framework (Vogelgesang et al., 2012). Before tomographic reconstruction, we performed flat-field correction of the projections and applied phase retrieval based on the transport of intensity equation (Paganin et al., 2002).

The microtomographic volume was imported to Dragonfly 2021.1 (Object Research Systems [ORS] Inc.) as a stack of. tif files and converted to ORSSession format for previsualization and segmentation. Previsualization consisted of rendering the entire data set and adjusting the color grading lookup table (LUT) and opacity to explore gross structure. *Segmentation* of CT data refers to the assignation of pixels or voxels to labels that correspond to anatomical entities, to facilitate visualization or quantitative analysis. Segmentation was performed manually, usually using (1) *ROI Painter > 2d View Tools > Multi-slice > Round Brush > Local Otsu > Upper* and *Segment > Define Range > OFF*, or (2) *ROI Painter > 2d View Tools > Multi-slice > Round Brush > Full* and *Segment > Define Range > ON* and adjusted manually to exclude non-focal tissues. The *Single slice* brush setting was used to refine edges and correct overlapping labels.

Regions of interest (ROIs) and multi-regions of interest (multi-ROIs) were both used to create and edit segmentation labels. Dragonfly ROIs and multROIs do not overwrite one another at equivalent levels of data hierarchy; classes within a multiROI do mutually overwrite. This can be leveraged to selectively choose overwrite behavior. ROIs and multiROIs are also interconvertible: classes can be extracted from multiROIs as ROIs, or ROIs can be combined into a multi-ROI. Boolean (logical) operators (e.g., AND, OR) can be applied during combination, such that extensive overlap in labels can be automatically corrected. A final consideration is that software execution is faster using multiROIs rather than the equivalent labels stored as ROIs. When the segmentation file exceeded the system's available video random access memory, multiROIs were exported as.ORSObject files and loaded into a new.ORSSession using the original data set. ROIs were initially cleaned using *Refine regions of interest > Process islands > Keep by largest*, using a value of *1* for unpaired and *2* for paired structures; then ROIs were manually cleaned. Segmentation labels were exported as image series for volume rendering using a custom code (K. Jandausch, FSU-Jena, pers. comm.). These series were cropped to the label extent, then imported to VG Studio Max 3.4.5 (Volume Graphics GmBH) for volume rendering, with Phong interpolation shading. Renders were projected using central perspective to accurately capture shape and spatial information using *Rendering > Central Perspective*; scale for perspective renders was obtained from equivalent orthographic projection using *Rendering > Parallel*.

2.7 | Image processing

Photomicrographs and SEMs were level-adjusted, sharpened, and arranged in Adobe Photoshop CS6 (Adobe Inc.). Brightness and contrast were adjusted using *Image > Auto Contrast* followed by *Image > Adjustments > Levels*. We used *Filter > Sharpen > Unsharp Mask* filter with starting values of *Amount* = 50%, *Radius* = 1.7 pixels and *Threshold* = 0 as recommended by AntWeb (v.8.64.2, California Academy of Science). Photographs of histological sections were typically sharpened with reduced *Radius* and/or increased *Threshold* values to avoid artifacts. Line drawings were created by tracing

micrographs or micro-CT reconstructions with the *Pen* tool in Adobe Illustrator CS6 and CC2020 (Adobe Inc.), which were also used to compose figures.

2.8 | Terminology

2.8.1 | General terminology

Treatments of hymenopteran anatomy vary widely in terminology, both for anatomical entities themselves and for positional and orientational terms. To reduce ambiguity in the present comparative work, we provide a detailed explanation of the approach taken here. Because we employ both homology-oriented and anatomical (homology-neutral) terms to compromise between evolutionary and comparative morphology, we have synthesized nomenclature from various sources and introduced new terms where existing schemata are ambiguous or nonexistent. See Section 4.4 for further discussion of nomenclatural and ontological perspectives.

Segments are referred to by tagma and position, from anterior to posterior. Relative orientation is concordant with numbering scheme. Hence, terms like *prior*, *preceding*, *previous* indicate relative anterior (cephalad), while terms like *following*, *subsequent* indicate relative posterior (caudad) orientation. Longitudinal figures are consistently oriented with the anterior direction to the left. We caution that some prior authors (e.g., Youssef, 1968) use a reversed orientation system compared to the present work in their descriptions and/or figures. Orientational terms for the genital segments (AVIII and AIX) are complicated by several factors: most of the sting sclerites are highly reduced and/or modified, to the point where obvious homologous landmarks are frequently absent; many sting structures are strongly curved, such that the terms "dorsal" and "ventral" may have different anatomical and functional meanings, or differ along the length of the structure; and the entire sting apparatus and its subparts have many degrees of possible rotation relative to the remaining gaster and to one another. For the gonapophyses and their derivative structures (see below), we primarily orient using the proximal-distal axis; the point at which the gonapophysis articulates with the gonocoxite is considered the most proximal. Dorsoventral orientation of gonapophyseal parts are considered functionally, in resting position (as figured) and at the location of the specific subpart referenced.

Abbreviations of tagmata (Figures 1a–e and 2a,b): **Th**, thorax; **A**, abdomen, **M**, metasoma. Abbreviations of intrasegmental regions: **T**, tergite; **S**, sternite (e.g., ATIII is the third abdominal tergite). Because we treat the entire abdomen, the abdominally inserting muscles of ThSIII (metasternum) are also considered. Note that abdominal segments and their sclerites are indexed with Roman numerals as they are associated with "A" (e.g., AIII), whereas abdominal muscles are indexed by their origins using Arabic numerals (e.g., 3volm) to avoid confusion with thoracic muscles (e.g., IIvolm).

The *abdomen* as considered here comprises 10 segments, including the *propodeum* (AI), *petiole* (AII), and internalized genital-postgenital segments (AVIII–X). Note that potential subsequent
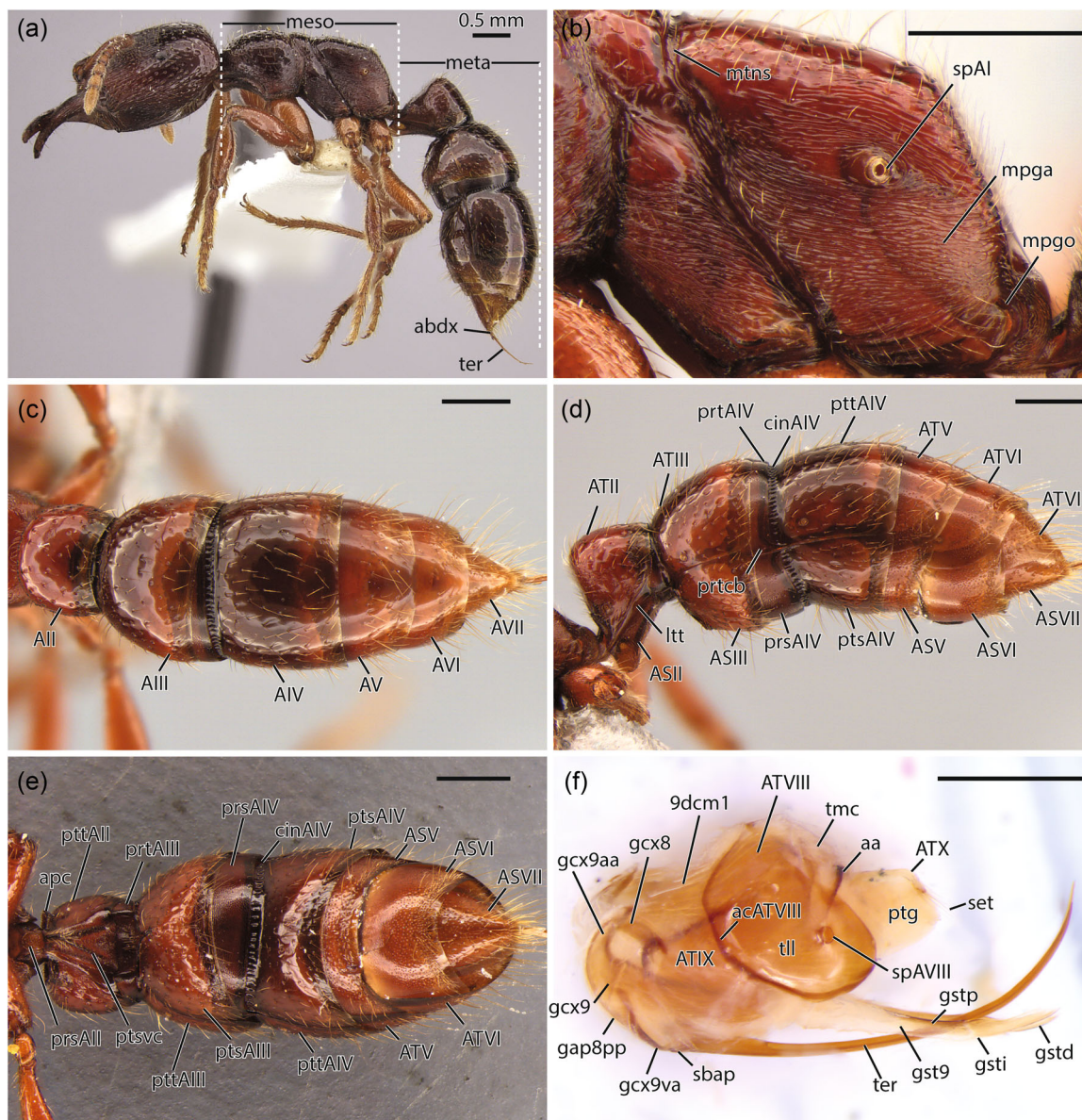
FIGURE 1 *Amblyopone australis*, habitus, segmentation, and sculpture of the abdomen; photomicrographs. (a) full body habitus, lateral view; image from www.AntWeb.org, CASENT 0260443, imager Will Ericson (b) detail of propodeum, lateral view, (c) metasoma, dorsal view, (d) metasoma, lateral view, (e) metasoma, ventral view, (f) genital and postgenital segments, dissected, lateral view. Scale bars: 0.5 mm. A, abdominal segment; aa, anal arc; abdx, external apex of the abdomen; ac, antecosta; apc, anterolateral petiolar carina; AS, abdominal sternite; AT, abdominal tergite; cin, cinctus; dcm, tergocoxal muscle; gap8pp, proximal process of gonapophysis VIII; gcx8, gonocoxite VIII; gcx9, ventral process of gonocoxite VIII; gcx9aa, anterior arm of gonocoxite IX; gcx9va, ventral arm of gonocoxite IX; gst9, gonostylus IX; gst9d, distal sclerite of the gonostylus; gst9i, distal sclerite of the gonostylus; ltt, laterotergite; ltt, laterotergite; meso, mesosoma; meta, metasoma; mpga, metapleural gland atrium; mpgo, metapleural gland orifice; mtns, metanotal sulcus; prs, presternite; prt, pretergite; prtcb, cuticular band of the fourth pretergite (ATIV); ptg, proctiger; pts, poststernite; ptsvc, ventrolateral carinae of the petiolar poststernite; ptt, posttergite; sbap, articular process of the sting bulb; set, seta; sp, spiracle; ter, terebra; tll, lateral lobes of ATVIII; tmc, medial connection of ATVIII

segments are not differentiated (see, e.g., Boudinot, 2018; Smith 1969, 1970; Snodgrass, 1935b). The *mesosoma* (**meso**, Figure 1a) is the tagma comprising the thoracic segments plus AI; the *metasoma* (**meta**, Figure 1a) comprises AII–X. The noun *gaster* and its adjectival form *gastral* refer (in *Amblyopone*) to segments AIII–X and are here used only in discussing muscular function or mechanical motion. We treat the *pregenital segments* of most female Hexapoda as

consisting of segments AI–VII (Figures 1a–e and 2a), the *genital segments* as AVIII and AIX, and the *postgenital segments* as AX–XII (Figures 1f and 2b) depending on postgenital development (Boudinot, 2018); in males, the first genital segment is AIX. The *anterior pregenital segments* comprise AI–AIV, which have highly modified skeletomusculature, while the *posterior pregenital segments* are the relatively unmodified AV–AVII.
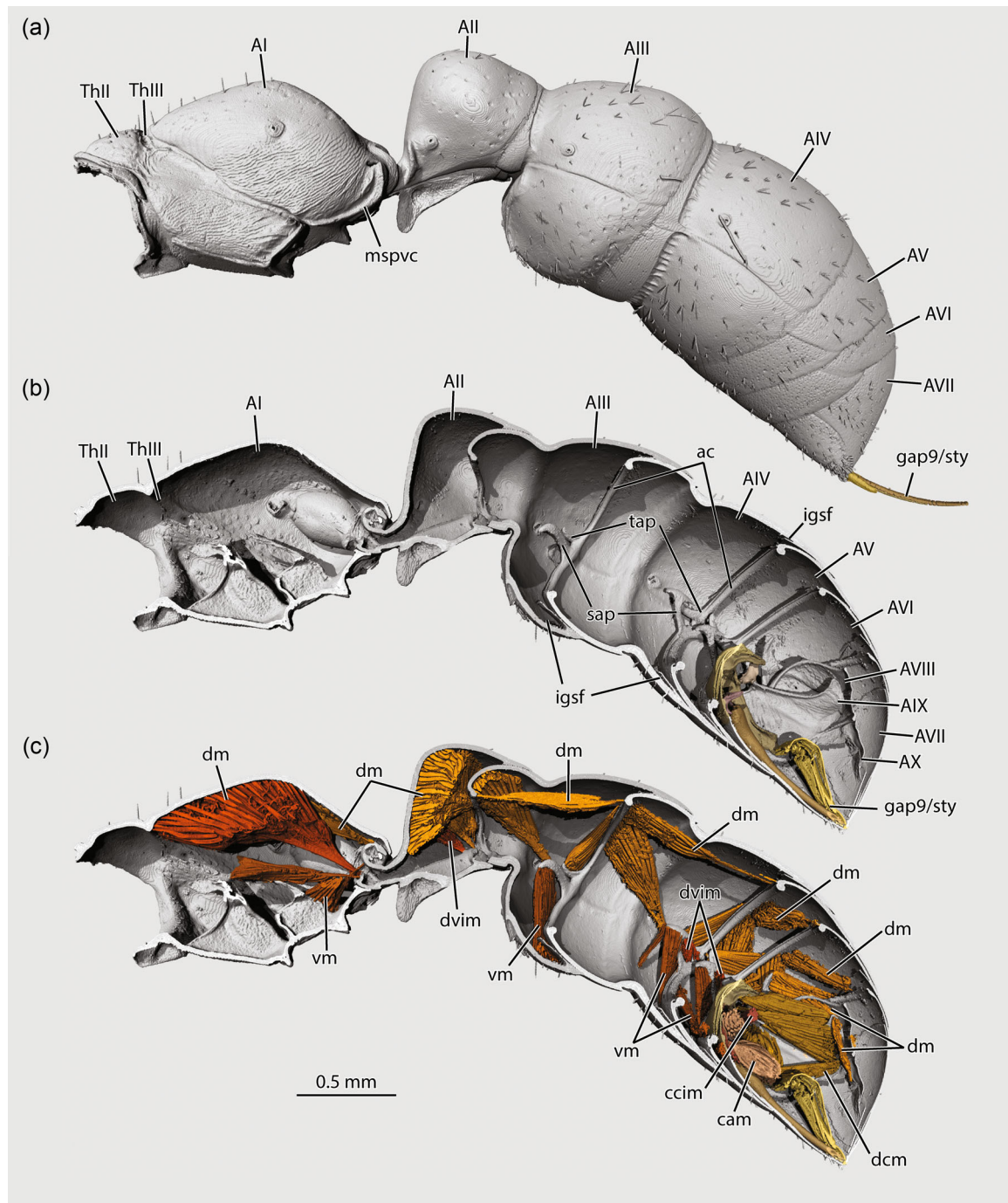
FIGURE 2 *Amblyopone australis*, external (a) and internal (b and c) habitus, with major integumentary (b) and muscular (c) features; 3D reconstruction, equivalent views. (a) external lateral view, (b and c) sagittal bisection. Scale bar: 0.5 mm. A, abdominal segment; AS, abdominal sternite; AT, abdominal tergite; cam, coxapophyseal muscle; ccim, coxocoxal muscle; dcm, tergocoxal muscle; dm, dorsal muscle; dvim, dorsoventral intrinsic muscle; gap9/sty, stylet of gonapophyses IX; igsf, intrasegmental fold; mspvc, ventrolateral mesopectal carina; sap, anterolateral sternal apodeme; tap, anterolateral tergal apodeme; Th, thoracic segment; vm, ventral muscle

An *apodeme* is a solid endoskeletal element that serves as a site of muscle attachment, while an *apophysis* is a hollow invaginated skeletal element, which may or may not bear muscle attachments. A *suture* is a groove or line that marks the fusion of ancestrally separate sclerites, whereas the term *sulcus* refers to a groove or line, usually corresponding to an internal ridge (Snodgrass, 1962). For the metasomata of Hymenoptera, the terms *tergite* and *sternite* indicate the dorsal and ventral sclerites, while *tergum* and *sternum* are applied to the dorsal and ventral body regions, including both conjunctivae and sclerites (Hymenoptera Anatomy Ontology, HAO; Yoder et al., 2010). The terms *medial* and *lateral* indicate position along the transverse body axis; *mesal* and *ectal* refer to the position within

or outside of the body wall, or the inner and outer surfaces of endoskeletal elements. We use *porrect* (adj.) for structures that are approximately orthogonal to the long axis of a referenced surface or plane; porrect apodemes extend anteriorly more or less horizontally in resting position, in which the antecosta is basically vertical in the dorsoventral axis. *Malleate* (adj.) means hammer-shaped and refers to a structure with a dilated, hammerlike apical process.

Surface sculpture is described following Harris (1979). Regarding setation (vestiture, pubescence), or the pattern of sensilla/sensilloid integumentary structures, we use the term *setae* to refer to hair-like, deflectable structures regardless of length and stature. Although the cellular structure of setae was not confirmed histologically, the gross morphology of sensilloid fields ascertained by light and electron microscopy suggests that those of the external body surfaces are generally *sensilla trichodea filiformis* (or setae in the strictest sense). Specifically, the hairs are narrowly tapering with no obvious pore structures, and frequently arise from punctae or cuticular depressions, suggesting the presence of a tormogenous socket. While this approach remains deductive from limited data, we prefer to at least attempt to connect our observations to discrete anatomical entities, rather than categorizing setation based on undefined length ratios. The internalized genital appendages bear several types of modified sensilla, which are referred to agnostically as *hairs*, with an accompanying description of form. For recent discussion of sensilloid structures and character concepts, see Boudinot et al. (2020) and Boudinot et al. (2021). Terms for setational stature follow Wilson (1955).

2.8.2 | Skeletal nomenclature

Because there has been no modern, comprehensive review of abdominal sclerite terminology (see e.g., Beutel et al., 2014) and as we intentionally deviate from certain prior usages, we define and explain here the general nomenclatural system used in the present study for the abdominal skeleton and other anatomical systems. We provide general definitions of key terms along with anatomical-spatial, developmental, and homological context to explicate both the meaning of our usages and their justification.

Pregenital abdomen. Specific terminology for skeletal elements of the pregenital segments is based on Snodgrass (1910, 1942), Bolton (1990c), Hashimoto (1996), and Keller (2011). Diverse nomenclature has been applied to the anterior regions of the metasomal segments, particularly in AII and AIII. This terminological confusion is due to the difficulty of identifying subparts of sclerites associated with secondary segmentation and is exacerbated by modification due to petiolation. Even when a sclerite is divided into anterior and posterior regions by a line of a given form, it may be difficult to find definitive or consistent landmarks indicating this division, especially across broad samples of taxa.

The tergites or sternites of adult insects are secondarily segmented (*sensu* Snodgrass, 1935b): the externally apparent incision between segments corresponds to an invaginated ridge of the sclerite, the *antecosta* (**ac**, Figure 2b). The narrow region anterad the antecosta is the *acrosclerite* (*acrotergite*, *acrosternite*), which is delineated externally by the *antecostal sulcus*. Both acrosclerite and antecosta are consistently differentiable in segments AIII–VII; in AVIII the antecosta is distinct but the antecostal sulcus and acrotergite are poorly developed; in AIX we infer that the anterior marginal carination represents the antecosta. In ants, the post-antecostal sclerite may be divided into anterior and posterior portions by a *cinctus*, a transverse sulcus or girdling constriction (Bolton, 1990a), resulting in a defined *presclerite* (*pretergite*, *presternite*; **prt**, **prs**, Figure 1d,e) and *postsclerite* (*posttergite*, *poststernite*; **ptt**, **pts**, Figure 1d,e). Previously, the term "acrosclerite" has been used for the entire presclerite in ants (e.g., Taylor, 1978), but we agree with Bolton (1990c) and Hashimoto (1996) that this application is inaccurate.

In AII (the petiole), there is a clear articulatory region formed by the presclerites, which are both constricted relative to and divided from the postsclerites by prominent carinae. The specialized articulatory presclerites of AIII may be referred to as the *helcial tergite* and *helcial sternite*, or *in toto* as the *helcium* (Bolton, 1990a, 1990b, 1990c). Among extant ants, cincti may also be present on segments AIV–VII (Bolton, 1994; Fisher & Bolton, 2016), but are absent in *Amblyopone* posterad AIV. In segments where a cinctus is absent, we do not formally distinguish pre- and postsclerites, although they are implied by differences in sculpture and setation (e.g., Bolton, 1990c). These undivided sclerites have distinct surface patterning, with two primary regions: an anterior contact surface that underlies and comes into regular contact with the tergum or sternum of the preceding segment, and is typically glabrous, and bears fine, uniform microsculpture; and a posterior region with variable, usually with more robust sculpture, and with setae.

In AIV–VII, the antecostae of both tergite and sternite bear a pair of *anterolateral apodemes* (*tergal apodemes*, **tap**, *sternal apodemes*, **sap**, Figure 2b); in AII and AIII, only the sternite bears such apodemes, which are modified in form. The posterior tergal margin of AII, and the posterior tergal and sternal margins of AIII–VIII, are invaginated, forming a thin sclerotic lamina, which continues as *conjunctiva* (membrane). The pocket formed by this invagination is the *intrasegmental fold* (**igsf**, Figure 2b); its membranous ventral face (on the tergum) or dorsal face (on the sternum) corresponds to the wall of the *intersegmental fold*. In most segments, the intrasegmental fold partially bears the large dorsal and ventral paramedial protractor muscles. This double fold of the conjunctiva has been figured previously (e.g., Plate 1, Janet, 1902), but to our knowledge the intra- and intersegmental folds have not been named separately.

Genital and postgenital abdomen. Sclerites of the sting apparatus are named using the gonocoxite-gonopod homology interpretation of Smith (1969, 1970), with modification, while their subparts are described mainly following the homology-neutral approach of Kugler (1978). The primary distinction in our basic conception relative to Smith is that the entire genital appendage is considered the "gonopod," which is divisible into a proximal "protopod" ("crustacea":

coxa/basis; Hexapoda: subcoxa/coxa) and a distal ramus or rami ("c": exopod/endopod; H: stylus/apophysis) (Boudinot 2018). Table 1 provides an abbreviated synopsis of terminological equivalencies for the genital-postgenital segments; see also Oeser, (1961) and Youssef (1968). Additional equivalencies are provided where relevant in the text.

Most broadly, the female appendages of AVIII and AIX both comprise a pair of proximal and ancestrally biramous *gonocoxites* (**gcx8**, **gcx9**, Figure 1f), the distal rami of which are the medially situated *gonapophyses* and the laterally situated *gonostyli* (**gst9**, Figure 1f). The gonapophyses form the "valves" of the sting, while the gonostyli are flexible, partially membranous structures, which clasp or "sheathe" the sting for part of its length when the sting is retracted. Gonocoxites VIII bear only gonapophyses, while those of AIX bear both gonapophyses and gonostyli. Whereas gonocoxites VIII are single, solid sclerites, those of AIX are deeply incised, with the *preincision* dividing the main body of gonocoxites IX from the narrower *ventromedial processes of gonocoxites IX* (= "rami of gonapophyses IX" or "second rami"; see Section 4.4 for rationale). We do not refer to the "postincision," or space between the posterior and ventral arms of gonocoxites IX (Kugler, 1978), but rather describe the shape of the posterior and ventral arms specifically.

Gonapophyses VIII and IX clasp one another via an *olistheter mechanism* (sliding rail) which comprises the *aulaces* (sg. *aulax*, groove) of VIII and the *rhachies* (sg. *rhachis*, tongue) of IX. The olistheter elements extend longitudinally along the dorsal (AVIII) or ventral (AIX) surfaces of the gonapophyses. Together, the gonapophyses form the sting, which comprises the proximal *sting base* and distal injective portion or *terebra* (**ter**, Figures 1f and 23a). *Sting base* here refers generally to the composite gonapophyseal region proximal to the terebra and distal to the proximal processes of gonapophyses VIII (not after Kugler, 1978, i.e., indicating the dorsomedian part of the sting bulb specifically).

The regions of gonapophyses VIII that bear the aulaces are referred to as the *lancets* (first valve/valvula), while the fused regions of IX which bear the rhachies are referred to as the *stylet* (second valve/valvula). The lumen enclosed by the stylet and lancets is the *venom canal* into which discharge the products of the venom gland, the Dufour's gland, and the sting bulb gland. The slender, elongate, grooved portion of gonapophyses VIII, proximal to the lancets, are the *proximal processes of gonapophyses VIII* (= "rami of gonapophyses VIII" or "first rami"). In their most proximal regions, the lancets bear small, partially membranous dorsal dilations or *valvilli* which project into the valve chamber of gonapophyses IX. Proximal to gonapophyses IX is a single Y-shaped sclerite, the *furcula* (Figures 21b,e and 24a,b) which is considered a fragment of the fused gonapophyseal bases (Hermann & Chao, 1983). Gonapophyses IX are fused dorsomedially, and are dilated at their base, forming the proximal *sting bulb* and distal *valve chamber*, delineated but not fully divided by a proximodorsal *sting bulb apophysis* (Figure 23). The dorsolateral condyles of the sting bulb are the *proximodorsal processes*; these articulate with the ventral arms of the furcula. The ventrolateral condyles of the sting bulb are the *articular processes*, which articulate with the ventromedial processes of the ninth gonocoxites. The proximodorsal process is separated from the articular process by the lateral *basal notch* (Figure 24a,b). Distad the valve chamber, the *inner and outer dorsal walls of gonapophyses IX* meet, marking the start of the terebra.

The reduced tergites of AVIII–IX are not referred to as "hemitergites" as they are in many aculeates, including some ants, because they retain a sclerotized *medial connection*, rather than being disjunct. ATIX is divided by the carinate *midplate line* into a *dorsal body* ("dorsal apodeme", Kugler, 1978) and *ventral body* (Figure 19a). Note that the *anal arc* (**aa**, Figure 1f) is used here after Kugler (1978), not as in Hermann (1969), that is, it refers to the posterodorsal sclerotized arc of ATIX, and is not synonymous with "anal plate" or ATX. The term *proctiger* is sometimes applied to the tenth tergite (anal plate) or even to the posterolateral lobe of ATIX (Daly, 1955); here, we refer to the tergite as ATX specifically and use proctiger to refer to the entire membranous region dorsad the anal opening of the hindgut, ventrad ATX, which probably includes the tightly associated membranes of AX and the hindgut (**ptg**, Figures 1f; 29a; and 30a; Yoder et al., 2010).

2.8.3 | Muscular nomenclature

Following von Kéler (1955), a muscle's *origin* (**O**) is its point of fixed attachment (punctum fixum, origo, Ursprung), and its *insertion* (**I**) is the point of movable attachment (punctum mobile, insertio, Angriffpunkt). To our descriptions we have added **F**, for the description of form. Muscles are assigned to segments based on their origin. They are *extrinsic* if they cross segmental borders of the main body tagma or connect an appendage to a main segment; they are *intrinsic* if they originate and insert on the same body segment, or within an appendage. Because muscles usually insert posterad their origin, those which are *reversed in position* insert anterad their origin (Snodgrass, 1935a). We avoid the term "tendon" to refer to muscle insertions, because in the strict sense it indicates the epidermal portion of the myotendinous junction ("tonofibrilla"), and we did not examine all insertions histologically (Chapman et al., 2013). Instead, we simply describe the form of insertions observed, for example, "long, slender" or "broad, extensive" insertions.

Generally, we follow the topographic main-group system for muscle naming (Friedrich & Beutel, 2008, 2010; Beutel et al. (2014). Topographic main groups refer to the general spatial position of muscle origin and insertion within and between segments. This system, however, has not been adapted to the abdomen, thus we have drawn on several sources, particularly Snodgrass (1935a, 1942, 1956), to establish a label system that is applicable across the Hexapoda. Table 2 lists all 55 skeletal muscles observed here, with abbreviated origin and insertion (see Results for full descriptions); Table S2 provides the full system, including male genital musculature, with correspondences to prior nomenclatures. In the pregenital abdomen, there are four primary groups, within which subgroups are differentiated: (1) dorsal or intertergal muscles, which

TABLE 1 Synopsis of terminological equivalencies for major features of the genital-postgenital segments.

Here	Kugler (1978)	Daly (1955)	Rietschel (1937)	Janet (1898a)
ATVIII	Spiracular plate	Tergum 8	Stigmenplatte	Plaque stigmatifère
ATIX	Quadrate plate	Tergum 9	Quadratische Platte	Plaque carré
ATIX dorsal body	Dorsal apodeme	-	Apodem der quadratischen Platte	-
Terebra	Aculeus	Sting	Stachel	Aiguillon
Gonocoxite VIII	Triangular plate	First valvifer	Winkel	Crosse
Gonocoxite IX	Oblong plate	Second valvifer	Oblonge Platte	Arceau ventral de l'anneau 12
Anal arc	Anal arc	Posterior band of tergum 9	-	Arc chitineaux de l'anneau 12
Gonostylus IX	Gonostylus	Third valvula	Stachelscheide	Valve de la gaine de l'aiguillon
ATX	Anal plate	Tergum 10	10ter Tergit	Arceau dorsal de l'anneau 12
Furcula	Furcula	Furcula	Gabelbein	Fourchette
Proximal process of gonapophysis VIII	Ramus 1	Ramus of first valvula	Stechborstenbogen	Arc laterál du stylet
Lancet	Lancet	First valvula	Stechborste	Stylet[a]
Ventral process of gonocoxite IX	Ramus 2	Ramus of second valvula	Stachelrinnenbogen	Rail du guidage du gorgeret
Stylet	Sting	Second valvula	Stachelrinne	Gorgeret
Sting bulb	Sting bulb	-	Stachelrinnenkolben	Partie supérieure du squelette du gorgeret
Articular process	Articular process	Basal process of the second valvula	Stachelrinnenbogengelenk	-
Proximodorsal process	Anterolateral process	(Part of base of second valvulae)	-	Arc chitineux de la partie supérieur du gorgeret
Sting bulb apophysis	Internal apophysis	-	-	Apophyse chitineuse
Valvillus	Valve of the lancet	Valve of the first valvula	Elastisches Plättchen	Lamelle du stylet/piston du stylet
Posterolateral lobe of the anal arc	-	proctiger	-	Arceau dorsal de l'anneau 12 (part)
Basal notch	Basal notch	-	-	Échancrure de la par l'arc laterál du gorgeret
Rhachis	-	-	Schiene der Stachelrinne	Rail du guidage
Aulax	-	-	-	Rainure du coulissage
Barbule	barb		Widerhaken	Dent de la côte du extrémité du stylet[b]
Here	**HAO preferred term**	**HAO URI**	**Other**	
ATVIII	Abdominal tergum 8	HAO_0000061		
ATIX	Female T9	HAO_0001873		
ATIX dorsal body	-	-		
Terebra	Terebra	HAO_0001004	(Sting) shaft	
Gonocoxite VIII	First valvifer	HAO_0000338	Gonangulum	
Gonocoxite IX	Second valvifer	HAO_0000927	Écaille latérale/écaille du gorgeret	
Anal arc	-	-		
Gonostylus IX	Third valvula	HAO_0001012	Gonoplac	

(Continues)

TABLE 1 (Continued)

Here	HAO preferred term	HAO URI	Other
ATX	Abdominal tergum 10	HAO_0000052	
Furcula	Furcula	HAO_0002498	
Proximal process of gonapophysis VIII	Ventral ramus of the first valvula	HAO_0000891	
Lancet	Dorsal ramus of the first valvula	HAO_0001579	
Ventral process of gonocoxite IX	Dorsal ramus of the second valvula	HAO_0002190	
Stylet	Ventral ramus of the second valvula	HAO_0001107	(Sting) shaft
Sting bulb	Bulb	HAO_0002177	
Articular process	Processus articularis	HAO_0001704	
Proximodorsal process	-	-	
Sting bulb apophysis	-	-	
Valvillus	Valvillus	HAO_0001619	
Posterolateral lobe of the anal arc	-	-	
Basal notch	-	-	
Rhachis	Rhachis	HAO_0000898	
Aulax	Aulax	HAO_0000152	
Barbule	-	-	

Note: The first column (terms used here) is repeated on the second page for ease of comparison. A dash (-) indicates that the term is absent in the given reference. HAO URI refers to Universal Resource Identifiers and can be accessed on the web by appending the given URI to the following URL: https://purl.obolibrary.org/obo/.

[a]We are aware of potential confusion surrounding the mixed usage of "stylet" and "lancet;" to our knowledge, however, the application of "stylet" to the lancet is limited to the French corpus at the turn of the 20th century and is not an established usage.

[b]Janet (1898a) states that the "stylet" (= lancet) of bees and some wasps are "dentélés sur les côtes de leur extrémité" (dentate on the sides of their apices) and incorrectly continues that "ceux des Fourmis sont lisses" (those of ants are smooth). The term "dent de la côte du extrémité du stylet" is drawn from the above description of the barbules of other Hymenoptera.

originate and insert on tergites (**dm**, Figure 2c), and may be *dorsal orthomedial* (**domm**), *dorsal paramedial* (**dpmm**), or *dorsal ortholateral* (**dolm**); (2) ventral or intersternal muscles (**vm**, Figure 2c), which originate and insert on sternites, and may be *ventral orthomedial* (**vomm**), *ventral paramedial* (**vpmm**), or *ventral ortholateral* (**volm**); and (3) dorsoventral or tergosternal muscles (**dvm**, Figure 2c), which originate on a tergite and insert on a sternite, and include the *dorsoventral intrinsic medial* (**dvimm**) and *dorsoventral intrinsic lateral muscles* (**dvilm**), and the *dorsoventral extrinsic paramedial muscles* (**dvxm**). The dorsal and ventral paramedial muscles are named for their intermediate position between the orthomedial and ortholateral muscles. The paramedials are designated as "lateral external dorsal" and "lateral external ventral" muscles by Snodgrass (1942), but do not run ectal to the dorsal ortholaterals ("lateral internal dorsals," Snodgrass, 1942) or ventral ortholaterals ("lateral internal ventrals," Snodgrass, 1942) in *Amblyopone*, thus we consider the original designation of "external" to be misleading.

In the more caudal segments, which are highly modified and may bear appendages, there are four additional groups: (1) *ventrodorsal extrinsic* or sternotergal muscles (**vdxm**), which originate on ASVII and insert on ATVIII; (2) *tergocoxal muscles* (**dcm**), which originate on a tergite and insert on a gonocoxite; (3) *coxocoxal muscles* (**ccim**), which run transversely between the gonocoxites; and (4) *coxapophyseal muscles* (**cam**), which originate on the ninth gonocoxites and insert on the furcula or elements of the sting base. The intraspiracular muscles are labeled M. *occlusor spiraculi*. Note that they were only observable in certain segments and transverse histological sections, and thus 3D-reconstruction and description of these muscles and their associated apodemes is limited or precluded. Spiracular dilator muscles (M. *dilator spiraculi*) were not observed here but are present in some ants (*e.g*, Janet, 1897). See Section 4.6 for discussion of the spiracular musculature; note also that the spiracular muscles are named after (Snodgrass, 1935a) and not according to the system described below for the other skeletal muscles.

TABLE 2 Skeletal muscles of the abdomen.

Designation	Name	Origin	Insertion
IIIvomm	*metafurca-abdominosternalis medialis*	Metafurca	Presternite ASII
IIIvolm	*metafurca-abdominosternalis lateralis*	Metadiscrimenal lamella	Anterolateral apodemes ASII
1domm	*tergo-tergalis orthomedialis*	Propodeum	Petiolar levator process
1dolm	*tergo-tergalis ortholateralis*	Propodeum	Anterolateral petiolar condyles
2domm	*tergo-tergalis orthomedialis*	Posttergite AII	Antecosta ATIII
2dpmm	*tergo-tergalis paramedialis*	Posttergite AII	Antecosta ATIII
2dolm	*tergo-tergalis ortholateralis*	Posttergite AII	Antecosta ATIII
2dvilm	*tergo-sternalis interior lateralis*	Posttergite AII	Posterolateral apodemes ASII
3domm	*tergo-tergalis orthomedialis*	Antecosta ATIII	Acrotergite ATIV
3dpmm	*tergo-tergalis paramedialis*	Posttergite ATIII	Anterolateral apodemes ATIV
3dolm	*tergo-tergalis ortholateralis*	Antecosta ATIII	Antecosta ATIV
3vpmm	*sterno-sternalis paramedialis*	Poststernite ASIII	Anterolateral apodemes ASIV
3volm	*sterno-sternalis ortholateralis*	Poststernite ASIII	Anterolateral apodemes ASIV
4domm	*tergo-tergalis orthomedialis*	Antecosta ATIV	Acrotergite ATV
4dpmm	*tergo-tergalis paramedialis*	Posttergite ATIV	Anterolateral apodemes ATV
4dolm	*tergo-tergalis ortholateralis*	Antecosta ATIV	Antecosta ATV
4vpmm	*sterno-sternalis paramedialis*	Poststernite ASIV	Anterolateral apodemes ASV
4volm	*sterno-sternalis ortholateralis*	Poststernite ASIV	Anterolateral apodemes ASV
5domm	*tergo-tergalis orthomedialis*	Anterior ATV	Acrotergite ATVI
5dpmm	*tergo-tergalis paramedialis*	Posterior ATV	Anterolateral apodemes ATVI
5dolm1	*tergo-tergalis ortholateralis minor*	Anterior ATV	Anterolateral apodemes ATVI
5dolm2	*tergo-tergalis ortholateralis major*	Anterior ATV	Anterolateral apodemes ATVI
5dvilm	*tergo-sternalis interior lateralis*	Anterolateral apodemes ATV	Anterolateral apodemes ASV
5vomm	*sterno-sternalis orthomedialis*	Antecosta ASV	Acrosternite ASVI
5vpmm	*sterno-sternalis paramedialis*	Posterior ASV	Anterolateral apodemes ASVI
6domm	*tergo-tergalis orthomedialis*	Anterior ATVI	Acrotergite ATVII
6dpmm	*tergo-tergalis paramedialis*	Posterior ATVI	Anterolateral apodemes ATVII
6dolm1	*tergo-tergalis ortholateralis minor*	Anterior ATVI	Anterolateral apodemes ATVII
6dolm2	*tergo-tergalis ortholateralis major*	Anterior ATVI	Anterolateral apodemes ATVII
6dvilm	*tergo-sternalis interior lateralis*	Anterolateral apodemes ATVI	Anterolateral apodemes ASVI
6dvxm	*tergo-sternalis exterior (paramedialis)*	Posterior ATVI	Anterolateral apodemes ASVII
6vomm	*sterno-sternalis orthomedialis*	Antecosta ASVI	Acrosternite ASVII
6vpmm	*sterno-sternalis paramedialis*	Posterior ASVI	Anterolateral apodemes ASVII
6volm	*sterno-sternalis ortholateralis*	Anterolateral apodemes ASVI	Anterolateral apodemes ASVII
7domm	*tergo-tergalis orthomedialis*	Anterolateral apodemes ATVII	Antecosta ATVIII
7dpmm	*tergo-tergalis paramedialis*	Posterior ATVII	Ventrolateral ATVIII
7dolm	*tergo-tergalis ortholateralis*	Anterolateral apodemes ATVII	Dorsal ATVIII
7dvimm1	*tergo-sternalis interior anteromedialis*	Antecosta ATVII	Posterior ASVII
7dvimm2	*tergo-sternalis interior posteromedialis*	Posterior ATVII	Anterolateral apodemes ASVII

(Continues)

TABLE 2 (Continued)

Designation	Name	Origin	Insertion
7dvilm	*tergo-sternalis interior lateralis*	Anterior ATVII	Anterolateral apodemes ASVII
7vdxm	*sterno-tergalis exterior*	Antecosta ASVII	Antecosta ATVIII
8domm	*tergo-tergalis orthomedialis*	Antecosta ATVIII	Posterodorsal apodemes ATIX
8dpmm	*tergo-tergalis paramedialis*	Dorsolateral ATVIII	Midplate line ATIX
8dolm	*tergo-tergalis ortholateralis*	Anterolateral ATVIII	Midplate line ATIX
8dcm	*tergo-coxalis (solus)*	Antecostal flanges ATVIII	Lateral apodemes gonocoxites VIII
8ccim	*coxo-coxalis interior*	Gonocoxites VIII	No medial insertion; muscle transverse
9domm	*tergo-tergalis orthomedialis*	Posterodorsal apodemes ATIX	Proctiger lobe
9dcm1	*tergo-coxalis anterior externalis*	Posterolateral flanges ATIX	Anterior arms gonocoxites IX
9dcm2	*tergo-coxalis anterior internalis*	Posterodorsal apodemes ATIX	Anterior arms gonocoxites IX
9dcm3	*tergo-coxalis lateralis*	Mesal ATIX	Posterior arms gonocoxitex IX
9dcm4	*tergo-coxalis medialis*	Anal arc	Posterior arms gonocoxitex IX
9cam1	*coxo-apophysealis major anterior*	Anterior arms gonocoxites IX	Furcula dorsal arm
9cam2	*coxo-apophysealis major posterior*	Posterior arms gonocoxites IX	Furcula ventral arms
9cam3	*coxo-apophysealis minor*	Ventromedial processes gonocoxites IX	Sting bulb articular processes
9ccim	*coxo-coxalis interior*	Posterior arms gonocoxites IX	No medial insertion; muscle transverse

Note: Full descriptions of origin, insertion, and form are given in Section 3.

Abbreviations: cam, coxapophyseal muscles; ccim, coxococoxal intrinsic muscles; dolm, dorsal ortholateral muscles; domm, dorsal orthomedial muscles; dpmm, dorsal paramedial muscles; dvilm, dorsoventral intrinsic lateral muscles; dvimm, dorsoventral intrinsic medial muscles; dvxm, dorsoventral extrinsic (paramedial) muscles; dcm, tergocoxal muscles; volm, ventral ortholateral muscles; vomm, ventral paramedial muscles; vpmm, ventral paramedial muscles; vdxm, ventrodorsal extrinsic muscles.

A Latinized name is provided for each skeletal muscle, in the form *Musculus origin-insertion (descriptors)*. Grammatically, the origin is given in the ablative singular, the insertion in the nominative singular of the relational adjective suffixed with *-alis*, and additional descriptor(s) in the nominative singular of the relational adjective, or a comparative degree of an adjective concluding in *-or* (e.g., "interior" indicating intrasegmentality, or "minor" indicating the smaller of two similar muscles). Muscle labels are designated with three parts: the segment of origin (e.g., **5**dolm2), the topographic region (e.g., 5**dolm**2), and a sequential identifying number if necessary (e.g., 5dolm**2**). Segments of origin are given in Arabic numerals (1–10) for the abdomen and Roman numerals (III) for the thorax; sequential identifiers are given in Arabic numerals for both tagmata. The sequential identifiers are given in order from anterior to posterior, and from medial to lateral where muscles overlap.

A number of extrinsic and intrinsic visceral muscles (those with at least one nonskeletal attachment) were also observed, which are described in Section 3.5 with their associated organs. These are named by their location or putative function and are not assigned numerical designations, except for the tergocardiac muscles, *M. tergocardiacalis*, which originate on a tergite and insert on the dorsal vessel, and are clearly segmental. We choose not to use the traditional term "alary muscle," which refers to the wing-like or deltoid shape of the tergocardiac muscles (Nation, 2008), to avoid the implication that they are associated with the wings. Other (probably) extrinsic visceral muscles are those of the venom and Dufour's gland ducts, *M. dilator glandulae venenalis*, *M. dilator glandulae Dufouris dorsalis*, and *M. dil. gl. Duf. ventralis*. Recognizable intrinsic visceral muscles of the alimentary tract are *M. ventriculi*, *M. sphincter pylori*, *M. retractor ani*, and *M. sphincter ani*. Besides those described above, several additional muscle groups can be recognized which do not occur in Aculeata or which were not observed here (Table S2).

2.8.4 | Gland nomenclature

Following the standard classification of exocrine glands by Noirot & Quennedey (1974), distinction is made between *class-1* and *class-3* glands (their classification initially also included Class-2, although these have been homologized with oenocytes: Billen & Šobotník, 2015; Noirot & Quennedey, 1991). Class-1 glands are formed by a monolayered epithelium of secretory cells. Class-3 glands are made up of a number of bicellular units, each unit comprising a *secretory cell* and its accompanying *duct cell*. The junction between the secretory cell and the duct cell is known as the *end apparatus*, which functions as a drainage system for the secretory products. Both Class-1 and Class-3 glands can open directly through the external cuticle, or can contain an internalized *reservoir* where secretion can be temporarily

stored. We do not adopt the classification system of Yek & Mueller (2011) for the metapleural gland atrium; see Section 4.1.4 for discussion of our rationale.

2.8.5 | Nomenclature for other soft tissue

Certain non-muscular soft tissues were partially reconstructable with micro-CT and are described briefly; note that the circulatory, digestive, reproductive, and nervous systems were not examined in detail with other methods. Terminology for the soft tissues generally follows (Chapman et al., 2013). Terms for the proventriculus are used after (Eisner & Brown, 1956).

The *circulatory system* of the abdomen includes the *dorsal vessel* or "heart," the pericardial cells, and the muscles of the dorsal diaphragm, as well as connective tissues and cells of potentially suspensory function that connect the dorsal vessel to the body wall. Because the circulatory organs were too poorly resolved to confidently identify the non-muscular cell types, we refer to them agnostically as *dorsal diaphragm cells*. The *tergocardiac muscles* are extrinsic visceral muscles that originate on the postantecostal tergite and insert on the dorsal diaphragm or the vessel itself. Accessory pulsatile organs of the sting apparatus were not observed, although pulsatile organs associated with the ovipositor have been reported for certain non-Hymenopteran taxa (Hillyer & Pass, 2020; Hustert et al., 2014; Pass, 2000).

The *alimentary tract* of the abdomen comprises three main regions, the *foregut*, *midgut*, and *hindgut*. The foregut includes the *esophagus* and *crop*, which are differentiated by the thickness and convolution of the intima, and the *proventriculus*. The proventriculus comprises two main sclerotized parts, the *bulb*, the walls of which are the lamellate *plicae*, and the s*tomodeal valve*, located within the midgut *ventriculus*; anteriorly the stomodeal valve is expanded into a disclike *anterior lip* which partially sits on the ectal anterior ventricular surface. The midgut is represented by the *ventriculus*, a large, bulbous chamber. The hindgut comprises three parts: (1) the *pylorus*, a campaniform chamber attached to the ventriculus and separated by a muscular sphincter and bearing the *Malpighian tubules*; (2) the *ileum*, a long, folded, tubelike organ; and (3) the *rectum*, which is basically a large, extensible sac with particularly thin intima, and which bears the *rectal pads* and the *anus* with its associated musculature.

The *reproductive organs* comprise the paired *ovaries*, each with four *ovarioles*, within which we distinguish the *vitellarium* and the proximal *lateral oviduct*; the lateral oviducts fuse medially, forming the *median oviduct*, which posteriorly expands into a partially sclerotized, multiply folded *distal oviduct*. We use the term *distal oviduct* due to uncertainty in the data set: we could not differentiate elements such as the bursa copulatrix, spermatheca, and vagina, if present; see Section 4.8.3. Ovarioles contain *oocytes* and *trophocytes*, the latter with multiple *trophocyte nuclei* and connected to the oocyte via subcellular *ring canals*. Note that the micro-CT data were of insufficient spatial resolution to segment further subdivisions of the ovarioles (e.g., terminal filaments, germaria), cell types (e.g., follicle cells), or other subcellular structures (e.g., fusomes).

The *central nervous system* comprises the *ventral nerve cord*, *ganglia*, and *peripheral nerves*. Due to variation in the fusion of neuromeres among taxa (Niven et al., 2008), the situation of the ganglia in situ relative to the segments, and because we did not examine segmentality of ganglia by their innervations, we refer to the six ganglia by their position (see Section 4.8.4) as the *second mesosomal ganglion*; *first*, *second*, *third*, and *fourth metasomal ganglia*; and *terminal ganglion*. The ganglia are joined by paired longitudinal branches of the nerve cord, or *connectives* (Klass, 2008b). We use *peripheral nerve* broadly for the lateral ramifications arising from the ganglia. We refer to the peripheral nerves as innervating tissues; however, according to some strict usages, nervules or neurons (rather than nerves) innervate tissues (e.g., Youssef, 1968). Because we did not histologically examine neuronal structure, *innervates* should here be taken to mean "peripheral nerve intimately associated with the named tissue and likely innervating it by way of one or more neurons."

3 | RESULTS

3.1 | Mesosoma and anterior pregenital abdomen

3.1.1 | ThII-III (mesopectal and metapectal regions)

Sclerites

The **metapectus** is completely fused with the **mesopectus** anteriorly and the **propodeum** posteriorly. The mesopectus bears internally a median ridge, the **mesodiscrimenal lamella** (msd, Figure 3b), which is marked externally by the depressed **mesodiscrimenal line** (sulcus; msdl, Figure 3a); the mesopectus, anterad the mesocoxae, bears a pair of arcuate transverse carinae, the **mesosternal processes** (msstp, Figure 3); the mesodiscrimenal lamella gives rise to a marginated, approximately triangular process, the **mesofurca** (msf, Figures 3b and 4b,d), which has a single pair of anterolateral arms that extend laterally toward the body wall; externally the mesofurca is indicated by the small **mesospinal pit** (msspp, Figure 3a); the mesofurca is medially fenestrated by the **neural foramen** (msnf, Figure 4b,d) through which runs the ventral nerve cord; the neural foramen is dorsally enclosed by a strip of sclerite, the **neural bridge** (msnb, Figure 4d). Externally and ventrally, the metapectus is marked by four features: (1) a transverse arc that contacts the mesocoxal foramina posteriorly, the **paracoxal line** (pcxs, Figure 3); (2) a medially situated impression, the **metafurcal pit** (mtfpp, Figure 3a); (3) a longitudinal and medially oriented line, the **metadiscrimenal line** (mtdl, Figure 3a), which ends posteriorly at the metafurcal pit; and (4) a pair of transversely oriented protuberances, the **metasternal processes** (mtstp, Figures 3 and 4), which surround the metafurcal pit, and are subtriangular in shape. Posterior to the metafurcal pit is a longitudinal carina which contacts the posterior margin of the metasternal area, which also contacts the propodeum laterally, closing the metacoxal
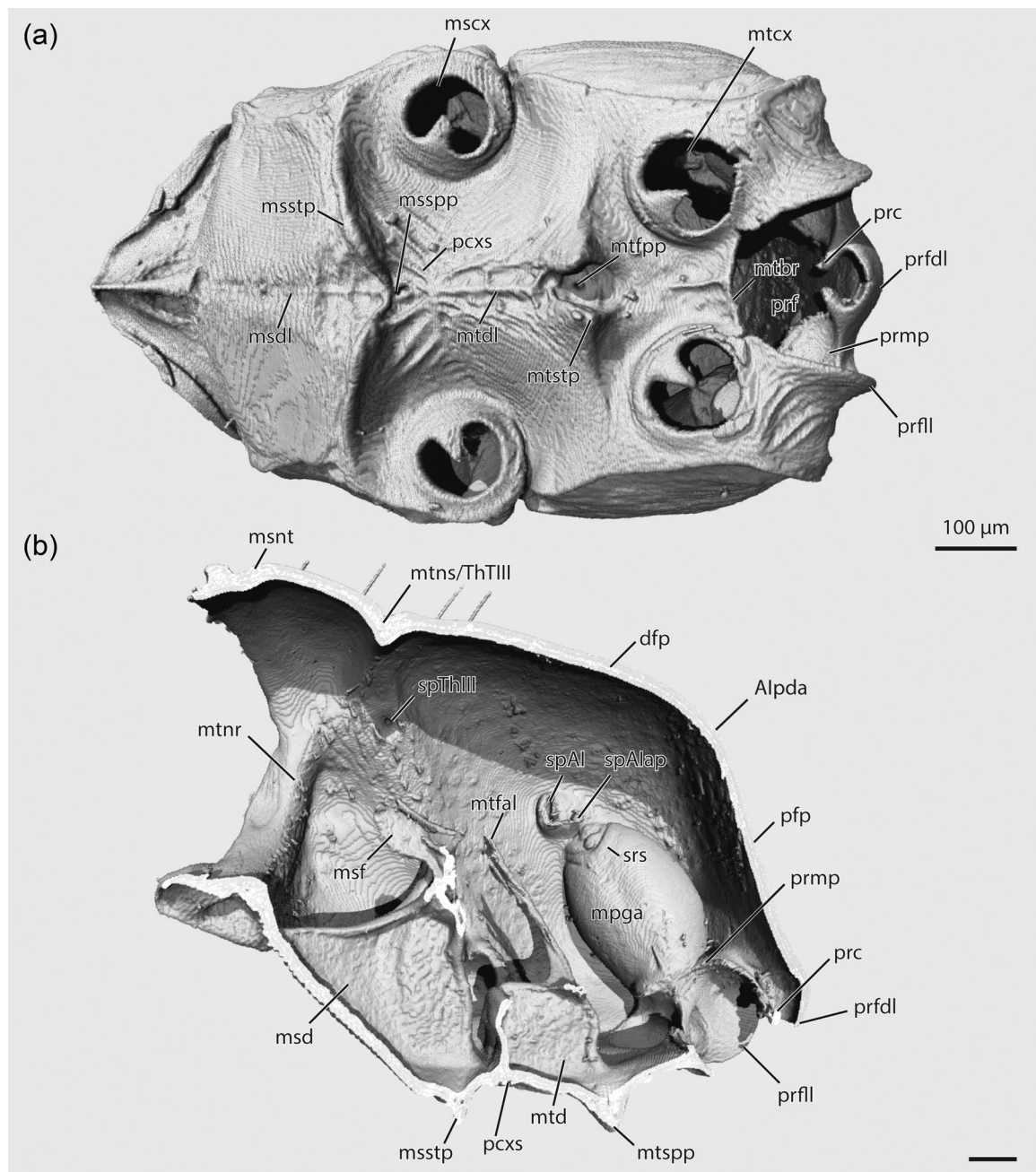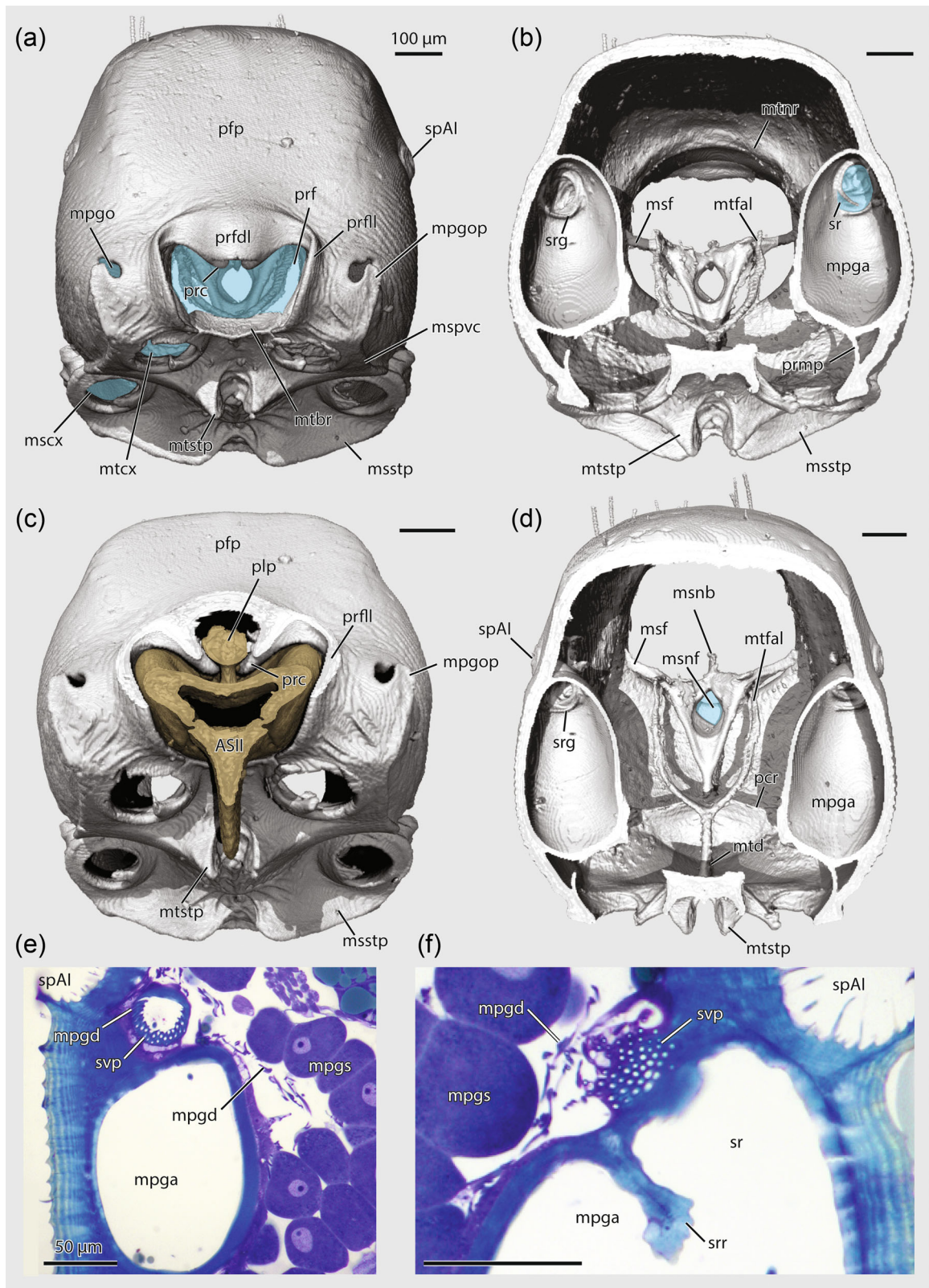
FIGURE 3 *Amblyopone australis*, skeleton of the mesosoma and abdominal segment I (propodeum). (a) external ventral view, (b) sagittal bisection. Scale bars: 100 μm. AIpda, posterodorsal angle of the propodeum; dfp, dorsal surface of the propodeum; mpga, metapleural gland atrium; mscx, mesocoxal foramen; msd, mesodiscrimen; msdl, mesodiscrimenal line; msf, mesofurca; msnt, mesonotum; msspp, mesospinal pit; msstp, mesosternal pit; mtbr, metasternal bridge; mtcx, metacoxal foramen; mtdl, metadiscrimenal line; mtdl, metadiscrimenal line; mtfal, anterior laminae of the metafura; mtfpp, metafurcal pit; mtnr, metanotal ridge; mtns, metanotal sulcus; mtstp, metasternal process; pcxs, paracoxal sulcus; pfp, posterior surface of the propodeum; prc, propodeal condyle; prf, propodeal foramen; prfdl, dorsal lobe of the propodeal foramen; prfll, lateral lobe of the propodeal foramen; prmp, mesal propodeal process; sp, spiracle; spAIap, spiracular apodeme; srs, secretory recess sulcus; ThT, thoracic tergite

foramina. Internally, the paracoxal and the metadiscrimenal lines correspond, respectively, with the **paracoxal ridge** (**pcr**, Figures 4d and 5c) and the large, median plate of the **metadiscrimenal lamella** (**mtd**, Figures 3b–5a); the paracoxal ridge extends laterally to the pleural wall and forms part of the **mesocoxal foramen** (**mscx**, Figures 3a and 4a), while the metadiscrimenal lamella posteriorly

bears the metafurca. The **metafurca** is a pair of spinelike apophyses that extend anterodorsally. Muscles inserting on AII (the petiole) originate on both the metadiscrimenal lamella and the **anterior laminae of the metafurca** (**mtfal**, Figures 3b and 4b,d).

The **metapleural gland atrium** (**mpga**, Figures 1b–5c) is a large, ovate invagination which can frequently be seen through the

FIGURE 4 (See caption on next page)
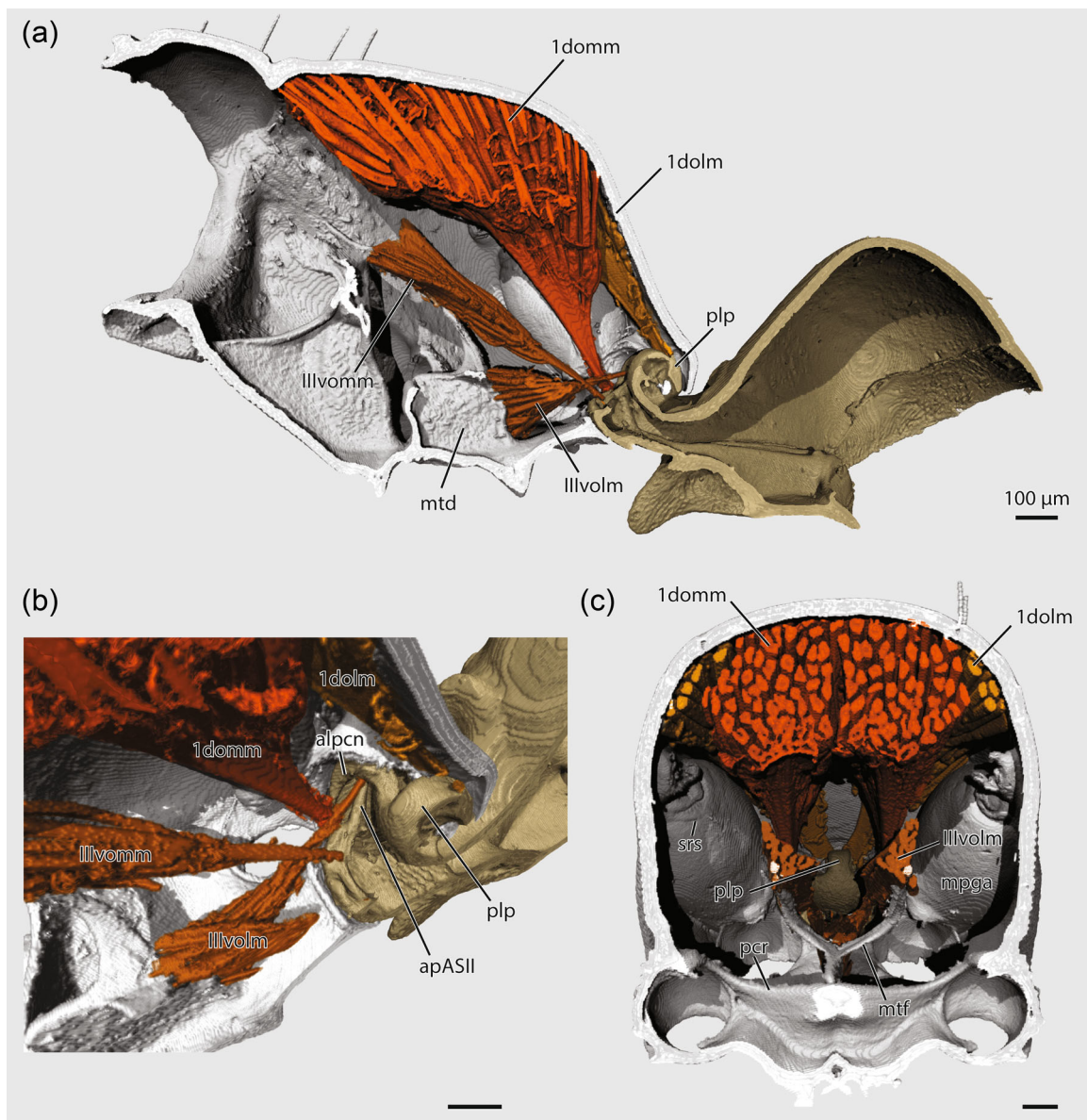
FIGURE 5 *Amblyopone australis*, skeletomusculature of the metasternum and abdominal segment I (propodeum) and articulation with abdominal segment II (petiole); three-dimensional reconstruction. (a) sagittal bisection, (b) anterior dorsomesal view, (c) anterior transverse dissection. Scale bars: 100 μm. alpcn, anterolateral petiolar condyle; ap, anterolateral apodeme; dolm, dorsal ortholateral muscle; domm, dorsal orthomedial muscle; mpga, metapleural gland atrium; mtd, metadiscrimenal lamella; mtf, metafurca; pcr, paracoxal ridge; plp, petiolar levator process; srs, secretory recess sulcus; volm, ventral ortholateral muscle; vomm, ventral orthomedial muscle

FIGURE 4 *Amblyopone australis*, skeleton of abdominal segment I (propodeum) and articulation with abdominal segment II (petiole) in 3D reconstruction (a–d); metapleural gland morphology in transverse histological sections (e–f). (a) propodeum, posteroventral external view; (b) mesosoma, anterior transverse dissection, (c) propodeum and petiole, posteroventral external view, petiole partially dissected, (d) propodeum, posterior transverse dissection, (e) metapleural gland, (f) detail of metapleural gland secretory recess. Cyan overlays in (a–d) indicate foramina. Scale bars, a–d: 100 μm. Scale bars, e–f: 50 μm. mpga, metapleural gland atrium; mpgd, metapleural gland duct cell; mpgo, metapleural gland orifice; mpgop, posterolateral process of the metapleural gland orifice; mpgs, metapleural gland secretory cell; mscx, mesocoxal foramen; msf, mesofurca; msnb, neural bridge of the mesofurca; msnf neural foramen of the mesofurca; mspvc ventrolateral mesopectal carina; msstp mesosternal pit; mtbr, metasternal bridge; mtcx, metacoxal foramen; mtd, metadiscrimenal lamella; mtfal, anterior laminae of the metafura; mtnr, metanotal ridge; mtstp, metasternal process; pfp, posterior surface of the propodeum; plp, petiolar levator process; plp, petiolar levator process; prc, propodeal condyle; prf, abdominal sternite; prfdl, dorsal lobe of the propodeal foramen; prfll, lateral lobe of the propodeal foramen; prmp, mesal propodeal process; sp, spiracle; sr secretory recess of the metapleural gland atrium; srg, spiral ruga of the secretory recess; srr, secretory recess ridge; svp, sieve plate of the secretory recess

translucent metapleural wall with light microscopy (Figure 1b); at its anterodorsal end is the **secretory recess (sr**, Figure 4b,d–f), a compartment partially differentiated by a strong invagination of the mesal atrial wall, the **secretory recess ridge (srr**, Figure 4e) corresponding to the external **secretory recess sulcus (srs**, Figures 3b and 5c); internally, the recess bears robust **spiral rugae (srg**, Figure 4b,d) which coil around the long axis of the atrium and which delineate the secretory recess from the remainder of the atrium ("receptacle," Tulloch et al., 1963); at its external apex, the secretory recess bears a distinct region of perforated cuticle, the **sieve plate (svp**, Figure 4f). The **metapleural gland orifice (mpgo**, Figures 1b and 4a) is posterodorsally oriented and roughly U-shaped in oblique posterior view; the orifice appears teardrop-shaped in posterior view, because the **posterolateral processes of the orifice (mpgop**, Figure 4a,c) occlude the anterolateral part of the orifice itself; the ridge on the posterolateral process is a continuation of the longitudinally oriented **ventrolateral mesopectal carina (mspvc**, Figures 2a and 4a). The **metapleural gland** itself is formed by two clusters of approximately 80–90 **secretory cells (mpgs**, Figure 4e,f) at each side. These large, spherical cells have a diameter of 50 μm, and are associated with **duct cells (mpgd**, Figure 4e,f) which connect to the atrium through the holes of the sieve plate (**svp**, Figure 4e,f).

Muscles

Ventral orthomedial muscles: (1) **IIIvomm**, *M. metaspina-abdominosternalis medialis* (Figure 5). **O**: Posteromedially on the anterodorsal metafurcal lamina; **I**: on the transverse carina of the anterior arc of the petiolar presternite, at the base of the anterolateral apodemes of ASII. **F**: Laterally thin, narrowly triangular, ventromedially directed, tapering to slender insertions. **Ventral ortholateral muscles**: (2) **IIIvolm**, *M. metafurca-abdominosternalis lateralis* (Figure 5). **O**: On the posterior surface of the base of the metadiscrimenal lamella; **I**: on the apices of the anterolateral apodemes of ASII. **F**: Small but robust, triangular, dorsolaterally directed; origins united at metadiscrimenal lamella, insertions diverging laterally. *Note*: **IIIvomm** and **IIIvolm** correspond with IIIvlm3 and IIIvlm2 of Friedrich & Beutel (2008) and Beutel et al. (2014).

3.1.2 | AI (propodeum)

Sclerites

In lateral external view the **propodeum** is approximately rhomboid, with the long axis oriented dorsoventrally, and without clear demarcation separating it from ThIII (**AI**, Figures 1a,b and 2a) The **dorsal propodeal surface (dfp**, Figure 3b) gently slopes posteroventrally; it is approximately equal in length to the **posterior propodeal surface (pfp**, Figures 3b and 4a,c), which it meets at a rounded **posterodorsal angle (AIpda**, Figure 3b). The **posterior propodeal surface** is gently inclined anteriorly from the transverse (vertical) plane. The **metanotal sulcus (mtns**, Figures 1b and 3b) separates AI from the **mesonotum (msnt**, Figure 3b) dorsally and laterally; internally, it corresponds to the **metanotal ridge**

(**mtnr**, Figures 3b and 4b); the metanotal sulcus is the only trace of the metanotum retained in workers, although the metanotum is a distinct sclerite in alates and developed to some degree in workers of various species (Aibekova et al., 2022; Boudinot et al., 2022a). The **propodeal spiracle (spAI**, Figures 1b–4a,c) is located near the center of the propodeum in lateral view (Figure 2a) and is close to the dorsalmost height of the metapleural gland atrium internally; a small, rod-shaped **spiracular apodeme (spAIap**, Figure 3b) projects from the anteroventral edge of the internal spiracular atrium. The **propodeal foramen (prf**, Figures 3a and 4a) is roughly reniform in shape; in posterior view, the foramen forms a smoothly rounded, inverted omega miniscule (ω-shape; Figure 4a); its lateral walls are posteriorly produced as the **lateral lobes of the propodeal foramen** (= propodeal lobes; **prfll**, Figures 3 and 4a,c) which are mesally concave, accommodating the lateral surfaces of the anterolateral petiolar condyles; the dorsomedian margin of the foramen is produced as a broad **dorsal lobe of the propodeal foramen (prfdl**, Figures 3 and 4a), which anteroventrally bears the paired **propodeal condyles (prc**, Figures 3 and 4a,c); these condyles articulate with the petiolar levator process (**plp**, Figures 4c and 6); the ventromedial portion of the propodeal foramen comprises the flat **metasternal bridge (mtbr**, Figures 3a and 4a). The entire inner margin of the propodeal foramen is finely carinate; its internal dorsal margin is formed by the arcuate **mesal propodeal processes** of the posterior propodeal wall (**prmp**, Figures 3b and 4b), which are tightly approximated with the mesal walls of the metapleural gland atria.

The surface sculpture of the propodeal dorsum, its posterior face, and approximately the dorsal third of the metapleural area in lateral view is smooth and shining, with coarse piligerous punctures bearing setae of varied length. The longitudinal midline (in dorsal view) and the area around the spiracle are glabrous. The ventral region of each metapleural area is finely imbricate. The area just dorsad the metacoxae is strigulate (Figure 1a,b).

Muscles (Figure 5)

Dorsal orthomedial muscles: (1) **1domm**, *M. tergo-tergalis orthomedialis*. **O**: Dorsomedial area of the propodeum; **I**: anteriorly on the anterolateral petiolar condyles, as they wrap in front of the presternite. **F**: Very large, feather-shaped, posteroventrally directed, tapering significantly toward insertions. **Spiracular muscles** were not resolved in the present data set. **Dorsal ortholateral muscles**: (2) 1dolm, *M. tergo-tergalis ortholateralis*. **O**: Dorsolateral areas of the propodeum; **I**: dorsolaterally on the petiolar levator process. **F**: Large, feather-shaped, ventromedially directed, tapering significantly to insertions.

3.1.3 | Sculpture and setation of the pregenital abdomen

Beyond the details provided above, the surface sculpture and setation are largely comparable between the pregenital segments (Figure 1a–e). The presclerites or anterior post-antecostal regions are glabrous and covered with fine, dense, strigulate sculpture. The
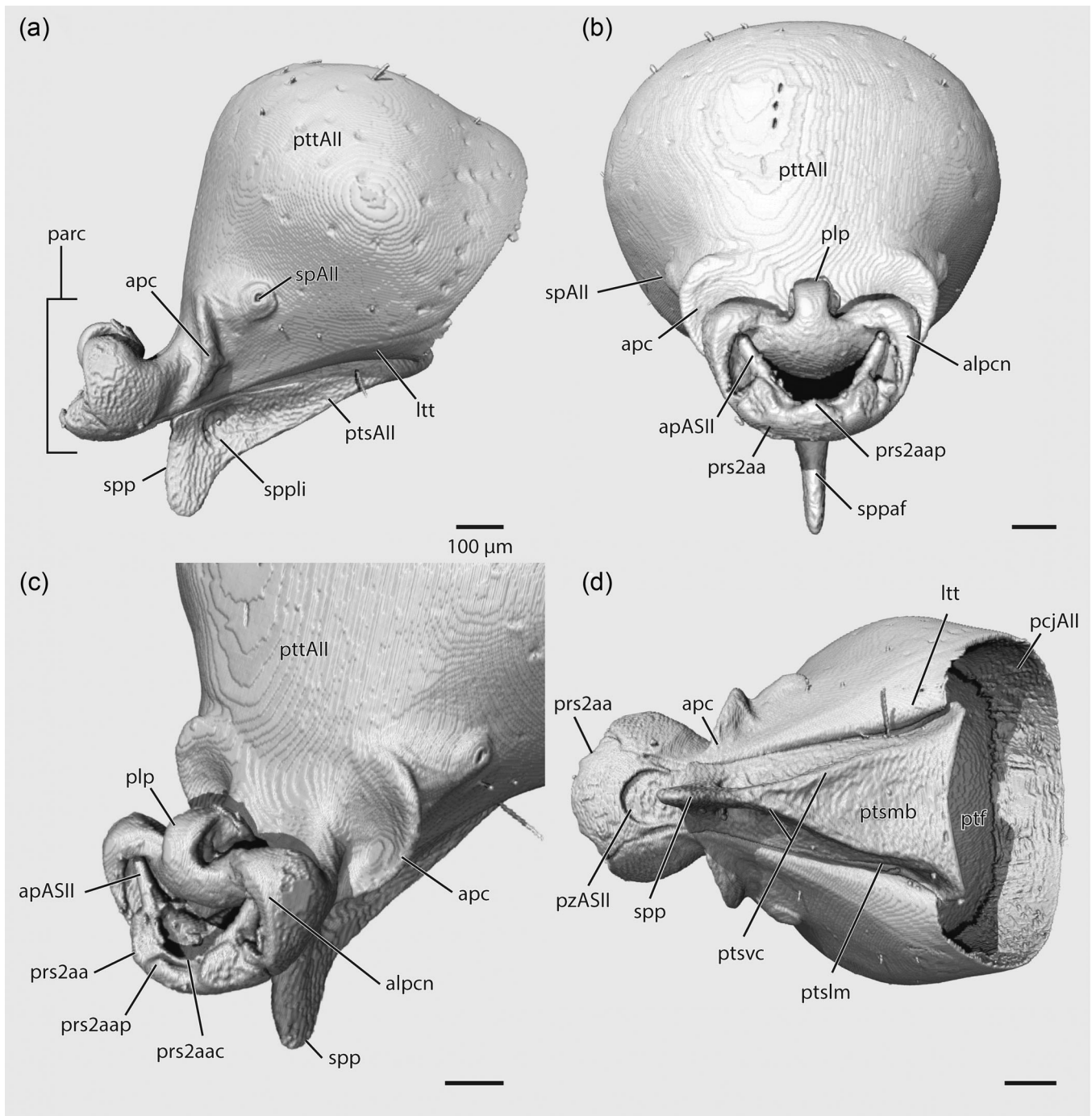
FIGURE 6 *Amblyopone australis*, skeleton of abdominal segment II (petiole); 3D reconstruction in (a) lateral view, (b) anterior view, (c) anterior oblique view, (d) ventral view. Scale bars: 100 μm. A, abdominal segment; alpcn, anterolateral petiolar condyle; apc, anterolateral petiolar carina; apc, anterolateral petiolar carina; ltt, laterotergite; parc, petiolar articulatory complex; pcj, posterior conjunctiva; plp, petiolar levator process; prs2aa, anterior arc of the petiolar presternite; prs2aac, transverse carina of the anterior arc of the petiolar presternite; prs2aap, dorsal process of the anterior arc of the petiolar presternite; ptf, posterior petiolar foramen; pts, poststernite; ptslm, lateral petiolar poststernite margination; ptsmb, medial body of the petiolar poststernite; ptsvc, ventrolateral carinae of the petiolar poststernite; ptt, posttergite; pz, proprioreceptive zone; sp, spiracle; spp, subpetiolar process; sppaf, anterior surface of the subpetiolar process; sppli, lateral impression of the subpetiolar process

postsclerites or posterior postantecostal regions are overall smooth and shining, except for piligerous punctae. The setae arising from these punctae are rather long, tapering, and flexuous, ranging from suberect to subdecumbent and varying somewhat in length with no

obvious spatial patterning. The distribution of punctae and associated setae is more or less uniform on the entire posttergite and poststernite of AII–AIV. In AV and AVI, the punctae are more concentrated towards the posterior margins of the sclerites and

are conspicuously denser and smaller on the sternites. On AVII the punctae are particularly dense on the ventral parts of the posterior tergite, and the entire posterior sternite, giving rise to particularly long setae apically. Additionally, ATVII has smaller punctulae with concordantly smaller associated setae interspersed with the larger punctae, while on the prior segments the entire field of punctae is of similar size.

3.1.4 | AII (M1; petiole)

Sclerites

ATII is divided into pre- and posttergites by the auriculate **anterolateral petiolar carinae** (**apc**, Figures 6 and 7); these carinae are located entirely anterad the petiolar spiracles, are margined posterobasally by a shallow sulcus, and have concave, dish-like anterior surfaces which function as contact surfaces with the ectal surfaces of the lateral lobes of the propodeal foramen when AII is fully elevated. The petiolar presclerites are divided into two regions: the anterior articulatory complex and the posterolateral contact surfaces. The **petiolar articulatory complex** (**parc**, Figure 6a) comprises the petiolar pretergite and presternite, and has a concave dorsal surface, thick anterolateral condyles, and an anteromedian process. The **petiolar levator process** (**plp**, Figures 4c, 5, 6b,c, and 8a) is located anterodorsally on the pretergite, and is roughly circinate in shape, that is., resembling the scroll of a violin; its dorsal part is a rectangular block, the sides of which are slightly impressed; dorsomedially the process bears a thin, roughly rectangular strip of sclerite that curves anteroventrally, connecting to the anteromedian margin of the pretergite (Figure 6c); the levator complex articulates with the propodeal condyles and dorsal lobe of the propodeal foramen (Figures 4c and 5a,b). The **anterolateral petiolar condyles** (**alpcn**, Figures 5b–7b) are approximately reniform in anterior view; they laterally overlap the dorsal margin of the presternite, and medially they connect to the petiolar levator process; the condyles articulate on their ectal surfaces with the mesal surfaces of the lateral lobes of the propodeal foramen; anteromesally they are excavated and accommodate the anterolateral apodemes of the sternite (Figure 5b).

The disc of the **petiolar presternite** bears a large, posteroventral, semicircular depression, the **proprioreceptive zone of AII** (**pzAII**, Figures 6d–8a) surrounded by thick cuticle; the sculpture of the external and internal surfaces of the proprioreceptive zone is corticinus to shallowly areolate (Figures 6d and 7c). In ventral view, the anterior region of the presternite is roughly tongue-like, with a rounded anterior margin. The **anterior arc of the petiolar presternite** is carinate (**pr2saa**, Figures 6–8a) and medially bears a small subtriangular **dorsal process** (**prs2aap**, Figures 6b–8a); posterad this process is a shallow sulcus followed by an arcuate **transverse carina of the anterior arc** (**prs2aac**, Figure 6c). The transverse carina posterolaterally continues into the digitate **anterolateral apodemes of the petiolar presternite** (**apASII**, Figures 5b–8a), which project dorsolaterally into the excavated inner part of the petiolar condyles; the anteroventral mesal surfaces of the apodemes bear small elliptical impressions; posteriorly, the apodemes connect to longitudinal ridges that continue posteriorly into the lumen of the segment. Muscle IIIvlm1 inserts at the base of these apodemes; muscle IIIvlm2 inserts on their apices (Figure 5b). It is possible that the transverse carina of the anterior arc corresponds to the antecosta, the sulcus of the anterior arc to the antecostal sulcus, and the dorsal process of the anterior arc to the acrosternite, since these features recapitulate the expected forms and spatial relationship of these structures in less highly modified segments.

The **petiolar posttergite** (petiolar node; **pttAII**, Figures 6a–c–8) is roughly cuneate in lateral external view, with a posterodorsally sloped anterior surface, rounded posterodorsal angle, and slightly convex dorsum; in anterior view it is subelliptical posterad the anterolateral petiolar carinae; it articulates broadly with AIII such that the posterior constriction of the petiole is wider than half the width of the petiole; it bears laterotergites ventrolaterally and spiracles anterolaterally. The **laterotergites** (**ltt**, Figures 6a,d and 7a,b) are subtriangular and are delineated dorsally by a fine crease externally, and a more pronounced sulcus internally; they slightly overlap with and fit into lateral longitudinal sulci of the dorsal margin of the poststernite over its length. The **petiolar spiracles** (**spAII**, Figures 6–8b) are elliptical, with their long axes subparallel to the apparent ventral margin of the tergite in lateral view; they are borne on low, roughly circular cuticular prominences. The **posterior petiolar foramen** (**ptf**, Figures 6d and 7) in posterior view resembles a broad omega majuscule (Ω; Figure 7); the ventrolateral impressions of the foramen are formed by the overlap of the laterotergites with the posterior lip of the poststernite; (Figure 7b) they accommodate the anterior ventrolateral corners of ATIII (Figure 8).

The **petiolar poststernite** is divisible into two main regions, the medial poststernite body and the posterior poststernite lip. The **medial poststernite body** (**ptsmb**, Figures 6d and 7a,c) comprises most of the sternite. It is subtriangular in lateral view, being produced anteromedially as the **subpetiolar process** (**spp**, Figures 6–8) and sloping posteriorly to its posterior margin. In ventral view it is subtrapezoidal (Figure 6d), with the posterior margin concave. The **anterior surface of the subpetiolar process** (**sppaf**, Figure 6b) is a simple ridge ventrally (distally), expanding dorsally (proximally) into a triangle. The subpetiolar process bears a subcircular **lateral impression** (**sppli**, Figures 6a–8) on each side, posteroventrad the anterolateral carinae and approximately ventrad the spiracle. The ventral surface of the medial poststernite body is marginated by the **ventrolateral carinae of the petiolar poststernite** (**ptsvc**, Figures 6d and 7b), which are united anteromedially at the subpetiolar process, and which sinuously diverge to the posterolateral corners of the poststernite body. These carinae are situated at lateral margins of the medial poststernite body and extend from the anterolateral dorsal corners of the poststernite body to its posterior margin; these carinae delimit the lateral poststernite articulations ventromedially. The **lateral poststernite articulations** are the extreme lateral portions of the medial poststernite body; they comprise the **lateral longitudinal sulcus of the poststernite** (**ptsls**, Figure 7b,d) and the **lateral rim of the poststernite** (**ptslr**, Figure 7b); the lateral sulcus
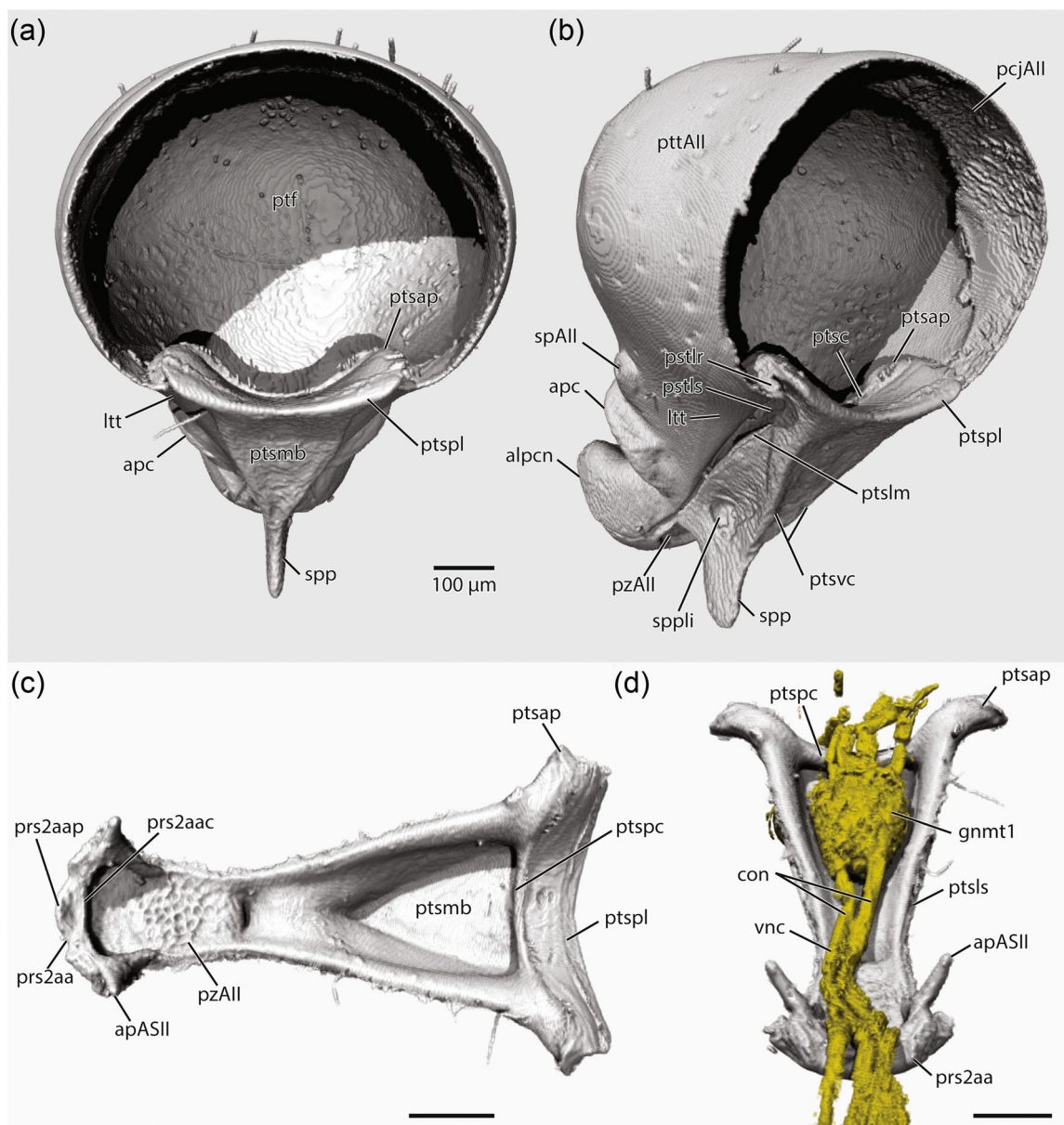
FIGURE 7 *Amblyopone australis*, skeleton of abdominal segment II (petiole); 3D reconstruction in (a) posterior view, (b) posterior oblique view, (c) dorsal view, tergite hidden; (d) anterodorsal view, tergite hidden, with ventral nerve cord. Scale bars: 100 μm. A, abdominal segment; alpcn, anterolateral petiolar condyle; apc, anterolateral petiolar carina; con, connective of the ventral nerve cord; gnmt1, first metasomal ganglion; ltt, laterotergite; pcj, posterior conjunctiva; prs2aac, transverse carina of the anterior arc of the petiolar presternite; ptf, posterior petiolar foramen; ptsap, posterolateral apodeme of the petiolar poststernite; ptslm, lateral petiolar poststernite margination; ptslr, lateral ridge of the petiolar poststernite; ptsls, lateral sulcus of the petiolar poststernite; ptsmb, medial body of the petiolar poststernite; ptspc, posterior petiolar poststernite carina; ptspl, posterior petiolar poststernite lip; ptspl, posterior petiolar poststernite lip; ptsvc, ventrolateral carinae of the petiolar poststernite; ptt, posttergite; pz, proprioreceptive zone; sp, spiracle; spp, subpetiolar process; sppli, lateral impression of the subpetiolar process; vnc, ventral nerve cord

receives the ventral margins of the laterotergites, while the lateral rim curves ventromedially in cross-section and contacts the laterotergite along its length. The lateral rims are posteriorly preapically expanded into rounded prominences, the **posterolateral apodemes of the poststernite** (**ptsap**, Figures 7 and 8), which are connected medially by the transverse, arcuate **posterior poststernite carina** (**ptsc**, Figures 7b–d and 8), which may form a contact surface with the antecosta of ASIII. The posterolateral apodemes are tightly connected by tough conjunctiva to the helcial tergite (AIII pretergite), such that in manual dissection the posterior poststernite plate frequently remains attached to AIII when segments are disarticulated, rather than being retained on the remaining AIII sternite. The posterior poststernite carina differentiates the medial poststernite body from the **posterior poststernite lip** (**ptspl**, Figures 7 and 8) which has a dorsal contact surface with the helcial sternite (AIII presternite) during abdominal flexion; this lip is
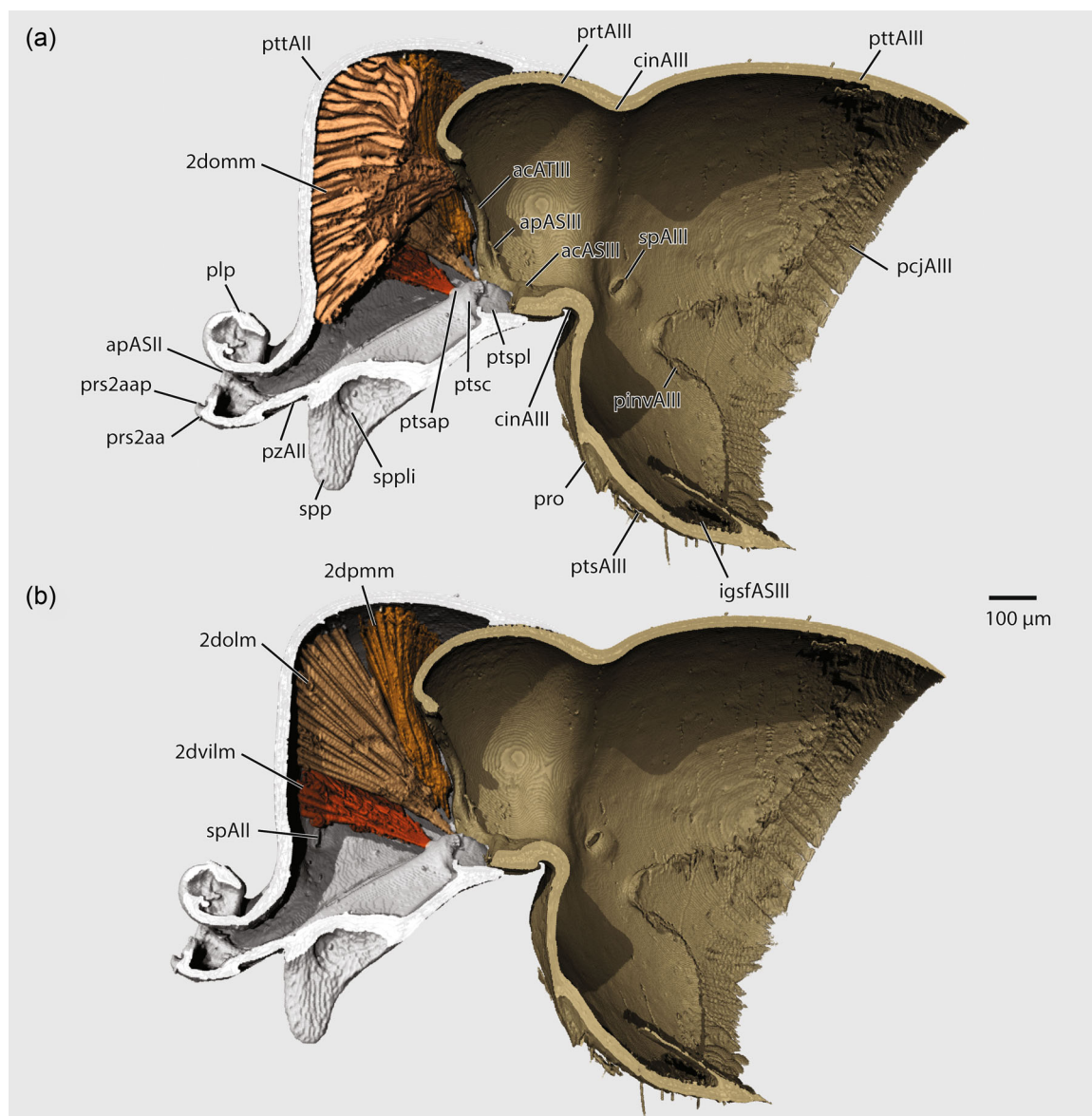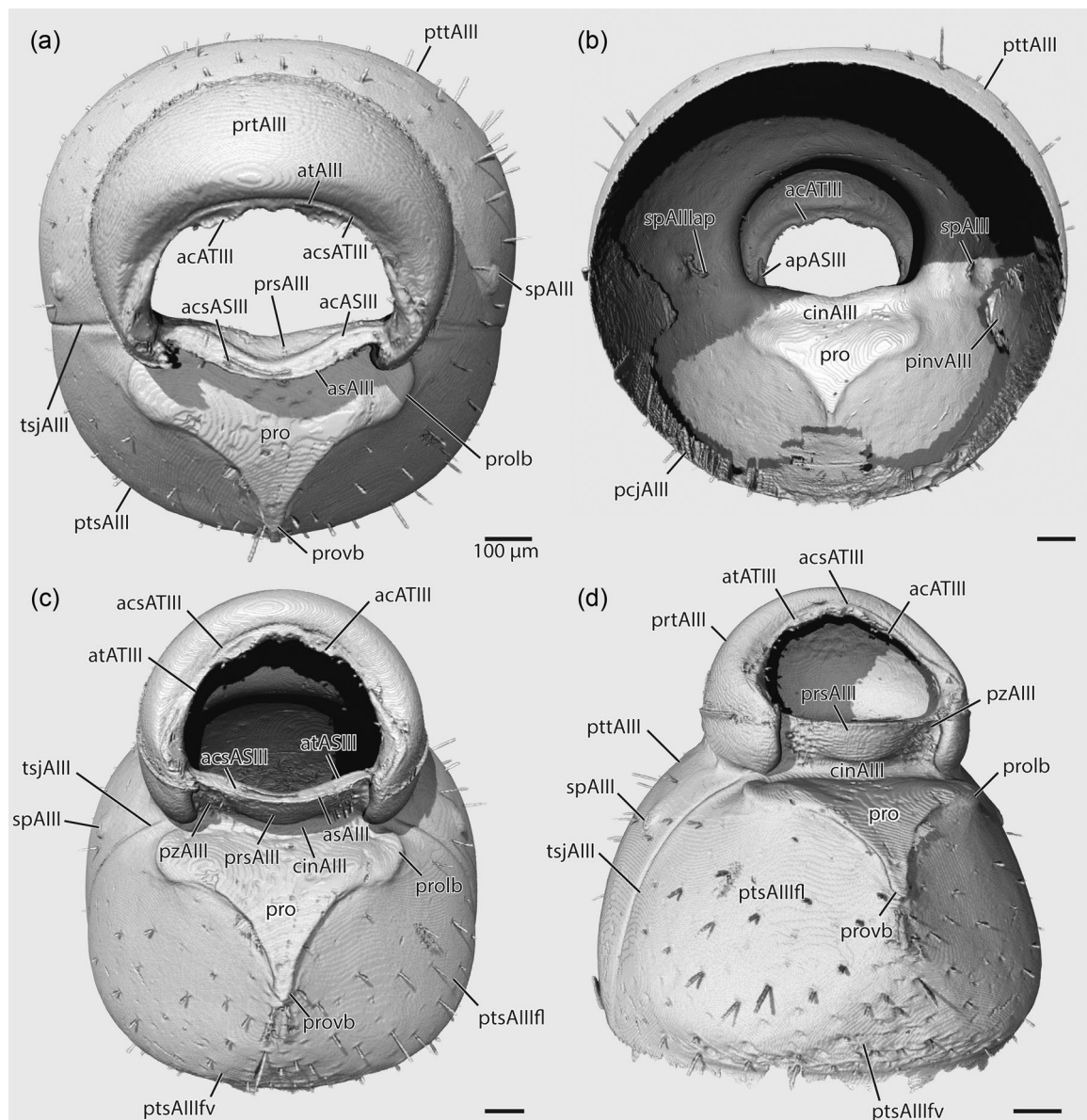
FIGURE 8 *Amblyopone australis*, skeleton of abdominal segments II–III and musculature of AII; 3D reconstruction, sagittal bisection, equivalent view, in (b) with 2domm hidden. Scale bar: 100 μm. A, abdominal segment; ac, antecosta; ap, anterolateral apodeme; cin, cinctus; dolm, dorsal ortholateral muscle; domm, dorsal orthomedial muscle; dvilm, dorsoventral intrinsic lateral muscle; igsf, intrasegmental fold; pinv, posterior (sclerotized) invagination; plp, petiolar levator process; pro, prora; prs2aa, anterior arc of the petiolar presternite; prs2aap, dorsal process of the anterior arc of the petiolar presternite; prt, pretergite; pts, poststernite; ptsap, posterolateral apodeme of the petiolar poststernite; ptsc, posterolateral apodeme of the petiolar poststernite; ptspl, posterior petiolar poststernite lip; ptt, posttergite; pz, proprioreceptive zone; sp, spiracle; spp, subpetiolar process; spp, subpetiolar process; sppli, lateral impression of the subpetiolar process

roughly rectangular and dorsally concave. In mesal view, the poststernite has a large longitudinal medial trough which is V-shaped in cross-section and is mostly occupied by the **first metasomal ganglion** (**gnmt1**, Figure 7d) and longitudinal **connectives** (**con**, Figure 7d) of the **ventral nerve cord** (**vnc**, Figure 7d); see also Section 3.5.4.

Anterad the anterolateral carinae, ATIII has fine scabrous sculpture, as does the entire subpetiolar process. Both regions bear denser, shorter setae than on the remaining tergite, these being appressed to erect (Figure 4d,e).

Muscles

Dorsal orthomedial muscles: (1) 2domm, *M. tergo-tergalis orthomedialis* (Figure 8a). **O**: Anterior and anterodorsal surfaces of the AII posttergite (petiolar node); **I**: anteromedially on ATIII antecosta (helcial tergite), flanking the midline. **F**: Very large, cuneate, posteriorly directed; coalesced as a single bundle anteriorly, inserting on a short bifurcation. **Dorsal paramedial muscles: (2) 2dpmm**, *M. tergo-tergalis paramedialis* (Figure 8b). **O**: Laterally on the dorsal surface of the AII posttergite (petiolar node); **I**: on the ventrolateral edges of the ATIII antecosta (helcial tergite), immediately laterad I:

FIGURE 9 *Amblyopone australis*, skeleton of abdominal segment III, 3D-reconstruction in (a) anterior view, (b) posterior view, (c) anteroventral view, (d) oblique anteroventral view. Scale bars: 100 µm. A abdominal segment; ac, antecosta; acs, antecostal sulcus; AS, abdominal sternite; as, acrosternite; AT, abdominal tergite; at, acrotergite; cin, cinctus; pcj, posterior conjunctiva; pinv, posterior (sclerotized) invagination; pro, prora; prolb, lateral boss of the prora; provb, lateral boss of the prora; prs presternite; prt, pretergite; pts, poststernite; ptsAIIIfl, lateral surface of the third poststernite (ASIII); ptsAIIIfv, ventromedial surface of the third poststernite (ASIII); ptt, posttergite; pz, proprioreceptive zone; sp, spiracle; spAIIIap, spiracular apodeme; tsj, tergosternal junction

2dlm1. **F**: Somewhat flat, ventrolaterally directed, tightly abutting 2dolm anteriorly and the posterior conjunctiva (intersegmental membrane) posteriorly. **Dorsal ortholateral muscles**: **(3) 2dolm**, *M. tergo-tergalis ortholateralis* (Figure 8b. **O**: Dorsolaterally on the anterior face of the AII posttergite (petiolar node), laterad O: 2domm, anterad O: 2dpmm; **I**: ventrolateral corners of the ATIII antecosta (helcial tergite). **F**: Large, broadly triangular, posteroventrally and laterally directed, with long narrow insertions. **Dorsoventral muscles**: **(4) 2dvilm**, *M. tergo-sternalis interior lateralis* (Figure 8b). **O**: Laterally on the anterior and anterolateral surfaces of the AII posttergite (petiolar node); **I**: on the posterolateral apodemes of the AII

poststernite. **F**: Flat, fan-shaped, posteroventrally directed. **Spiracular muscles** were not resolved in the present data set.

3.1.5 | AIII (M2)

Sclerites

The **third abdominal segment** is divided by a broad **cinctus** (**cinAIII**, Figures 8a and 9b,d) into the anterior presclerites, which are modified as an articular complex, and the posterior postsclerites. The **helcium** is a complex formed by the highly modified

presclerites; it is substantially smaller than the postsclerites; it is located supraaxially, that is, it mainly lies dorsad the **tergosternal junction** (**tsjAIII**, Figure 9a,c,d) of the postsclerites. The internal margins of the **helcial sclerites** are insensibly fused (Figure 10a); externally the **helcial tergite** overhangs the presternite completely (Figure 9d). The **helcial tergite** (**prtAIII**, Figures 8 and 9) is cuculiform (hood-shaped) in lateral view, with an overhanging anterodorsal margin; in anterior view, it is semicircular in shape, overlapping the presternite ventrolaterally (Figure 9a,c,d). Therefore, the **helcial sternite** (**prsAIII**, Figure 9) is only distinct anteromedially; in anterior view it is gently arcuate; in lateral view, it projects slightly below the pretergite ventrally. The **proprioreceptive zones of AIII** (**pzAIII**, Figure 9c,d) are the concavities formed where the pretergite overhangs the presternite ventrolaterally; these zones bear short, erect setae, which are notably shorter and denser than those of the postsclerites. The **antecostal sulcus of ATIII** (**acsATIII**, Figure 9) is distinct, and divides the narrow **acrotergite** (**atAIII**, Figure 9) from the posterior **antecosta** (**acATIII**, Figures 8–10a); the **antecostal sulcus of ASIII** (**acsASIII**, Figure 9) is shallow, but the **acrosternite** (**asAIII**, Figure 9a,c) is still differentiable as the poorly developed, narrow carina on the anterior presternital margin. **Anterolateral apodemes of presternite AIII** (**apASIII**, Figures 8–10a) are developed, while those of tergite AIII are absent, similar to AII; the apodemes are modified in form, being quite small and digitate, and running closely along the ventrolateral pretergite (Figure 9b); uniquely to AIII, these apodemes lack any muscle attachment, and thus may be vestigial. The **helcial cinctus** (**cinAIII**, Figures 8 and 9c,d) is a transverse sulcus that separates the presclerites and postsclerites; it rings the segment completely; it is margined anteriorly by a carina which curves posteriorly ventrad the level of the spiracle, but not near the tergosternal junction; the cinctus is deep and cross-ribbed by carinulae externally; internally it is not musculated.

The **third abdominal posttergite** (**pttAIII**, Figures 8 and 9) is sutured immovably to the **third abdominal poststernite** (**ptsAIII**, Figures 8 and 9); both postsclerites are large and bulbous, but otherwise relatively unmodified in shape. The **prora** (**pro**, Figures 8 and 9) is a cuticular outgrowth and thickening that is developed anteriorly on the third poststernite; in frontal view, it is broadly cordate, with the margin of the raised **anterolateral bosses** (**prolb**, Figure 9a,c,d) narrowly tapering ventromedially to their posteroventral apex, the raised **ventromedial boss** (**provb**, Figure 9a,c,d); internally the prora lacks a lumen, although it does form a concavity (Figure 9b); at its widest point it exceeds the width of the presternite. The poststernite is differentiable into three slightly flattened surfaces, structured by the prora: two **lateral surfaces** (**ptsAIIIfl**, Figure 9c,d) delineated medially by the lateral margins of the prora; and a single **ventromedial surface** (**ptsAIIIfv**, Figure 9c,d), which is approximately triangular, and delimited anteriorly by the ventral boss of the prora.

The **third abdominal spiracles** (**spAIII**, Figures 8 and 9) are round and borne on low, subcircular cuticular prominences; they are laterally directed and anteriorly oriented; they are situated above the tergosternal suture by a little more than once the diameter of the spiracular prominence diameter, and posterior from the presternite by a little more than twice such a diameter.

The **third abdominal posterior invaginations** (**pinvAIII**, Figures 8 and 9b) connect to the **posterior conjunctiva** (**pcjAIII**, Figures 8 and 9b), are partially sclerotized, and form roughly digitate, anteriorly projecting cuticular thickenings as the level of the tergosternal junction. The **intrasegmental folds** (**igsfASIII**, Figures 8 and 10a) are quite large and well-sclerotized.

The prora bears dense, subdecumbent to erect setae which are somewhat shorter and coarser than those of the remaining segment.

Muscles (Figure 10)

Dorsal orthomedial muscles: (1) **3domm**, *M. tergo-tergalis orthomedialis*. O: Dorsomedially on the ATIII antecosta (helcial tergite); I: anteromedially on the AIV acrotergite. F: Elongate, spindle-shaped, anteroposteriorly oriented; coalesced anteriorly at a single origin, diverging posteriorly to several insertion points. **Dorsal paramedial muscles**: (2) **3dpmm**, *M. tergo-tergalis paramedialis*. O: Dorsolaterally on the posterior ATIII posttergite, partially within the intrasegmental fold; I: on the dorsal surface of the ATIV apodemes. F: Large, flat, broadly triangular, anteroventrally and laterally directed, inserting broadly on the entire dorsal apodemal surface. **Dorsal ortholateral muscles**: (3) **3dolm**, *M. tergo-tergalis ortholateralis*. O: Dorsolaterally on the ATIII antecosta (helcial tergite); I: medially on the ATIV antecosta, at the base of the ATIV apodemes. F: Large, elongate-triangular, ventrolaterally directed, with long insertions. **Ventral paramedial muscles**: (4) **3vpmm**, *M. sterno-sternalis paramedialis*. O: Ventrolaterally on the posterior AIII poststernite, partially within the intrasegmental fold; I: on the ventral and ectal surfaces of the ASIV apodemes. F: Large, flat, and broadly triangular; anterodorsally and medially directed. **Ventral ortholateral muscles**: (5) **3volm**, *M. sterno-sternalis ortholateralis*. O: At the midline on the posterior poststernite; I: apicomesally on the anteroventral apices of the ASIV apodemes, anteromediad the most anterior I: 3vpmm. F: Slender, filiform, dorsolaterally directed. **Spiracular muscles** were not resolved in the present data set.

3.1.6 | AIV (M3)

Sclerites

The **fourth abdominal tergite** and **sternite** are fused for the length of the entire segment. The **fourth abdominal antecostae** (**acATIV**, **acASIV**, Figures 10 and 11b,d) are strongly inflexed and fused, forming a distinct continuous rim in internal view; the **fourth abdominal acrotergite** (**atAIV** Figures 10 and 11b) and **acrosternite** (**asAIV**, Figures 10 and 11b) are well-developed and divided from the antecostae by the **antecostal sulci** (**acsASIV**, Figure 10a); they continue as anterior carinae on the anterolateral apodemes of the
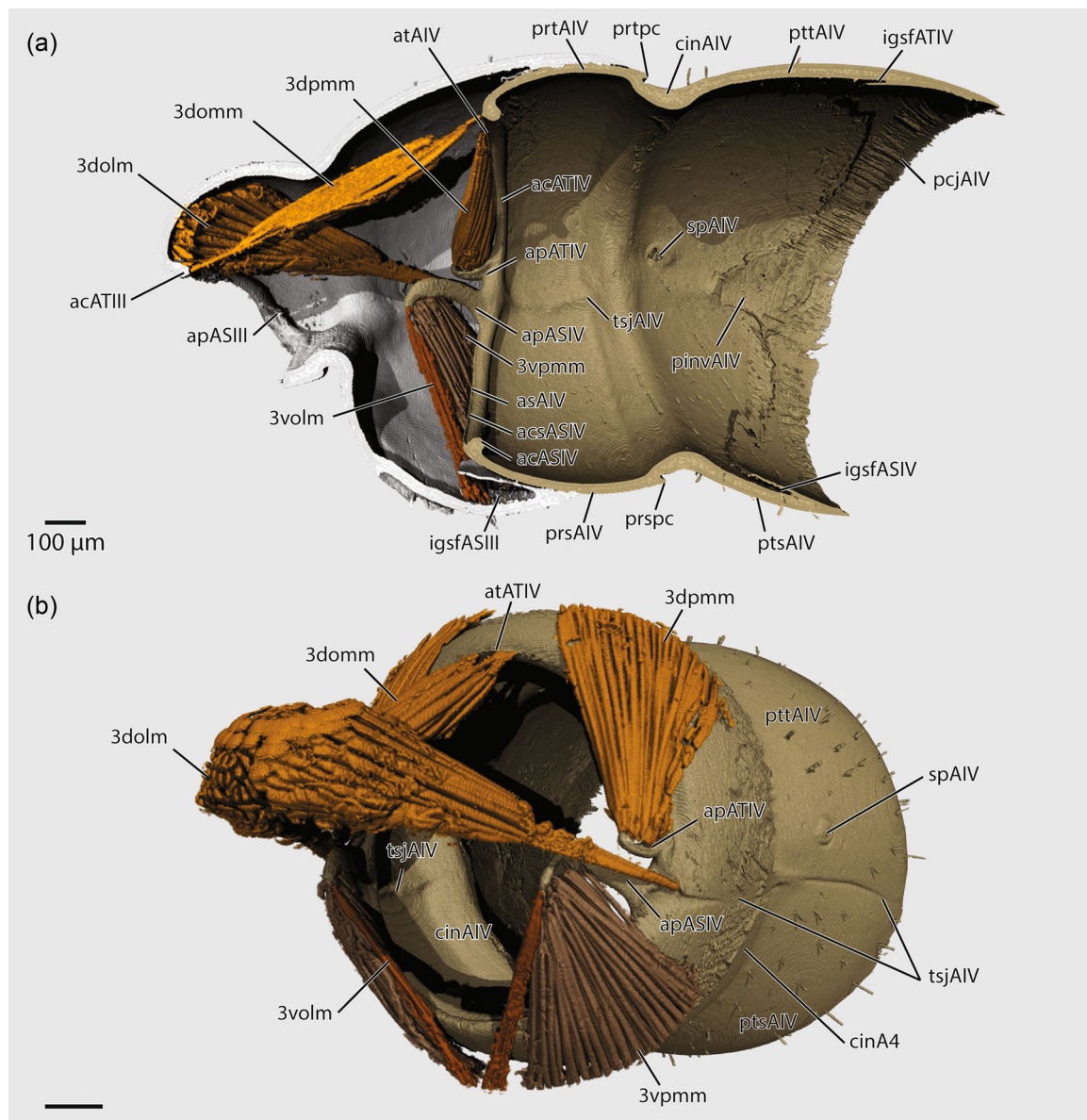
FIGURE 10 *Amblyopone australis*, skeleton of abdominal segments III–IV and musculature of AIII, 3D reconstruction in (a) sagittal bisection and (b) oblique anterior view, AIII hidden. Scale bars: 100 μm. A, abdominal segment; ac, antecosta; ap, anterolateral apodeme; AS, abdominal sternite; as, acrosternite; AT, abdominal tergite; at, acrotergite; cin, cinctus; dolm, dorsal ortholateral muscle; domm, dorsal orthomedial muscle; dpmm, dorsal paramedial muscle; igsf, intrasegmental fold; pcj, posterior conjunctiva; pinv, posterior (sclerotized) invagination; prscp, dorsal process of the anterior arc of the petiolar presternite; prscp, dorsal process of the anterior arc of the petiolar presternite; prt, pretergite; prtpc, posterior carina of the fourth pretergite (ATIV); pts, poststernite; ptt, posttergite; sp, spiracle; tsj, tergosternal junction; volm, ventral ortholateral muscle; vpmm, ventral paramedial muscle

tergite and sternite. The **fourth abdominal cincti** (**cinAIV**, Figures 10 and 11a) of the tergum and sternum are continuous with one another, forming a wide, transverse sulcus that divides the pre- and postsclerites; the cinctus is cross-ribbed, that is, with scrobiculate sculpture (Figure 11a); the internal ridge of the cinctus is not musculated (Figures 10a and 11b). The **fourth abdominal presclerites** (**prtAIV**, **prsAIV**, Figures 10a and 11a) are slightly smaller in diameter relative to the postsclerites; they are aligned along their length, rather than having the pretergite overhanging the presternite laterally as in AIII; in lateral view, their lateral tergosternal margin is nearly evenly

concave (Figure 11a); they are delimited posteriorly by the **posterior carinae of the fourth abdominal pretergite** (**prtpc**) and **presternite** (**prspc**, Figures 10a and 11a,b), which border the cincti anteriorly. Immediately dorsad the **tergosternal junction** (**tsjAIV**, Figures 10 and 11a), at the external interface of the pre- and postsclerites is a longitudinally oriented strip of sclerite, which forms a narrow **cuticular band of the pretergite** (**prtcb**, Figures 1d and 11a) which extends from the posterior carina to the anterior pretergite, forming a bridge across the cinctus. Both presclerites bear large anterolateral apodemes. The **anterolateral apodemes of ATIV** (**apATIV**, Figures 10

and 11a,b) arise from the ventralmost point of the pretergite; they are falcate, upcurved, and approximately porrect; they are shorter than the sternal apodemes (about ½ the length). The **anterolateral apodemes of ASIV (apASIV**, Figures 10 and 11a,b) are large, falcate, downcurved, and additionally bend inward, such that their apices are medial to both their own bases, and the tergal apodemes (Figure 10b).

Posterad the cinctus, the postsclerites are basically unmodified, besides being tergosternally fused. The **fourth abdominal posttergite (pttAIV**, Figures 10 and 11a,b) is slightly longer than the **fourth abdominal poststernite (ptsAIV**, Figures 10 and 11a,b). The **fourth abdominal spiracles (spAIV**,

Figures 10 and 11a) are located posterad the tergal cinctus and are separated from the pretergital carina by about four of their own maximum diameters, and from the tergosternal margin by about two of their own maximum diameters. The spiracles are small, elliptical and are borne on low discs, which are scarcely raised above the surface of the surrounding tergite; the spiracular apodeme was not resolved but may be present. As in AIII, the **fourth abdominal posterior invaginations (pinvAIV**, Figure 10a) form lateral digitate sclerotized thickenings at the tergosternal junction which connect to the well-developed posterior conjunctiva (**pcjAIV**, Figure 10a).
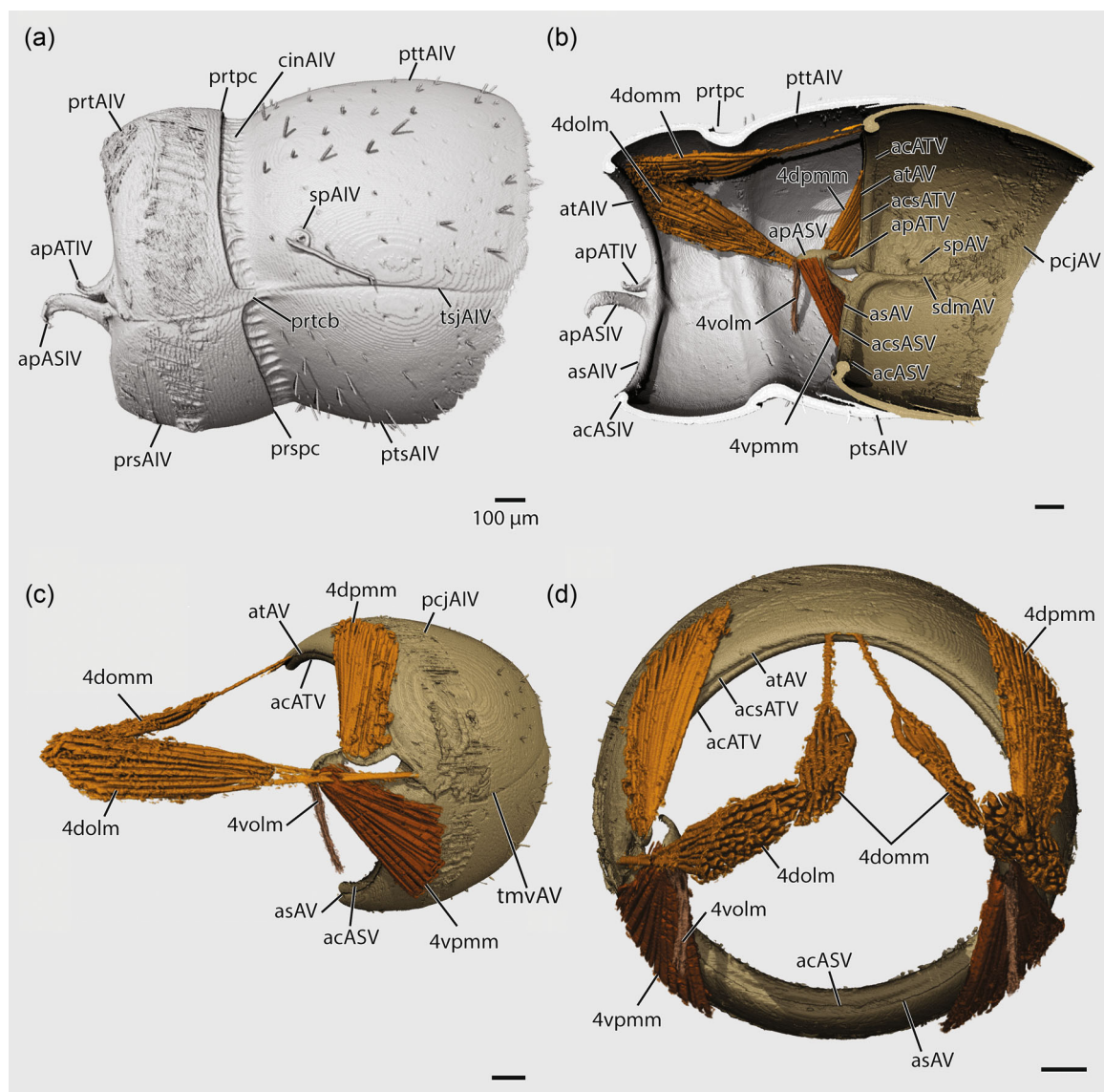
FIGURE 11 *Amblyopone australis*, skeleton of abdominal segments IV–V and musculature of AIV, 3D-reconstruction, in (a) external lateral view, AV hidden, (b) sagittal bisection, (c) oblique ectal view, AIV hidden, (d) anterior view, AIV hidden. Scale bars: 100 μm. ac, antecosta; ap, anterolateral apodeme; as, acrosternite; at, acrotergite; cin, cinctus; dolm, dorsal ortholateral muscle; domm, dorsal orthomedial muscle; pcj, posterior conjunctiva; prs, presternite; prspc, posterior carina of the fourth presternite; prt, pretergite; prtcb, cuticular band of the fourth pretergite (ATIV); prtpc, posterior carina of the fourth pretergite (ATIV); pts, poststernite; ptt, posttergite; sdm, dorsolateral sternal margination; sp, spiracle; tmv, ventral margin of the tergite; tsj, tergosternal junction; volm, ventral ortholateral muscle; vpmm, ventral paramedial muscle
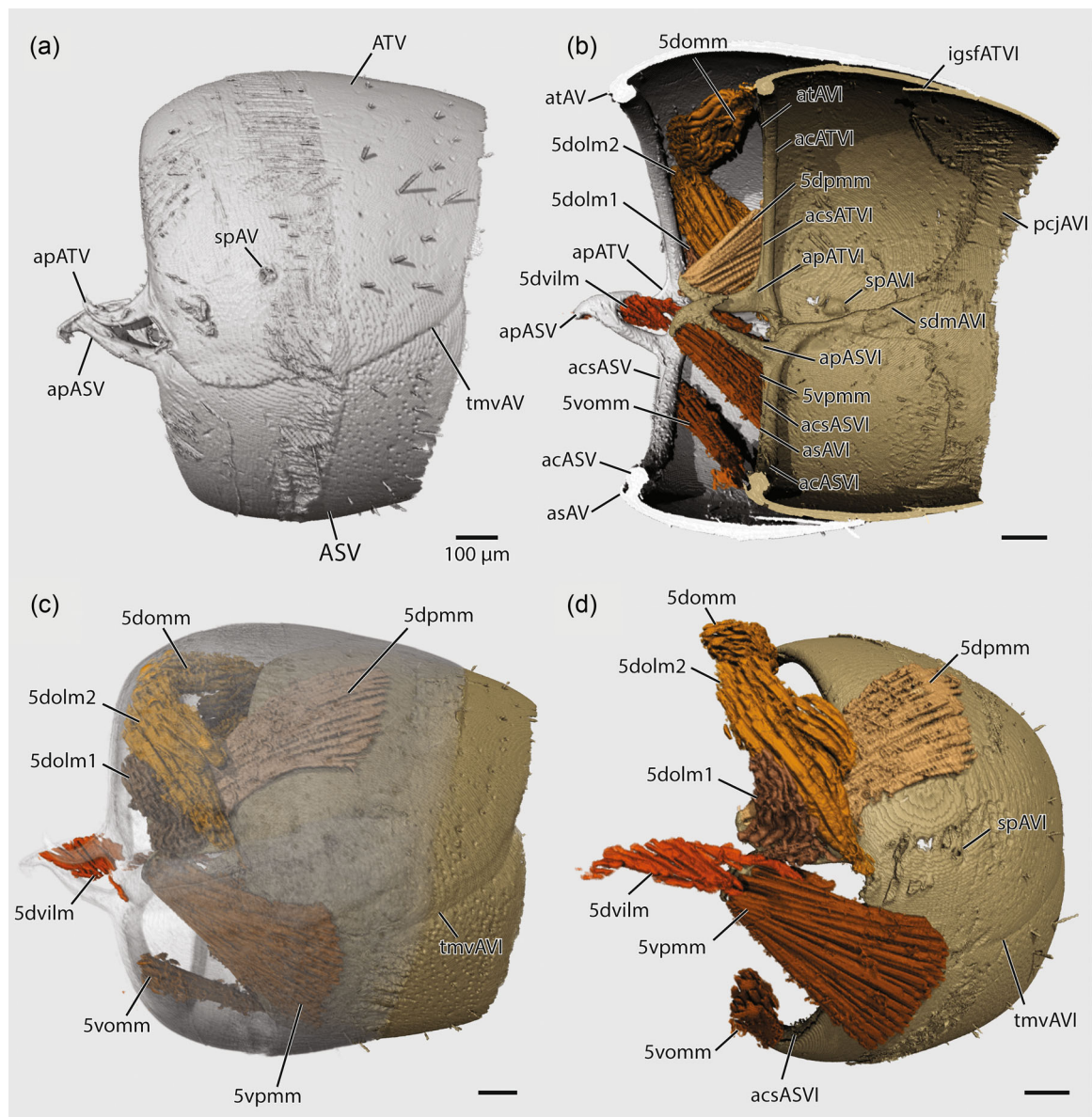
FIGURE 12 *Amblyopone australis*, skeleton of abdominal segments V–VI and musculature of AV, 3D reconstruction in (a) external lateral view, AVI hidden, (b) sagittal bisection, (c) external lateral view, AV translucent, (d) oblique ectal view, AV hidden. Note that the apparent hole just anterad the sixth spiracle is an artifact; the surface of this region is closed and continuous. Scale bars: 100 μm. A, abdominal segment; ac, antecosta; acs, antecostal sulcus; ap, anterolateral apodeme; AS, abdominal sternite; as, acrosternite; as, acrosternite; AT, abdominal tergite; at, acrotergite; at, acrotergite; dolm, dorsal ortholateral muscle; domm, dorsal orthomedial muscle; dpmm, dorsal paramedial muscle; dvilm, dorsoventral intrinsic lateral muscle; igsf, intrasegmental fold; pcj, posterior conjunctiva; sdm, dorsolateral sternal margination; sp, spiracle; tmv, ventral margin of the tergite; vomm, ventral orthomedial muscle; vpmm, ventral paramedial muscle

Muscles (Figure 11b–d)

Dorsal orthomedial muscles: **(1) 4domm**, *M. tergo-tergalis orthomedialis*.**O**: Dorsomedially on the ATIV antecosta, flanking the midline; **I**: anteromedially on the AV acrotergite. **F**: Elongate, spindle-shaped, posteromedially oriented, with very long narrow insertions. **Dorsal paramedial muscles**: **(2) 4dpmm**, *M. tergo-tergalis paramedialis*. **O**: Dorsolaterally on the posterior AIV posttergite, partially within the intrasegmental fold; **I**: on the dorsal surface and partially the ectal surface of the ATV anterolateral apodemes. **F**: Large, flat, broadly triangular, anteroventrally and laterally directed, inserting broadly on

the entire dorsal apodemal surface. **Dorsal ortholateral muscles**: **(3) 4dolm**, *M. tergo-tergalis ortholateralis*. **O**: Dorsolaterally on the ATIV antecosta, ventrolaterad O: 4domm; **I**: on the ATV antecosta, at the base of the ATV anterolateral apodemes. **F**: Elongate-triangular, posteroventrally and laterally directed, with long slender insertions. **Ventral paramedial muscles**: **(4) 4vpmm**, *M. sterno-sternalis paramedialis*. **O**: Ventrolaterally on the posterior AIV poststernite, partially within the intrasegmental fold; **I**: on the ventral, ectal, and mesal surfaces of the anterior process of the ASIV anterolateral apodemes. **F**: Large, flat, broadly triangular; insertions wrapping

around the malleate apodemal process. **Ventral ortholateral muscles**: **(5) 4volm**, *M. sterno-sternalis ortholateralis*. **O**: Ventrolaterally on the AIV poststernite, just posterad the cinctus, at around 1/3rd the height of the sternite in lateral view; **I**: on the apices of the ASV anterolateral apodemes. **F**: Small, slender, filiform, dorsomedially directed.

3.2 | Posterior pregenital abdomen

3.2.1 | AV (M4)

Sclerites

The fifth abdominal segment lacks a cinctus. Overall, the segment is roughly barrel-shaped; its anterior margin in lateral view is not concave, but subvertical, with the tergite projecting slightly anterad the sternite. The **fifth abdominal tergite** (**ATV**) and **sternite** (**ASV**, Figure 12a) are unfused and subequal in anteroposterior length; the **ventral margin of the tergite** (**tmvAV**, Figures 11c and 12a) overhangs the sternite ectally. The **fifth abdominal acrotergite** (**atAV**, Figures 11b–d and 12b) and **acrosternite** (**asAV**, Figures 11b–d and 12b) are somewhat more developed than those of AIV and are delimited by deeper **antecostal sulci** (**acsATV**, Figures 11d; **acsASV**, 11b and 12b). The **fifth abdominal antecostae** (**acATV**, Figures 11b–d and 12b; **acASV**, 11b–d and 12b) are also somewhat more robust than those of the preceding segment; they are unfused at their bases (Figure 11b). The **anterolateral apodemes of ATV** (**apATV**, Figures 11b–d and 12a–c) are falcate, upcurved, and porrect; they arise laterad those of the sternite (Figure 12a). The **anterolateral apodemes of ASV** (**apASV**, Figures 11b–d and 12a–c) are large, upcurved, and malleate. The malleate process has a thin dorsal flange, which has a convex dorsal profile in lateral view, and concave lateral surfaces. The **dorsal margin of the sternite** is strongly carinate, with the **dorsolateral sternal margination** (**sdm**, Figure 11b) continuing from the antecosta of ASV. The **fifth abdominal spiracles** (**spAV**, Figures 11b and 12a,b) are small and located on the glabrous anterior contact surface of the tergum; they are therefore usually concealed; the intraspiracular apodeme was not resolved but is likely to be present. The **posterior conjunctiva** (**pcjAV**, Figure 11b) is somewhat anteriorly prolonged around the tergosternal junction, but is not produced into distinctly sclerotized posterior invaginations as in AIII and AIV.

Muscles (Figures 12b–d and 13)

Dorsal orthomedial muscles: **(1) 5domm**, *M. tergo-tergalis orthomedialis*. **O**: Dorsolaterally on the anterior surface of ATV, just posterad the antecosta; **I**: anteromedially on the AVI acrotergite. **F**: Moderately sized; posteriorly and strongly medially directed. **Dorsal paramedial muscles**: **(2) 5dpmm**, *M. tergo-tergalis paramedialis*. **O**: Dorsolaterally on the posterior AV tergite, partially within the intrasegmental fold; **I**: on the dorsal and ectal faces of the ATVI anterolateral apodemes. **F**: Large, flat, broadly triangular, anteroventrally directed. **Dorsal ortholateral muscles**: **(3) 5dolm1**, *M. tergo-tergalis ortholateralis minor*.

O: Ventrolaterally on the anterior surface of ATV, immediately posterad the antecosta, ventrad **O**: 5dolm2; **I**: ectally on the base of the ATVI anterolateral apodemes, anterad **I**: 5dpmm. **F**: Small, cuneate, posteroventrally directed; possibly a subdivision of 5dolm2. **(4) 5dolm2**, *M. tergo-tergalis ortholateralis major*. **O**: Anterolaterally on the anterior surface of ATV, on and immediately posterad the antecosta, ventrolaterad **O**: 5domm; **I**: on the base of the ATVI anterolateral apodemes, laterad **I**: 5dpmm. **F**: Broadly triangular, posteroventrally directed. **Dorsoventral muscles**: **(5) 5dvilm**, *M. tergo-sternalis interior lateralis*. **O**: Mesally on the base of the ATV anterolateral apodemes; **I**: ectally on the anterior process of the ASV anterolateral apodemes. **F**: Very small, asymmetrically fan-shaped, anteromedially directed. **Ventral orthomedial muscles**: **(6) 5vomm**, *M. sterno-sternalis orthomedialis*. **O**: Laterally on the ASV antecosta; **I**: medially on the AVI acrosternite. **F**: Somewhat small, roughly triangular, posteriorly and strongly medially directed. **Ventral paramedial muscles**: **(7) 5vpmm**, *M. sterno-sternalis paramedialis*. **O**: Ventrolaterally on the posterior AV sternite, partially within the intrasegmental fold; **I**: on the ectal and ventral surfaces, and the anterior apex, of the apical process of the ASVI anterolateral apodemes. **F**: Large, flat, broadly triangular; anterodorsally and slightly medially directed; insertions wrapping around the malleate apodemal process. **Intraspiracular occlusor muscles** (*M. occlusor spiraculi*) present.

3.2.2 | AVI (M5)

Sclerites

The sixth abdominal segment is similar to AV in all aspects of gross morphology (Figures 12a and 14a), with the following exceptions: the
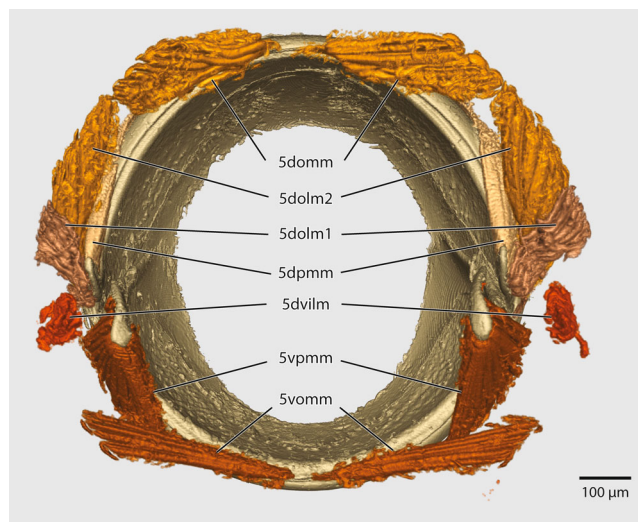
FIGURE 13 *Amblyopone australis*, musculature of abdominal segment V, 3D reconstruction, anterior view. Scale bar: 100 μm. dolm, dorsal ortholateral muscle; domm, dorsal orthomedial muscle; dvilm, dorsoventral intrinsic lateral muscle; vomm, ventral orthomedial muscle; vpmm, ventral paramedial muscle

segment is anteroposteriorly shorter; both the tergal and sternal **anterolateral apodemes** (**apATVI**, **apASVI**, Figures 12b and 14) are larger, and the tergal apodemes are longer relative to those of the sternite, being subequal in length; the dorsal surfaces of the apical processes of the anterolateral sternal apodemes are more poster-odorsally slanted in lateral view, that is, the anterior apices of the malleate processes are directed more ventrally than in AV (Figure 14a). Otherwise, AVI shares the following features with AV: the segment is short barrel-shaped, the **sixth abdominal tergite** (**ATVI**) and **sternite** (**ASVI**, Figure 14a) are unfused and subequal in length; the **ventral margin of the tergite** (**tmvAVI**, Figures 12c,d and 14a) overhangs the sternite laterally; the **dorsolateral sternal margination** (**sdmAVI**, Figure 12b) is well-developed and continuous with the sternal antecosta; the **acrotergite** (**atAVI**) and **acrosternite** (**asAVI**, Figures 12b and 14b), are well-developed with relatively broad **antecostal sulci** (**acsATVI**; Figure 12b; **acsASVI**, 12b,d) cincti are absent; the **sixth abdominal spiracles** (**spAVI**, Figures 12b,d and 14a) are small and located on the glabrous anterior contact surface of the tergite, thus usually concealed; the intraspiracular apodeme was not resolved, but is likely to be present; and the **posterior conjunctiva** (**pcjAVI**, Figure 12b) is somewhat anteriorly prolonged around the tergosternal junction, but is not produced into distinctly sclerotized posterior invaginations.

Muscles (Figure 14b–d)

Dorsal orthomedial muscles: **(1) 6domm**, *M. tergo-tergalis orthomedialis* **O**: Dorsolaterally on the anterior surface of ATVI, slightly removed from the antecosta; **I**: anteromedially on the AVII acrotergite. **F**: Moderately sized; posteriorly and strongly medially directed. **Dorsal paramedial muscles**: **(2) 6dpmm**, *M. tergo-tergalis paramedialis*. **O**: Dorsolaterally on the posterior AVI tergite, within the intrasegmental fold; **I**: dorsally, ectally, and apically on the ATVII anterolateral apodemes. **F**: Large, flat, broadly triangular; anteroventrally and slightly medially directed, with extensive insertion area. **Dorsal ortholateral muscles**: **(3) 6dolm1**, *M. tergo-tergalis ortholateralis minor*. **O**: Anterolaterally on the anterior surface of ATVI, immediately posterad the antecosta, ventrad O: 6dolm2; **I**: ectally on the base of the ATVII anterolateral apodemes, anteroventrad I: 6dolm2. **F**: Small, cuneate, posteroventrally directed; possibly a subdivision of 6dolm2. **(4) 6dolm2**, *M. tergo-tergalis ortholateralis major*. **O**: Dorsolaterally on the anterior surface of ATVI, on and immediately posterad the antecosta, ventrolaterad O: 6domm; **I**: ectally on the base of the ATVII anterolateral apodemes, posterodorsad I: 6dolm1. **F**: Broadly triangular, posteroventrally directed; running partially laterad 6dolm1 and mediad 6dvxm. **Dorsoventral muscles**: **(5) 6dvilm**, *M. tergo-sternalis interior lateralis*. **O**: Mesally on the base of the ATVI anterolateral apodeme, laterad 6volm; **I**: ectally on the apical processes of the ASVI anterolateral apodemes. **F**: Very small, asymmetrically fan-shaped; anteromedially directed. **(6) 6dvxm**, *M. tergo-sternalis exterior (paramedialis)*. **O**: Laterally on the posterior AVI tergite, just posterad I: 6dolm2, very slightly dorsad the spiracle; **I**: ectally on the basal crest of the ASVII anterolateral apodemes. **F**: Small, flat, ribbon-like, ventromedially directed; note that these muscles were poorly resolved in micro-CT and may be partially damaged. **Ventral**

orthomedial muscles: **(7) 6vomm**, *M. sterno-sternalis orthomedialis*. **O**: Laterally on the ASVI antecosta; **I**: anteromedially on the AVII acrosternite, at the very midline. **F**: Somewhat flat, posteroventrally and strongly medially directed; insertions immediately adjacent or coincident. **Ventral paramedial muscles**: **(8) 6vpmm**, *M. sterno-sternalis paramedialis*. **O**: Ventrolaterally on the posterior AVI sternite, within the intrasegmental fold; **I**: ectally, ventrally, and apically on the apical processes of the ASVII anterolateral apodemes. **F**: Large, flat, broadly triangular; anterodorsally and slightly medially directed, insertions wrapping around the malleate apodemal process. **Ventral ortholateral muscles**: **(9) 6volm**, *M. sterno-sternalis ortholateralis*. **O**: Mesally on the base of the ASVI anterolateral apodeme; **I**: ectally on the apical processes of the ASVII anterolateral apodemes. **F**: Small, slender, ribbonlike, medially directed. **Intraspiracular occlusor muscles** (*M. occlusor spiraculi*) present.

3.2.3 | AVII (M6)

Sclerites

Abdominal segment VII is the terminal external segment; overall, it is roughly cone-shaped, tapering apically to the **external apex of the abdomen** (**abdx**, Figure 15a); it lacks a cinctus. The **seventh abdominal tergite** (**ATVII**) is larger than the sternite (**ASVII**; Figure 15a); the **ventral margin of the tergite** (**tmvAVII**, Figure 15a) overhangs the sternite ectally for the length of the entire segment; the profile of the ventral margin of the tergite is sinuate in lateral view, such that anterior area of the tergite is laterally lobate and deeper than the posterior half. Both pairs of **anterolateral apodemes of AVII** are relatively large compared to those of prior segments; the **anterolateral apodemes of ATVII** (**apATVII**, Figures 14b and 15a,b) are large, falcate, upcurved, and have the mesal surfaces somewhat impressed laterally; the **anterolateral apodemes of ASVII** (**apASVII**, Figures 14b and 15a,b) are slightly longer than those of the tergite and are notably wider than the sternal apodemes of preceding segments; their malleate apices are broader than those of ASV and ASVI; the **antecosta of ATVII** (**acATVII**, Figures 14b and 15b) is well-developed and continues onto the dorsal edge of the anterolateral tergal apodeme; its **antecostal sulcus** (**acsATVII**, Figure 15b) is quite narrow but still differentiates the thin **acrotergite** (**atATVII**, Figure 15b); the **antecostal sulcus of ASVII** (**acsASVII**, Figures 14b and 15b) is also shallow, but broader than that of the tergite, and the **acrosternite** (**asAVII**, Figures 14b and 15b) is more distinct than the acrotergite; the **antecosta of ASVII** (**acASVII**, Figures 14b and 15b) continues strongly onto the anteroventral edge of the anterolateral apodeme; posteriorly, the posterodorsal edge, where the apodeme enters the segmental lumen, has a strongly developed **basal crest** (**apbc**, Figure 14b); immediately posterad the basal crest, the profile of the strongly carinate **dorsolateral sternal margination** (**sdmAVII**, Figure 14b) curves dramatically, forming a distinct **posterodorsal angle** (**spda**, Figure 14b) and becoming more or less horizontal posteriorly. It is possible that this carina is in fact part of the antecosta, rather than the dorsolateral sternal margination, or that
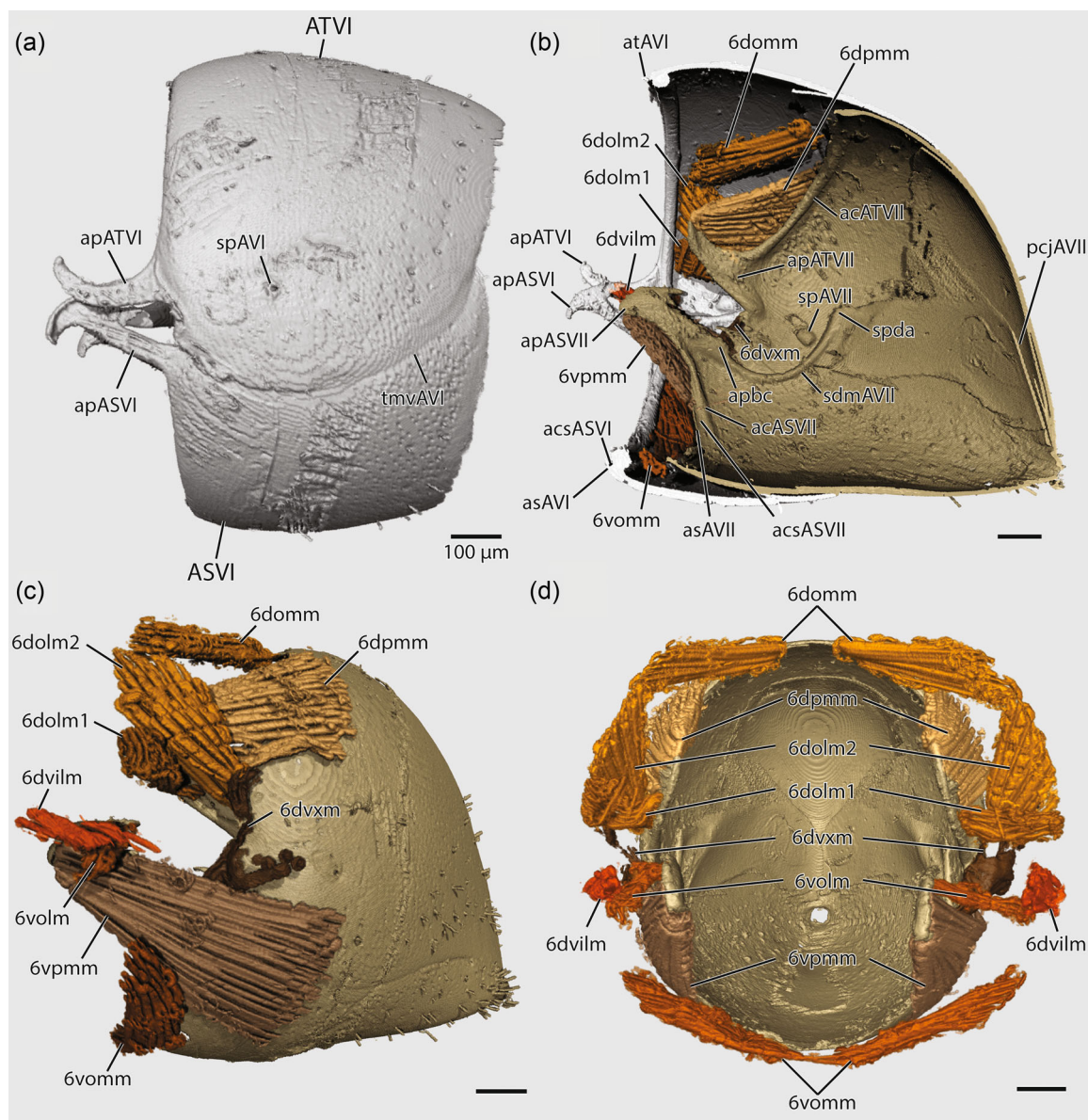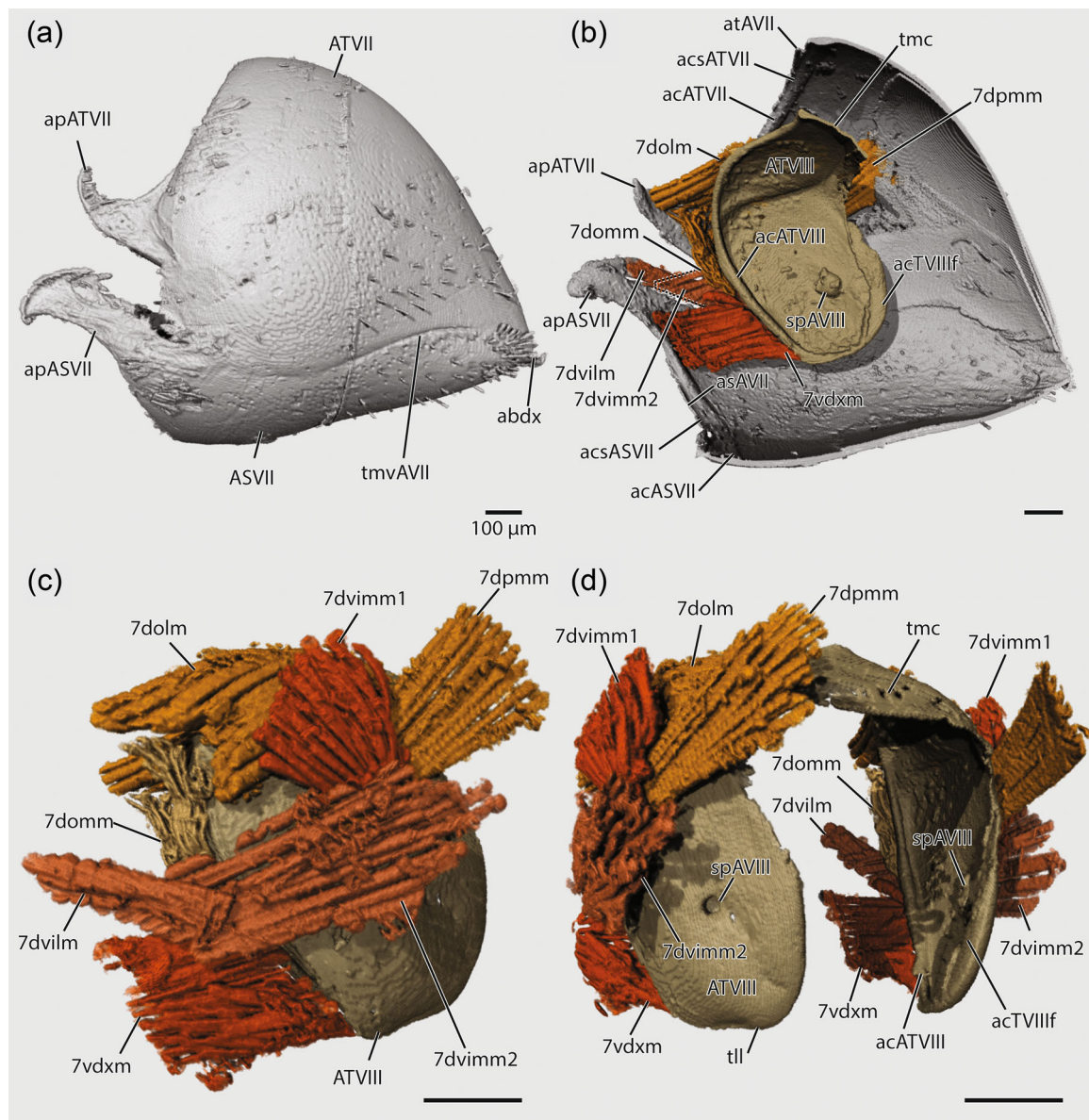
FIGURE 14 *Amblyopone australis*, skeleton of abdominal segments VI–VII and musculature of AVI, 3D reconstruction in (a) external lateral view, AVII hidden, (b) sagittal bisection, (c) ectal view, AVI hidden, (d) anterior view, AVI hidden. Scale bars: 100 µm. A, abdominal segment; acs, antecostal sulcus; ap, anterolateral apodeme; apbc, basal crest of the anterolateral sternal apodeme of AVII; AS, abdominal sternite; as, acrosternite; AT, abdominal tergite; at, acrotergite; dolm, dorsal ortholateral muscle; domm dorsal orthomedial muscle; dpmm, dorsal paramedial muscle; dvilm, dorsoventral intrinsic lateral muscle; dvxm, dorsoventral extrinsic (paramedial) muscle; igsf, intrasegmental fold; pcj, posterior conjunctiva; sdm, dorsolateral sternal margination; sp, spiracle; tmv, ventral margin of the tergite; volm, ventral ortholateral muscle; vomm, ventral orthomedial muscle; vpmm, ventral paramedial muscle

the sternal margination is itself antecostal; however, a landmark delimiting these two carinae is absent. The **posterior conjunctiva** (**pcjAVII**, Figure 14b) of both tergum and sternum are highly developed and tightly associated with the membranous remnants of AVIII (i.e., those parts not belonging to the eighth tergite or appendages), forming a chamber which encloses the sting apparatus. The **seventh abdominal spiracles** (**spAVII**, Figure 14b) are small and situated in the anterior third of the tergite, slightly ventrad the level of the base of the anterolateral apodeme of ATVII; the spiracular apodeme was not resolved but may be present.

Muscles (Figure 15b–d)

Dorsal orthomedial muscles: (1) 7domm, *M. tergo-tergalis orthomedialis*. O: Mesally on the ATVII anterolateral apodemes, from around the longitudinal midpoint to the base, mediad O: 7dlm1; **I**: anteroventrally on the ATVIII antecosta leading edge. **F**: Small and ribbonlike but robust; posteriorly directed. **Dorsal paramedial muscles: (2) 7dpmm**, *M. tergo-tergalis paramedialis*. **O**: Dorsolaterally on the posterior AVII tergite, within the large intrasegmental fold; **I**: ectally on the ventrolateral part of ATVIII, dorsad the antecosta, anterad the spiracles. **F**: Flat, broadly triangular, anteroventrally

FIGURE 15 *Amblyopone australis*, skeletomusculature of abdominal segment AVII and skeleton of ATVIII, 3D reconstruction in (a) external lateral view, (b) sagittal bisection, (c) ectal view, AVII hidden, (d) oblique posterior view, AVII hidden. Scale bars: 100 μm. abdx, external apex of the abdomen; ac, antecosta; acs, antecostal sulcus; acs, antecostal sulcus; acTVIIIf, antecostal flange of ATVIII; ap, anterolateral apodeme; AS, abdominal sternite; as, acrosternite; AT, abdominal tergite; at, acrotergite; dolm, dorsal ortholateral muscle; domm, dorsal orthomedial muscle; dpmm, dorsal paramedial muscle; dvilm, dorsoventral intrinsic lateral muscle; dvimm, dorsoventral intrinsic medial muscle; sp, spiracle; tll, lateral lobes of ATVIII; tmc, medial connection of ATVIII; tmv, ventral margin of the tergite; vdxm, ventrodorsal extrinsic muscle

directed; somewhat smaller and originating further anteriorly on the tergite relative to the dorsal paramedials of the prior segments. **Dorsal ortholateral muscles**: **(3) 7dolm**, M. *tergo-tergalis ortholateralis*. **O**: Dorsally and partly mesally on the ASVII anterolateral apodemes; **I**: dorsomedially on the dorsal surface of ATVIII, flanking the subrectangular medial connection. **F**: Large, broad, flat, subrectangular; posterodorsally and medially directed. **Dorsoventral muscles**: **(4) 7dvimm1**, M. *tergo-sternalis interior anteromedialis*. **O**: Laterally on the ATVII antecosta, posterodorsad the bases of the anterolateral apodemes; **I**: on the posterodorsal angle of the AVII sternite, immediately mesad O: 7dvimm2. **F**: Flat, broadly

triangular, posteroventrally directed. **(5) 7dvimm2**, M. *tergo-sternalis interior posteromedialis*. **O**: Laterally on the posterior AVII tergite, around the posterodorsal angle of the sternite, laterad I: 7dvimm1; **I**: dorsally on the dorsal carina of the ASVII anterolateral apodemes, posteromediad I: 7dvilm. **F**: Broad, flat, approximating a parallelogram in shape; anteroventrally directed, running closely mediad 7dvim3. **(6) 7dvilm**, M. *tergo-sternalis interior lateralis*. **O**: Ventrolaterally on the anterior surface of ATVII, ventrad and slightly posterad the bases of the anterolateral apodemes; **I**: on the posterior surface of the apical processes of the ASVII anterolateral apodemes. **F**: Slender, anteriorly directed, running closely laterad
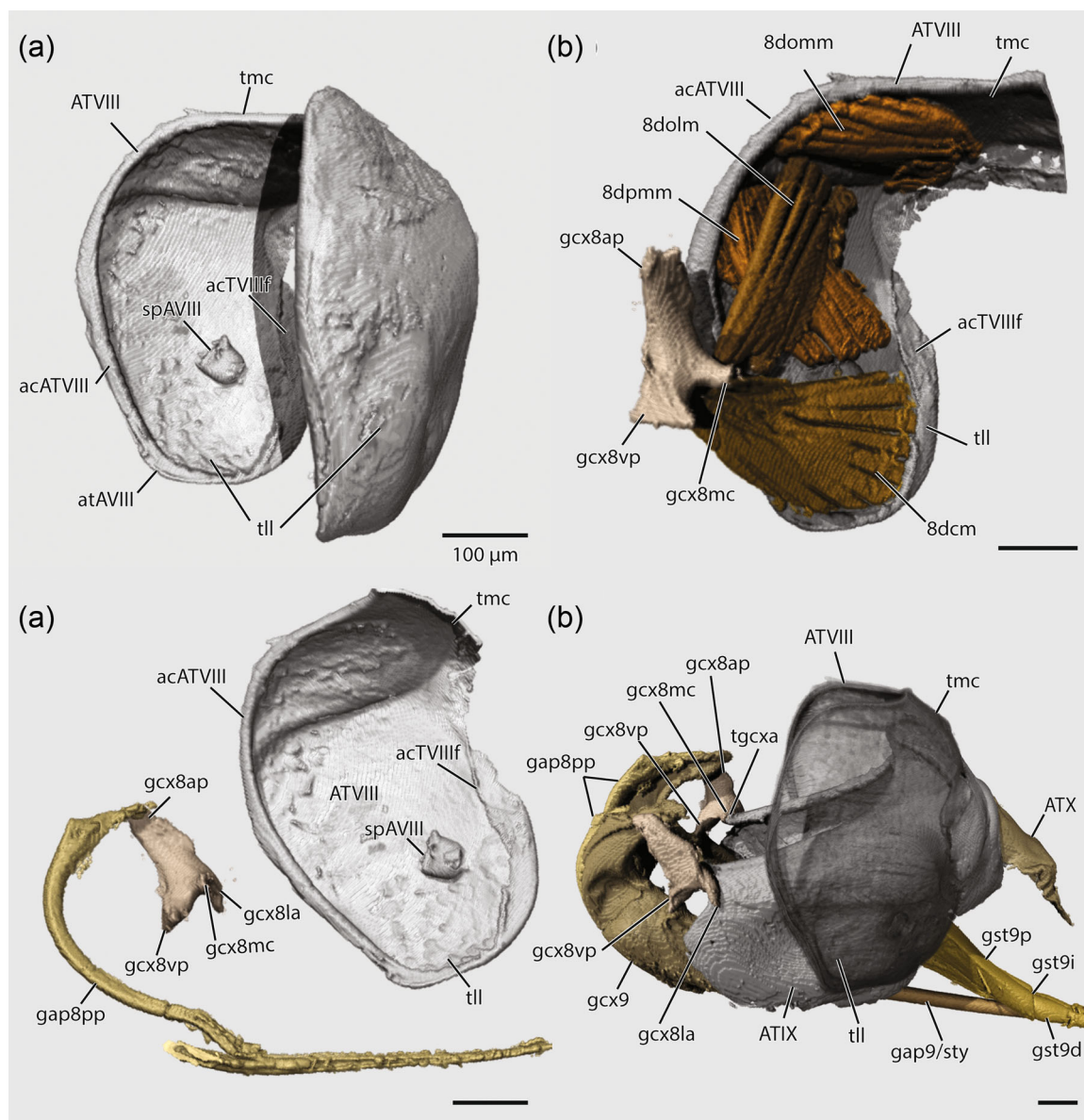
FIGURE 16 *Amblyopone australis*, skeletomusculature of abdominal segment VIII and skeleton of the genital-postgenital segments, 3D-reconstruction. (a) abdominal tergite VIII, oblique anterior view, (b) abdominal tergite VIII and gonocoxite VIII, anterior view, (c) abdominal tergite VIII and eighth genital appendages, sagittal bisection, (d) skeleton of the genital-postgenital segments, lateral view, ATVIII translucent. Scale bars: 100 μm. ac, antecosta; acTVIIIf, antecostal flange of ATVIII; AT, abdominal tergite; at, acrotergite; dcm, tergocoxal muscle; dolm, dorsal ortholateral muscle; domm, dorsal orthomedial muscle; dpmm, dorsal paramedial muscle; gap8pp, proximal process of gonapophysis VIII; gap9/sty, stylet of gonapophyses IX; gcx8ap, anterior process of gonocoxite VIII; gcx8la, lateral apodeme of the posterior process of gonocoxite VIII; gcx8mc, medial condyle of the posterior process of gonocoxite VIII; gcx8vp, ventral process of gonocoxite VIII; gcx9, gonocoxite IX; gst9d, distal sclerite of the gonostylus; gst9i, gonostylar incision; gst9p, proximal sclerite of the gonostylus; sp, spiracle; tgcxa, tergogonocoxital articulation; tll, lateral lobes of ATVIII; tmc, medial connection of ATVIII

7dvim2. **Ventrodorsal extrinsic muscles**: **(7) 7vdxm**, *M. sternotergalis exterior***O**: Laterally on the ASVII antecosta, at its junction with the ASVII anterolateral apodemes; **I**: anteroventrally on the ATVIII antecosta leading edge, immediately ventrad I: 7domm. **F**: Flat, nearly rectangular, posterodorsally directed, insertion occupying the entire anteroventral edge of the ATVIII antecosta ventrad I: 7dmm1. **Spiracular muscles** were not resolved in the present data set.

3.3 | Genital and postgenital abdomen

3.3.1 | AVIII (M7)

Sclerites

The eighth abdominal segment is represented by the reduced, spiracle-bearing tergite, and the modified genital appendages; the remainder of the segment is membranous and participates

with the membranes of AVII in forming a chamber enclosing the terminal segments. The **eighth abdominal tergite** (**ATVIII**, Figures 15b–d–18b,c and 20a,b) is continuously sclerotized but can be differentiated into two transversely bowed **lateral lobes** (**tll**, Figures 15d, 16, and 18c,d) connected by a roughly rectangular, sclerotized **medial connection** (**tmc**, Figures 15b–d–17b–d) that becomes more membranous posteromedially; the junction of the lateral lobes and the medial connection forms a blunt inflexed ridge on the mesal surface of the lateral lobe, within which originate the dorsal paramedial muscles **8dpmm** (Figures 16b and 17); the tergite is more or less vertically oriented with respect to the seventh segment at rest (Figure 15b) but can be retracted or protracted to a nearly horizontal position, with the ventral apices directed anteriorly or posteriorly. The **antecosta of ATVIII** (**acATVIII**, Figures 15b,d–17a,b) is well-developed; it provides margination along the leading edges of the lateral lobes; on the mesal surface of the lateral lobe, the antecosta expands into a thin **antecostal flange** (**acATVIIIf**, Figures 15b,d and 16a–c; "posterodorsal lobe"; Kugler, 1978) before becoming indistinct dorsally as it joins the posteroventral membrane of the medial connection; the tergocoxal muscles 8dcm partially originate in the concavity formed by the antecostal flanges (Figures 16b and 17a). The **eighth abdominal acrotergite** (**atAVIII**, Figure 16a) is indistinctly indicated by an offset ventrolateral ridge anterad the antecosta on the anteroventral part of the lateral lobes of the tergite The **eighth abdominal spiracles** (**spAVIII**, Figures 15b,d, 16a,c, and 18b) are located on the lateral lobes, at around a third of the around the ventral third of the tergite height; they are relatively large, round, and posterolaterally directed; they are supplied by well-developed tracheal trunks which may be associated with major sting muscles (see Section 4.6; Figure 35); the internal spiracular atrium is large, ovate, and anteroposteriorly inclined (Figure 16a,c); the intraspiracular apodeme was not resolved in any preparation but is likely to be present.

The **genital appendages of the eighth segment** are the **eighth gonocoxites** and their **eighth gonapophyses**; they are entirely disjunct from and located anterad the tergite. The **eighth gonocoxites** (**gcx8**, Figures 16b–d–22a,b) are approximately triangular in lateral view, and each comprises three processes on a central body: (1) the **anterior process** (**gcx8ap**, Figures 16b–d, 17a,c,d, 19a, 21b,d,e, and 22b; "body of the triangular plate" Kugler, 1978) is laterally compressed, approximately falcate in profile, and slightly concave mesally; it is dorsally carinate; it articulates ectally with the proximal part of the anterior arm of the ninth gonocoxite; it gives rise to the **proximal process of the eighth gonapophysis**; (2) the **posterior process** ("dorsoapical process", Kugler, 1978) comprises a short, downcurved, falcate **lateral apodeme** (**gcx8la**, Figures 16c,d; 17a,c; 19a; 21b–e; and 22b) and a **medial condyle** (**gcx8mc**, Figures 16b–d; 17b,c; 18c; 21b,c,e; and 22b), which is transversely divided by an **articulatory sulcus** (**gcx8as**, Figures 21b; 22b; and 25a); the posterior process articulates with the dorsoapical corners of the ninth tergital antecosta at the **VIII-IX tergogonocoxital articulation** (**tgcxa**, Figures 16d–19a): the anterior margin of the ninth antecosta fits into the articulatory sulcus of the medial condyle, while the lateral

apodeme articulates with the ectal surface of the ninth tergite. The apex of the lateral apodeme is the insertion site of the tergocoxal muscle **8dcm** (Figure 17a,c); (3) the **ventral process** (**gcx8vp**, Figures 16b–d; 17; 18e; 19a; 21d; and 22b; "ventroapical process", Kugler, 1978) is subtriangular in lateral view, with an anterior carina which offsets the posterior region from the posterior process of the eight gonocoxite; in posterior view its outline is subrectangular and apically expanded, with the ventrodistal margins sharply truncate; this truncate margin articulates via a condyle mechanism with the posterior arm of the ninth gonocoxite at the **VIII–IX intergonocoxital articulation** (**igcxa**, Figures 19b; 21a,c–e; and 25c4). The **eighth gonapophyses** arise from the anterior process of the eighth gonocoxite at a narrow junction; their **proximal processes** (**gap8pp**, Figures 1f; 16c; 17a–c; 18a,c,e; 21b–e; and 22a,d–g) are slender, filiform, and deeply grooved; they curve posteroventrally along the anterior margin of gonocoxites IX, tightly adjoining the ventromedial processes of gonocoxites IX, and converge medially approximately between, but ventrad the eighth gonocoxites, just anterad the furcula; at their juncture they give rise to the **aulaces of the lancet olistheter** (**au**, Figure 25c6), which are dorsolaterally oriented and subrectangular in cross section. Each groove is partially enclosed dorsolaterally by short, curved condyles, which clasp the rhachies of the stylet. The presence of the olistheter mechanism demarcates the proximal gonapophyseal processes from the distal **lancets** (**gap8/lan**, Figures 17a–c; 19a; 20b; 21c,e; and 23c); as they enter the sting base, the lancets give rise to paired **valvilli** (**vvl**, Figure 23c1,2), small proximodorsal dilations, the dorsolateral walls of which are some-what less sclerotized. A single pair of valvilli was resolved in transverse histological cross-sections (Figure 23c1,2), while a sagittal section indicates there may be two or three pairs (Figure 28a). The valvilli are proximally somewhat digitate in cross-section, forming an inverted Y-shape medially which projects into the valve chamber; more distally the valvilli become narrower and more membranous until they close; the fusion of the medial and lateral dorsal walls of the valvilli forms an unpaired sclerotic flap on each lancet, which serves as an **arm of the dorsomedial seal of the venom canal** (**sda**, Figure 23c3–6); in the region where the valvilli are closed but the pockets of the sting bulb are unfused, the arm of the dorsomedial seal appears to directly contact the **ventral membrane of the venom gland duct** (**vgd**, Figure 23c3–5). Ventromedially each lancet bears an **arm of the ventromedial seal** (**sva**, Figure 25c3–6), a narrow, vertical flap which projects into the venom canal; the arms of the ventromedial seal can be intimately approximated with one another (Figure 25c6). Apically each lancet bears 5 min, triangular, proximally directed **barbules** (**bar**, Figure 26a,b), which are increasingly widely spaced in the proximal direction.

Muscles

Dorsal orthomedial muscles: (**1**) **8domm**, *M. tergo-tergalis orthome-dialis* (Figures 16b and 17). **O**: Dorsolaterally on the ATVIII antecosta and just posterad the antecosta on the mesal surface of the lateral lobes; **I**: ectally on the posterodorsal apodeme of the ATIX dorsal body. **F**: Broad, flat, somewhat curved, posteromedially directed.
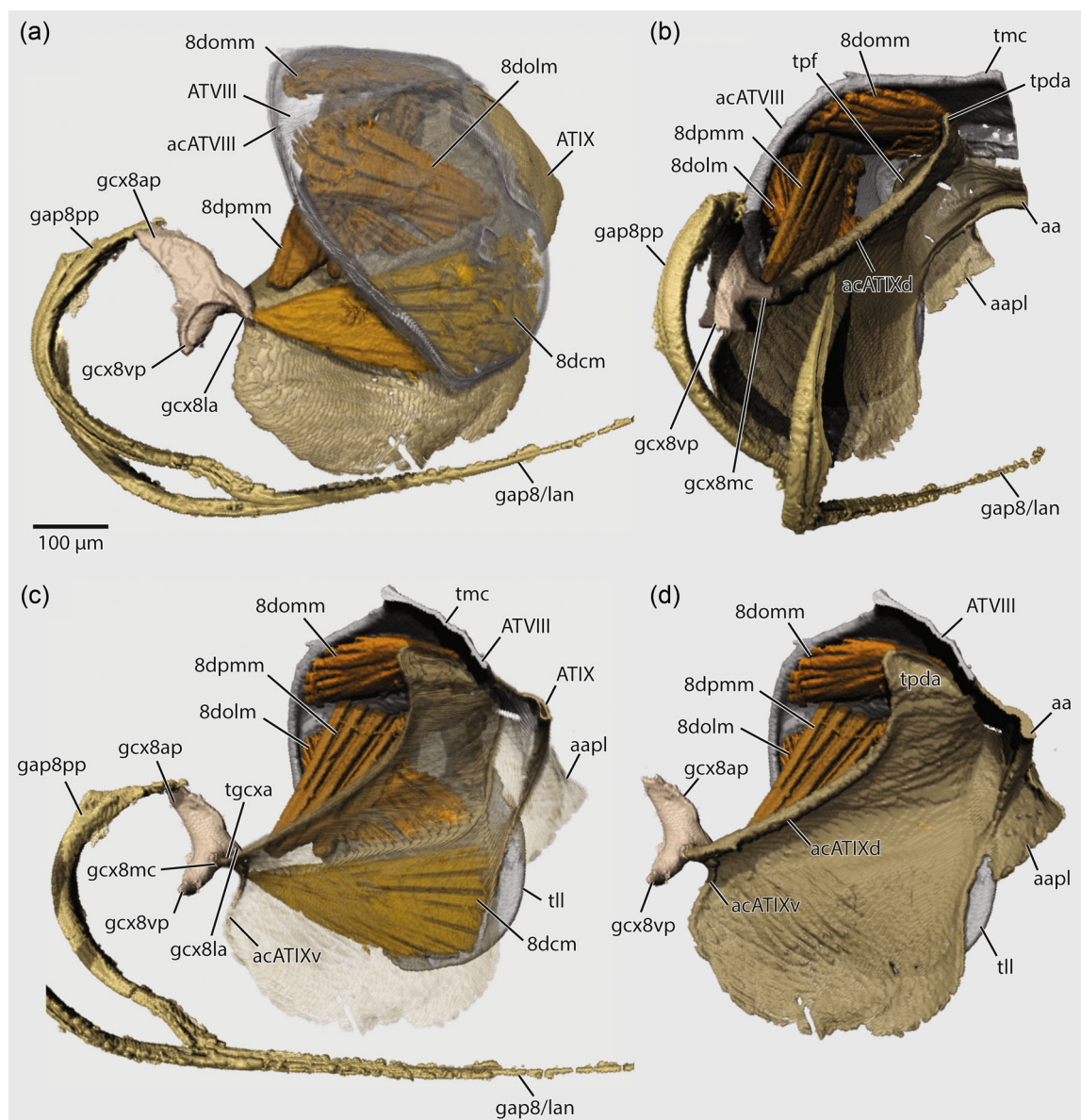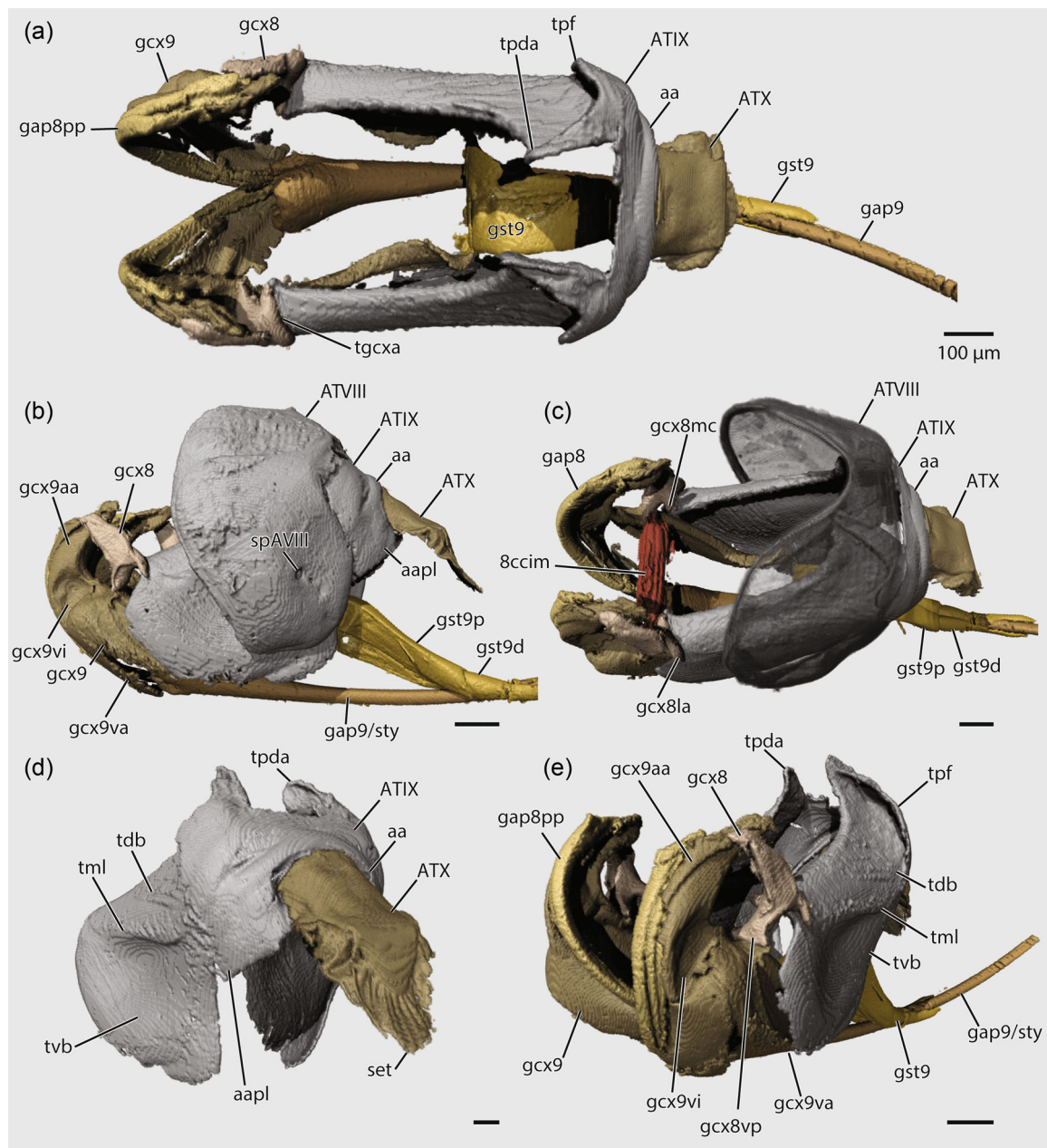
FIGURE 17 *Amblyopone australis*, skeleton of AVIII and ATIX, and musculature of ATVIII, 3D reconstruction. (a) lateral view, ATVIII translucent, (b) oblique anterior view, (c) sagittal bisection, ATIX translucent, (d) mesal view. Scale bar applies to all subfigures: 100 μm. aa, anal arc; aapl, posterolateral lobe of the anal arc; ac, antecosta; acATIXd, dorsal body antecosta of ATIX; acATIXv, ventral body antecosta of ATIX; acTVIIIf, antecostal flange of ATVIII; AT, abdominal tergite; at acrotergite; dcm, tergocoxal muscle; dolm, dorsal ortholateral muscle; domm, dorsal orthomedial muscle; dpmm, dorsal paramedial muscle; gap8/lan, lancet of gonapophysis VIII; gap8pp, proximal process of gonapophysis VIII; gap9/sty, stylet of gonapophyses IX; gcx8ap, anterior process of gonocoxite VIII; gcx8la, lateral apodeme of the posterior process of gonocoxite VIII; gcx8mc, medial condyle of the posterior process of gonocoxite VIII; gcx8vp, ventral process of gonocoxite VIII; gcx9, gonocoxite IX; gst9d, distal sclerite of the gonostylus; gst9i, gonostylar incision; gst9p, proximal sclerite of the gonostylus; sp, spiracle; tgcxa, tergogonocoxital articulation; tll, lateral lobes of ATVIII; tmc, medial connection of ATVIII; tpda, posterodorsal apodeme of the dorsal body of ATIX; tpf, posterolateral flange of the dorsal body of ATIX

Dorsal paramedial muscles: **(2) 8dpmm**, *M. tergo-tergalis paramedialis* (Figures 16b and 17). **O**: Dorsolaterally on the mesal surface of the lateral lobes, on the inflexed ridge where the lobe adjoins the medial connection; **I**: anteriorly on the midplate line carina of ATIX. **F**: Nearly rectangular, flat, anteroventrally directed. **Dorsal ortholateral muscles**: **(3) 8dolm**, *M. tergo-tergalis ortholateralis* (Figures 16b and 17). **O**: Anterolaterally on the mesal surface of the lateral lobe, anterolaterad

O: 8dpm1; **I**: posteriorly on the midplate line carina of ATIX. **F**: Similar in shape to 8dpm1 but reflected around the transverse axis; nearly rectangular, flat, posteroventrally directed. **Tergocoxal muscles**: **(4) 8dcm**, *M. tergo-coxalis (solus)* (Figures 16b; 17; and 20a,b). **O**: Posteroventrally on the mesal surface of the lateral lobe, within the concavities formed by the antecostal flanges; **I**: apically on the lateral apodeme of the posterior process of
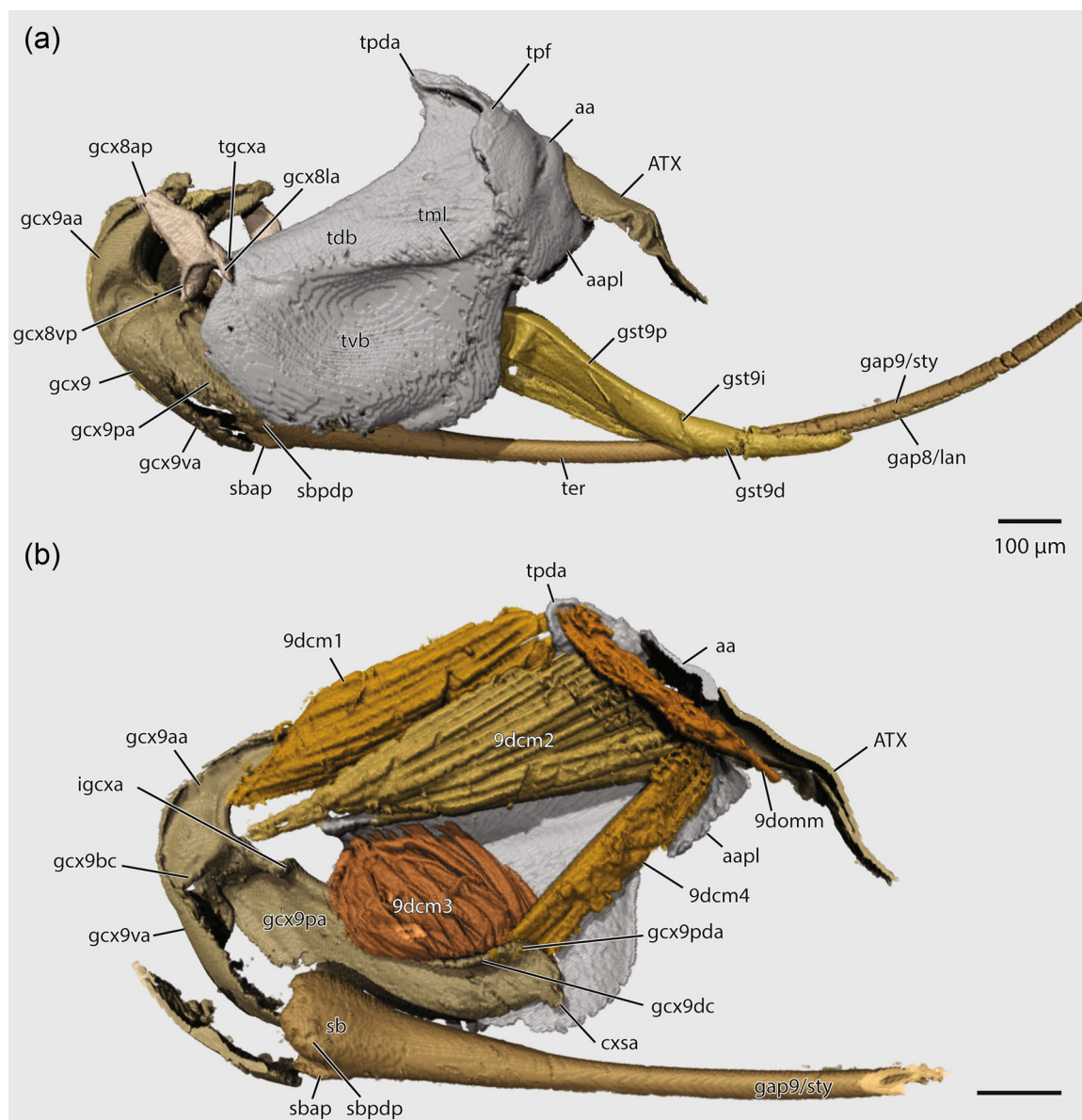
FIGURE 18 *Amblyopone australis*, skeleton of the genital-postgenital segments, 3D reconstruction in (a) dorsal view, ATVIII hidden, (b) lateral view, ATVIII hidden (c) oblique dorsal view, ATVIII translucent, (d) oblique posterior view, ATX and ATX only, (e) oblique anterior view, ATVIII hidden. Scale bars: 100 μm. aa, anal arc; aapl, posterolateral lobe of the anal arc; AT, abdominal tergite; ccim, coxocoxal muscle; gap8pp, proximal process of gonapophysis VIII; gap9/sty, stylet of gonapophyses IX; gcx8, gonocoxite VIII; gcx8la, lateral apodeme of the posterior process of gonocoxite VIII; gcx8mc, medial condyle of the posterior process of gonocoxite VIII; gcx8vp, ventral process of gonocoxite VIII; gcx9, gonocoxite IX; gcx9aa, anterior arm of gonocoxite IX; gcx9va, ventral arm of gonocoxite IX; gcx9vi, ventral ectal impression of the anterior arm of gonocoxite IX; gst9, gonostylus IX; gst9d, distal sclerite of the gonostylus; gst9p, proximal sclerite of the gonostylus; set seta; sp, spiracle; tdb, dorsal body of ATIX; tgcxa, tergogonocoxital articulation; tml, midplate line of ATIX; tpda, posterodorsal apodeme of the dorsal body of ATIX; tpf, posterolateral flange of the dorsal body of ATIX; tvb, ventral body of ATIX

gonocoxite VIII. **F**: Large, broadly triangular, flat, anterodorsally directed. **Coxocoxal intrinsic muscles**: **(5) 8ccim**, *M. coxo-coxalis interior* (Figures 18c; 22a,b,d; 24e; and 25). **O**: Apicomesally on the ventral process of gonocoxites VIII; I: medial insertion absent; muscle is transverse. **F**: Broadly spindle shaped. **Intraspiracular occlusor** muscles (*M. occlusor spiraculi*) present.

3.3.2 | AIX (M8)

Sclerites

The sclerites of the ninth abdominal segment are represented by the highly modified tergite and the genital appendages. The **ninth abdominal tergite** (**ATIX**, Figures 16d and 17–20) is divided into

FIGURE 19 *Amblyopone australis*, skeleton of the genital-postgenital segments and musculature of ATIX, 3D-reconstruction in (a) lateral view, (b) sagittal bisection. Scale bars: 100 μm. aa, anal arc; aapl, posterolateral lobe of the anal arc; AT, abdominal tergite; ccim, coxocoxal muscle; cxsa, coxostylar articulation; dcm, tergocoxal muscle; domm, dorsal orthomedial muscle; gap8/lan, lancet of gonapophysis VIII; gap8pp, proximal process of gonapophysis VIII; gap9/sty, stylet of gonapophyses IX; gcx8, gonocoxite VIII; gcx8ap, anterior process of gonocoxite VIII; gcx8la, lateral apodeme of the posterior process of gonocoxite VIII; gcx8mc, medial condyle of the posterior process of gonocoxite VIII; gcx8vp, ventral process of gonocoxite VIII; gcx9, gonocoxite IX; gcx9aa, anterior arm of gonocoxite IX; gcx9bc, basal carina of the anterior arm of gonocoxite IX; gcx9dc, dorsal carina of the posterior arm of gonocoxite IX; gcx9pda, posterodorsal apodeme of the posterior arm of gonocoxite IX; gcx9va, ventral arm of gonocoxite IX; gcx9vi, ventral ectal impression of the anterior arm of gonocoxite IX; gst9, gonostylus IX; gst9d, distal sclerite of the gonostylus; gst9i, gonostylar incision; gst9p, proximal sclerite of the gonostylus; sb, sting bulb; sbap, articular process of the sting bulb; sbpdp, proximodorsal process of the sting bulb; set, seta; sp, spiracle; tdb, dorsal body of ATIX; ter, terebra; tgcxa, tergogonocoxital articulation; tml, midplate line of ATIX; tpda, posterodorsal apodeme of the dorsal body of ATIX; tpf, posterolateral flange of the dorsal body of ATIX; tvb, ventral body of ATIX

the subisometric **dorsal body** (**tdb**) and **ventral body** (**tvb**) by the carinate **midplate line** (**tml**, Figures 18b,d,e; 19a; and 20d,e), which runs longitudinally from the anterior to posterior borders of the tergite. The **ninth abdominal antecosta** is here interpreted as comprising the strong dorsal carina on the dorsal and anterior margins of the dorsal body, the **dorsal body antecosta** (**acATIXd**,

Figure 17b,d), and the small, fine carina on the anterior edge of the ventral body, the **ventral body antecosta** (**acATIXv**, Figure 17c,d), which becomes indistinct ventrally; the antecostae of the dorsal and ventral bodies are continuous on the anterior edge of the tergite. The dorsal body bears a **posterodorsal apodeme** (**tpda**, Figures 17b,d; 18a,d,e; 19; and 20c–e), which is large and fin-like; it
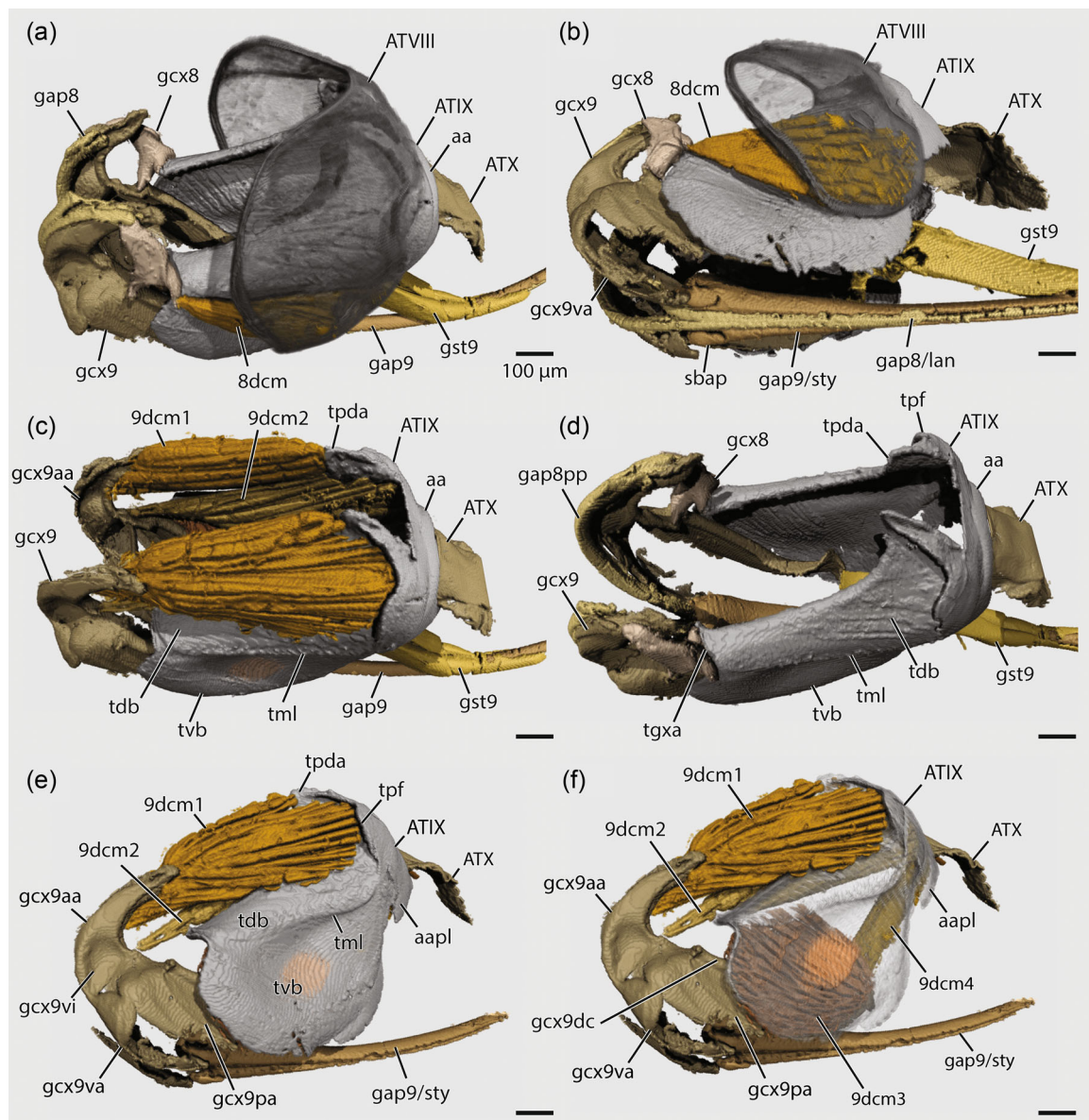
FIGURE 20 *Amblyopone australis*, skeleton of the genital-postgenital segments and musculature of ATIX, 3D-reconstruction; ATVIII is translucent in (a–b) and hidden in (c–f); ATIX is translucent in (f). Muscles are hidden in (a) and (d). Scale bars: 100 μm. aa, anal arc; aapl, posterolateral lobe of the anal arc; AT, abdominal tergite; dcm, tergocoxal muscle; gap8, gonapophysis VIII; gap8/lan, lancet of gonapophysis VIII; gap8pp, proximal process of gonapophysis VIII; gap9, gonapophysis IX; gap9/sty, stylet of gonapophyses IX; gcx8, gonocoxite VIII; gcx9, gonocoxite IX; gcx9aa, anterior arm of gonocoxite IX; gcx9aa, anterior arm of gonocoxite IX; gcx9dc, dorsal carina of the posterior arm of gonocoxite IX; gcx9pa, posterior arm of gonocoxite IX; gcx9va, ventral arm of gonocoxite IX; gcx9vi, ventral ectal impression of the anterior arm of gonocoxite IX; gst9, gonostylus IX; sbap, articular process of the sting bulb; tdb, dorsal body of ATIX; tgxa, tergogonocoxital articulation; tml, midplate line of ATIX; tpda, posterodorsal apodeme of the dorsal body of ATIX; tpf, posterolateral flange of the dorsal body of ATIX; tvb, ventral body of ATIX

is recurved such that its apex is directed anteriorly; at the apex, the dorsal body antecosta connects to a carina on the posterior edge of the apodeme, which expands laterally into a large **posterolateral flange** (**tpf**, Figures 17b; 18a,e; 19a; 20d,e) forming a concavity within which originates the tergocoxal muscle 9dcm1 (Figure 20c,e,f). The apices of the posterodorsal apodeme are additionally bent laterally, and the proctiger muscle **9domm** originates mesally on this bent region (Figure 19b). The **ventral body** is vaguely rectangular in shape,

and is less strongly sclerotized than the dorsal body, other than the small ventral body antecosta and the **anal arc** (**aa**, Figures 17b–d; 18a–e; 19; 20a,c,d; and 26g), which is a posteromedial, arcuate, sclerotized strip, which medially unites the posterodorsal apodemes of the dorsal body. The anteromedial disc of the anal arc is weakly sclerotized; the posterolateral corners of the anal arc are expanded into roughly triangular **posterolateral lobes of the anal arc** (**aapl**, Figures 17b–d; 18b,d; 19; and 20e,f), the mesal
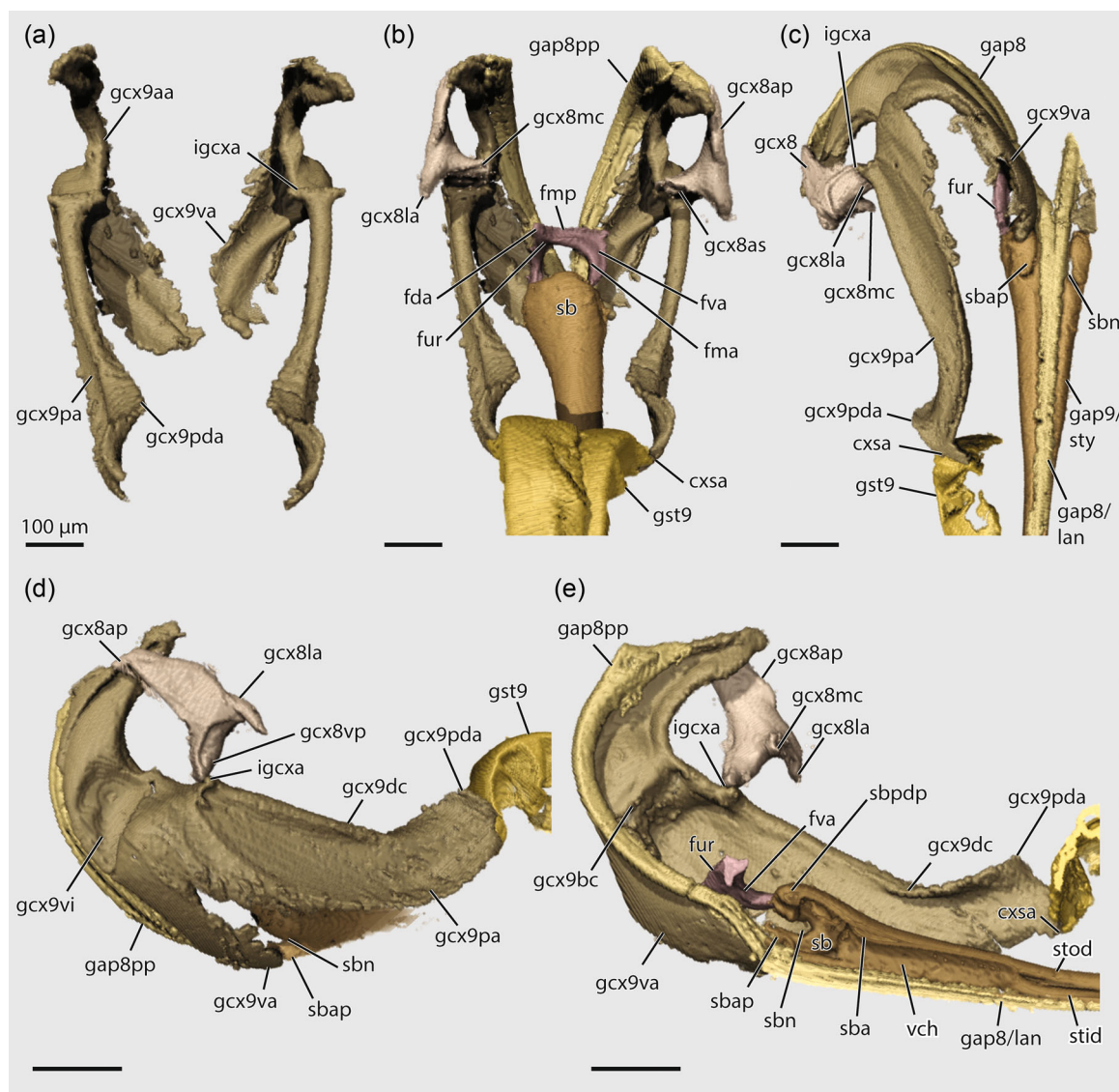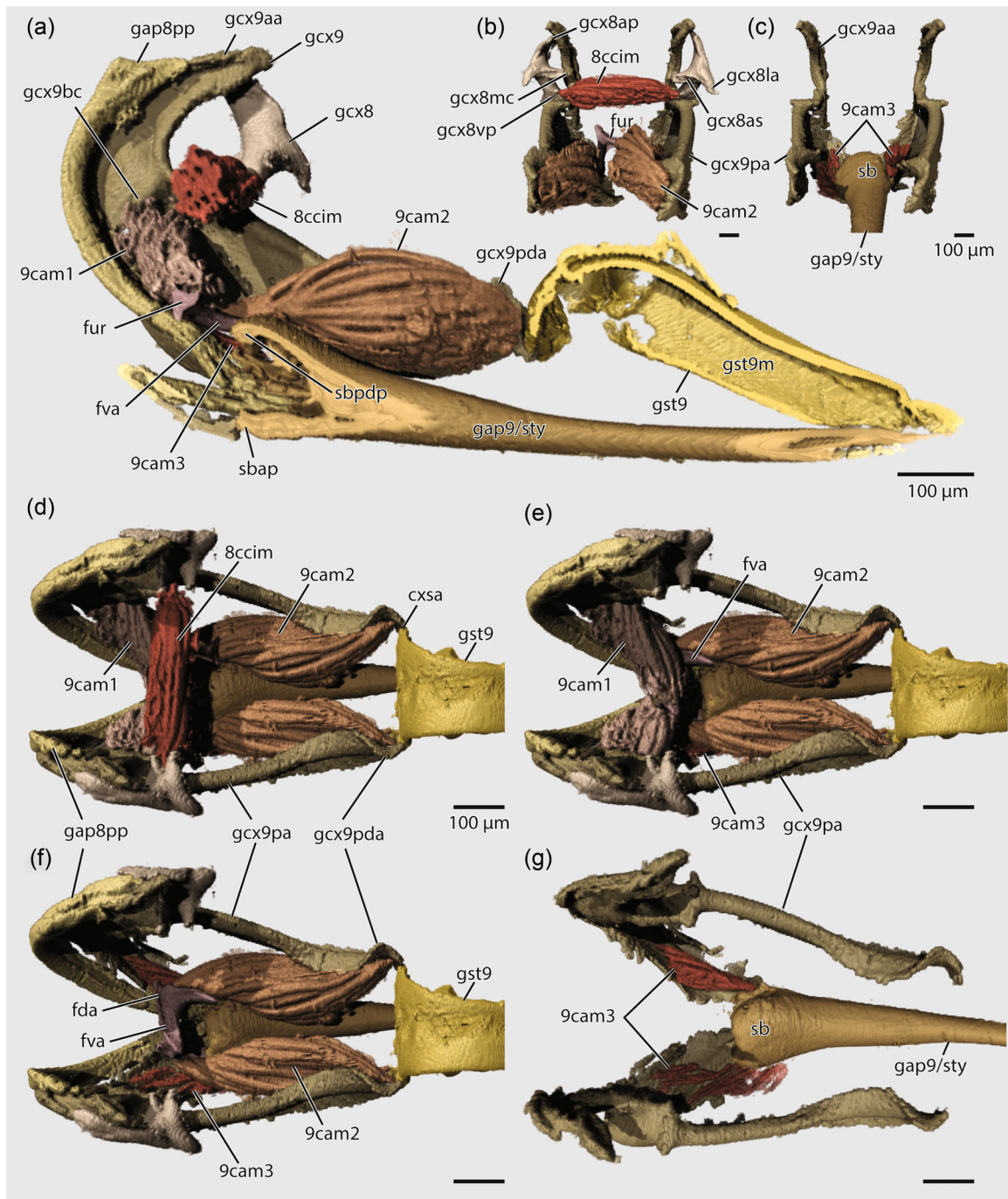
FIGURE 21 *Amblyopone australis*, skeleton of the genital appendages, 3D-reconstruction. (a) gonocoxites IX, dorsal view, (b) genital appendages, dorsal view, (c) genital appendages, ventral view, left half of body, (d) gonocoxites, oblique ectal view, (e) genital appendages, sagittal bisection, mesal view. Scale bars: 100 μm. cxsa, coxostylar articulation; fda, dorsal arm of the furcula; fma, anterior furcular margination; fmp, posterior furcular margination; fur, furcula; fva, ventral arm of the furcula; gap8pp, proximal process of gonapophysis VIII; gap9/sty, stylet of gonapophyses IX; gcx8ap, anterior process of gonocoxite VIII; gcx8as, articulatory sulcus of the posterior process of gonocoxite VIII; gcx8la, lateral apodeme of the posterior process of gonocoxite VIII; gcx8mc, medial condyle of the posterior process of gonocoxite VIII; gcx9aa, anterior arm of gonocoxite IX; gcx9dc, dorsal carina of the posterior arm of gonocoxite IX; gcx9pa, posterior arm of gonocoxite IX; gcx9pda, posterodorsal apodeme of the posterior arm of gonocoxite IX; gcx9va, ventral arm of gonocoxite IX; gcx9va, ventral arm of gonocoxite IX; gcx9vi, ventral ectal impression of the anterior arm of gonocoxite IX; gst9, gonostylus IX; igcxa, VIII-IX intergonocoxital articulation; sb, sting bulb; sba, sting bulb apophysis; sbap, articular process of the sting bulb; sbap, articular process of the sting bulb; sbn, basal notch of the sting bulb; stid, inner dorsal wall of the stylet; stod, outer dorsal wall of the stylet; vch, valve chamber

surfaces of which bear the tergocoxal muscles **9dcm4** (Figures 19b and 20f); the posterior anal arc is intimately connected to **ATX** (Figure 26g).

The **genital appendages of the ninth abdominal segments** comprise the ninth gonocoxites, the distolateral ninth gonostyli, and the distomedial ninth gonapophyses. The **ninth gonocoxites (gcx9**, Figures 16d; 18a,b,e; and 19) are much larger than the eighth and more complex in shape; they are divided into three primary regions:

(1) an anterior arm, (2) a posterior arm, and (3) a ventral arm. **(1)** The **anterior arm of gonocoxite IX (gcx9aa**, Figures 18b; 19; 20c,e,f; 21a,d,e; and 22a) is laterally compressed and roughly corniform (horn-shaped) in lateral view. It articulates at its dorsal apex with the anterior process of gonocoxite VIII, at which point it also gives rise to the **ventromedial process of gonocoxite IX**. Its ectal surface bears a concave **ventral impression (gcx9vi**, Figures 18b,e; 20e; and 21d); its mesal surface bears a longitudinal **basal carina (gcx9bc**,

FIGURE 22 *Amblyopone australis*, skeletomusculature of the genital appendages, 3D-reconstruction. (a) sagittal bisection, (b) gonocoxites, posterior view, (c) ninth genital appendages, posterior view, (c–g) dorsal view, muscle groups selectively hidden. Scale bars: 100 μm. cam, coxapophyseal muscle; ccim coxocoxal muscle; cxsa, coxostylar articulation; fur, furcula; fva, ventral arm of the furcula; gap8pp, proximal process of gonapophysis VIII; gap9/sty, stylet of gonapophyses IX; gap9pp, stylet of gonapophyses IX; gcx8, gonocoxite VIII; gcx8ap, anterior process of gonocoxite VIII; gcx8as, articulatory sulcus of the posterior process of gonocoxite VIII; gcx8la, lateral apodeme of the posterior process of gonocoxite VIII; gcx8mc, medial condyle of the posterior process of gonocoxite VIII; gcx8vp, ventral process of gonocoxite VIII; gcx9aa, anterior arm of gonocoxite IX; gcx9aa, anterior arm of gonocoxite IX; gcx9bc, basal carina of the anterior arm of gonocoxite IX; gcx9pa, posterior arm of gonocoxite IX; gcx9pda, posterodorsal apodeme of the posterior arm of gonocoxite IX; gst9m, membranous medial surface of the gonostylus; gst9m, membranous medial surface of the gonostylus; sb, sting bulb; sbap, articular process of the sting bulb; sbpdp proximodorsal process of the sting bulb
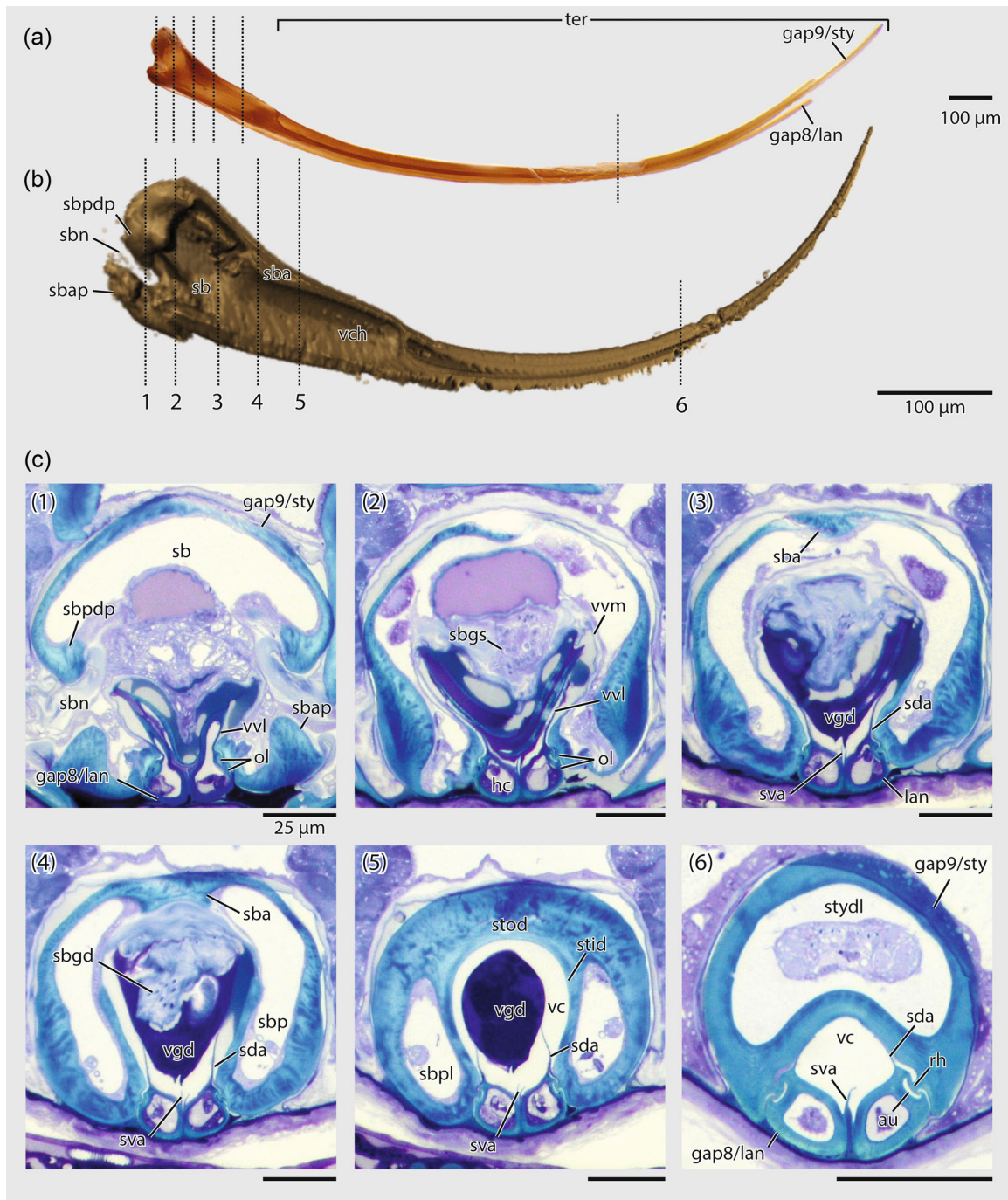
FIGURE 23 *Amblyopone australis*, morphology of the sting. (a) Photomicrograph, sting base and terebra, (b) 3D reconstruction, sting base and stylet, (c) transverse histological section series. Numbered dashed lines in (a–b) correspond approximately to the location where the sections in (c) were acquired. Scale bars, a–b: 100 µm. Scale bars, c1–6: 25 µm. au, aulax of the lancet olistheter; gap8/lan, lancet of gonapophysis VIII; gap9/sty, stylet of gonapophyses IX; hc, hemocoel; ol, olistheter; rh, rhachis of the stylet olistheter; sb, sting bulb; sba, sting bulb apophysis; sbap, articular process of the sting bulb; sbgd, sting bulb gland duct; sbgs, sting bulb gland secretory cell; sbn, basal notch of the sting bulb; sbpdp, proximodorsal process of the sting bulb; sbpdp, proximodorsal process of the sting bulb; sbpl, sting bulb pocket lumen; sda, lancet arm of the dorsomedial seal of the venom canal; stid, inner dorsal wall of the stylet; stod, outer dorsal wall of the stylet; stydl, dorsomedian lumen of the stylet; sva, lancet arm of the ventromedial seal of the venom canal; ter, terebra; vc, venom canal; vch, valve chamber; vgd, venom gland duct; vvl, valvillus
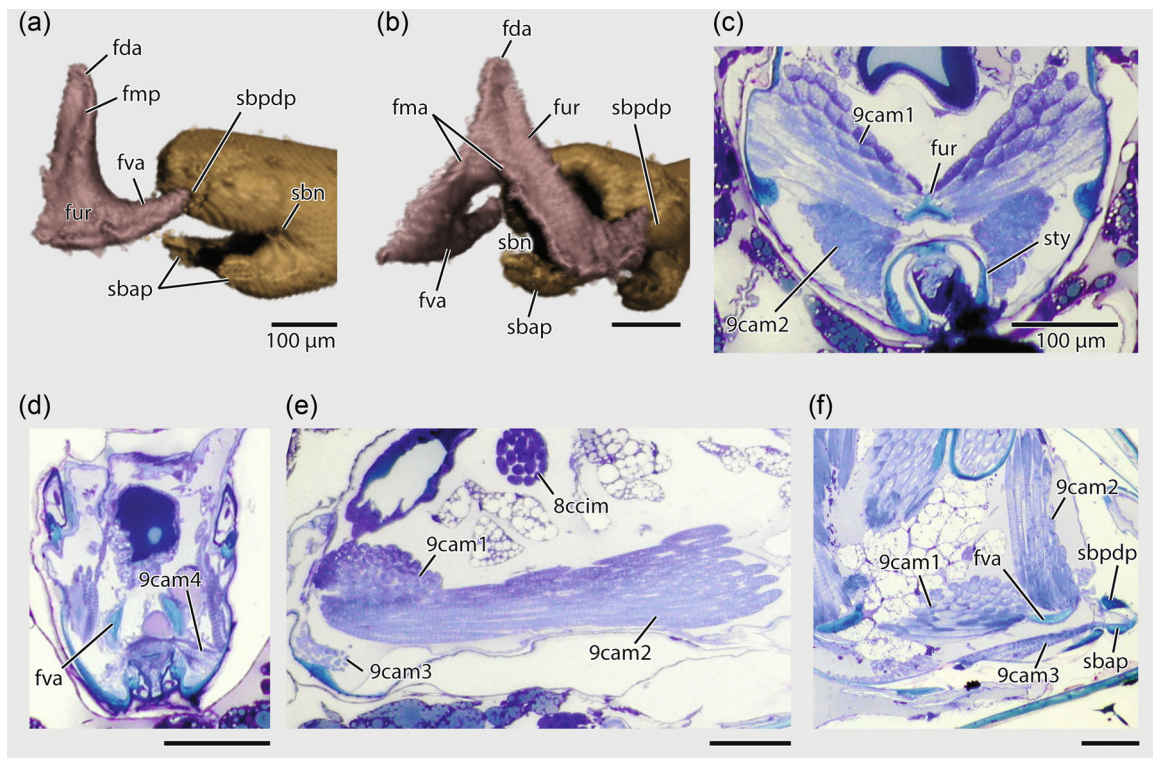
FIGURE 24 *Amblyopone australis*, skeletomusculature of the furcula and sting base. (a) Three-dimensional (3D)-reconstruction, ectal view, (b) 3D-reconstruction oblique anterior view, (c–d) transverse histological sections, (e–f) sagittal histological sections. Scale bars: 100 μm. cam, coxapophyseal muscle; ccim, coxocoxal muscle; fda, dorsal arm of the furcula; fma, anterior furcular margination; fmp, posterior furcular margination; fur, furcula; fva, ventral arm of the furcula; sbap, articular process of the sting bulb; sbn, basal notch of the sting bulb; sbpdp, proximodorsal process of the sting bulb; sty, stylet

Figures 19b; 21e; and 22a), which separates it from the anterior and ventral arms and partially bears the origin of the coxapophyseal (furcular) muscle 9cam1 (Figure 22a,d,e). **(2)** The **posterior arm of gonocoxite IX (gcx9pa**, Figures 19; 20e,f; 21; and 22d–g) is the largest portion of the sclerite. It is broadly falcate, and bent inwards preapically around the anteroposterior axis; it has a strong **dorsal carina (gcx9dc**, Figure 19b; 20f; and 21d,e) along its entire length, which basally forms a small condylar knob at the **VIII–IX inter-gonocoxital articulation (igcxa**, Figures 19b and 21a,d,e) with the ventral process of gonocoxite VIII; the posterior arm bears a **posterodorsal apodeme (gcx9pda**, Figures 19b; 21a,c–e; and 22d,f), which forms a medial, carinate shelf and on which originates the coxapophyseal muscle 9cam2 (Figure 22a,b,d–f). At its posteroventral apex is a small, ventromedially oriented lobe, the **coxostylar articulation (cxsa**, Figures 19b; 21b,c,e; and 22d), which gives rise to the **ninth gonostylus**. **(3)** The **ventral arm of gonocoxite 9 (gcx9va**, Figures 18b,e; 19; 20b,e,f; 21a,c–e) is more or less arcuate, sweeping posteroventrally below the posterior gonocoxital arm, and secondarily directed medially; it is overall poorly sclerotized and difficult to distinguish from the ligulate membrane and the ventromedial gonocoxital processes. Overall, the **ventromedial gonocoxital processes** are intimately opposed to both the ventral gonocoxital arms and the proximal processes of gonapophyses VIII. They were indistinctly resolved and were not able to be segmented

or visualized separately here, so further description is not presently possible.

The **ninth gonostyli (gst9**, Figures 18a; 20a–d; 21–d; and 22a,d) are situated laterad the ninth gonapophyses and arise from the apices of the posterior arms of the ninth gonocoxites; they are approximately rectangular in cross section, and are medially grooved, thus able to clasp the ectal surfaces of the terebra; their proximal articulations are narrow and condylic, that is, the stylus base coordinates with the gonocoxital apex mechanically, rather than being separated by membrane as in some Aculeata (Kumpanenko et al., 2019). From their narrow articulation, the styli curve dorsally, then posteroventrally, forming the roughly falcate "sheaths" of the terebra; they are quite thin and flexible, being most poorly sclerotized ventrally, with the mesal surfaces entirely membranous. The **gonostylar incision (gst9i**, Figures 1f; 19a; and 26c) divides each stylus into proximal and distal sclerites at around two-thirds of the stylus length; in lateral view the **proximal gonostylar sclerite (gst9p**, Figures 1f; 18b,c; 19a; and 26c,d) is subrectangular apically, while the **distal gonostylar sclerite (gst9d**, Figures 1f; 18b,c; 19a; and 26c) is more digitate. The proximal gonostylar sclerite bears a few widely separated hairs, some quite short and conical, others much longer (**set**, Figure 26d); the **medial membranous surface** of each stylus (**gst9m**, Figures 22a and 26c–e) is densely clothed with cuticular microtrichia (**cmt**, Figures 26c–e). The gonostylar incision is
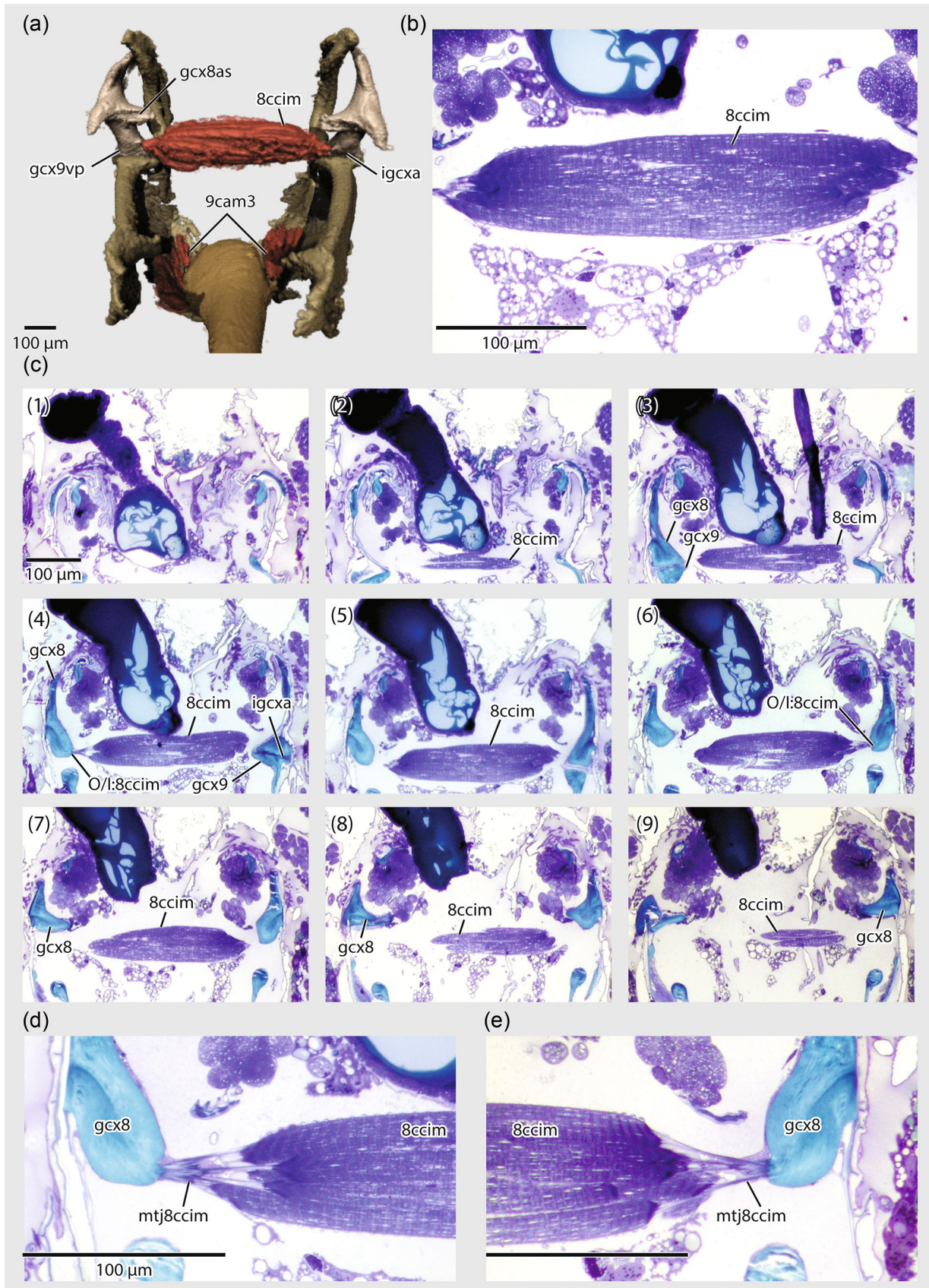
FIGURE 25 (See caption on next page)

surrounded by quite short, flat, triangular, appressed hairs that are mostly distributed on the proximal part of the distal gonostylar sclerite (**set**, Figure 26f).

The **ninth gonapophyses** (**9gap**) are medially fused and divided into two unpaired structures, the proximal furcula, and the distal ninth gonapophyseal component of the sting base, sting bulb, valve chamber, and the stylet of the terebra. The **furcula** (**fur**, Figures 21b,e; 22a,b; 24a–c; and 28a) is disjunct from all other sclerites; it is located proximad the sting base, anterad the sting bulb between the posterior arms of gonocoxites IX, and dorsad gonapophyses VIII (Figure 21b); it is in the shape of an inverted Y in posterior view, with a median dorsal arm and two ventrolateral arms. The **dorsal furcular arm** (**fda**, Figures 21b; 22f; 24a,b) is subtriangular; the **ventral furcular arms** (**fva**, Figures 21b,e; 22f; 24a,b,d,f; and 28b) are curved, appearing crescentiform in lateral view, tapering slightly towards their posterior apices (Figure 24a), and extending laterally to a position dorsad the preapical part of the posterior arm of gonocoxite IX. The **anterior furcular margination** (**fma**) and **posterior furcular margination** (**fmp**, Figures 21b and 24a,b) comprise carinae that marginate the ventral arms, continuing onto the anterior and posterior faces. On each face the carinae fuse dorsomedially on the dorsal arm, such that the furcula is ventromedially ecarinate (Figure 24b); the distal apices of the ventral furcular arms articulate with the proximodorsal processes of the sting base (Figure 24a,b).

The sting base bears **proximodorsal processes** (**sbpdp**, Figures 19; 21e; 22a; 23c1; 24a,b; and 28a; "anterior processes" Kugler, 1978), which are strongly sclerotized, inflexed condyles that articulate with the ventral arms of the furcula; the ventrolateral part of the proximodorsal processes form roughly triangular, ventrally directed lobes. The dorsomedian portion of the sting base between the proximodorsal processes ("basal ridge," Kugler, 1978), is continuously sclerotized, but less strongly than the processes themselves; the processes form the proximodorsal wall of the **sting bulb** (**sb**, Figures 19b; 21b,e; 22c; and 23c1), a subglobular chamber which decreases in all dimensions posteriorly. Proximoventrally, the sting bulb bears the **articular processes of the sting bulb** (**sbap**, Figures 19; 20b; 21c–e; 22a,b; 23c1; and 24a,b; "*processi articulares*"), which are short, curved, slightly tapering condyles which articulate with the apices of the ventral arms of gonocoxites IX. The articular processes are separated from the proximodorsal processes by the **basal notches of the sting bulb** (**sbn**, Figures 21c; 23c1; and 24a,b), which are more-or-less U-shaped lateral incisions. Distally, the proximodorsal, medial **sting bulb apophysis** (**sba**, Figures 21e; 23b,c3,c4; and 28a) delimits the sting bulb from the distal **valve chamber** (**vch**, Figures 21e and 23b), although the apophysis does not fully septate these regions. The **terebra** (**ter**, Figures 1f and 23a) is considered to begin at the juncture of the **inner and outer dorsal walls of gonapophyses IX** (**stid**, **stod**, Figures 21e and 23c5). In dorsal external view, the sting bulb and valve chamber correspond to a depressed, less robustly sclerotized region bordered on its lateral and distal edges by a fine carina. The internal structure of the fused ninth gonapophyses differs along their length, with four primary regions recognizable in cross-section from proximal to distal: (1) the dorsal margin is fused and continuous, with the lateral margins incised at the basal notches (Figure 23c1); (2) the dorsomedian sting bulb wall becomes more weakly sclerotized; the ventromesal margins are invaginated and partially membranous, forming U-shaped lateral pockets (Figure 23c2–3); (3) the sclerotized walls of the **pockets of the sting bulb** (**sbp**) close by fusing to the dorsomedian wall as part of the sting bulb apophysis, such that there are two, lateral, teardrop-shaped **pocket lumina** (**sbpl**) continuous with the haemocoel surrounding the medial **venom canal** (**vc**, Figure 23c4–5); and (4) the pocket lumina fuse medially into a single, reniform **dorsomedial lumen** (**stydl**) dorsad the venom canal, indicating the start of the terebra (Figure 23c6).

The **stylet** of the ninth gonapophyses (**gap9/sty**, Figures 18a,b,e; 19; 20; 21c; 22a,e; and 23) tapers slightly from its base to the apex of the sting. The **rhachies of the stylet olistheter** (**rh**, Figures 23c6 and 26a) are ventromedially converging in orientation; each consists of a longitudinal ridge, mushroom-shaped in cross-section, which fits into the corresponding aulax; ventrolaterally, the stylet overhangs the ectal margin of the lancet (Figure 23c). The **apex of the stylet** (**styx**, Figure 26a) is rounded, and is wider than and continues slightly beyond the sharply tapering **apices of the lancets** (**lanx**, Figure 26a) when relaxed. The lancets can be exserted beyond the stylet (Figure 26b); the gap between the stylet and lancet apices permits the issue of venom; the stylet externally bears two minute, triangular, proximally directed **barbules** (**bar**, Figure 26b), beneath which the stylet is slightly depressed.

Muscles

Dorsal orthomedial muscles: **(1) 9domm**, *M. tergo-tergalis orthomedialis* (Figures 19b; 29a; and 30a,b). **O**: Mesally on the posterodorsal apodeme of the ATIX dorsal body; **I**: dorsoapically on the proctiger lobe, ventrad ATX, dorsad *M. retractor ani*. **F**: Slender, elongate, posteroventrally directed. *Note*: These may be dorsal ortholateral muscles; see Section 4.5. **Tergocoxal muscles**: **(2) 9dcm1**, *M. tergo-coxalis anterior externalis* (Figures 1f; 19b; and 20c,e,f). **O**: Posteriorly on the ectal surface and anterodorsal edge of the posterolateral

---

FIGURE 25 *Amblyopone australis*, morphology of the eight coxocoxal intrinsic muscle. (a) Three-dimensional-reconstruction of gonocoxites and stylet, posterior view. (b–e) transverse histological sections, (b) at the anteroposterior midpoint of 8ccim, (c) progressive section series through 8ccim at 10 μm spacing, (d–e) attachments to gonocoxites VIII, right (d) and left (e) sides of body. Scale bars: 100 μm. cam, coxapophyseal muscle; ccim, coxocoxal muscle; gcx8, gonocoxite VIII; gcx8as, articulatory sulcus of the posterior process of gonocoxite VIII; gcx9, gonocoxite IX; gcx9vp, ventral ectal impression of the anterior arm of gonocoxite IX; igcxa, VIII–IX intergonocoxital articulation; mtj8ccim, myotendinous junction; O/I, muscle attachment (origin/insertion)
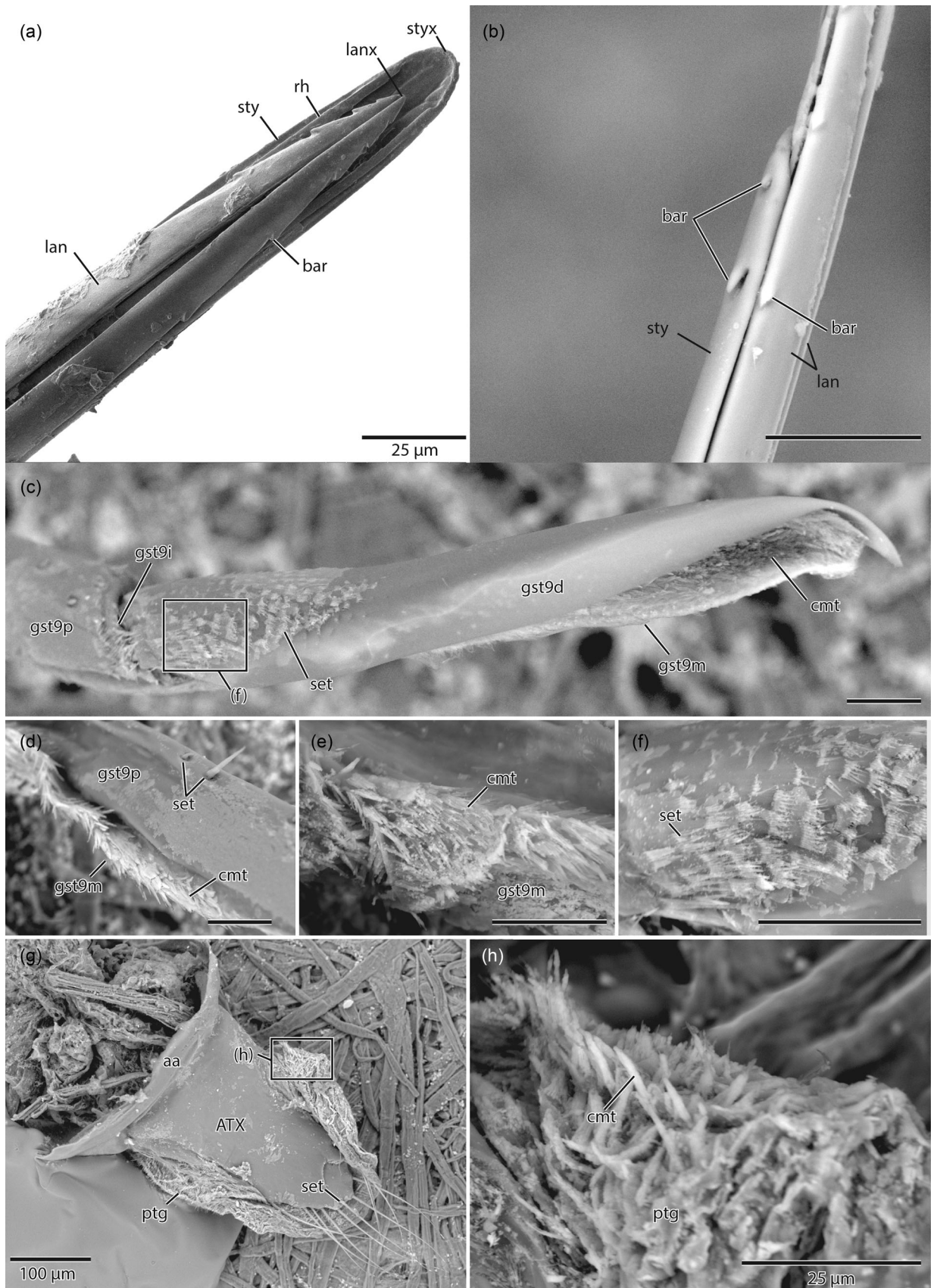
FIGURE 26 (See caption on next page)

flange of the ATIX dorsal body; **I**: apically and subapically on the posterior edge of the proximal anterior arm of gonocoxite IX, dorsad I: 9dcm2. **F**: Large, somewhat triangular, but with extensive insertion, anteroventrally directed. **(3) 9dcm2**, *M. tergo-coxalis anterior internalis* (Figures 19b and 20c,e,f). **O**: Posteriorly on the mesal surface of the posterodorsal apodeme of the ATIX dorsal body, mediad 9dcm1, laterad 9domm; **I**: on the base of the posterior edge of the anterior arm of gonocoxite IX, just dorsad the intergonocoxital articulation, at the level of the basal carina of the anterior arm. **F**: Large, broadly triangular, anteroventrally directed. **(4) 9dcm3**, *M. tergo-coxalis lateralis* (Figures 19b and 20f). **O**: Anterodorsally on the mesal surface of ATIX, just ventrad the dorsal body antecosta, on the ventral body antecosta; **I**: apically on the ectal surface and dorsal carina of the posterior arm of gonocoxite IX, on the posterodorsal apodeme and coxostylar articulation. **F**: Large, subglobular bundle (when relaxed), posteroventrally directed. **(5) 9dcm4**, *M. tergo-coxalis medialis* (Figures 19b and 20f). **O**: On the mesal surface of the posteroventral lobe of the anal arc; **I**: dorsally on the posterodorsal apodeme of the posterior arm of gonocoxite IX, mediad I: 9dcm3. **F**: Somewhat narrow, rectangular, anteroventrally and somewhat medially directed. **Coxapophyseal muscles**: **(6) 9cam1**, *M. coxo-apophysealis major anterior* (Figures 22a,d,e and 24c,e,f). **O**: On and ventrad the basal carina of the anterior arm of gonocoxite IX, anterad the intergonocoxital articulation; **I**: ectally on the dorsal arm of the furcula. **F**: Robustly spindle-shaped, anteromedially directed. **(7) 9cam2**, *M. coxo-apophysealis major posterior* (Figures 22a–f and 24c,e,f). **O**: Preapically on the mesal surface of the posterior arm of gonocoxite IX; **I**: apically and ectally on the ventral arms of the furcula. **F**: Large, vaguely spindle-shaped, curved, anteriorly directed. **(8) 9cam3**, *M. coxo-apophysealis minor* (Figures 22a,c,e–g; 24d–f; and 25a). **O**: On the ventromedial process of gonocoxite IX, as it runs behind the ventral arm of gonocoxite IX, at around the ventral third of the arm's height in posterior view; **I**: on the articular processes of the sting bulb. **F**: Small, narrowly triangular, anteroventrally directed. *Note*: These muscles were poorly resolved, and the ventromedial processes of gonocoxites IX were not segmented separately from gonocoxites IX, so the origin and insertion given here should be treated provisionally. To the degree that the origin and insertion were resolved, they match the expected positions in other taxa; but see the Discussion. **Coxocoxal intrinsic muscles**: **(9) 9ccim**, *M. coxo-coxalis interior* (Figure 28b), **O**: posteroventrally on the mesal surface of the posterior arm of gonocoxite IX; **I**: medial insertion absent; muscle is transverse; **F**: overall forming a fine transverse, diaphragm-like sheet;

anteroposteriorly thin; origins broadly triangular, medial portion narrow; runs intimately dorsad the dorsal occlusor muscle of the Dufour's gland duct.

3.3.3 | AX (M9)

Sclerites

The tenth abdominal segment is strongly reduced; its remnant is represented by a small unpaired tergital fragment, the **tenth abdominal tergite** (**ATX**, Figures 18–20 and 26g). This weakly sclerotized, approximately triangular to lobate plate articulates basally with the anal arc or posteromedial sclerotized band of ATIX (**aa**; Figures 18d; 19; and 26g). The distal apex of ATX bears around 10 long, smooth-shafted, flexuous setae (**set**, Figures 1f; 18d; and 26g) arising from narrow sockets. The entire ventral region of AX, the proctiger (**ptg**, Figures 1f; 26g,h; 29a; and 30a), is membranous and dorsally encloses the anus; this membrane is highly convoluted and clothed with cuticular microtrichia (**cmt**, Figure 26h).

Muscles

AX has no intrinsic skeletal musculature; the proctiger is moved by the orthomedial muscles of the ninth tergite (**9domm**, Figure 19b). The retractor of the anal bursa, *M. retractor ani*, may originate on the proctiger membranes, which belong partially to AX, but have no skeletal attachment (see Sections 3.5.2, 4.8.2).

3.4 | Metasomal exocrine glands and gland musculature

3.4.1 | Exocrine glands

Six exocrine glands are found in the posterior region of the abdomen (Figures 27 and 28). The paired **pygidial gland** at each side has 50–60 spherical cells with a diameter around 35 μm; these **secretory cells** (**pygs**, Figure 27b) are connected by **duct cells** (**pygd**, Figure 27b) to a median **reservoir** space (**pygr**, Figure 27b) formed by the invaginated intersegmental conjunctiva between ATVI and ATVII. We did not recognize the pygidial gland in the micro-CT scans, as the regions around the segmental articulations are filled with poorly resolved connective tissue that precludes discrimination of the gland cells. The **gonostyli gland**

FIGURE 26 *Amblyopone australis*, morphology of the distal terebra, ninth gonostylus, and tenth segment, **scanning electron microscope** (SEM). (a) apical terebra, ventral view; image courtesy of Roberto Keller, (b) apical terebra, lateral view, (c) gonostylus IX, mesal view, (d) proximal sclerite of gonostylus IX, oblique posterodorsal view, (e) mesal surface of gonostylus IX, mesal view, (f) detail proximal setae of the distal sclerite of gonostylus IX, corresponding to the outlined rectangle in (c), (g) abdominal segment X, dorsal view, (h) detail of proctiger membrane, corresponding to outlined rectangle in (g). Scale bars, a–f, g: 25 μm. Scale bar, g: 100 μm. aa, anal arc; AT, abdominal tergite; bar barbule; cmt, cuticular microtrichia; gst9d, distal sclerite of the gonostylus; gst9i, gonostylar incision; gst9m, membranous medial surface of the gonostylus; gst9p, proximal sclerite of the gonostylus; lan, lancet; lanx, apex of the lancet; ptg, proctiger; rh, rhachis of the stylet olistheter; set, seta; sty, stylet; styx, apex of the stylet

comprises a few isolated **secretory cells** (**gstgs**, Figure 27c) with a diameter of 20 μm inside each of the (ninth) gonostyli; they are connected by **duct cells** (**gstgd**, Figure 27c) that guide the secretion to the gonostylar surface. The **sting shaft gland** (**shg**, Figure 27a and 29a) is formed by an elongated patch of 80–100 round **secretory cells** (**shgs**, Figure 27d,e) that lay atop the proximal part of the stylet ("sting shaft"); slender **duct cells** (**shgd**, Figure 27d,e) carry the secretion to the ventral sting chamber. The **venom gland** is the largest abdominal organ, occupying much of the internal volume of AIV–AVI (**vg**, Figures 27a and 29a); the **venom gland duct** (**vgd**, Figures 23c3–5; 27a; 28; and 29a) has a length of approximately 1 mm and connects the sting base with an ellipsoid **reservoir** (**vgr**, Figure 27a) with a length of 1 mm and a diameter of 0.5 mm. Two slender **secretory filaments** (**vgf**, Figure 27a,f) with a length of almost 2 mm open posterodorsally into the reservoir near the connection with the venom duct (Figure 27a); the secretory filaments have a diameter of about 40 μm and contain the secretory cells that produce the actual venom. The secretory cells are arranged around a narrow central **lumen** (**vgfl**, Figure 27f), to which they are connected with short duct cells by **end apparati** (**ea**, Figure 27f). An internalized convoluted gland of the reservoir was not observed in histology or micro-CT and may be absent as in other Amblyoponinae (Schoeters et al., 1999). The **Dufour's gland** is a tubiform sac with a length around 1 mm and a diameter of 100–150 μm; its **secretory cells** (**dgs**, Figure 27g) are arranged in a monolayered epithelium with a thickness around 10 μm and an **apical cuticle** (**dgc**, Figure 27g) of 2 μm that lines the large central **reservoir** (**dgr**, Figure 27a,g). Both, the venom gland and Dufour's gland, enter the sting bulb, with the venom gland duct dorsad the Dufour's gland duct (**dgd**, Figures 27a and 28a,b); both gland ducts lie closely dorsad the median oviduct (Figure 29a). The ducts of the two glands open in the proximal portion of the sting bulb, in a tissue bulb that contains the **ducts of the sting bulb gland** (**sbgd**, Figures 23c4 and 28a). The few **secretory cells** of the sting bulb gland (**sbgs**, Figures 23c4 and 28a) have a diameter around 20 μm and are positioned between the dorsal wall of the venom gland and the dorsal wall of the sting bulb (Figure 28a).

3.4.2 | Musculature of the venom and Dufour's gland ducts

One muscle was observed inserting directly on the venom gland duct, and two on the Dufour's gland duct. While we predict all of these muscles to be extrinsic, originating on a sclerite, the origins were not resolved, precluding an origin-insertion oriented nomenclature; see Section 2.8.3. Additionally, muscle 9ccim is usually considered along with the other muscles of the Dufour's gland apparatus (Billen, 1982b, 1990a; Schoeters & Billen, 1996). We describe it with the skeletal musculature of AIX (Section 3.3.2.2) but discuss it with the other gland musculature (Section 4.7.2).

No dorsal musculature of the venom gland duct was observed; the mass of tissue surrounding the ventral venom gland duct represents *M. dilator glandulae venenalis* (**mven**, Figure 28b). *M. dilator glandulae Dufouris dorsalis* (**mdd**, Figure 28b) and *M. dilator glandulae Dufouris ventralis* (**mdv**, Figure 28b) insert on the dorsal and ventral walls of the slit-like Dufour's gland duct respectively. Both the venom gland dilator and the dorsal Dufour's gland dilator are likely paired, as in other stinging (Billen, 1990a) and non-stinging ants (Schoeters & Billen, 1996), but see Section 4.7.2 on homology of the venom gland muscles. The ventral Dufour's gland dilator is probably unpaired.

3.5 | Dorsal diaphragm, alimentary tract, reproductive organs, and central nervous system

3.5.1 | Dorsal diaphragm and vessel

The dorsal cardiac organs were only partially observable, in the region of ATV and ATVI. Overall, they were poorly and patchily resolved. The abdominal **dorsal cardiac vessel** ("heart") was only resolved in micro-CT in the region of ATIV (**dcv**, Figure 29b), but was visible more posteriorly in a few transverse histological sections targeted to visualize the pygidial gland (Figure 27b); the anterior vessel is very narrow and tubulate; ostia were not differentiable. In the micro-CT data, large, discrete **dorsal diaphragm cells** (**ddc,** Figure 29a,b) cells are visible flanking the remnants of the medial vessel; these probaby represent pericardial cells, but might include fat body, suspensory cells, or a combination of the above (Chapman et al., 2013). Longitudinal cardiac muscles were not resolved; however, the fine, dorsomedian transverse fibers presumably attaching to the dorsal vessel were partially resolved, giving a vague indication of the vessel's shape and size. Additionally, the origins of the extrinsic tergocardiac muscles were observed for AV and AVI. The tergocardiac muscles (**dkm**, Figure 29a,b) are coalesced medially as part of the diaphragm, but have long, distinct attachments and as such can be designated segmentally. Only a few large fibers of the tergocardiac muscles were resolved in both segments; these however show an indication of the "alate" or deltoid shape expected. These muscles, **5, 6dkm**, *M. tergocardiacalis* (Figure 29b), originate ventrolaterally on the respective tergite, on or just posterad the antecosta, and insert dorsomedially on the dorsal vessel.

3.5.2 | Alimentary tract

The intima of all ectoderm-derived gut elements has a somewhat granular appearance in the micro-CT data, which likely represents indistinctly resolved intrinsic circular musculature. The **esophagus** (**es**, Figure 29a,c) is elongate, narrow, and curves sinusoidally, with a ventral bend, as it enters AII; posteriorly it widens in diameter at around the longitudinal midpoint of AII, at which point the intima becomes convoluted and thickened as it transitions to the crop.
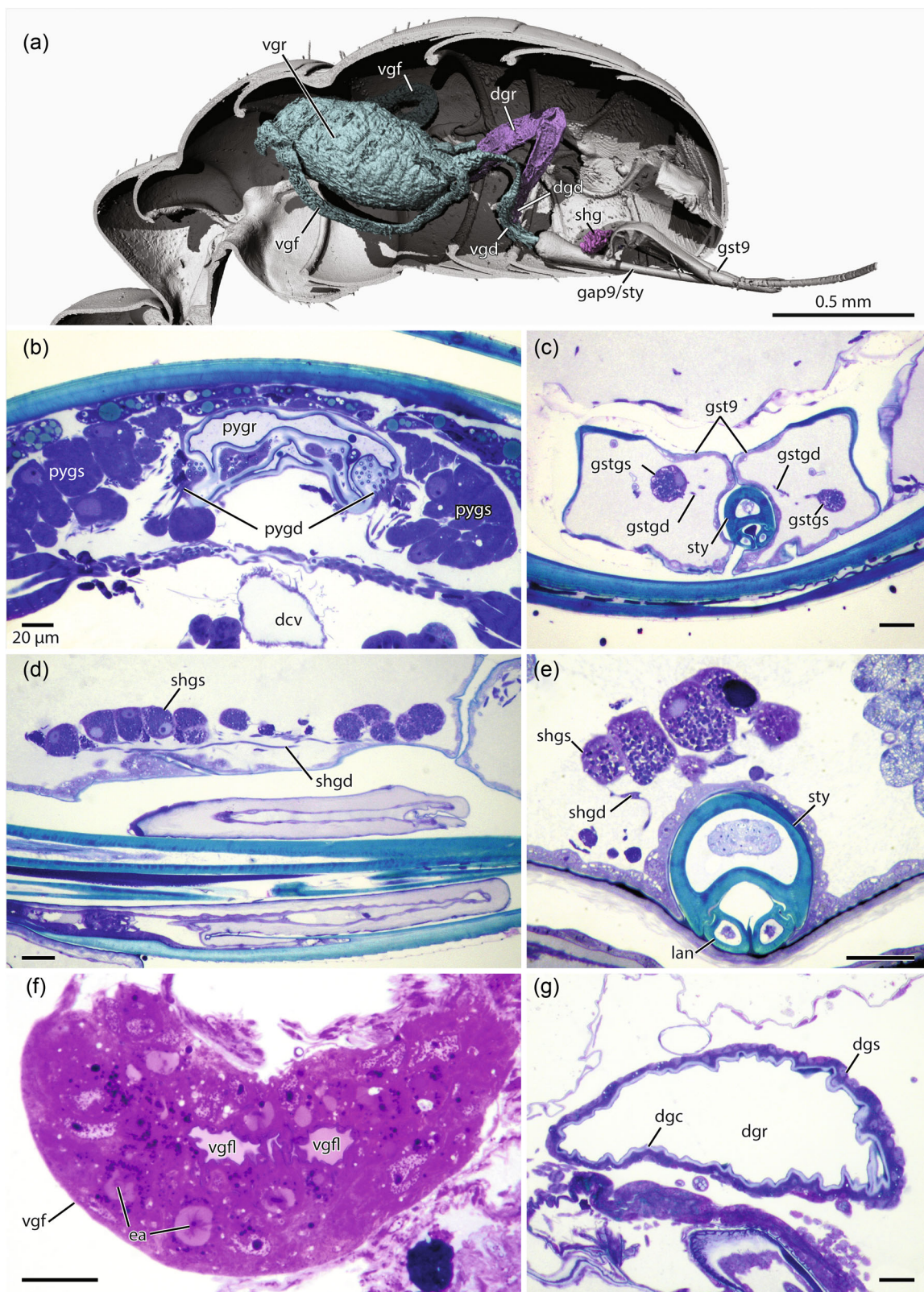
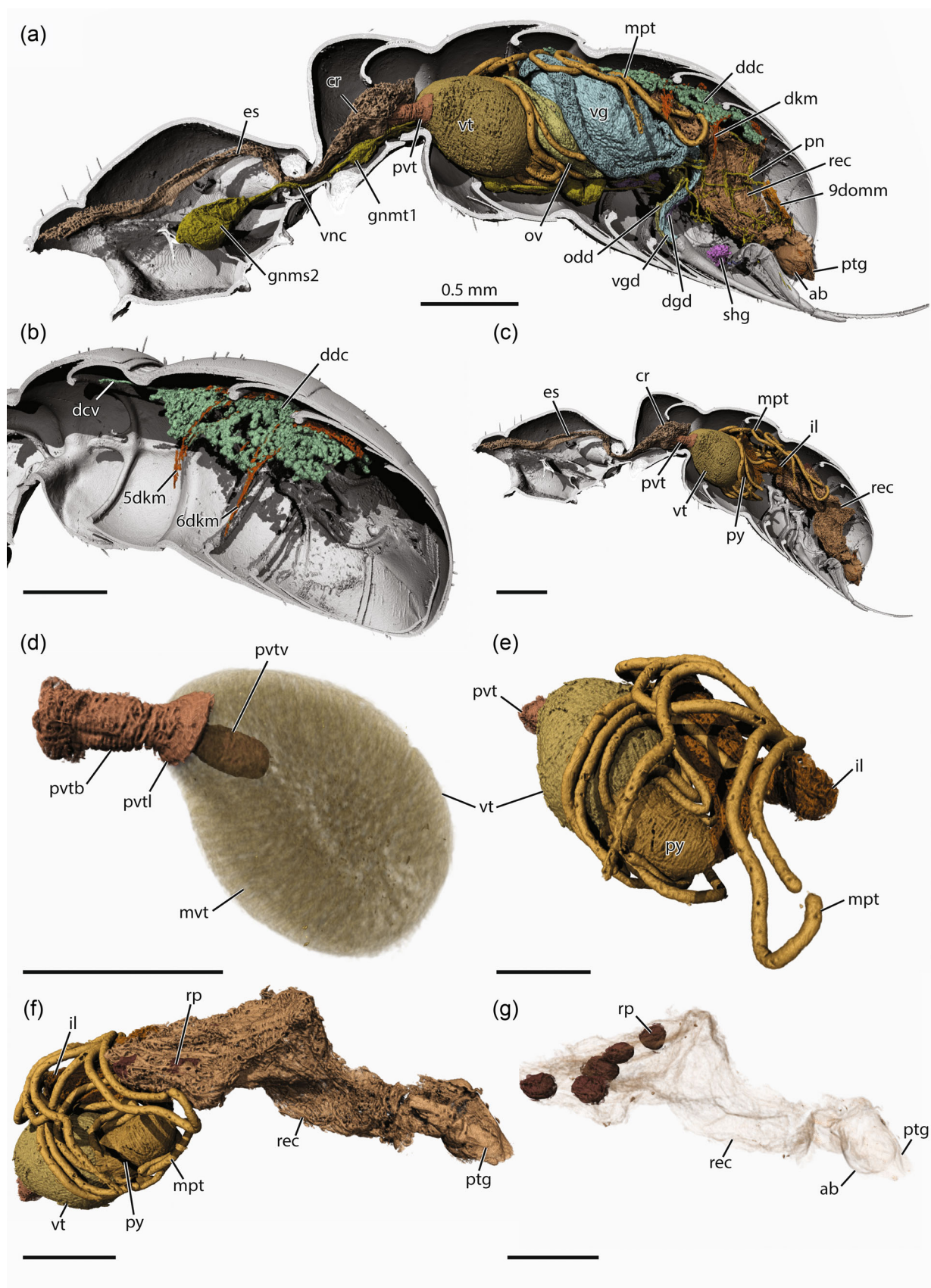**FIGURE 27** (See caption on next page)
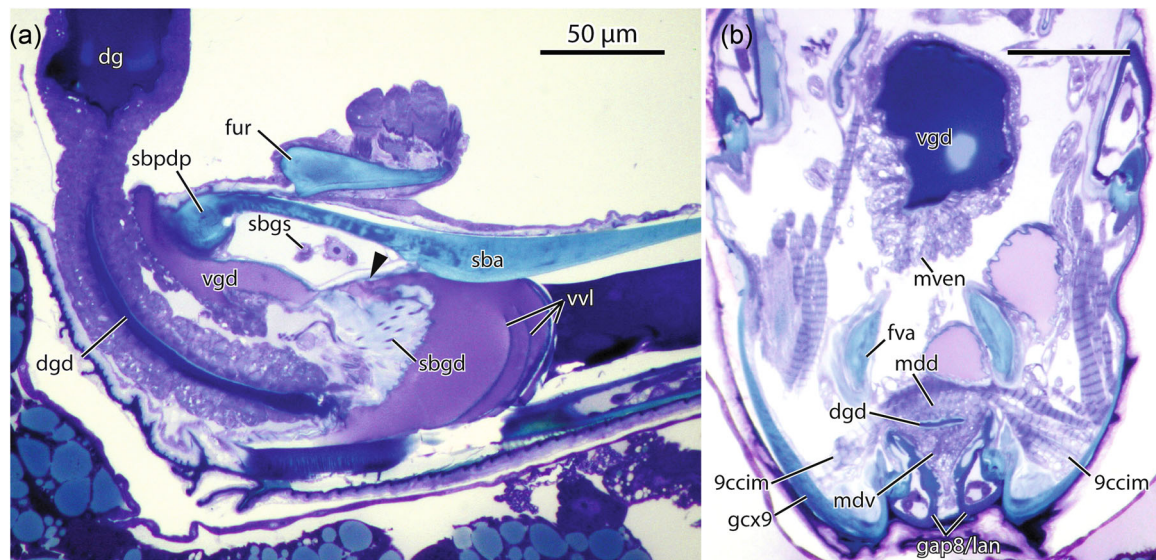
FIGURE 28 *Amblyopone australis*, exocrine glands of the sting base and musculature of the venom and Dufour gland ducts in (a) sagittal and (b) transverse histological sections. Black arrowhead in (a) indicates possible sclerotized connection of the sting bulb apophysis and venom gland duct dorsum. Scale bars: 50 μm. dg Dufour gland; dgd, Dufour gland duct; fur, furcula; fva, ventral arm of the furcula; gap8/lan, lancet of gonapophysis VIII; gcx9, gonocoxite IX; mdd, *M. dilator* glandulae Dufouris dorsalis; mdv, *M. dilator* glandulae Dufouris ventralis; mven, *M. dilator* glandulae venenalis; sba, sting bulb apophysis; sbgd, sting bulb gland duct; sbgs, sting bulb gland secretory cell; sbpdp, proximodorsal process of the sting bulb; vgd, venom gland duct; vvl, valvillus

The **crop** (**cr**, Figure 29a,c) is a relatively small pouch extending partially into the lumen of AII and surrounding the proventriculus dorsally and laterally in the anterior region of AIII; its intima is quite thick and highly convoluted, appearing somewhat thinner posteriorly, and folded inwards posteroventrally as it covers the dorsum of the proventriculus. The observable morphology of the **proventriculus** (**pvt**, Figure 29a,c–e) is as described by Eisner (1957): the **bulb** (**pvtb**, Figure 29d,e) and the **stomodeal valve** (**pvtv**, Figure 29d) are similar in overall size; the bulb parts are hexamerous (sometimes appearing superficially pentamerous in a given section), the plicae are partially membranous and arranged in a spiral around the longitudinal axis (not figured), and the proventriculus is overall poorly sclerotized; the number of longitudinal muscle bundles could not be ascertained; we also observe a much wider **anterior lip of the stomodeal valve** (**pvtl**, Figure 29d) than figured by Eisner (1957) for *A. australis*. Note that the anteriormost tissues of the proventricular bulb could not be discriminated clearly. The **ventriculus** (**vt**, Figure 29a,c–f) is a large, simple, approximately ovate chamber; its wall is thick, and likely contains a dense layer of muscle fibers, *M. ventriculi* (**mvt**, Figure 29d); cecae are absent; as the only endodermal component

of the digestive system, the ventriculus lacks a cuticular lining; however, its microvillar layer ("wall") is notably thicker than the hindgut intima. The **pylorus** (**py**, Figure 29e,f) is large and campaniform, separated from the ventriculus by a thick ring of muscular tissue, *M. sphincter pylori* (not figured); the pylorus gives rise to 10 **Malpighian tubules** (**mpt**, Figure 29a,c,e,f). The **ileum** (**il**, Figure 29c,e,f) is long and doubled over, with relatively thickened, convoluted intima. The **rectum** (**rec**, Figure 29a,c,f,g) is quite large and sac-like; its intima is thin and poorly resolved in the micro-CT data, with the entire rectum partially collapsed in the scanned specimen; six subcircular to ovate **rectal pads** (**rp**, Figure 29e,f) are present in the anterior region of the rectum, near the junction with the ileum; the rectal pads are probably arranged radially, but are distorted in the scan; they have a distinct cuticular envelope, while their interior is highly convoluted in the scan, these convolutions corresponding to the invaginations of the basal plasma membrane. Apically, the rectum bends dorsally and bears a dilation, the **anal bursa** (**ab**, Figure 29f,g), which has thicker membrane and is partially divided from the rectal lumen by membrane; dorsally the anal bursa connects to the ventral membrane of the tenth tergum, forming the lobate flap of the **proctiger** (**ptg**,

FIGURE 27 *Amblyopone australis*, exocrine glands of the posterior metasoma. (a) Three-dimensional (3D)-reconstruction, lateral view, sclerites sagittally bisected, (b–g) histological sections along the sagittal axis (d) and the transverse axis (b, c, e–g). Scale bar, a: 0.5 mm. Scale bars, b–g: 20 μm. dcv dorsal (cardiac) vessel; dg, Dufour gland; dgc, Dufour gland apical cuticle; dgr, Dufour gland reservoir; dgs, Dufour gland secretory cell; dgs, Dufour gland secretory cell; ea, end apparatus; gst9, gonostylus IX; gstg, gonostyli gland; gstgd, gonostyli gland duct cell; gstgs, gonostyli gland secretory cell; lan, lancet; pyg, pygidial gland; pygr, pygidial gland reservoir; pygs, pygidial gland secretory cell; shg, sting shaft gland; shgd, sting shaft gland duct cell; shgs, sting shaft gland secretory cell; sty, stylet; vg, venom gland; vgf, venom gland secretory filament; vgfl, lumen of venom gland secretory filament

FIGURE 29 (See caption on next page)

Figures 29a,f,g and 30a). The wall of the anal bursa has a circular layer of muscle, *M. sphincter ani* (**msan**, Figure 30b) the dorsal margins of which also receive the insertions of a group of longitudinal muscles apparently originating anteriorly on the proctiger, *M. retractor ani* (**mran**, Figure 30b); the ninth dorsal orthomedial muscles, 9domm, insert dorsoapically on the proctiger (Figure 30b) and are probably involved in excretion along with the nonskeletal anal muscles.

3.5.3 | Reproductive organs

Ovaries (**ov**, Figure 29a) are present and well-developed, with four **ovarioles** (**ovl**, Figure 30c) each; the ovarioles are meroistic polytrophic as expected for Hymenoptera (Chapman et al., 2013). The **lateral oviducts** (**odl**, Figure 30c) are large and well-sclerotized on their lateral edges, with a sclerotized **distal arch** (**odla**, Figure 30c) at the aperture of the oviduct, where it adjoins the distal **vitellarium** (**vit**, Figure 30c,d) in which oogenesis occurs. Posteriorly, the lateral oviducts join medially as the **median oviduct** (**odm**, Figure 30c); after a short stretch the median oviduct is laterally expanded and thickened, forming the **distal oviduct** (**odd**, Figures 29a and 30c), a dilated region which is sclerotized laterally and membranous dorsomedially, and which is dish-like in the scanned specimen; this thickened flap is distally infolded, forming a small dorsoventral pocket; distad this fold, the ventral wall of the oviduct is notably more strongly sclerotized than the dorsal wall, which is extremely thin and intimately approximated with the venom and Dufour's gland ducts (Figure 29a), forming a roughly triangular sclerotized lobe (Figure 30c, black arrowhead). Spermathecae were not observed.

The median oviduct and distal oviduct run closely ventrad the ducts of the venom and Dufour's glands and dorsad gonapophyses VIII; it apparently opens at the most proximal part of the sting base. **Oocytes** (**ooc**, Figure 30c,d) and multinucleate **trophocytes** (**trc**, Figure 30c,d) are present, connected by cytoskeletal **ring canals** (**rc**, Figure 30d; Gutzeit et al., 1993); five or more trophocyte nuclei per cell (**trcn**, Figure 30d) were resolved; yellow bodies were not observed. Musculature of the oviduct was not observed.

3.5.4 | Central nervous system

The abdominal **ventral nerve cord** (**vnc**, Figures 29a and 30e) has five discrete **ganglia**, connected by two parallel, longitudinal **connectives** (**con**, Figures 7d and 30e) of the cord; four fibers are apparently present between the second mesosomal and first metasomal ganglia, and between the first and second metasomal ganglia (Figure 7d), but these may not represent connectives (they were only partially resolved); the nerve cord was also not resolved in a small area around the presternite of AIII. The connectives appear to coalesce as a single branch from the fourth metasomal to the terminal ganglion, but they may be paired and closely approximated; posteriorly, only one distinct connective was clearly resolved in micro-CT, but this is situated laterally, suggesting the presence of the other.

The **second mesosomal ganglion** (**gnms2**, Figures 29a and 30e) is large and situated more or less mesad the metapleural gland atria; it is visibly composite, with three lobes; the **first metasomal ganglion** (**gnmt1**, Figures 7d and 30e) is located in the petiole, and occupies much of the petiolar poststernital volume (Figure 7d); the **second metasomal ganglion** (**gnmt2**, Figure 30e) is well-separated from the first, located in the anterior region of ASIV; the third and fourth metasomal and terminal ganglia are positioned closely together, in the posterior region of AIV and the anterior region of AV. The **third metasomal ganglion** (**gnmt3**, Figure 30e is somewhat smaller and subglobular; the **fourth metasomal ganglion** (**gnmt4**, Figure 30e is larger and more elongate-ovate; the **terminal ganglion** (**gnt**, Figure 30e) is large and subspherical. Peripheral nerves (**pn**, Figures 29a and 30e) were only well-resolved arising from the terminal ganglion; these are long and highly ramified and innervate (at least) the posterior ileum, the rectum, the muscles of AIX, the median oviduct, and the ducts of the Dufour and venom glands (Figure 29a).

4 | DISCUSSION

4.1 | Pregenital skeleton

4.1.1 | Apodemes

Segments AIV–AVII bear a single pair of anterolateral apodemes on the antecostae of the tergite and sternite, while AII and AIII bear only modified sternal apodemes. In AII the sternal apodemes are functional, serving as insertion sites for the ventral muscles of the metasternum; in AIII they are likely nonfunctional, as they do not receive muscle attachments, and are closely approximated to the tergital antecosta. This condition in AIII is likely related to the general

FIGURE 29 *Amblyopone australis*, morphology of nonskeletomuscular organ systems (a), the dorsal diaphragm (b), and the alimentary tract (c–g); 3D reconstruction. (a) soft tissue habitus, sagittal bisection; (b) dorsal diaphragm, oblique posterior view of sagittal bisection; (c) alimentary tract, sagittal bisection; (d) proventriculus and ventriculus, lateral view, ventriculus translucent; (e) proventriculus, ventriculus, pylorus, and ileum, oblique posterior view; (f) ventriculus and hindgut, lateral view; (g) rectum (translucent). Scale bars: 0.5 mm. ab, anal bursa; cr, crop; dcv, dorsal (cardiac) vessel; ddc, dorsal diaphgragm cell; ddc, dorsal diaphgragm cell; dgd, Dufour gland duct; dkm, tergocardiac muscle; domm, dorsal orthomedial muscle; es, esophagus; gnms2, second mesosomal ganglion; gnmt1, first metasomal ganglion; il, ileum; mpt, Malpighian tubule; mvt, *M. ventriculi*; ov, ovary; pn, peripheral nerve; ptg, proctiger; pvt, proventriculus; pvtb, bulb of the proventriculus; pvtl, anterior lip of the proventriculus; pvtv, stomodeal valve; rec, rectum; rp, rectal pad; shg, sting shaft gland; vag, vagina; vg, venom gland; vgd, venom gland duct; vnc, ventral nerve cord; vt, ventriculus
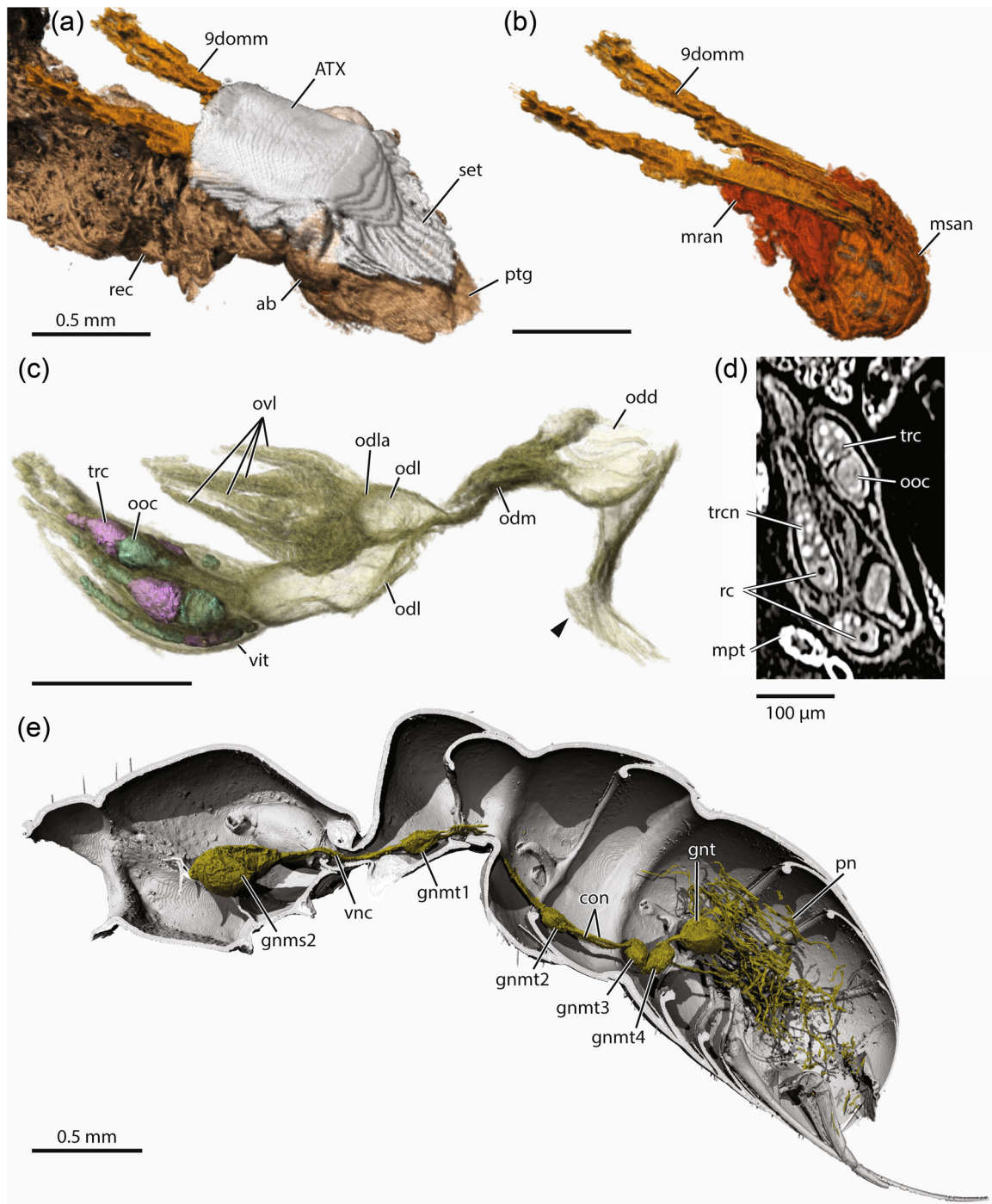
FIGURE 30 *Amblyopone australis*, excretory, reproductive, and central nervous organs; three-dimensional (3D)-reconstruction (a–c, e), sagittal CT section (d). (a) tenth abdominal segment and rectum, oblique posterior view; (b) muscles of the anus and proctiger, equivalent view to (a); (c) reproductive organs, translucent, oblique ectal view (d) left ovary, sagittal section; (e) central nervous system, sagittal bisection. Black arrowhead indicates sclerotized lobe of the distal oviduct. Scale bars, a–c, e: 0.5 mm. Scale bar, d: 100 μm. ab, anal bursa; con, connective of the ventral nerve cord; domm, dorsal orthomedial muscle; gnms2, second mesosomal ganglion; gnmt1–4, first to fourth metasomal ganglion; gnt terminal ganglion; mpt, Malpighian tubule; mran, *M. rectractor ani*; msan, *M. sphincter ani*; odla, distal arch of the lateral oviduct; odla, distal arch of the lateral oviduct; odm, median oviduct; ooc, oocyte; ovl, ovariole; pn, peripheral nerve; ptg, proctiger; rc, ring canal; rec, rectum; set, seta; trc, trophocyte; trcn, trophocyte nucleus; vag, vagina; vit, vitellarium; vnc, ventral nerve cord

loss and modification of muscle groups in relation to tergosternal fusion in the anterior metasoma (see below). While the tergal apodemes are always simple in form, those of ASV–ASVI bear elaborate, malleate apical process, increasing the area for muscle attachment.

The posterodorsal angle of the seventh sternite in *Amblyopone* superficially resembles another apodeme, such as the lateral apodeme of *Apis* (Snodgrass, 1942). However, the pattern of muscle insertion on the anterolateral apodemes in ASVII is conserved with that of prior segments, and only a dorsoventral intrinsic muscle inserts on the posterodorsal angle (7dvimm1); its homolog in *Apis* does not insert on the lateral apodeme, but similarly on a posterolateral expansion of the sternite (Snodgrass, 1942). It seems therefore that the posterodorsal angle is not homologous to the lateral apodeme but is a consequence of the dorsolateral sternal profile and its continuity with the antecosta.

4.1.2 | Sternal apodemes in the ants

Preliminary sampling of various outgroups and all major lineages of ants, except the leptanillomorphs, reveals that a single pair of sternal apodemes in the posterior pregenital abdomen is the predominant character state within both Formicidae and among major Hymenopteran clades (Table 3). Beyond the primary observations on ants here, a single pair of anterolateral apodemes was also reported in in the anterior metasoma of the male of *Dorylus* sp. (Short, 1959), the seventh sternite of *Solenopsis richteri* (Callahan et al., 1959), and all pregenital segments of *Myrmica rubra* (Janet, 1902). Preliminary segmentation of the male of *Lioponera* sp. demonstrates a single pair of malleate anterolateral sternal apodemes in the posterior pregenital segments.

Some ant species have no apodemes on one or more segments; a second pair is not known to be present in workers, but has been derived on ASIX in the males of some *Leptomyrmex* species (Barden et al., 2017). When the apodemes are present, their degree of development and the expansion of their apices into malleate processes varies both among and within lineages. This pattern of variation suggests that trait values of the sternal apodemes may be systematically informative at several taxonomic levels.

Some subjective correlations can be drawn between the development of the sternal apodemes and several general morphological characters of the ants in Table 3: (1) the thickness of the cuticle; (2) the development of the sting; (3) hypertrophied anterior gastral segments; and (4) body size. Note that these putative relationships were not interrogated quantitatively or statistically. In general, larger ants with thicker exoskeletons, enlarged anterior gastral segments, and a functional sting have larger, more robust apodemes with more dilated apical processes. In the Formicinae and Dolichoderinae the sting is nonfunctional; formicines have minute falcate apodemes on ASVI and may lack apodemes entirely in at least AV, while the sampled dolichoderines appear to lack apodemes on both ASV and ASVI. This suggests that the loss of the sting is

associated with reduced abdominal strength and range of motion. Gross gastral movements facilitated by the mesosomal and petiolar muscles may suffice for these ants, which spray venom or disseminate semiochemicals from the abdomen from a distance. Considerable insight into this question will be provided by sampling *Aneuretus*, the stinging sistergroup of Dolichoderinae.

Alternately, the apparent relationship between sting and apodeme loss might be primarily due to the tendency of lineages of stinging ants to have more robust skeletons, that is, we acknowledge the probability of autocorrelation in the four morphological variables considered above. In *A. australis*, the anterolateral apodemes of each segment receive the protractors, which are large dorsal and ventral paramedial muscles. The ventral paramedials are notable among the intersternals in that they are consistently present and similarly developed, even when their antagonists, the ventral orthomedials, are absent. The consistent presence of the tergal and sternal protractors, and their nearly identical form, suggests that their function is well-conserved. The variable expression of elements that participate in this function may therefore indicate a change in selective pressure on abdominal mobility, or the development of an alternative mechanical solution with comparable functional outcomes. Whether the lack of apodemal insertion areas is compensated for by a muscular rearrangement, or if it implies reduced strength and/or mobility of the metasomal segments, will require additional anatomical investigation at a minimum, and preferably biomechanical study.

4.1.3 | Sternal apodemes in the Hymenoptera

The presence of sternal apodemes in general appears to be a multiply derived state in insects. There may be none, a single anterolateral pair, a more posterior lateral pair, both lateral pairs, and one or two anteromedian apodemes. Among the ametabolous and hemimetabolous insects, sternal apodemes are absent in, for example, Archaeognatha (Bitsch, 1973; Matsuda, 1957), Zoraptera (Hünefeld, 2007), Mantodea and Blattodea (Klass, 2008b; Shankland, 1965), Enicocephalomorpha (Hemiptera; Davranoglou et al., 2017), and Psocodea (Badonnel, 1934). A single lateral pair occurs in Dermaptera (Klass, 2001), and Cicadidae (Hemiptera; Vasvary, 1966). Two pairs of apodemes are present in at least some Odonata (Klass, 2008a) and some Orthoptera (Snodgrass, 1935a), though other orthopterans lack ventral sclerites entirely (Consoulas & Theophilidis, 1992). In the Endopterygota, sternal apodemes are absent in various Diptera (Bonhag, 1951; Ovtshinnikova & Galinskaya, 2016; Ovtshinnikova, Galinskaya, & Lukashevich, 2018; Pollock, 1999), Siphonaptera (Snodgrass, 1947), and the neuropteroid groups Chrysopidae (Miller, 1933) and Raphidioptera (Matsuda, 1957). In Hymenoptera, two pairs of sternal apodemes, anterior and lateral, occur in at least the anterior abdomen of *Urocerus* ("symphyta"), and in all the pregenital metasomal segments of *Apis* (Short, 1959; Snodgrass, 1942). A single pair of anterolateral sternal apodemes occurs in several aculeate groups, including other Apidae (*Bombus*), Vespidae,

TABLE 3 States of the sternal apodemes of the posterior pregenital segments in ants and major aculeate clades.

Family	Subfamily	Genus	Species	Sex	ASV	ASVI	Form	Notes
Formicidae	Amblyoponinae	*Amblyopone*	*australis*	w	1	1	M	
Formicidae	Amblyoponinae	*Stigmatomma*	*pallipes*	w	1	1	M	
Formicidae	Dolichoderinae	*Anonychomyrma*	cf. *murina*	w	0	0	-	AVI very slightly angular but not produced into apodemes
Formicidae	Dolichoderinae	*Dolichoderus*	*cuspidatus*	w	0	0	-	
Formicidae	Dolichoderinae	*Leptomyrmex*	*fragilis*	w	0	0	-	AVI very slightly angular but not produced into apodemes
Formicidae	Dolichoderinae	*Tapinoma*	*sessile*	w	0	0	-	
Formicidae	Dorylinae	*Dorylus*	indet.	w	1	1	F	Subgenus *Anomma*; small workers examined
Formicidae	Dorylinae	*Eciton*	*vagans*	w	1	1	F	
Formicidae	Dorylinae	*Labidus*	*praedator*	w	1	1	F	
Formicidae	Dorylinae	*Simopone*	*conradti*	w	1	1	F	Apodemes large, somewhat dilated
Formicidae	Ectatomminae	*Ectatomma*	*tuberculatum*	w	1	1	M	
Formicidae	Ectatomminae	*Gnamptogenys*	cf. *rastrata*	w	1	1	M	
Formicidae	Formicinae	*Camponotus*	nr. *sericeus*	w	0	1	F	Apodemes minute
Formicidae	Formicinae	*Camponotus*	*whitei*	w	0	1	F	Apodemes minute
Formicidae	Formicinae	*Formica*	*moki*	w	1	1	F	Apodemes very small
Formicidae	Formicinae	*Myrmelachista*	*mayri*	w	0	0	-	
Formicidae	Myrmeciinae	*Myrmecia*	*pilosula*	w	1	1	M	
Formicidae	Myrmicinae	*Atta*	*cephalotes*	w	1	1	F	Large minor workers examined
Formicidae	Myrmicinae	*Crematogaster*	*mutans*	w	1	1	F	Apodemes minute
Formicidae	Myrmicinae	*Manica*	*invidia*	w	1	1	R	
Formicidae	Myrmicinae	*Pogonomyrmex*	*subdentatus*	w	1	1	F	
Formicidae	Ponerinae	*Bothroponera*	*crassa*	w	1	1	F	
Formicidae	Ponerinae	*Diacamma*	cf. *rugosum*	w	1	1	M	
Formicidae	Ponerinae	*Odontomachus*	*bauri*	w	1	1	M	
Formicidae	Proceratiinae	*Proceratium*	*deelemani*	w	1	1	F	Apodemes quite elongated
Formicidae	Pseudomyrmecinae	*Pseudomyrmex*	*salvini*	w	1	1	F	
Formicidae	Pseudomyrmecinae	*Tetraponera*	*rufonigra*	w	1	1	F	
Chyphotidae	Typhoctinae	*Typhoctes*	cf. *peculiaris*	♀	1	1	F-T	Apodemes fairly large but less sclerotized than antecosta or posterior sternite
Chyphotidae	Cyphotinae	*Cyphotes*	indet.	♂	1	1	F	Apodemes elongate-falcate
Mutillidae	indet.	indet.	indet.	♂	1	1	F	Apodemes elongate-falcate
Pompilidae	Pepsinae	*Pepsis*	indet.	♀	1	1	F	Apodemes large, robust, externally marginated, leaving a trapezoidal, depressed medial portion
Thynnidae	Myzininae	*Myzinum*	*dubiousum*	♀	1	1	F	
Thynnidae	Myzininae	*Myzinum*	*dubiousum*	♂	1	1	F	
Vespidae	Eumeninae	*Ancistrocerus*	cf. *campestris*	♀	1	1	F-T	

TABLE 3 (Continued)

Family	Subfamily	Genus	Species	Sex	ASV	ASVI	Form	Notes
Apidae	Apinae	*Apis*	*meliifera*	w	2	2	F (anterior); D (posterior)	
Apidae	Apinae	*Apis*	*meliifera*	♀	2	2	F (anterior); D (posterior)	
Chrysididae	Loboscelidiinae	*Loboscelidia*	indet.	♀	1	1	R	Apodemes very narrow and elongated, with truncate or slightly recurved apices
Chrysididae	Chrysidinae	*Chrysis*	indet.	♂	1	1	T	Apodemes triangular in anterior pregenital segments, ASV and ASVI with deeply emarginate anterior border, leaving broadly triangular anterolateral prolongations
Chrysididae	Cleptinae	*Cleptes*	*alienus*	♂	1	2?	R	Anterior pregenital segments with broadly truncate apodemes; AVI anterolaterally incised, leaving an anterolateral pair of truncate apodemes and a posterolateral lobe which might be apodemal
Chrysididae	Amiseginae	*Adelphe*	*anisomorphae*	♂	1	?	T	AVI extremely reduced, precluding determination from the illustrations

Note: Dashed lower border divides primary observations on ants from primary observations on outgroups. Solid bold lower border divides primary observations from literature references. Species column abbreviations: cf., onfer, species determination somewhat uncertain; indet., taxon indetermined; nr., near, taxonomy possibly insufficient for species determination; -, inapplicable (apodemes absent). Sex column symbols: w, worker; ♂, male; ♀, female. Numbers in columns ASV and ASVI indicate number of apodeme pairs on abdominal sternites V and VI. Form column refers to the overall shape of the apodemes. A question mark (?) indicates uncertainty, see **Notes** column. Literature references: *Apis*, Snodgrass (1942); *Loboscelidia*, Day (1979); *Chrysis*, *Cleptes*, *Adelphe*, Kimsey (1992).

Abbreviations: D, digitate; F, falcate; M, malleate; R, truncate; T, triangular; F-T, falcate-triangular.

(Short, 1959), Megachilidae (Fischer, 1956), and some Chrysididae (Day, 1979; Kimsey, 1992). Other chrysidids have clear anterolateral apodemes on the anterior pregenital segments, while the posterior pregenital and genital-postgenital segments are highly reduced but retain anterolateral sternal prolongations (Kimsey, 1992). In male *Auplopus* (Pompilidae), ASVI bears one definitive pair of anteromedial apodemes, and has pronounced, rounded anterolateral angles (Kimsey, 1992; Loktionov & Lelej, 2008). We observed a single pair of apodemes in ASV and ASVI in the female of *Typhoctes* cf. *peculiaris* and the male of *Chyphotes* sp. (Chyphotidae), a *Pepsis* female (Pompilidae), the female *Chalybion californicum* (Sphecidae), the male and female of *Myzinum dubiosum* (Thynnidae), the female of *Ancistrocerus* cf. *campestris* (Vespidae), and an unidentified male mutillid (Table 3).

Because of this variability in the development of the sternal apodemes at quite different phylogenetic depths, we cannot confidently infer the transformation series leading to the ant condition. Possibilities include: (1) the sternal apodemes of ants are autapomorphic to the family; (2) a single pair of apodemes is the plesiomorphic state for Hymenoptera, and the two pairs in apoids and other clades are singly or severally derived from an "ant-like" state; or (3) two pairs of sternal apodemes is the ordinal plesiomorphy, as suggested by their presence in at least some

"symphyta" and Apoidea, and the single pair in ants represent (3a) the loss of one pair, or (3b) fusion of the anterior and lateral pairs, the latter being the explanation proposed by Short (1959). If (3) is true, we consider (3b) to be more parsimonious than (3a) due to the pattern of muscle insertions. In *Apis*, the ventral orthomedial, ventral paramedial, and dorsoventral extrinsic muscles insert on the anterior sternal apodemes, while the dorsoventral intrinsic muscles insert on the lateral apodemes (Snodgrass, 1942). In contrast, the anterolateral apodemes of *Amblyopone* receive the insertions of all four groups. Deeper sampling is necessary to resolve these outstanding questions.

4.1.4 | Metapleural gland atrium

The metapleural gland is the canonical synapomorphy of Formicidae, which is usually retained in females across taxa, with a few notably exceptional lineages (Bolton, 1994, 2003; Boudinot, 2015; Hölldobler & Engel-Siegel, 1985). The ultrastructure of the gland and, to an extent, the atrium, have received careful attention in a number of descriptive and comparative works (Billen & van Boven, 1987; Billen, 2017; Gusmão et al., 2001; Hölldobler & Engel-Siegel, 1985; Schoeters & Billen, 1992, 1993; Tulloch et al., 1963, 1963; Tulloch, 1936; Yek & Mueller, 2011). However, the overall skeletal

morphology of the metapleural gland atrium, in particular its anterior region, has been inadequately treated, with most focus on the gland orifice (e.g., Keller, 2011). We consider that the present "one- and two-chambered" categorization of the atrium (Yek & Mueller, 2011) insufficiently captures the variation evident in this region. The two-chambered form is defined by a "clear constriction between a membranous collecting sac and a sclerotized atrium" (Yek & Mueller, 2011, p. 780). However, we find that the degree of sclerotization of the "collecting sac" (= secretory receptacle) and its degree of differentiation by a constriction are both variable among lineages (Hölldobler & Engel-Siegel, 1985; Tulloch et al., 1963). In fact, the figure which illustrates the "membranous collecting sac" characteristic of the two-chambered design (fig. 3 of Yek & Mueller, 2011) is reproduced with modification from Tulloch et al. (fig. 1, 1963), who describe this area as being differentiated by "differences in wall texture," with specific reference to the sieve plates and spiral rugae, rather than by degree of sclerotization (p. 92). In *A. australis*, the secretory recess is clearly differentiable by the presence of the sieve plate and the strongly developed spiral rugae (Figure 4), and is internally delimited by the large secretory recess ridge. On the other hand, the entire atrium is strongly and similarly sclerotized, and is externally only weakly constricted at the secretory recess sulcus (Figures 3 and 4). According to the former characters, the atrium matches the illustration of Tulloch et al. (1963), except in the number of sieve plates, which by extension should imply a two-chambered design. Contrarily, the latter combination of characters would classify it as a one-chambered atrium (Yek & Mueller, 2011). While we appreciate the likely systematic and functional importance of compartmentalization of the atrium, and the comparative utility of recognizing these parts, additional investigation is required to accurately characterize the apparent cline of trait variation. One possibly important difference in subregions of the atrium is the degree of fusion or continuity with the body wall.

4.1.5 | Invaginations

In addition to the dorsal and ventral intrasegmental folds, the ventral margin of the posttergite and dorsal margin of the poststernite bear infoldings, which continue as membrane. That of the posttergite extends dorsally into the body cavity, while that of the presternite continues ventrally into the body cavity. In AIII–AIV, which are tergosternally fused, these invaginations are basally fused to one another and overall enlarged and sclerotized, forming a digitate cuticular thickening posteriorly connected to the intersegmental conjunctivae. These thickenings can frequently be seen through the translucent tergites without magnification. In manual dissection, the membranous portions can be easily removed, leaving the sclerotized thickenings apparent. Preliminary observations across major ant nodes indicate that this condition is usually absent and may therefore have systematic value. Additionally, since the membranes of the dorsal and ventral intersegmental folds form clear contact surfaces for the successive presclerites, it is likely that these lateral processes

have functional significance as well, possibly in moderating frictional forces, or stabilizing the gaster as during retraction and flexion.

4.2 | Pregenital skeletomusculature

4.2.1 | Overview

Most segments of the abdomen are highly modified. ATI is fused to the metathorax and ASI is lost, as expected for the Apocrita; AII–AIV participate in gross movements of the gaster (Hashimoto, 1996), and AIII–AIV are tergosternally fused. AVII encloses and moves elements of the sting apparatus, which comprises the remnants of AVIII and AIX, while AX is extremely reduced to a small tergal fragment that lacks intrinsic skeletal musculature. By contrast, AV and AVI have simple presclerites, are not tergosternally fused, and show little reduction of musculature relative to other aculeates, particularly in AVI (Snodgrass, 1956; Youssef, 1968). We therefore consider the unreduced muscular and simple skeletal state of AVI to be the closest approximation of the neopteran groundplan in ants for the pregenital abdominal segments in the following discussion (see Section 4.3 on homology inference).

The abdominal muscles originating in the mesosoma match those of *Myrmica rubra* (Janet, 1898b) *Formica* (Aibekova et al., 2022; Markl, 1966), and *Myrmecia nigrocincta* (Liu et al., 2019): a ventral orthomedial muscle (IIIvomm) runs from the metafurca to the petiolar presternite and a ventral ortholateral muscle (IIIvolm) runs from the metadiscrimen to the petiolar anterolateral apodemes. We note that IIIvolm corresponds to IIIvlm3 of the neopteran groundplan (Friedrich & Beutel, 2008), suggesting partial or at least ancestral homology of the posterior portion of the metadiscrimen with the metaspina, although it has been labeled as IIIvlm7 by Liu et al. (2019). We observed the same muscles of AII–III as Hashimoto (1996) for *A. australis*, except we describe the dorsal paramedial 2dpmm, which Hashimoto (1996) does not figure. In *Myrmica rubra*, in which both AII and AIII are petiolated, with nodiform posttergites, 2dpmm is apparently absent (Janet, 1894), but 3dpmm is well-developed; Janet (1894) infers 3dpmm to be rotators of the gaster.

In *Amblyopone*, the number of muscle groups in each segment increases in the posterior direction from AI to AVI: the metafurca and AI each bear two muscle groups, AII and AIII have four, AIV has five, AV has seven, and AVI has nine. The functional implications of the modifications of AII–AIII are an increase in power (Hashimoto, 1996) with concomitant modification of the range of motion (Dlussky & Fedoseeva, 1988). The pattern of muscle reduction and elongation in the anterior direction therefore suggests a transition in selection on strength in the anterior metasoma to selection on fine motor control in the posterior metasoma. Mid-abdominal musculature should be evaluated in future studies, as it remains neglected, although possibly quite conserved.

4.2.2 | Variation

Excluding the spiracular muscles, which were not examined in detail, AVI of *A. australis* has the same muscles as *Apis* (Snodgrass, 1942)

with three primary differences: (1) the dorsoventral intrinsic medial (= second lateral) muscle is absent; (2) the dorsal ortholateral muscles are bipartite (6dolm1, 6dolm2 = 167 of Snodgrass); and (3) the dorsoventral intrinsic lateral muscles (5–7dvilm = 160, 171, 182 of Snodgrass) have their origin on the anterolateral tergal apodeme, rather than the anteroventral tergite. The third difference implies that either (a) the origin of the dvilm (and other) muscles can shift across the antecosta, or (b) that the antecosta of *Apis* curves ventrolaterally around the tergite. Unfortunately, Snodgrass (1942) did not sufficiently illustrate the tergites of *Apis* to evaluate the condition of the acrosclerite from the literature alone. Furthermore, tergal apodemes are also likely multiply derived in various insect lineages. In Archaeognatha the dvilm originate on or just posterad the antecosta (Bitsch, 1973). In *Dissosteira* (Orthoptera) and *Geotrupes* (Coleoptera) the dvilm originate on a post-antecostal part of the tergite (Hieke, 1966; Snodgrass, 1935b). That the tergal muscles can display at least some range of origin positions is also evinced by 3, 4, and 7domm. Specifically, 3 and 4domm originate posteromedially on the antecosta, while 7domm originates on the anterolateral tergal apodemes and, in *Apis*, the origin of 3domm (133 of Snodgrass, 1942) is immediately posterad the antecosta. It is possible that origin of 3domm on the antecosta is a derived condition, as it was observed by Hashimoto (1996) in Myrmicinae, Pseudomyrmecinae, Myrmeciinae, Ectatommini, and *Cerapachys*, but not in Ponerini or other aculeates. Development of the dorsolateral sternal margination and its apparent continuity with the antecosta suggests that (b) above may also be biologically plausible.

4.2.3 | Potential consequences of tergosternal fusion

With the exception of the intrinsic dorsoventral muscles (2dvilm), the anterior pregenital segments lack dorsoventral musculature. As noted by Hashimoto (1996), this is probably in relation to tergosternal fusion, because the entire fused segment can be moved by the dorsal ortholateral muscles which insert ventrally at the tergosternal junction. Additionally, the major movements of the gaster effected by the muscles of AII–AIV are depression, elevation, and rotation; compression of the anterior segments is apparently not an important function. Since these segments are also larger and more sclerotized than those following, which can telescopically retract, loss of compressive function seems like a reasonable mechanical optimization. We hypothesize that 2dvilm may serve to brace the unfused petiole during the rigorous act of stinging.

The absence or reduction of ventral musculature in the anterior segments may also be related to tergosternal fusion. In general, the ventral orthomedial and ortholateral muscles appear to be modified away from their retractive function across the abdomen. It is possible that the protractors of the tergum and sternum (dorsal and ventral paramedial muscles) compensate for this reduction in conjunction with the tergal retractors (dorsal orthomedial and ortholateral muscles). Dilation of the segment followed by retraction of the

following tergum may produce telescoping of the posterior segments. However, mechanical investigations in the present study were limited to gross manual manipulation of segments in the undissected abdomen, so any functional interpretations are conjectural to some degree.

4.3 | Pregenital muscular system

We base general and serial homology hypotheses for the skeleto-musculature on the criteria of Remane (1952), that is, **relative spatial orientation and identity** of origins and insertions, **similarity in structure** of apodemes and muscles, both among segments and between ants and other aculeates, and **intermediate degrees of modification** from the "full" complement of muscles and simple shape of segment AVI. Before invoking the origin of new muscle groups, we first consider the hypothesis that the observed musculature is the result of reorganization or reduction. The trend of muscle simplification has been demonstrated in Hymenoptera (Klopfstein et al., 2015), among other insect clades (Beutel et al., 2021). Based on outgroup comparisons (Table S2; Boudinot et al., 2020), we consider the "simple" skeletal state of segments AV and AVI in *A. australis* to be least derived, thus potentially retaining most of the muscle groups that may be ancestral to the Aculeata or higher clades. Therefore, we expect that muscles observed in the postgenital and anterior pregenital abdomen are homonomous with some of those in AV and AVI.

It must be noted that the supposedly "basal" position of the Amblyoponinae within Formicidae has led to inaccurate inferences about the evolutionary context of skeletomuscular characters in the past. For example, the broad attachment of AII to AIII is a derived condition in amblyoponines (Bolton, 2003; Boudinot et al., 2020, 2022b), not a symplesiomorphy with outgroup aculeates (Hashimoto, 1996; Wilson et al., 1967). We therefore encourage caution in interpreting characters as plesiomorphies due to an assumed "primitive" phylogenetic position, and especially of the amblyoponine plan as paradigmatic of the ancestral ant sting (Kugler, 1978). Explicitly, by definition all extant taxa are equally temporally separated from their most recent common ancestor, so the concept of a "basal lineage" is oxymoronic. Additionally, the terminalia of female eusocial aculeates might be especially prone to reduction homoplasy as different lineages converge on similar biomechanical optima in the adaptation of the ovipositor from a multifunctional to a primarily stinging organ.

At the risk of repetition, we summarize the serial correspondences and functional patterns of abdominal muscles in *A. australis* below for the sake of clarity for discussion (Figures 31–34).

(1) **Dorsal orthomedial muscles**, *M. tergo-tergalis orthomedialis* (Figures 31; 32a; and 34a–c,e); **2domm**, originating on the anterior surface of the petiolar node and inserting on the helcial tergite; **3, 4, 7domm**, originating on the antecosta and inserting on the following acrotergite; **5, 6domm**, originating just

posterad the antecosta and inserting on the following acrotergite. The dorsal orthomedials are retractors of the tergum in AIV–AVI. In AII and AIII they are elevators of the gaster (Hashimoto, 1996). In AVII they are much reduced and insert ventrally, and as such are probably depressors of ATVIII, as suggested by Callahan et al. (1959) for the myrmicine *Solenopsis*.

(2) **Dorsal paramedial muscles**, *M. tergo-tergalis paramedialis* (Figures 31; 32b; and 34a–c); **2dpmm**, originating on the dorsolateral petiolar node and inserting on the ventrolateral helcial tergite; **3–7dpmm**, originating on the posterior tergite and reversed in position, inserting on the following anterolateral tergal apodemes. In AII the dorsal paramedials have an intermediate position, as the entire posterior volume of the segment is occupied by the helcium. In AVII they originate in a more anterolateral position than in AIII–AVI, but still lie within the intrasegmental fold, which is hypertrophied as part of the sting chamber. The dorsal paramedials are protractors of the tergum (Snodgrass, 1942); in AII they are depressors of the gaster.

(3) **Dorsal ortholateral muscles**, *M. tergo-tergalis ortholateralis* (Figures 31; 32c; and 34a–c); **2dolm**, originating anterolaterally on the petiolar node and inserting on the antecosta of the helcial tergite; **3**, **4dolm**, originating on the antecosta and inserting on the following antecosta, at the base of the anterolateral tergal apodemes; **5**, **6dolm1–2**, originating just on or posterad the antecosta, and inserting at the base of the following anterolateral tergal apodemes; **7dolm**, originating dorsally on the ASVII anterolateral apodemes and inserting

dorsomedially on ATVIII. In AII and AIII, the dorsal ortholaterals are antagonists of the dorsal orthomedials, functioning as depressors of the gaster (Hashimoto, 1996). The ventral insertion and overall orientation in AIV suggest a similar function in jointly depressing the subsequent segments. In AV and AVI the dorsal ortholaterals are retractors of the tergum (Snodgrass, 1942). In AVII they have a medial orientation, and as such might retract, pronate, or elevate ATVIII, which can move freely within the haemocoel to some degree. We note that Snodgrass (1942) interpreted the dorsal orthomedial and ortholateral muscles originating on AVII as laterals and medials, respectively. We base our present identification of these muscles on the spatial ordering of the muscles along the transverse axis, the insertion of 7domm on the antecosta, and the insertion of 7dolm more posteriorly on the tergite; these patterns reiterate the spatial relationships of their serial homologs in the preceding segments.

(4) **Dorsoventral intrinsic medial muscles**, *M. tergo-sternalis interior anteromedialis* (Figures 31; 33a; and 34b); **7dvimm1**, originating on the ATVII antecosta, inserting on the posterodorsal angle of the AVII sternite; *M. tergo-sternalis interior posteromedialis*, **7dvimm2**, originating posteriorly on the AVII tergite, reversed in position, inserting dorsally on the ASVII anterolateral apodeme. Generally, dorsoventral muscles are segmental compressors (Snodgrass, 1935a), and this function seems reasonable for 7dvimm2. The insertion of 7dvimm1 suggests a retractive or possibly elevatory function. We note that Snodgrass (1942) includes both reversed dorsoventral intrinsic
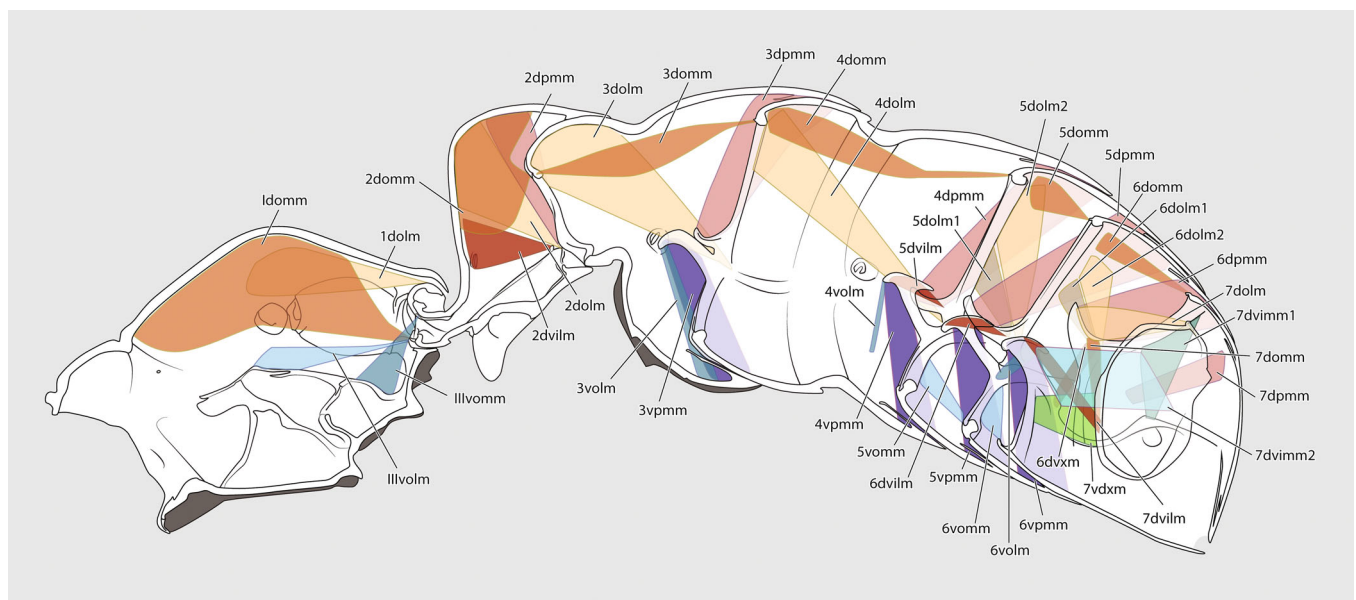
FIGURE 31 *Amblyopone australis*, pregenital muscles, diagrammatic, shown in sagittal bisection. Sclerites and muscles are partially translucent to show overlapping structures. dolm, dorsal ortholateral muscle; domm, dorsal orthomedial muscle; dpmm, dorsal paramedial muscle; dvilm, dorsoventral intrinsic lateral muscle; dvimm, dorsoventral intrinsic medial muscle; dvxm, dorsoventral extrinsic (paramedial) muscle; vdxm, ventrodorsal extrinsic muscle; volm, ventral ortholateral muscle; vomm, ventral orthomedial muscle; vpmm, ventral paramedial muscle
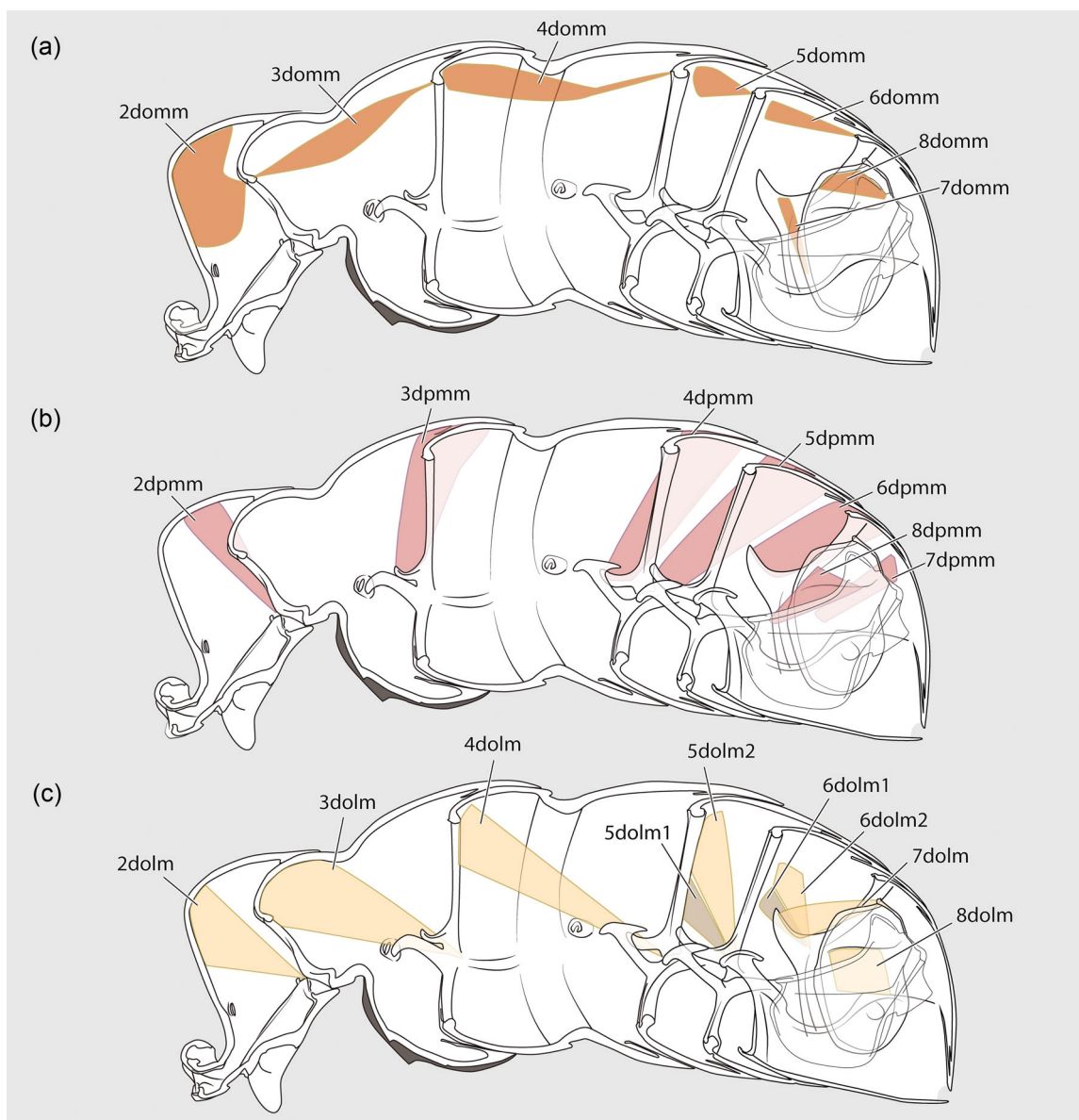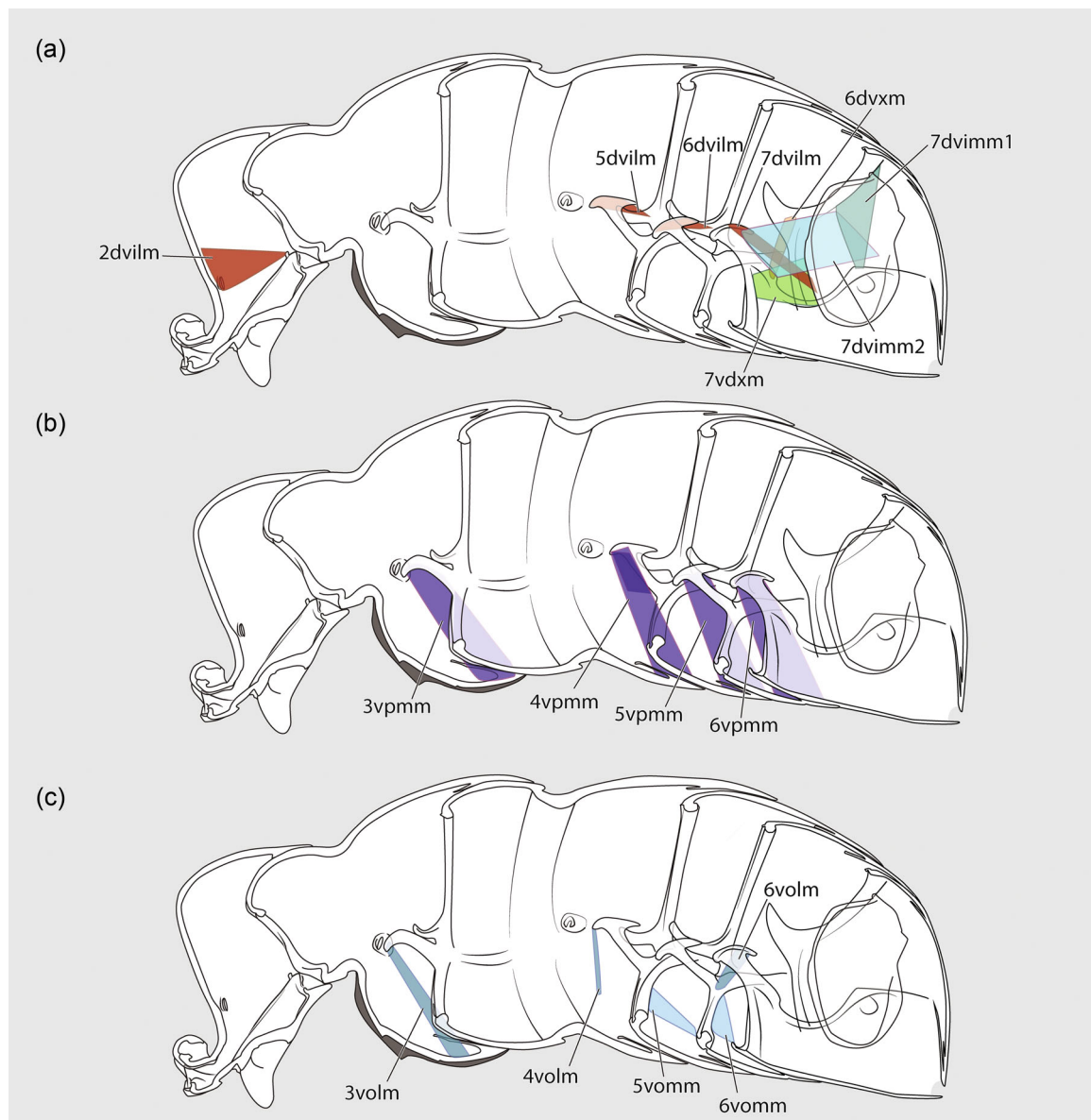
FIGURE 32 *Amblyopone australis*, dorsal musculature of the abdomen, diagrammatic, shown in sagittal bisection. Sclerites and muscles are partially translucent to show overlapping structures. (a) Dorsal orthomedial muscles, (b) dorsal paramedial muscles, (c) dorsal ortholateral muscles. dolm, dorsal ortholateral muscle; domm, dorsal orthomedial muscle; dpmm, dorsal paramedial muscle

muscles, 7dvimm2 and 7dvilm, under the same designation, M. 182, although he describes them separately.

(5) **Dorsoventral intrinsic lateral muscles**, M. *tergo-sternalis interior lateralis* (Figures 31; 33a; and 34a,b); **2dvilm**, originating anterolaterally on the petiolar node, inserting on the postero-lateral apodemes of the AII poststernite; **5–7dvilm**, originating on the anterolateral tergal apodeme and inserting on the sternal apodeme of the same segment. In AII, the compressive function of the dorsoventral intrinsic muscles may be rendered more complex by the relative rigidity, flexibility, and articulation of the poststernital-helcial complex. We hypothesize that contraction of 2dvilm renders the petiole more rigid, which may prevent the tergosternal connection from tearing during

extreme contraction of the other three petiolar muscles. Further support during gastral depression is provided by the prora, which comes into contact with the petiolar poststernite when the gaster is completely downflexed. Janet (1894) suggests that the dorsoventral intrinsic muscles of the petiolated AIII in *Myrmica rubra* are involved in respiratory movement, which might also be the case for 2dvilm in *Amblyopone*. The dorsoventral intrinsic laterals in AV–AVII may also serve as segment tensors, keeping their respective, unfused terga and sterna together against potential tearing forces exerted by the action of the intersegmental muscles. Such a function is circumstantially supported by the absence of dorsoventral intrinsic muscles in segments AIII and AIV, which are

FIGURE 33 *Amblyopone australis*, dorsoventral and ventral musculature of the abdomen, diagrammatic, shown in sagittal bisection. Sclerites and muscles are partially translucent to show overlapping structures. (a) Dorsoventral and ventrodorsal muscles, (b) ventral paramedial muscles, (c) ventral orthomedial and ventral ortholateral muscles. dvilm, dorsoventral intrinsic muscle; dvimm, dorsoventral intrinsic medial muscle; dvxm, dorsoventral extrinsic (paramedial) muscle; vdxm, ventrodorsal extrinsic muscle; volm, ventral ortholateral muscle; vomm, ventral ortholateral muscle; vpmm, ventral paramedial muscle

tergosternally fused. Moreover, their main orientation in AV–AVIII is longitudinal, suggesting a function that is not strictly compressive. Alternatively, it is possible they play a role in maintaining the anterolateral apodemes of the tergite laterad those of the sternite, or in holding both pairs to the body wall during movements of the posterior segments. The former function was reported by Hashimoto (1996) for the dorsal and ventral paramedial muscles of AII–AIII in taxa with both tergal and sternal apodemes on these segments.

(6) **Dorsoventral extrinsic paramedial muscles**, *M. tergo-sternalis exterior paramedialis* (Figures 31; 33a; and 34a), **6dvxm**,

originating posterolaterally on the AVI tergite, inserting ectally on the ASVII anterolateral apodeme. In *Apis*, the dorsoventral extrinsic muscles are present in AIII–AVI (Snodgrass, 1942); in *A. australis* they are present only in AVI. They are possibly segmental compressor, but interpreting the function of 6dvxm is complicated by its poor resolution in our micro-CT data. This was probably due to both endogenous and external factors. 6dvxm is distorted in the scan, and seems partially degraded, probably due to damage in preservation, while the apparently thin, ribbon-like nature of the muscle likely makes it more susceptible to such damage. We encourage future investigation of the precise structure of these muscles to confirm their
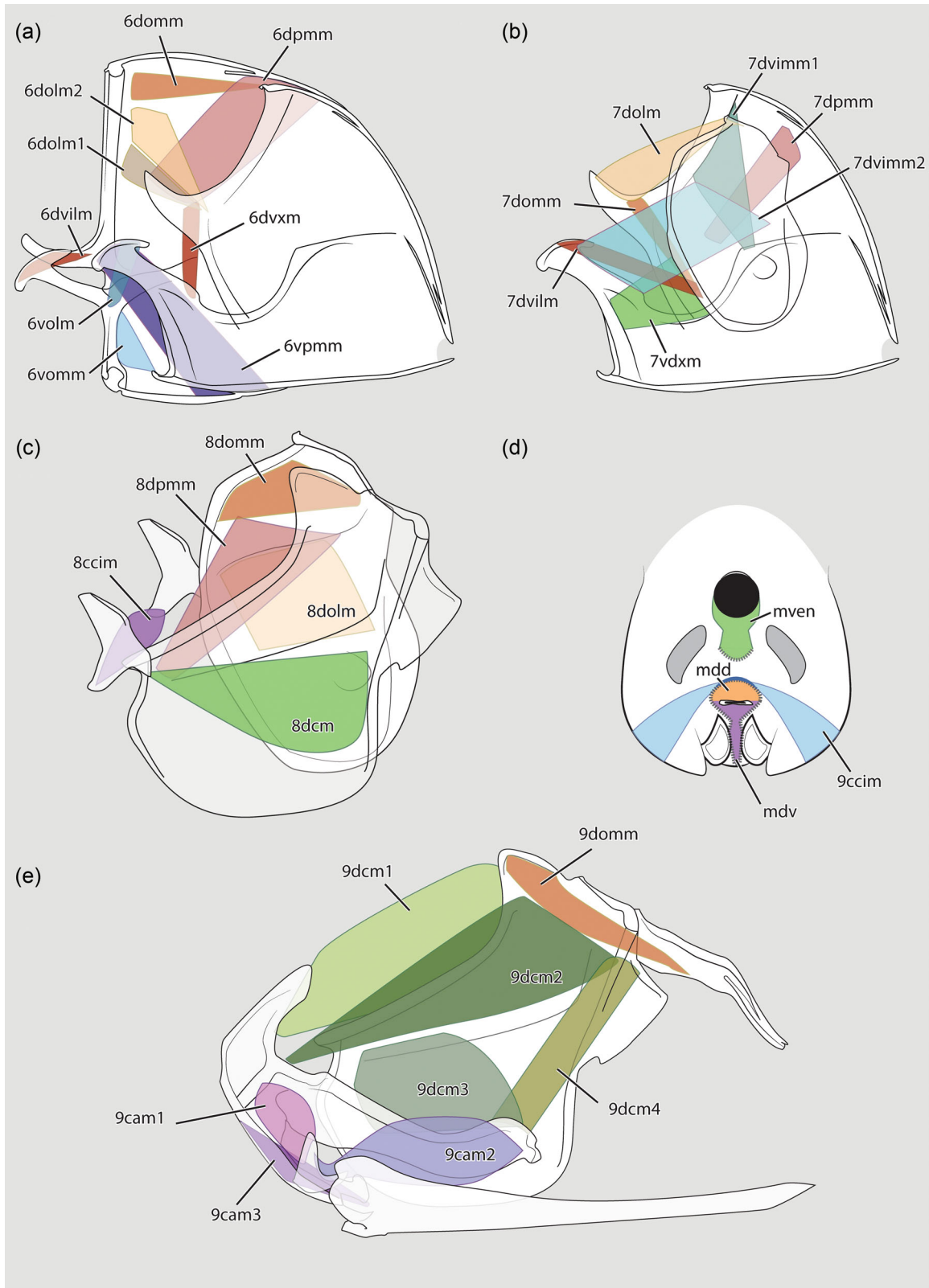
FIGURE 34 (See caption on next page)

orientation and form, and to elucidate factors hindering their reconstruction here.

(7) **Ventral orthomedial muscles**, *M. sterno-sternalis orthomedialis* (Figures 31; 33c; and 34a); **5, 6vomm**, originating laterally on the antecosta and inserting medially on the following acrosternite. In *Apis* the ventral orthomedials are present in AIII–AVI in the worker and queen, and AVII in the queen only (Snodgrass, 1942). In *Apis* they have a definitive anteroposterior orientation and are retractors of the sternum (Snodgrass, 1942). In *A. australis* their orientation appears strongly oblique, although this may be partially due to the close approximation of the segments in situ. However, their medial insertion suggests they are still retractors. Their absence in the anterior pregenital segments is likely related to tergosternal fusion, which facilitates movement of the entire segment by the dorsal and ventral ortholateral muscles.

(8) **Ventral paramedial muscles**, *M. sterno-sternalis paramedialis* (Figures 31; 33b; and 34a); **3–6vpmm**, originating posterolaterally on the posterior sternite, within the intrasegmental fold, reversed in position, inserting on the anterolateral sternal apodemes of the following segment. The ventral paramedials correspond in shape and function to their dorsal analogs, and are protractors of the sternum (Snodgrass, 1942). They are unreduced, being present and well-developed in entire pregenital metasoma, while the ventral orthomedial and ortholaterals are frequently reduced or absent.

(9) **Ventral ortholateral muscles**, *M. sterno-sternalis ortholateralis* (Figures 31; 33c; and 34a); **3volm**, originating ventromedially on the posterior poststernite and inserting on the ASIV anterolateral apodemes; **4volm**, originating laterally on the poststernite and inserting on the ASV anterolateral apodemes; **6volm**, originating mesally on the ASVI anterolateral apodeme and inserting on the apical process of the ASVII anterolateral apodeme. In *Apis*, the ventral ortholaterals are anteroposteriorly oriented sternal retractors (Snodgrass, 1942), which appear to differ in function in *Amblyopone*, where the volm are much smaller than the other ventrals. Their orientation is basically dorsoventral in AIII and AIV, and oblique in AVI. Hashimoto (1996) inferred 3volm to be a pronator of the sternum, which seems like a reasonable function for all the ventral ortholaterals observed here.

(10) The **ventrodorsal extrinsic muscle**, *M. sterno-tergalis exterior* (Figures 31; 33a; and 34b); **7vdxm** is the only sternotergal muscle in the abdomen. As such, it cannot be homologized with any other

abdominal muscles in *Amblyopone*, although it is easily identifiable with its homolog in other aculeates (Daly, 1955; Snodgrass, 1910). It is possible that absence of muscles from AVII to the genital appendages (e.g., Daly, 1955; Snodgrass, 1942) is a synapomorphy of the vespiform aculeates, as there is a sternogonapophyseal muscle from ASVII to gonapophyses VIII in the "chrysidoid" families of Aculeata, the "symphytan" Hymenoptera, and in various other Holometabola (Barbosa et al., 2021; Hünefeld et al., 2012; Vilhelmsen, 2000). However, we do not formally propose it as such, since our primary observations were limited to a single species, and as the apparent pattern relies on a limited number of publications. Furthermore, Daly (1955) does not list this muscle in his treatment of the chrysidid *Parnopes edwardsii*, indicating the need for further study to confirm polarity across aculeate clades.

In addition to the skeletal muscles described here, and the tergocardiac muscles of the dorsal diaphragm (see Sections 3.5.1, 4.8.1), we predict the presence in ants of extrinsic visceral muscles of the ventral diaphragm, which originate on sternites and which anastomose to form a transverse septum surrounding the ventral nerve cord (Richards, 1963; see also Section 4.8.4). These muscles could not be observed here.

4.4 | Sclerites of the genital and postgenital segments

Overall, the sting apparatus and proctiger of *Amblyopone* are well-developed. Tergites VIII and IX have sclerotized median connections, which may be the plesiomorphic condition for aculeates, having been repeatedly lost in ants to form detached hemitergites (Daly, 1955). Kugler (1978) proposed two conditions as plesiomorphies of the sting apparatus in the amblyoponine *Stigmatomma pallipes*, which we also observed in *A. australis*: the tergites are overall large, well-sclerotized, and well-musculated; and the sting shaft (terebra) is relatively undifferentiated and upcurved in profile. Notably, the furcula is present; it is fused to gonapophyses IX in most Dorylinae and in *Simopelta* (Ponerinae; Bolton, 1990b; Borowiec, 2016).

The mesal structure of the lancet olistheter, with extremely narrow arms of the dorsomedial seal, has not been exactly described in ants for which the sting was observed in cross-section. A similarly structured arm, though not quite as narrow, is known from various outgroup Hymenoptera, for example, *Sierolomorpha* and *Rhopalosoma* (Quicke et al., 1992) Given their form and contact with the venom

FIGURE 34 *Amblyopone australis*, musculature of the posterior pregenital, genital, and postgenital segments, diagrammatic, in sagittal bisection (a–c, e) and transverse section (d). (a) Abdominal segments VI–VII, (b) abdominal segments VII–VIII, (c) abdominal tergite VIII, (d) muscles of the venom and Dufour gland ducts; (e) muscles of AIX. Dashed outline in (d) indicates unresolved origin. cam, coxapophyseal muscle; ccim, coxocoxal muscle; dcm, tergocoxal muscle; dolm, dorsal ortholateral muscle; domm, dorsal orthomedial muscle; dpmm, dorsal paramedial muscle; dvilm, dorsoventral intrinsic lateral muscle; dvimm, dorsoventral intrinsic medial muscle; dvxm, dorsoventral extrinsic (paramedial) muscle; mdd, *M. dilator glandulae Dufouris dorsalis*; mdv, *M. dilator glandulae Dufouris ventralis*; mven, *M. dilator glanduale venenalis*; vdxm, ventrodorsal extrinsic muscle; volm, ventral ortholateral muscle; vomm, ventral orthomedial muscle; vpmm, ventral paramedial muscle

gland duct (proximally) and dorsal wall of the venom canal (distally), these arms certainly participate in forming a pressure seal. The functional implications of combined action of this dorsal seal and the better-characterized ventromedial seal deserve future attention.

The valvilli of gonapophyses VIII were only visible in a limited number of histological sections, indicating limitations in the other techniques levied here (see Section 4.9). Only one pair of valvilli was fully resolved in transverse histological series; a second pair is likely present, as in *Stigmatomma pallipes* (Quicke et al., 1992), although only resolved in limited sagittal sections (vvl, Figure 28a); the apparent three structures in Figure 28a may represent the disassociated parts of the first pair and the undamaged second pair. The tendency of the intimately associated pairs of valvilli to be resolved as a single structure has been noted previously (Quicke et al., 1992). We note that many authors use the term "valve" rather than "valvillus" to describe these structures, and "valve" has also been applied *in toto* to multiple pairs of valvilli when they are present but not differentiable in a given examination. This may lead to a lack of clarity, given the use of "valve" to also describe the entire dorsal and ventral components of the terebra, that is, the stylet and lancets themselves.

We have further taken issue with referring to the proximal processes of gonocoxites VIII as the "first rami" or "rami of the first valvulae/lancets/gonapophyses VIII," and the ventromedial processes of gonocoxites IX as the "second rami" or "rami of the second valvulae/stylet/gonocoxites IX" (as in, e.g., Daly, 1955; Ernst et al., 2013; Hermann & Chao, 1983; Kugler, 1978; Kumpanenko & Gladun, 2018; Matushkina, 2011; Packer, 2003; Snodgrass, 1942; Vilhelmsen, 2000). Regarding both terms, we reject the use of "rami" due to category conflation. Specifically, the "first rami" are part of gonapophyses VIII, while the "second rami" are part of gonocoxites IX. More generally, rami are the distal mobile elements of biramous appendages (i.e., in Hymenoptera, the gonapophyses and gonostyli themselves). Regarding the "rami of gonapophyses IX," the structure under consideration is actually a continuous element of the cuticle of gonocoxites IX. The traditional label implies that the "rami" belong to the gonapophyses, and thus has the potential or actual effect of causing cognitive dissonance when learning and applying terms for the ninth segmental appendages. Furthermore, it is the ventromedial processes of gonocoxites IX, which bear the origins of the coxapophyseal muscles 9cam3.

We discourage the assignment of homonymous terms to dissimilar or conceptually dependent, hierarchically nested structures within a given nomenclatural schema, or of adopting an approach in which such homonyms are permissible. Although we do not here use a strictly controlled vocabulary in reference to a published ontology such as HAO, or parse our descriptions into machine-readable ontological classes and relationships (e.g., Silva & Feitosa, 2019), we root our nomenclatural outlook in certain principles common to major biological ontologies and directed acyclic graphs generally. Specifically, each anatomical entity is described by a unique term, which can be related to other unique terms through a series of dependent relationships indicated by "of," or in other words, a *part_of*

relationship (Dessimoz & Škunca, 2017; Gremse et al., 2011; Yoder et al., 2010). This system avoids combinations such as "the anterior valve of the dorsal valve of the ventral valve of the first-valvifer-first valvula complex," which would here be presented as "the anterior valvillus of the lancet of the gonapophysis of the gonopod of the sternum of the eighth segment of the abdomen."

4.5 | Muscles of the genital and postgenital segments

Because the mechanical functions of the sting have been extensively studied in many Hymenoptera, we did not investigate sting muscle function in detail here. All examined muscles of the sting apparatus are identifiable with their homologs in the "poneroid" *Paraponera clavata* (Daly, 1955), but two muscles known from the latter were not found (M. 6, 10). Muscle 6 of Daly (1955) originates on ATVII dorsad 7dolm and inserts on ATVIII ventrad 7dolm; M. 10 originates on the sternal apodeme distad 7dvimm 2 and inserts at the ventroapical margin of ATIX. Although neither have been reported in other ants or aculeates for which data are available, M. 6 corresponds to a dorsal paramedial muscle and M. 10 to a lateral ventrodorsal muscle, almost certainly a subdivision of 7vdxm, given the absence of other sternotergal muscles in the hymenopteran abdomen. Further study is necessary, as many authors do not code longitudinal tergal muscles of AVII (Table 4).

4.5.1 | Serial homologs of the pregenital muscles (Figure 34c)

Although the ventral sclerites of the genital and postgenital segments are absent, reduced to membrane, or represented only by the genital appendages, the dorsal musculature of AVIII can be homologized with those of the pregenital segments. Some shifts in overall orientation relative to the pregenital muscles have occurred, but the transverse spatial relationships are preserved. The dorsal orthomedial muscle, 8domm, originates dorsomediad the other groups and inserts on the posterodorsal apodeme of the ATIX dorsal body. The dorsal paramedial muscle 8dpmm retains its reversed position, originating ventromediad 8domm and inserting anteriorly on the ATIX midplate line. A single paired dorsal ortholateral, 8dolm, originates ventrolaterad 8dpmm and inserts posteriorly on the ATIX midplate line; this muscle is notably shorter (anteroposteriorly) and broader than the preceding dorsal ortholaterals.

4.5.2 | Tergocoxal muscles (Figure 34c,e)

One tergocoxal muscle was observed for AVIII (8dcm) and four for AVIX (9dcm1–4). Hünefeld et al. (2012) inferred that two tergocoxal muscles were present in the groundplan of the Holometabola for both AVIII and AIX. There is an additional ninth tergocoxal muscle in

TABLE 4 Homology of ovipositor muscles across major hymenopteran clades.

Amblyopone australis — Here	Paraponera — Daly (1955)	Myrmeciinae — Kugler (1980)	Anthophila; Sphecidae; Vespidae — Rietschel (1937)	Apis mellifera — Snodgrass (1942)	Ampulicidae; Sphecidae — Graf et al. (2021)	Pompilidae (Cryptocheilus versicolor) — Kumpanenko and Gladun (2018)	Chrysidoidea — Barbosa et al. (2021)	Ceraphronoidea — Ernst et al. (2013)	"Symphyta" — Vilhelmsen (2000)	Notes
-	6	-	-	-	-					1
7dolm	7	+	1	178	dT7-T8					
7domm	8	+	2	177	vT7-T8					2
7dpmm	9	+	3	179	pT7-T8					
7vdxm	11	+	8	184	S7-T8					3
-	10	-	-	-	-					
7dvimm1	2	+	5a	183						
7dvimm2	1	+	5b	182						
7dvilm	3	+	4	182						
-	-	-	-	-	-	-	M1	M1	M1	
8domm	12	+	11	187	-	M2	-	?	M2	4
8dolm	13	+	10	188	lT8-T9	M3	M3	M3	M3	
8dpmm	14	+	?	?	dT8-T9	?	M2	M2	-	4
8dcm	24	+	14	192	T8-1vf	M4	M4	M4	M4	
8ccim	25†	+	-	-	-	-	-	-	-	
	22		12	189		-	-	-	-	5
	23		13	190	T8-T8					6
	-				vT8-T9†					7
9domm	30	+	22	200		-	-	-	+	8
9dcm1	26†	+	17a	198a	dT9-2vfa	M5a	M5	M5	M5	9
9dcm2	27†	+	17b	198b	dT9-2vfb	M5b	M6	M5	M5	9
9dcm3	28†	+	18	199	vT9-2vf	M6	M7	M6	M6	9
?	?	?	?	?	?	?	M8	?	?	10
9dcm4	29†	+	18	199	pT9-2vf	M7	M9	M7	M7	10
-	-	-	-	-	-	-	-	M8	M8	11

TABLE 4 (Continued)

Amblyopone australis	Paraponera	Myrmeciinae	Anthophila; Sphecidae; Vespidae	Apis mellifera	Ampulicidae; Sphecidae	Pompilidae (Cryptocheilus versicolor)	Chrysidoidea	Ceraphronoidea	"Symphyta"	
-	-	-	-	-	-	-	-	-	M9	12
-	-	-	-	-	-	-	-	-	M10	13
9cam1	42	+	19b	197	m2vf-fu	M8	M11	-	-	14
9cam2	43	+	19a	197	l2vf-fu	M9	M13	-	-	14
9cam3	40	+	20	196	?	M10	M10	-	M11	15
?	41†	+	-	-	-	-	M12	M9	M12?	16
9ccim	-	-	-	-	-	-	?	?	?	16
-	-	-	-	-	2vf-2vf†	-	-	-	-	16
-	-	-	-	-	-	M11	-	-	-	17

Note: The top row provides an abbreviated list of the taxa studied in the given reference which are listed below in greater detail after the Notes. Blue fill: present; yellow fill: absent or not observed; green fill: not coded; black fill: inapplicable. Symbols: **+** present, no name given; **-** absent; **?** not observed, see **Notes** column. Double vertical border divides observations on ants from outgroups. Dashed bold vertical border divides Aculeata from non-aculeates. Numbers in the Notes column correspond to the statements below. **Note 1**, M6 is a dorsal paramedial muscle (dpmmm). **Note 2**, Snodgrass (1942) includes both reversed dorsoventral muscles of ATVII under the designation 182, but describes them separately, and explicitly notes the correspondence to Rietschel's 5b; Snodgrass (1910) did not observe this muscle. **Note 3**, M10 is a subdivision of 7vdxm. **Note 4**, Sources with "?" give only two dorsal longitudinal muscles from AVIII to AIX, so the identification of the dorsal longitudinal musculature is provisional and may differ among taxa. **Note 5** Spiracular occlusor of ATVIII. **Note 6**, Spiracular dilator of ATVIII. **Note 7**, Only observed by Graf et al. (2021) in *Ampulex*. **Note 8**, The precise homology of 9domm is uncertain. Vilhelmsen (2000) mentions muscles attaching to the rectum but does not describe them or designate them numerically; these may represent the intrinsic visceral muscles. **Note 9**, Also observed by Daly (1955) in *Formica*. **Note 10**, The homology of the tergogonocoxital muscles among taxa is somewhat ambiguous due to the presence of an additional "posterior T9-2vf" muscle in some groups; see Section 4.5. **Note 11**, ATIX-genital membrane muscles. **Note 12**, Gonocoxite VIII-genital membrane muscles. **Note 13**, Gonocoxite IX-genital membrane muscles. **Note 14**, Inapplicable when the furcula is absent. **Note 15**, Only observed by Daly (1955) in *Formica*; see Section 4.5. **Note 16**, Sources with "?" may not have coded these muscles since they can appear as visceral muscles; 9ccim is possibly homologous with 2vf-2vf in *Sceliphron*, see Section 4.5. **Note 17**, Intragonapophyseal muscles of the sting bulb walls to the venom duct flap apodeme.

Taxonomic representation: Kugler (1980): *Myrmecia, Nothomyrmecia*. Riteschel (1937): Apidae (*Apis, Bombus*); Colletidae (*Prosopis*); Sphecidae (*Ammophila*); Vespidae (*Dolichovespula, Macrovespa, Polistes, Vespa*); note that Rietschel (1937) follows a *Bauplan* descriptive system, only explicitly noting which taxa were observed when a muscle is absent; this column is a collation of all present muscles described, see reference for patterns of absence. Graf et al. (2021): Sphecidae (*Sceliphron destillatorium*); Ampulicidae (*Ampulex compressa*). Barbosa et al. (2021): all chrysidoid families except Plumariidae. Ernst et al. (2013): Ceraphronidae (*Aphanogmus, Ceraphron, Trassedia*); Megaspilidae (*Conostigmus, Dendrocerus, Lagynodes, Megaspilus*). Vilhelmsen (2000) describes the musculature of *Xyela* specifically, and discusses variation among the other "symphytan" taxa listed: Tenthredinoidea; Pamphilioidea; Cephoidea; Siricidae; Xiphydriidae; Orussoidea; Stephanoidea; Megalyroidea; Evanoidea; Cynipoidea.

some chrysidoids and symphytan Hymenoptera, which complicates the homologization of 9dcm4 (Barbosa et al., 2021; Smith, 1972). Barbosa et al. (2021) term these the posteromedial and posterolateral T9-2vf muscles (M8, 9), while Smith (1972) considers them to be dorsal and lateral gonostylar muscles. Positionally, 9dcm4 appears to correspond to the lateral pair, but no conclusive inference can be made presently. It is also possible that the identity of these posterior tergocoxal muscles differs among taxa.

4.5.3 | Minor coxapophyseal muscles (Figure 34e)

The muscle 9cam3 corresponds to Daly's muscle 40 (1955). Due to preservational artifacts, the precise insertion of 9cam3 could not be determined, but it appears to insert ectally on the articular processes of the sting bulb. The exact insertion of this muscle varies among taxa, likely in relation to the diversity in form of the proximodorsal and articular processes of the sting and the basal notch. For example, the insertion of 9cam3 is on the articular process in Chrysidoidea (Barbosa et al., 2021), while in *Cryptocheilus* (Pompilidae) the minor coxapophyseal muscle inserts within the broad, shallow basal notch itself (M.10, Kumpanenko & Gladun, 2018). The fact that 9cam3 was only visible in a few images in the CT-data set and a limited number of sagittal and transverse histological sections indicates that the other sting bulb muscle may have been "hidden" between sections.

Daly's (1955) M. 41 is possibly present but difficult to observe. We base this interpretation on a few slices from histological preparations, which show an indication of muscle tissue in the expected location. However, the thin nature of these muscles and their medial position among the smallest and most convoluted parts of the abdomen makes them difficult to either manually dissect or to resolve in tomography. On the other hand, Daly (1955) only explicitly notes the presence of muscle 41 in *Formica*, in which the entire sting apparatus is extremely modified and reduced, and suggests that it may be a modification of M. 40.

Uncertainty in micro-CT reconstruction of the minor coxapophyseal muscles was noted for Ampulicidae and Sphecidae by Graf et al. (2021). These authors acquired scans at lower resolution than in the present study and required stitching of several independent scans. The fact that an improvement of around 1–2 μm/pixel resolution enabled reconstruction of a muscle which could otherwise not be unambiguously ruled present or absent implies that an even higher resolution scan of just the sting apparatus could reveal if a second muscle is present in *Amblyopone*. However, many parameters of the scan, and organismal traits, differed between our study and Graf et al. (2021), so we aware of the limitations of this analogy. An additional complicating factor in our case is that the scanned *Amblyopone* specimen has some of the sting elements torqued to the side, making it more difficult to differentiate folded membrane from flexible sclerite and distorted muscle fibers of the abdominal apex.

4.5.4 | The eighth coxocoxal intrinsic muscle (Figures 25 and 34e)

Muscle 8ccim is a transverse bundle that runs horizontally between the ventral processes of gonocoxites VIII. No medial insertion of this enigmatic muscle was observed here nor was it identified in *Paraponera* or *Formica* by Daly (1955), who also does not list this muscle for any other aculeate. We confirmed the lack of a medial insertion via histology, which demonstrates a clear myotendinous junction (**mtj8ccim**, Figure 25d,e) between the lateral portions of 8ccim and gonocoxites VIII, and no connection to any structure medially (Figure 25b,c). The eighth coxocoxal muscle is present in *Paraponera* and *Formica* (Daly, 1955), *Myrmecia* and *Nothomyrmecia* (Kugler, 1980), and *Myrmica rubra* (Janet, 1902), but it was not recorded in *Solenopsis richteri* (Callahan et al., 1959). A clear homolog of this muscle is absent beyond the Formicidae, and its presence in the taxa listed above indicates that 8ccim spans at least the "poneroformicoid" node. The broad distribution of this muscle among sampled ants and absence outside of the family indicates that 8ccim is a synapomorphy of the Formicidae.

It is possible, however, that 8ccim corresponds to a modified genital membrane muscle found in non-aculeate Hymenoptera, which are otherwise absent in Formicidae. For example, in Ceraphronoidea, there is a superficially similar transverse muscle originating on gonocoxites VIII, and inserting on the septate anterior genital membrane (ventral conjunctiva of the ninth gonocoxites, Ernst et al., 2013). If this "muscle 8" is homologous with 8ccim, this could falsify the hypothesis that absence of genital membrane musculature per se is an aculeate autapomorphy (Barbosa et al., 2021). The similarity in form and position of 8ccim with muscle 8 (Ernst et al., 2013) could also indicate hemiplasy, that is, that both character states are orthologous and derived, but appear homoplasious due to idiosyncratic lineage sorting (Avise & Robinson, 2008). The polarity and development of 8ccim in the remaining "poneroformicoid" clades, and in the leptanillomorphs, deserves investigation. Intriguingly, a transverse muscle of the eighth genital appendages is considered the sole unambiguous apomorphy of the female postabdomen in Antliophora (Hünefeld, 2009). This suggests that pressure on mechanical function in the postgenital skeletomusculature may lead to apparently convergent forms, even when these are autapomorphies of distantly related taxa.

Because 8ccim lacks a medial insertion, its contraction would draw the ventral processes of gonocoxites VIII together, and may serve to pronate the entire sclerites. Such contraction could have several concomitant effects, however, because gonocoxites VIII articulate with gonocoxites IX, the proximal processes of gonapophyses VIII, and with ATIX. Inferring the function of 8ccim is further complicated by the lack of analogously transverse muscles in the remainder of the Hymenopteran abdomen. Truly transverse abdominal muscles do occur in insects, but they are mostly visceral muscles inserting on the dorsal and ventral diaphragms (Snodgrass, 1935b). In Hymenoptera, the transverse sternal muscles form a somewhat diaphanous ventral

diaphragm, which intimately covers the ventral nerve cord and may be pulsatile and/or serve as a protective membrane (Richards, 1963; Snodgrass, 1935a). These muscles differ in sarcomeric structure from skeletal muscles, from which they diverge from a shared ontogenetic path during organogenesis (Chapman et al., 2013). In tomographic sections the ventral visceral muscles strongly resemble integumental conjunctiva, rather than striated muscle, and were not segmented or examined in any detail here.

The ninth coxocoxal intrinsic muscle, 9ccim, is similar in form to 8ccim, though much smaller, and is clearly functionally associated with the Dufour's gland duct apparatus (Figures 28b and 34d; Billen, 1982a, 1990a). Inferring the potential homology of these muscles will require further investigation of the polarity and states of 9ccim in other ants. Without any other clear homolog for 8ccim, some analogs may be valuable to consider. A similar muscle of possible comparative value runs transversely between the ninth gonocoxites in *Sceliphron destillatorium* (Sphecidae), in which 8ccim is absent (Graf et al. 2021). As with 8ccim, there is no medial insertion of this muscle ("2vf-2vf") and the function has not been definitively inferred (Graf et al., 2021); its potential association with the Dufour's gland and homology with 9ccim deserve examination. Janet (1902) noted an apparent transverse muscle in ATIX, but he interpreted it to be an occlusor of the rectum; this muscle may correspond to 9ccim or possibly *M. retractor ani* (see Section 4.8.2). A more informative comparison for 8ccim might be the transverse pregenital sternal muscles of certain orthopterans, which modulate the sternite width (Consoulas et al., 1993). Given the probable systematic value and functional importance of the well-developed 8ccim in ants, we encourage detailed, phylogeny-informed future study of the gonocoxital muscles across Apocrita. An investigation of the polarity and states of the genital membrane are also merited but will likely entail different methods than those used here, which tend to resolve membranes more poorly than sclerite and muscle.

4.5.5 | Proctiger muscle

The ninth dorsal orthomedial muscles (9domm) insert on the proctiger membrane itself, rather than on the sclerotized part of ATX. This is the condition in *Myrmecia* and *Nothomyrmecia* (Kugler, 1980) and Apidae, although apparently not in *Paraponera* (Daly, 1955). Given the presence of several proctiger muscles in apids, it is unclear whether 9domm is homologous with the proctiger muscles in *Paraponera*, or if they represent independent reductions from an ancestral state. It is further unclear if 9domm is truly the orthomedial, or an ortholateral muscle, which has taken a medial position as the tergite surface area reduced and the other musculature simplified. Finally, Janet (1902) figures a transverse "*muscle de fermeture du rectum*" (pg. 61) intrinsic to ATIX, rather than longitudinal proctiger muscles, which has not been described elsewhere in ants.

4.6 | Spiracular muscles and tracheae

We were able to confirm histologically that the intraspiracular occlusor muscles are unambiguously present in AV, AVI, and AVIII. However, the resolution of the micro-CT data was insufficient to confidently identify or exclude these muscles, and the histological sections available were of the posterior abdomen only. Additionally, the spiracular muscles were only visible in a transverse section series, thus precluding a description of their three-dimensional structure. We expect the occlusors to be present and functional in the preceding pregenital segments as well. Besides the primary observations here, we base this prediction on the following: (1) such muscles are present and functional in other ants and aculeates; (2) the spiracles are not reduced relative to the segments for which muscles were observed; and (3) we observed certain suggestive tomographic data. Specifically, apodemes of the expected form were occasionally partially visible in the CT-scan within the internal spiracular foramina, as well as small pieces of softer tissue resembling muscle remnants. We did not segment or describe these tissues in detail, as the attempt to reconstruct a poorly resolved structure can provide more misleading results than meaningful data.

In aculeates with two pairs of sternal apodemes, the spiracular dilator muscles of the pregenital segments arise from the lateral sternal apodemes (see Section 4.1). Therefore, the apparent absence of spiracular dilators in *Amblyopone* might inform inference of the nature of the single pair of sternal apodemes in ants (Daly, 1955; Snodgrass, 1942). The eighth spiracles of *Paraponera* have dilator muscles, but these originate from the tergite as in other aculeates (Daly, 1955), so they do not necessarily provide comparative information. Preliminary segmentation of the posterior pregenital abdomen of a male *Lioponera* sp. demonstrates the sixth *M. dilator spiraculi*, which originate post-antecostally on the dorsolateral sternal margination. Spiracular dilators are less consistently present than occlusors in insects generally (Snodgrass, 1935a; von Kéler, 1955). Confirming the presence or absence of these muscles may require freshly euthanized specimens and/or higher-resolution tomography. To investigate this question, we encourage further tomographic study of the pregenital segments.

4.6.1 | Eighth segmental spiracles

An initially surprising observation is that the tracheae of the eighth spiracles are highly developed, with robustly sclerotized taenidia, and are even visible in the scan (**trach**, Figure 35). Visualizing the respiratory system of insects is possible with synchrotron micro-CT, but achieving high resolution generally requires live, anaesthetized (e.g., Poinapen et al., 2017) or recently euthanized specimens (e.g., Socha et al., 2010), and/or noxious stains such as osmium tetroxide (e.g., Pereanu et al., 2007). Large, well-sclerotized tracheae of the eighth tergite have been described and figured for other
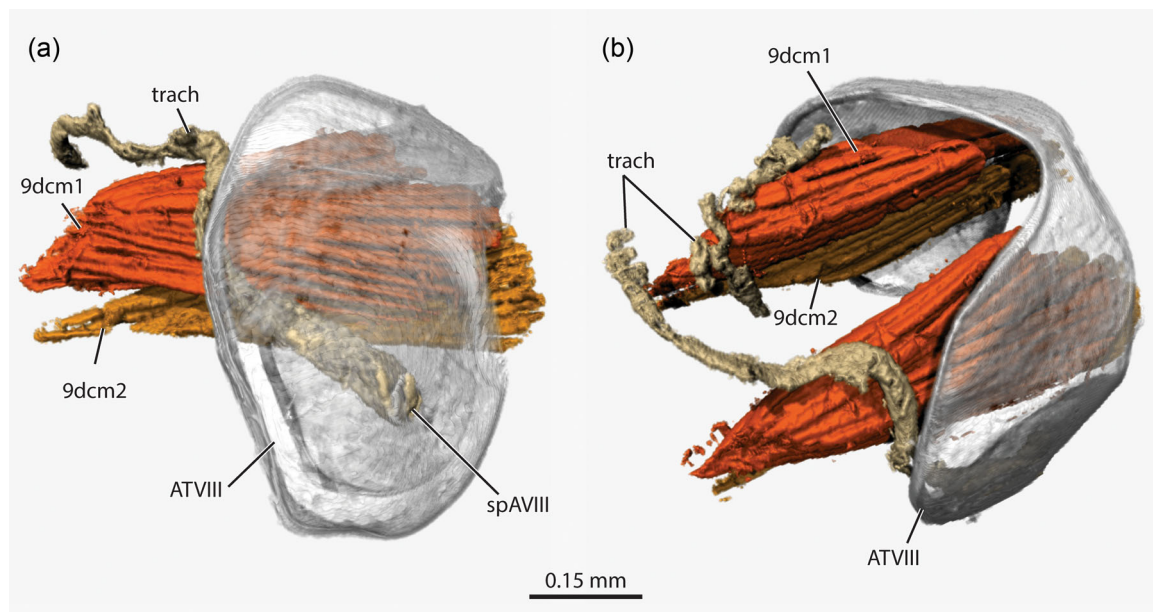
FIGURE 35 *Amblyopone australis*, tracheae of abdominal segment VIII and possible association with the tergocoxal muscles; 3D reconstruction, ATVIII translucent (a) lateral view; (b) oblique dorsoectal view. Scale bar: 0.15 mm. AT, abdominal tergite; dcm, tergocoxal muscle; sp, spiracle; trach, trachea

Hymenoptera (see, e.g., Figures 3 and 4 of Packer, 2003). In *A. australis*, these tracheae appear to be associated with the large anterior tergocoxal muscles, 9dcm1–2 (Figure 35), but this observation should be considered provisional and indeed may be artefactual; we did not histologically investigate tracheolar commerce with the muscles. ATVIII is entirely enclosed within the abdomen (Figure 2b), and is presumably not exposed to the atmosphere, even in full extension of the sting. It is possible that these tracheae are primarily involved in removal of carbon dioxide, for example, from 9dcm1–2 during the metabolic exertion of stinging.

In general, gas exchange in insects is complex, cyclical, and may involve phases with the spiracles closed (Lighton & Garrigan, 1995). For example, tracheal compression in the head and thorax, a convective process effected by muscular action, can increase oxygen diffusion from tracheoles into tissues when the spiracles are closed (Westneat, 2003). The eighth spiracles are fully musculated in *Paraponera clavata* and *Formica obscuripes* (Daly, 1955); in the myrmicine *Myrmica rubra*, Janet (1893) noted that the eighth spiracles and their occlusor muscles were "*notablement plus dével-oppés que ceus des arceaux précédents*" (p. 607), and a preliminary segmentation of a male *Odontomachus* sp. demonstrates both muscles of the large eighth spiracles. These observations suggest that if these internalized respiratory structures are not directly involved in gas exchange, they may play a role in baroregulation of the body cavity or skeleton, with consequent respiratory or expiratory effects. An archaic interpretation, introduced in the context of the *Apis* worker, is that the large eighth tracheae are involved in exsertion of the sting through air pressure, but this has been experimentally falsified (Rietschel, 1937; Trojan, 1935).

4.7 | Metasomal exocrine glands and associated musculature

4.7.1 | Metasomal exocrine glands

The pygidial gland was clearly resolved in histology, but could not be visualized in the micro-CT data set. This limitation was due to the poor resolution of tissues in the intersegmental regions. Much of the volume of the scanned specimen, including the intersegmental areas, is filled with what appears as a spiderweb-like matrix composed of roughly round to amorphous, densely interconnected subunits. This material probably includes elements of fat body and other organs, and connective tissues, but appears uniform and thus could not be segmented. This poorly resolved tissue is not uncommon in micro-CT scans of ants, a problem probably influenced by specimen age, preservation medium, staining, and scan parameters. It seems likely that scanning a freshly euthanized specimen would ameliorate this limitation to a degree.

No convoluted gland was observed within the venom gland in any preparation. The convoluted gland is absent in the amblyoponine genera *Stigmatomma*, *Mystrium*, *Prionopelta*, and *Onychomyrmex* (Schoeters et al., 1999); presence or absence could likely be confirmed by further histological sectioning of the venom gland reservoir. The sting bulb gland has previously been observed only in Myrmeciinae (Billen, 1990b) and *Protanilla wallacei* (Billen, Bauweleers, et al., 2013); this unusual phylogenetic distribution underscores the need for further sampling. The sting shaft gland is here observed for the second time in ants, being previously described only from the ponerine *Myopias hollandi* (Billen, Stroobants, et al., 2013).

4.7.2 | Muscles associated with the venom gland and Dufour's gland

The major glands of the sting apparatus are the venom gland and the Dufour's gland, both of which have a large median duct that enters the sting base (Figures 27a and 29a). The venom gland duct receives a single ventral muscle (*M. dilator glandulae venenalis*, **mven**; Figures 28b and 34d), while the Dufour's gland duct receives the insertion of both a dorsal and ventral group of muscles (*M. dilator glandulae Dufouris dorsalis et ventralis*, **mdd**, **mdv**; Figures 28b and 34d), and is affected indirectly by the action of **9ccim** (Figures 28b and 34d). None of these gland-associated muscles were resolvable in micro-CT, and even in histological preparations only the origins of 9ccim could be ascertained. Additional histological study will be crucial to clarify the details of the origins and forms of these muscles.

The venom gland duct apparatus includes dorsal muscles associated with the proximodorsal sting bulb apophysis in some taxa. In *Myrmica rubra*, the apophysis is continuous with a sclerotized fragment or secondary sclerotization of the dorsal surface of the venom gland duct ("*mince lame chitineuse*"), which receives paired occlusors (*M. ferm. ven.*; Janet, 1898a, 1898c). In *A. australis*, the sting bulb apophysis is distinct, and appears to anteriorly contact a sclerotized flap which is continuous with the venom gland duct (Figure 28a, black arrowhead), but dorsal muscles of the gland duct are absent. In *Solenopsis richteri*, both the sting bulb apophysis and the dorsal occlusor are absent, although the ventral dilator is retained (Callahan et al., 1959). In *Cryptocheilus* (Pompilidae), an intragonapopphyseal muscle ("M11") occurs within the sting bulb. This muscle originates on the dorsolateral walls posterad the articular processes and inserts on the proximolateral apodemes of the "flap of the venom duct," a clearly articulated plate (Kumpanenko & Gladun, 2018). This "flap" has an invaginated ventromedial portion which apparently corresponds to the proximodorsal sting bulb apophysis. Kumpanenko and Gladun (2018) state that the flap has been described in ants by Kugler (1978) and Callahan et al. (1959). Unfortunately, a terminological equivalency is not provided. Kugler (1978) defines the "internal apophysis" and states that it is involved with closing the venom duct by reference to Janet (1898a), but does not show either a mobile sclerite of the sting bulb or the "*lame chitineuse*." Callahan et al. (1959) note that the chitinous apophysis associated with the venom gland is absent. In this case, the "flap of the venom duct" may indicate the complex of partially sclerotized epithelial and visceral muscular tissue surrounding the duct ("*armature chitineuse*," Janet, 1898c). Alternately, it might refer to the "epithelial lip" which is associated with the Dufour's gland (Callahan et al., 1959).

The homology of the ventral venom gland duct muscles, *M. dilator glandulae venenalis*, could not be determined due to both experimental limitations and variability among ants. These muscles were only visible in a limited number of transverse histological sections and their origins could not be determined. In *M. rubra*, the dorsal and ventral venom gland duct muscles originate on the posterior arm of gonocoxite IX (*M. ferm. ven., M. ouv. ven.*;

Janet, 1898a), while in *Myrmecia gulosa*, muscles with the same insertion originate on ASVII (M.7; Billen, 1990a). In *Solenopsis richteri*, the ventral muscle originates at the articulation of the ventral arm of gonocoxite IX and the articular process of the sting bulb (Callahan et al., 1959). These differences in origin underscore the need for further comparative histology.

The Dufour's gland duct is affected by two dilator muscles inserting directly on the gland walls, *M. dil. gl. Duf. dorsalis et ventralis* (= M2, M3; Billen, 1982a, 1990a) and by the ninth coxocoxal intrinsic muscle 9ccim (= M1; Billen, 1982a, 1990a), which forms a diaphragm-like sheet immediately dorsad *M. dil. gl. Duf. dorsalis*. The dorsal dilator comprises the dense mass of muscular tissue surrounding the dorsum of the duct. The ventral dilator appears to possibly originate on the mesal faces of the proximal lancets in the prevalvillar region and possibly on the mesal walls of the valvilli themselves, and/or on the mesal and ventromedial membranes of the lancets in this region (Figure 28b). Uncertainty in the origin of the ventral dilator was also noted by Billen (1982b) in *Formica sanguinea*.

The variability in the skeletomusculature and glandular morphology in the sting base, between different aculeate groups and within ants, indicates diversity in the biomechanics of venom dosage and ejection, and gland product segregation. This observation has been much discussed previously but remains understudied both proximally and ultimately. In ants, the ultrastructure and chemistry of the venom and Dufour's glands have rarely been studied in the explicit context of the extrinsic musculature and surrounding sclerites, although focus on them has otherwise been intensive (Billen, 1982b, 1985, 1990b; Billen & van Boven, 1983, 1987; Billen & Gotwald, 1988; Billen & Taylor, 1993; Billen et al., 1984, 1986, 1987, 1988, 2000, 2001, 2013; Callahan et al., 1959; Piek, 1986; Schoeters & Billen, 1996; Schoeters et al., 1999). Most of the described variation in the sting base skeleton is limited to two-dimensional line drawings (Kugler, 1978, 1978, 1980, 1992) with usually brief or no discussion of soft tissue.

In general among aculeates, a distinction is made between the *valve-pump* and *injection type* of venom ejection (van Marle & Piek, 1986). The valve-pump type is effected by skeletomuscular action causing protraction-retraction of the lancets and piston-like behavior of the valvilli. The injection type is effected by contraction of muscles within the wall of the venom gland reservoir or ductus venatus (van Marle & Piek, 1986). These categories provide a useful heuristic for inferring functional morphology, namely, presence or absence of valvilli; however, the categories do not address the action of the extrinsic occlusor and dilator muscles of the venom gland and Dufour's gland ducts. Including a description of these muscles (or noting their definitive absence) may therefore both improve the heuristic value of the valve-pump/injection scheme, or provide evidence of additional nuance not currently captured in this conception.

Overall, our observations and the literature demonstrate that this anatomical region houses a rich, complex character system that deserves focused study. In particular, histological techniques, microscopic slide preparation, and fluorescence microscopy may be instrumental in describing the sting base; the latter was leveraged by

Kumpanenko & Gladun (2018), for example, to demonstrate the presence of resilin-like proteins, providing information on the flexibility of the sting elements.

4.8 | Other soft tissues

The non-muscular soft tissues were relatively poorly resolved in our micro-CT data set, and because our focus was the skeletomusculature, we did not examine these organ systems in detail with other techniques. Nevertheless, we consider even a brief overview to be valuable in providing comparative morphological information.

4.8.1 | Dorsal diaphragm

The tergocardiac muscles are clearly present in AV and AVI; the total number of tergocardiac muscle pairs is quite likely to be greater than two, but could not be ascertained. Tergocardiac muscles vary in number across insects, and may be reduced relative to the number of abdominal segments. For example, Polyneoptera generally have a pair of tergocardiac muscles on each of the 10 abdominal segments (and often one or two thoracic pairs; Nutting, 1951) while in Paraneoptera the number can be as few as four (Chapman et al., 2013). In some Lepidoptera, there are seven (Kuwasawa et al., 1999); Diptera may have eight (Andereck et al., 2010). Among the Hymenoptera, both *Apis* and *Myrmica* possess five pairs of tergocardiac muscles; in *Apis* these are of segments AIII–AVII, (Snodgrass, 1956), while in *Myrmica* they are of segments AIV–AVIII (Janet, 1902). This difference suggests loss of tergocardiac muscles may be associated with petiolation of the anterior metasoma, a pattern which deserves quantitative interrogation in ants. Additionally or alternatively, the number of tergocardiac muscles may vary in relation to body size.

4.8.2 | Alimentary tract

The crop, which is usually voluminous in ants (Caetano, 1990) appears quite small. However, this organ is membranous and extensible, and in the scanned specimen the crop is empty of fluid and partially collapsed. Because the crop does not maintain its full volume by air retention as in some insects (Chapman et al., 2013), any size assessment is provisional. Nevertheless, a small crop is reasonable given the association of this organ with food storage and the lack of known trophallaxis in *Amblyopone* (Chapman et al., 2013; Meurville & LeBoeuf, 2021; Solis et al., 2009).

The proventricular bulb is unusual in being hexamerous, as the usual state in ants is tetramery (Eisner & Brown, 1956; Eisner, 1957). The bulb is well-musculated with both longitudinal and circular muscles, although the precise number and arrangement of muscle bundles could not be ascertained. The pylorus bears a thick ring of tissue at its junction with the ventriculus which is likely the muscular pyloric sphincter, although the cellular structure of this high-contrast tissue was not unambiguously determined (Chapman et al., 2013). In their description of the digestive tract of *Paratrechina longicornis* (Formicinae) Solis et al. (2009) describe a "chamber" located "between the ileum and the ventriculus, where the Malpighian tubules converge" (pg. 56), previously called "*bexiga*" (Caetano et al., 2002) and propose this structure to be a formicid autapomorphy. It is presently unclear to us how this chamber differs from the pylorus, which has been partially described in ants as early as ("*orifice pylorique*" of Janet, 1902) and is generally recognized as one of the compartmentalizations of the alimentary canal (Chapman et al., 2013). Cuticular spines of the anterior ileum/pylorus, which have been described in *Dinoponera* (Ponerinae) and *Paraponera* (Caetano, 1990), were not observed.

The number of Malpighian tubules varies widely in ants, from as few as four in *Monomorium floricola* (Solis et al., 2013) to approximately 50 in some "poneroids" (Arab & Caetano, 2002).

The 10 Malpighian tubules observed here had uniform high contrast, precluding differentiation of subregions by epithelial cell structure (Arab & Caetano, 2002). We observed six rectal pads, as in Ponerinae, Pseudomyrmecinae, and Formicinae (Caetano, 1990); they appear distributed mainly in the anterior region of the rectum, but are evidently distorted in location and orientation along with the overall poorly resolved rectum. The rectal pads have bilayered walls. The outer wall is somewhat sclerotized, forming a thin "shell," which looks annular in sections and which might correspond to the "chitin ring" surrounding the rectal pads in *Dinoponera* (Caetano, 1990, p. 128). The inner wall is membranous and continuous with the dense internal convolutions, indicating that it is the basal plasma membrane. The anus and its musculature are superficially similar to the condition in *Myrmica* (Janet, 1902), and we similarly observe two large peripheral nerves associated with the anal tissues; unlike Janet (1902), we did not resolve a transverse occlusor of the anus, but a longitudinal *M. retractor ani* and circular *M. sphincter ani*, in addition to 9domm. The possible mode of action in the excretory process involves retraction of the proctiger membranes dorsad the anus by 9domm, followed by positioning of the anus through relaxation or partial contractions of *M. ret. ani* once the appropriate angle is attained, *M. sph. ani* can dilate to allow passage of excreta.

4.8.3 | Reproductive organs

The ovaries are well-developed and comprise four ovarioles each. The ovarioles appear to be active, containing oocytes at various stages of development. The distal parts of the vitellaria contain small, only partially distinct cells; more proximally, there are large cells with several highly contrasting organelles, which we infer to be trophocytes and nuclei; most proximally are large, uniformly contrasting cells, which we infer to be oocytes. The presence of intercalated oocytes and trophocytes indicates meroistic polytrophic ovarioles, which are present in most Endopterygota (Chapman et al., 2013) including ants (Billen, 1982a; Gobin et al., 1998; Khila &

Abouheif, 2008, 2010; Okada et al., 2010; Ramsay et al., 2020). Without a comparative point of reference, we cannot determine if the trophocytes are in the process of degeneration, which could suggest egg production, although the nuclei are qualitatively larger and less dense than predicted for degenerating trophocytes. Trophic eggs have been reported in *Amblyopone* (Gobin et al., 1998), but in a species with gamergates, which are absent in *A. australis*. Additionally, the species referenced by Gobin et al. (1998) may in fact belong to the genus *Stigmatomma*, to which the majority of erstwhile *Amblyopone* species were subsequently transferred (Yoshimura & Fisher, 2012). Young nonreproductive workers of *Diacamma* were observed to have oocytes and active trophocytes, while workers older than 180 days had both degenerated oocytes and trophocytes, in this case indicating loss of oogenic activity (Okada et al., 2010). The apparently active cells in the *Amblyopone* ovarioles might therefore not be evidence of egg production capacity but due to young age. The relative size of the oocytes to the trophocytes suggests that the former may have matured more than those of *Diacamma* workers by the onset of inactivity; however, our data were insufficient to quantify the developmental stage (King, 1970; Okada et al., 2010).

The distal portion of the oviduct was poorly resolved but shows some apparent differentiation into subregions. The median oviduct is distally dilated into an area which appears dish-like in our data set, but may properly be a pouch, with the dorsomedian membranes degraded or damaged; distad this area is a sclerotized, folded area forming a somewhat triangular, lobate area immediately proximal to the apex and opening of the oviduct. Because we could not determine the entire fine structure of these regions, and because the reproductive tract of workers (especially the oviduct) is understudied in ants, we refer to this entire region as the *distal oviduct*. It is possible that the dish-like region corresponds to a bursa copulatrix; the distal fold may be associated with musculature of the oviduct which was not resolved. An additional complication in our data set is that the dish-like dilation is closely approximated with a large peripheral nerve, which makes delimitation of the oviduct walls more difficult.

4.8.4 | Central nervous system

The abdominal central nervous system comprises the longitudinal connectives, or "main branches" of the ventral nerve cord, and the ganglia, which may represent single segmental neuromeres or fusions of two or more neuromeres (Niven et al., 2008). In Insecta generally, there are two large paired lateral connectives, and a small unpaired median nerve (Chapman et al., 2013; Klass, 2008b; Shankland, 1965). The median nerve was not resolved here, while in the anterior segments, a second pair of lateral connectives appears to be present. The latter observation, however, is probably artefactual, with these ancillary branches actually corresponding to either peripheral nerves or mislabeled fibers of the ventral diaphragm, or being attributable to damage causing separation of the components of the connectives. A single connective was reconstructed between the fourth

metasomal and terminal ganglia, which may be a true fusion (e.g., Birket-Smith, 1971) or an artifact of the close approximation of the branches.

The number of abdominal ganglia varies widely among insects, from the ordinal to subspecific level, due to variable patterns of neuromere fusion (Niven et al., 2008). Among the Hymenoptera there are as few as two abdominal ganglia in the Cynipidae and as many as eight in Tenthredinidae and *Sirex* (Brandt, 1879; Smith, 1972). There may even be a difference in ganglion count between males and females of the same species (Brandt, 1879). Among the ants, we observe six abdominal ganglia in *A. australis*; *Solenopsis invicta* has five (Choi et al., 2009) and *Myrmica rubra* has seven (Janet, 1902). Additionally, the site of fusion or anastomosis of nerves or neuromeres can be intraganglionic or extraganglionic (Klass, 2008b). This variation facilitates the occurrence of homoplasy and exacerbates its inferential effects (Niven et al., 2008). For these reasons, and due the limitations of the data set and our present scope, we do not attempt to homologize the ganglia of *A. australis* with those of other ants or Hymenoptera. Further, we do not provide homological or topographical descriptions of the peripheral nerves or their commerce with tissues, beyond a rough overview of the apparent association of the larger fibers of the terminal ganglion with certain organs. While a detailed description of the abdominal nervous system is merited, especially in a comparative-morphological and phylogenetic context, such study will certainly require different methods than those levied here, specifically in terms of freshly killed specimens, stains, and embedding (e.g., Klass, 2008b). Overall, the high degree of variability in the ventral nerve cord and ganglia in phylospace, but also through ontogeny, implies a complicated system of genetic, selective, functional, and developmental factors, the nature and interactions of which deserve attention.

Although we refrain from making definitive homology inferences about the nervous system, some general patterns can be considered. The fusion of the anterior two (or more) abdominal neuromeres to the metathoracic neuromere is frequently derived in Insecta, while the fusion of neuromeres AVIII–AX (and potential subsequent segments) into the terminal ganglion is probably the groundplan for Entognatha (Niven et al., 2008). On the other hand, the middle abdominal neuromeres are usually unfused (Niven et al., 2008). These patterns of consolidation may be associated with the anterior positional migration of ganglia in various Hymenoptera (Niven et al., 2008), which was also observed here. Presuming these fusions to be plesiomorphic, then the pattern of ganglion identity in *Amblyopone* would closely mirror that proposed for *Solenopsis* (Choi et al., 2009). Specifically, this would indicate the following homologies: second mesosomal ganglion = neuromeres ThII + ThIII + AI + AII; first metasomal ganglion = neuromere AIII; second metasomal ganglion = neuromere AIV; third metasomal ganglion = neuromere AV; fourth metasomal ganglion = neuromere AVI; terminal ganglion = neuromeres AVII + AVIII + AIX + AX. This is basically the same scheme inferred for *Apis* (Snodgrass, 1910), based on the segmental identity of the tissues innervated by the peripheral nerves of each ganglion.

4.8.5 | Space optimization

Gross modification of body segments can physically constrain the size, shape, and function of internal organs. For example, adult ants, like most Hymenoptera, are incapable of ingesting solid food particles beyond the infrabuccal pouch, since the esophagus must be extremely narrow to pass through the anterior metasomal segments. A compelling observation here is that the small crop is located largely within AII (the petiole; Figure 29a,c). Additionally, the first metasomal ganglion is located within the internal trough of the petiolar poststernite medial body (Figure 7d) and the second metasomal ganglion lies within the anterior region of ASIV. Further, the tergocardiac muscles of *Myrmica* are absent in both petiolated "waist" segments, AII and AIII (Janet, 1902). These observations raise the question of how the digestive, nervous, and circulatory organs are arranged in different lineages with a postpetiole (nodiform AIII), a larger crop, different metasomal ganglion counts, or a combination thereof. Because much study of the soft tissues neglects description or depiction of the organs in situ, we encourage future authors to consider exploring the relative spatial arrangement of these parts in specimens which are (at least partially) intact, before disarticulating or removing the organs for focused examination.

4.9 | Comparison of techniques and value of fundamental research

The multimodal approach employed here provides an opportunity to discuss the relative merits and drawbacks of the techniques used. Manual dissection with photomicroscopy provided clarity on elements of the base of the terebra, which were not resolved in micro-CT, nor visible in SEM due to the electron opacity of the ninth gonapophyses. On the other hand, the muscles were much more difficult to distinguish in manual dissection, and the technique is destructive, therefore only suitable when sufficient sampling has taken place and effectively prohibited for rare taxa. Since the difficulty of manual dissection and light imaging increases with decreasing body size and degree of sclerotization, the disadvantages of this technique are amplified in smaller ants and those of generally softer-bodied subfamilies like the Formicinae and Dolichoderinae.

Scanning electron microscopy permitted visualization of the structure of ATX, setae, and the barbules of the stylet and lancets. A higher vacuum SEM approach, including chemical dehydration and fixation, plus sputter-coating, would provide enhanced resolution and possibly depth of field. Critical-point drying would also enable SEM of dissected soft tissue and of partially membranous, delicate structures such as the valvilli. However, the low-vacuum machine used here does not require special preparation techniques and as such could be used quickly and cheaply within the constraints of our materials and facilities. Because original SEMs were acquired after identifying structures that could not be otherwise visualized, we feel that this method was sufficient for the present work, but encourage higher-resolution SEM imaging of sclerites, especially those of the valvilli, the sting base and terebral elements, and of setae across the body.

Histology provided the greatest detail of any technique applied here, and histological sections are, to a large extent, durable and reproducible in the same ways discussed below for CT (see, e.g., Matte & Billen, 2021). Skeletomuscular structures that were only resolved in histological sections include the spiracular muscles of AV, AVI, and AVIII, the valvilli of gonapophyses VIII, and the muscles of the venom and Dufour's gland ducts. The pygydial and sting bulb glands were only resolved histologically; the metapleural, Dufour, venom, sting shaft, and gonostylus glands were visible in the micro-CT scan. Additionally, histology confirmed the lack of a medial insertion for 8ccim and 9ccim. The major disadvantages of the histological approach are in specimen preparation, which requires live insects as starting material, and the limitation of any given section series to a single axis.

Micro-CT enables high-resolution three-dimensional reconstruction of internal anatomy to the scale of a few hundred nanometers. When applied to a targeted body region, micro-CT approximates the low range of the resolving power of SEM. However, as the resolution and number of stitched subscans increase, so does the required scan time and data set file size; modifications to the scan parameters and specimen preparation may also be required. Higher magnification scans limited to a single segment, or to the sting apparatus, may resolve the organs which were most poorly visible herein—specifically, the spiracular skeletomusculature, the dorsoventral extrinsic muscles of AVI and the coxapophyseal muscles, the fine details of the proximal processes of the gonapophyses, and the internal elements of the proximal sting.

One potential advantage of CT over histology is that in the latter, absolute contrast between tissues is determined at the time of staining and embedding. In conventional CT-scans, the X-ray absorption of tissues constrains relative contrast, thus soft tissue imaging usually requires staining (e.g., with iodine in absolute ethanol). Synchrotron light sources, however, provide additional phase contrast, enabling visualization of soft tissues without the need for staining (Betz et al., 2007).

An important factor is that micro-CT works with ethanol-preserved (Püffel et al., 2021) and dry-mounted specimens (Rühr et al., 2021) as well as with fossils preserved in a matrix (Boudinot et al., 2022a; Schwermann et al., 2016; Soriano et al., 2010; van de Kamp et al., 2018). We note that much of the value of CT-data is in their manipulability within visualization and analysis software, beyond rendering for study and communication. For this reason, we have made both the original CT-data set and our segmentation files accessible on Zenodo at doi.org/10.5281/zenodo.5553396 and encourage users of this text to explore these data interactively in three dimensions in addition to reviewing the figures published herein (the segmentation file is in.ORSSession format and requires Dragonfly, while the data set is a series of.tiff images suitable for most CT software).

The most important benefit of CT-data may be that they can are preserved even if the original specimen is lost or destroyed. The scan data exist digitally and can thus be backed up trivially and in a

decentralized, redundant manner. This capacity facilitates a specimen-oriented approach to morphology, which is often impossible due to the destructive nature of much anatomical investigation. Dissected organs can be preserved, but their preparation in situ is lost, and they become subject to degradation or preservational distortion. By contrast, digital three-dimensional anatomical data sets are linked to specimen-level metadata, and are easily shared among users and interconverted between datatypes. Therefore, beyond durability of data, digital anatomy facilitates reproducibility by permitting unlimited reanalysis of the same individual.

Replicability and durability of material at the individual specimen level are well-established tenets of systematics, embodied by physical types, and molecular genetics, with re-analyzable sequence data linked to specimen data from which they were extracted. Our hope is that the use of digital 3D-techniques will increasingly move morphology towards a similar paradigm. The fact that generating digital anatomical datasets facilitates future research is demonstrated by the present study: the CT-scan used here was originally generated as part of preliminary data exploration for an unrelated project. We hope therefore to emphasize the value of fundamental research, including hypothesis-free generation and exploration of 3D-anatomical data, or "night science" (Yanai & Lercher, 2019, 2020b, 2020a).

5 | CONCLUSION

The complete abdominal skeletomusculature and metasomal exocrine glands of the worker cast of the "poneroid" ant *Amblyopone australis* are described for the first time, using an integrative approach which synthesizes manual and digital techniques. We characterize the abdominal segmental groundplan and its exceptions in the context of serial homology and comparison to outgroup taxa. We formalize a nomenclatural system applicable generally to the abdomen of Hexapoda. We observe several traits meriting further investigation, especially in combination with phylogeny, to elucidate their evolutionary, structural, and functional implications. Specifically, we discuss the patterns of absence and variability in the sternal apodemes of insects, note the absence of the ASVII-gonapophyses VIII muscles in the "vespiform" aculeates, and propose the presence of muscle 8ccim as a synapomorphy of ants. We further discuss the homology and number of ATIX-proctiger muscles, the development and function of the postgenital tracheae, and the development of the arms of the dorsomedial seal of the lancets. We describe the metapleural and posterior metasomal glands, noting the apparent absence of the convoluted gland, the presence of the sting shaft gland for the first time outside of Ponerinae, and the first observation of the sting bulb gland in Amblyoponinae. We provide a morphological overview of the nervous, reproductive, digestive, and circulatory systems, confirming the unusual structure of the proventricular bulb, and fully characterizing the muscles of the anus for the first time in ants. We make methodological suggestions in the context of the strengths and limitations of the techniques used and outstanding research foci.

A comparative investigation of the abdominal skeletomusculature of a comprehensive sample of ants, in an explicitly phylogenetic context, would inform character transformation across Formicidae. We specifically predict that a comparison of the posterior pregenital segments will be valuable for understanding strength and directionality of selective forces at various node depths. A degree of skeletomuscular trait plasticity is apparent in aculeate lineages, given the variability of muscle origins and the presence or absence of skeletal traits such as the anterolateral sternal apodemes. Further, certain apomorphic states of the helcial skeletomusculature are known to be convergent in "poneroids" and "formicoids" (Fisher & Bolton, 2016; Hashimoto, 1996; Perrault, 2004), indicating that even complex, functional abdominal characters may be subject to homoplasy due to functional causes. Modern hymenopterists are advantaged by the development of robust independent molecular phylogenies within and across lineages, enabling mapping of character states to well-supported topologies (e.g., Barbosa et al., 2021), rather than primarily inferring phylogeny from difficult, highly variable, and often conflicting or autocorrelated traits. It is our aim that the present work will help provide a framework for future descriptive and comparative study of the ant abdomen, preferably across a wide sampling of clades, and serve to underscore the importance of anatomical data generation and primary research.

CONFLICTS OF INTEREST

The authors declare no conflicts of interest.

DATA AVAILABILITY STATEMENT

The data that support the findings of this study, including original CT and segmentation files, are available in Zenodo at doi.org/10.5281/zenodo.5553396

PERMISSION TO REPRODUCE MATERIAL

The micrograph in Figure 1a is reproduced from AntWeb.org with attribution as required. Permission for the SEM in Figure 26a was provided by Roberto Keller.

ORCID

Ziv E. Lieberman 🔟 https://orcid.org/0000-0001-6352-327X
Johan Billen 🔟 https://orcid.org/0000-0002-2392-7293
Thomas van de Kamp 🔟 http://orcid.org/0000-0001-7390-1318
Brendon E. Boudinot 🔟 https://orcid.org/0000-0002-4588-0430

REFERENCES

Aguiar, A. P., Deans, A. R., Engel, M. S., Forshage, M., Huber, J. T., Jennings, J. T., & Yu, D. S. K. (2013). Animal biodiversity: An outline of higher-level classification and survey of taxonomic richness: Order Hymenoptera. *Zootaxa*, *3703*(1), 51–62. https://doi.org/10.11646/zootaxa.3703.1.12

Aibekova, L., Boudinot, B. E., Beutel, R. G., Richter, A., Keller, R. A., Hita Garcia, F., & Economo, E. P. (2022). The skeletomuscular system of the mesosoma of *Formica rufa* workers (Hymenoptera: Formicidae). *Insect Systematics and Diversity*. Press. https://doi.org/10.1093/isd/ixac002

Andereck, J. W., King, J. G., & Hillyer, J. F. (2010). Contraction of the ventral abdomen potentiates extracardiac retrograde hemolymph propulsion in the mosquito hemocoel. *PLoS One*, *5*(9), e12943. https://doi.org/10.1371/journal.pone.0012943

Arab, A., & Caetano, F. H. (2002). Segmental specializations in the Malpighian tubules of the fire ant *Solenopsis saevissima* Forel 1904 (Myrmicinae): An electron microscopical study. *Arthropod Structure & Development*, *30*(4), 281–292.

Avise, J. C., & Robinson, T. J. (2008). Hemiplasy: A new term in the lexicon of phylogenetics. *Systematic Biology*, *57*(3), 503–507. https://doi.org/10.1080/10635150802164587

Badonnel, A. (1934). Recherches sur l'anatomie des Psoques, par André Badonnel. *Bulletin Biologique de France et de Belgique*, *18*(Suppl), 11–241.

Barbosa, D. N., Vilhelmsen, L., & Azevedo, C. O. (2021). Morphology of sting apparatus of Chrysidoidea (Hymenoptera, Aculeata). *Arthropod Structure & Development*, *60*, 100999. https://doi.org/10.1016/j.asd.2020.100999

Barden, P., Boudinot, B. E., & Lucky, A. (2017). Where fossils dare and males matter: Combined morphological and molecular analysis untangles the evolutionary history of the spider ant genus *Leptomyrmex* Mayr (Hymenoptera: Dolichoderinae). *Invertebrate Systematics*, *31*(6), 765–780. https://doi.org/10.1071/IS16067

Betz, O., Wegst, U., Weide, D., Heethoff, M., Helfen, L., Lee, W.-K., & Cloetens, P. (2007). Imaging applications of synchrotron X-ray phase-contrast microtomography in biological morphology and biomaterials science. I. General aspects of the technique and its advantages in the analysis of millimetre-sized arthropod structure. *Journal of Microscopy*, *227*(1), 51–71. https://doi.org/10.1111/j.1365-2818.2007.01785.x

Beutel, R. G., Friedrich, F., & Economo, E. P. (2021). Patterns of morphological simplification and innovation in the megadiverse Holometabola (Insecta). *Cladistics*, *cla*, *38*, 12483–245. https://doi.org/10.1111/cla.12483

Beutel, R. G., Friedrich, F., Yang, X.-K., & Ge, S.-Q. (2014). *Insect morphology and phylogeny: A textbook for students of entomology*. De Gruyter. https://doi.org/10.1515/9783110264043

Billen, J. (1982a). Ovariole development in workers of *Formica sanguinea* Latr. (Hymenoptera: Formicidae). *Insectes Sociaux*, *29*(1), 86–94. https://doi.org/10.1007/BF02224529

Billen, J. (1982b). The Dufour gland closing apparatus in *Formica sanguinea* Latreille (Hymenoptera, Formicidae). *Zoomorphology*, *99*(3), 235–244. https://doi.org/10.1007/BF00312297

Billen, J. (1990a). Morphology and ultrastructure of the Dufour's and venom gland in the ant *Myrmecia gulosa* (Fabr.) (Hymenoptera: Formicidae). *Australian Journal of Zoology*, *38*, 305–315.

Billen, J. (1990b). The sting bulb gland in *Myrmecia* and *Nothomyrmecia* (Hymenoptera: Formicidae): A new exocrine gland in ants. *International Journal of Insect Morphology and Embryology*, *19*(2), 133–139. https://doi.org/10.1016/0020-7322(90)90023-I

Billen, J. (2017). The metapleural gland of *Aneuretus simoni* (Formicidae, Aneuretinae). *Asian Myrmecology*, *9*(e009005). https://doi.org/10.20362/AM.009005

Billen, J., Attygalle, A. B., Morgan, E. D., & Ollett, D. G. (1987). The contents of the Dufour gland of the ant *Pogonomyrmex occidentalis*, *Chemistry and Biology of Social Insects* (pp. 426–427). Verlag J. Peperny.

Billen, J., Bauweleers, E., Hashim, R., & Ito, F. (2013). Survey of the exocrine system in *Protanilla wallacei* (Hymenoptera, Formicidae). *Arthropod Structure & Development*, *42*(3), 173–183. https://doi.org/10.1016/j.asd.2013.01.001

Billen, J., Evershed, R. P., Attygalle, A. B., Morgan, E. D., & Ollett, D. G. (1986). Contents of Dufour glands of workers of three species of *Tetramorium* (Hymenoptera: Formicidae). *Journal of Chemical Ecology*, *12*, 669–685.

Billen, J., Evershed, R. P., & Morgan, E. D. (1984). Morphological comparison of Dufour glands in workers of *Acromyrmex octospinosus* and *Myrmica rubra*. *Entomologia Experimentalis et Applicata*, *35*, 205–207.

Billen, J., & Gotwald, W. H., Jr. (1988). The crenellate lining of the Dufour gland in the genus Aenictus: A new character for interpreting the phylogeny of Old World army ants (Hymenoptera, Formicidae, Dorylinae). *Zoologica Scripta*, *17*, 293–295.

Billen, J., Grasso, D. A., Mori, A., & Le Moli, F. (2001). Structural and functional changes of the Dufour gland in gynes of the amazon ant *Polyergus rufescens* (Hymenoptera, Formicidae). *Zoomorphology*, *121*, 55–61.

Billen, J., Ito, F., Tsuji, K., Schoeters, E., Maile, R., & Morgan, E. D. (2000). Structure and chemistry of the Dufour gland in

Pristomyrmex ants (Hymenoptera, Formicidae). *Acta Zoologica*, 81, 159–166.

Billen, J., Jackson, B. D., & Morgan, E. D. (1988). Secretion of the Dufour gland of the ant *Nothomyrmecia macrops* (Hymenoptera: Formicidae). *Experientia*, 44, 715–719.

Billen, J. P. J. (1985). Comparative ultrastructure of the poison and Dufour glands in Old and New World army ants (Hymenoptera, Formicidae). *Actes Des Colloques Insectes Sociaux*, 2, 17–26.

Billen, J., & Šobotník, J. (2015). Insect exocrine glands. *Arthropod Structure & Development*, 44(5), 399–400. https://doi.org/10.1016/j.asd.2015.08.010

Billen, J., Stroobants, Z., Wenseleers, T., Hashim, R., & Ito, F. (2013). Diversity and morphology of abdominal glands in workers of the ant genus *Myopias* (Formicidae, Ponerinae). *Arthropod Structure & Development*, 42(3), 165–172. https://doi.org/10.1016/j.asd.2012.12.001

Billen, J., & Taylor, R. W. (1993). Notes on the aberrant venom gland morphology of some Australian dolichoderine and myrmicine ants (Hymenoptera, Formicidae). *Belgian Journal of Zoology*, 123(2), 59–163.

Billen, J., & van Boven, J. K. A. (1983). The chemical composition of the Dufour gland contents of workers of the ant *Formica cunicularia*: A test for recognition of the species. *Annales de La Société Zoologique de Belgique*, 113(suppl. 1), 283–289.

Billen, J., & van Boven, J. K. A. (1987). The metapleural gland in Old World army ants: A morphological and ultrastructural description (Hymenoptera, Formicidae). *Revue de Zoologie Africaine*, 101, 31–41.

Birket-Smith, J. (1971). The abdominal morphology of *Povilla adusta* Navas (Polymitarcidae) and of Ephemeroptera in general. *Insect Systematics & Evolution*, 2(2), 139–160. https://doi.org/10.1163/187631271X00176

Bitsch, J. (1973). Morphologie abdominale des machildes (Insecta Thysanura) I. Squelette et musculatures des segments prégénitaux. *Annales de Sciences Naturelles, Zoologie, Paris*, 12(15), 173–200.

Blanke, A., Watson, P. J., Holbrey, R., & Fagan, M. J. (2017). Computational biomechanics changes our view on insect head evolution. *Proceedings of the Royal Society B: Biological Sciences*, 284(1848), 20162412. https://doi.org/10.1098/rspb.2016.2412

Bolton, B. (1990a). Abdominal characters and status of the cerapachyine ants (Hymenoptera, Formicidae). *Journal of Natural History*, 24(1), 53–68. https://doi.org/10.1080/00222939000770051

Bolton, B. (1990b). Army ants reassessed—The phylogeny and classification of the doryline section (Hymenoptera, Formicidae). *Journal of Natural History*, 24, 1339–1364.

Bolton, B. (1990c). The higher classification of the ant subfamily Leptanillinae (Hymenoptera: Formicidae). *Systematic Entomology*, 15, 262–282.

Bolton, B. (1994). Identification Guide to the Ant Genera of the World. Harvard University Press.

Bolton, B. (2003). Synopsis and classification of Formicidae. *Memoirs of the American Entomological Institute*, 71, 1–370.

Bonhag, P. F. (1951). The skeleto-muscular mechanism of the head and abdomen of the adult horsefly (Diptera: Tabanidae). *Transactions of the American Entomological Society (1890-)*, 77(2), 131–202.

Borowiec, M. L. (2016). Generic revision of the ant subfamily Dorylinae (Hymenoptera, Formicidae). *ZooKeys*, 608, 1–280. https://doi.org/10.3897/zookeys.608.9427

Boudinot, B. E. (2015). Contributions to the knowledge of Formicidae (Hymenoptera, Aculeata): A new diagnosis of the family, the first global male-based key to subfamilies, and a treatment of early branching lineages. *European Journal of Taxonomy*, (120). https://doi.org/10.5852/ejt.2015.120

Boudinot, B. E. (2018). A general theory of genital homologies for the Hexapoda (Pancrustacea) derived from skeletomuscular correspondences, with emphasis on the Endopterygota. *Arthropod Structure & Development*, 47(6), 563–613. https://doi.org/10.1016/j.asd.2018.11.001

Boudinot, B. E., Khouri, Z., Richter, A., Griebenow, Z. H., van de Kamp, T., Perrichot, V., & Barden, P. (2022b). Evolution and systematics of the Aculeata and kin (Hymenoptera), with emphasis on the ants (Formicoidea: †@@@idae fam. nov., Formicidae). *bioRxiv*. https://doi.org/10.1101/2022.02.20.480183

Boudinot, B. E., Moosdorf, O. T. D., Beutel, R. G., & Richter, A. (2021). Anatomy and evolution of the head of *Dorylus helvolus* (Formicidae: Dorylinae): Patterns of sex- and caste-limited traits in the sausagefly and the driver ant. *Journal of Morphology*, jmor, 282, 21410–21658. https://doi.org/10.1002/jmor.21410

Boudinot, B. E., Perrichot, V., & Chaul, J. C. M. (2020). †*Camelosphecia* gen. nov., lost ant-wasp intermediates from the mid-Cretaceous (Hymenoptera, Formicoidea). *ZooKeys*, 1005, 21–55. https://doi.org/10.3897/zookeys.1005.57629

Boudinot, B. E., Richter, A., Katzke, J., Chaul, J. C. M., Keller, R. A., Economo, E. P., Beutel, R. G., & Yamamoto, S. (2022a). Evidence for the evolution of eusociality in stem ants and a systematic revision of † *Gerontoformica* (Hymenoptera: Formicidae). *Zoological Journal of the Linnean Society*, zlab097. https://doi.org/10.1093/zoolinnean/zlab097

Brandt, E. (1879). Vergleichend-anatomische Untersuchungen über das Nervensystem der Hymenopteren. *Horae Societatis Entomologicae Rossica*, 15, 31–50.

Brothers, D. J. (1975). Phylogeny and classification of the aculeate Hymenoptera, with special reference to Mutillidae. *The University of Kansas Science Bulletin*, 50(11), 483–648.

Brothers, D. J., & Carpenter, J. M. (1993). Phylogeny of Aculeata: Chrysidoidea and Vespoidea (Hymenoptera). *Journal of Hymenoptera Research*, 2(1), 76.

Brown, W. L., Jr. (1954). Remarks on the internal phylogeny and subfamily classification of the family Formicidae. *Insectes Sociaux*, 1, 21–31

Brown, W. L., Jr. (1967). A new *Pheidole* with reversed phragmosis (Hymenoptera: Formicidae). *Psyche: A Journal of Entomology*, 74(4), 331–339.

Caetano, F. H. (1990). Morphology of the digestive tract and associated excretory organs of ants. In R. K. Vander Meer, K. Jaffe, & A. Cedeno (Eds.), *Applied myrmecology: A world perspective* (pp. 119–129). Westview Press.

Caetano, F. H., Zara, F. J., & Jaffé, K. (2002). *Formigas: Biologia e anatomia*. F.H.C.

Callahan, P. S., Blum, M. S., & Walker, J. R. (1959). Morphology and histology of the poison glands and sting of the imported fire ant (*Solenopsis saevissima* v. *richteri* Forel). *Annals of the Entomological Society of America*, 52(5), 573–590. https://doi.org/10.1093/aesa/52.5.573

Carpenter, J. M. (1986). Cladistics of the Chrysidoidea (Hymenoptera). *Journal of the New York Entomological Society*, 94(3), 303–330.

Cecilia, A., Rack, A., Douissard, P. -A., Martin, T., dos Santos Rolo, T., Vagovič, P., Hamann, E., van de Kamp, T., Riedel, A., Fiederle, M., & Baumbach, T. (2011). LPE grown LSO: Tb scintillator films for high-resolution X-ray imaging applications at synchrotron light sources. *Nuclear instruments and methods in physics research section A: Accelerators, spectrometers, detectors and associated equipment*, 648, S321–S323.

Chapman, R. F., Simpson, S. J., & Douglas, A. E. (2013). *The insects: Structure and Function (Fifth edition)*. Cambridge University Press.

Choi, M.-Y., Raina, A., & Vander Meer, R. K. (2009). PBAN/pyrokinin peptides in the central nervous system of the fire ant, *Solenopsis invicta*. *Cell and Tissue Research*, 335(2), 431–439. https://doi.org/10.1007/s00441-008-0721-6

Consoulas, C., Hustert, R., & Theophilidis, G. (1993). The multisegmental motor supply to transverse muscles differs in a cricket and a bushcricket. *Journal of Experimental Biology*, 185(1), 335–355. https://doi.org/10.1242/jeb.185.1.335

Consoulas, C., & Theophilidis, G. (1992). Anatomy, innervation and motor control of the abdominal dorsal muscles of *Decticus albifrons* (Orthoptera). *Journal of Insect Physiology*, 38(12), 997–1010. https://doi.org/10.1016/0022-1910(92)90009-3

Daly, H. V. (1955). A comparative study of the sting of aculeate Hymenoptera. University of Kansas.

Davranoglou, L.-R., Baňař, P., Schlepütz, C. M., Mortimer, B., & Taylor, G. K. (2017). The pregenital abdomen of Enicocephalomorpha and morphological evidence for different modes of communication at the dawn of heteropteran evolution. *Arthropod Structure & Development*, 46(6), 843–868. https://doi.org/10.1016/j.asd.2017.08.006

Day, M. C. (1979). The affinities of *Loboscelidia* Westwood (Hymenoptera: Chrysididae, Loboscelidiinae). *Systematic Entomology*, 4(1), 21–30. https://doi.org/10.1111/j.1365-3113.1979.tb00608.x

Dessimoz, C. & Škunca, N., (Eds.). (2017). *The gene ontology handbook*. Springer New York. https://doi.org/10.1007/978-1-4939-3743-1

Dlussky, G. M., & Fedoseeva, E. B. (1988). Origin and early stages of evolution in ants. In (Ed.) Ponomarenko, A. G., *Melovoi biocenoticheskii krizis i rannie etapy evolyucii nasekomyh* (pp. 70–144). Izdatelstvo Nauka.

dos Santos Rolo, T., Ershov, A., van de Kamp, T., & Baumbach, T. (2014). In vivo X-ray cine-tomography for tracking morphological dynamics. *Proceedings of the National Academy of Sciences*, 111(11), 3921–3926.

Douissard, P.-A., Cecilia, A., Rochet, X., Chapel, X., Martin, T., van de Kamp, T., Helfen, L., Baumbach, T., Luquot, L., Xiao, X., Meinhardt, J., & Rack, A. (2012). A versatile indirect detector design for hard X-ray microimaging. *Journal of Instrumentation*, 7(09), P09016.

Egerton, R. F. (2005). *Physical principles of electron microscopy: An introduction to TEM, SEM, and AEM*. Springer.

Eisner, T. (1957). A comparative morphological study of the proventriculus of ants (Hymenoptera: Formicidae). *Bulletin of the Museum of Comparative Zoology*, 116, 439–490.

Eisner, T., & Brown, W. L., Jr. (1956). The evolution and social significance of the ant proventriculus. In (Ed.) Becker, E. C., *Proceedings of the Tenth International Congress of Entomology* (2, pp. 503–508). Mortimer Ltd.

Ernst, A., Mikó, I., & Deans, A. (2013). Morphology and function of the ovipositor mechanism in Ceraphronoidea (Hymenoptera, Apocrita). *Journal of Hymenoptera Research*, 33, 25–61. https://doi.org/10.3897/jhr.33.5204

Fischer, R. L. (1956). The muscular mechanism of the male metasoma and genitalia of *Megachile fortis* Cresson (Hymenoptera: Megachilidae). *The Canadian Entomologist*, 88(12), 657–673. https://doi.org/10.4039/Ent88657-12

Fisher, B. L., & Bolton, B. (2016). *Ants of Africa and Madagascar: A Guide to the Genera*. University of California Press.

Friedrich, F., & Beutel, R. G. (2008). The thorax of *Zorotypus* (Hexapoda, Zoraptera) and a new nomenclature for the musculature of Neoptera. *Arthropod Structure & Development*, 37(1), 29–54. https://doi.org/10.1016/j.asd.2007.04.003

Friedrich F., & Beutel R. G. (2010). The thoracic morphology of *Nannochorista* (Nannochoristidae) and its implications for the phylogeny of Mecoptera and Antliophora. *Journal of Zoological Systematics and Evolutionary Research*, 48(1), 50–74. https://doi.org/10.1111/j.1439-0469.2009.00535.x

Gauld, I. D., & Bolton, B. (Eds.). (1988). *The Hymenoptera*. Oxford University Press.

Gobin, B., Peeters, C., & Billen, J. (1998). Production of trophic eggs by virgin workers in the ponerine ant *Gnamptogenys menadensis*. *Physiological Entomology*, 23(4), 329–336. https://doi.org/10.1046/j.1365-3032.1998.234102.x

Graf, S., Willsch, M., & Ohl, M. (2021). Comparative morphology of the musculature of the sting apparatus in *Ampulex compressa* (Hymenoptera, Ampulicidae) and *Sceliphron destillatorium* (Hymenoptera, Sphecidae). *Deutsche Entomologische Zeitschrift*, 68(1), 21–32. https://doi.org/10.3897/dez.68.58217

Gremse, M., Chang, A., Schomburg, I., Grote, A., Scheer, M., Ebeling, C., & Schomburg, D. (2011). The BRENDA Tissue Ontology (BTO): The first all-integrating ontology of all organisms for enzyme sources. *Nucleic Acids Research*, 39(suppl_1), D507–D513. https://doi.org/10.1093/nar/gkq968

Gusmão, L. G., de, Caetano, F. H., & Nakano, O. (2001). Ultramorphology of the metapleural gland in three species of Atta (Hymenoptera, Formicidae, Ultramorphology of the metapleural gland in three species of Atta (Hymenoptera, Formicidae): Iheringia. *Série Zoologia*, 33–36. https://doi.org/10.1590/S0073-47212001000200003

Gutzeit, H. O., Zissler, D., & Fleig, R. (1993). Oogenesis in the honeybee *Apis mellifera*: Cytological observations on the formation and differentiation of previtellogenic ovarian follicles. *Roux's Archives of Developmental Biology*, 202(3), 181–191. https://doi.org/10.1007/BF00365309

Habenstein, J., Amini, E., Grübel, K., Jundi, B. el, & Rössler, W. (2020). The brain of *Cataglyphis* ants: Neuronal organization and visual projections. *Journal of Comparative Neurology*, 528(18), 3479–3506. https://doi.org/10.1002/cne.24934

Harris, R. A. (1979). A glossary of surface sculpturing. *Occasional Papers in Entomology. State of California Department of Food and Agriculture*, 28, 1–31. https://doi.org/10.5281/zenodo.26215

Hashimoto, Y. (1996). Skeletomuscular modifications associated with the formation of an additional petiole on the anterior abdominal segments in aculeate Hymenoptera. *Japanese Journal of Entomology*, 64, 340–356.

Hermann, H. R., & Chao, J.-T. (1983). Furcula, a major component of the hymenopterous venom apparatus. *International Journal of Insect Morphology and Embryology*, 12(5–6), 321–337. https://doi.org/10.1016/0020-7322(83)90027-2

Hermann, H. R. (1969). The hymenopterous poison apparatus: Evolutionary trends in three closely related subfamilies of ants (Hymenoptera: Formicidae). *Journal of the Georgia Entomological Society*, 4, 123–141.

Hieke, F. (1966). Vergleichende funktionelle Anatomie der Abdominalmuskulatur einiger männlicher Coleopteren unter besonderer Berücksichtigung des Genitoanalkomplexes. *Deutsche Entomologische Zeitschrift*, 13(1), 1–168.

Hillyer, J. F., & Pass, G. (2020). The insect circulatory system: Structure, function, and evolution. *Annual Review of Entomology*, 65(1), 121–143. https://doi.org/10.1146/annurev-ento-011019-025003

Hölldobler, B., & Engel-Siegel, H. (1985). On the metapleural gland of ants. *Psyche: A Journal of Entomology*, 91, 201–224.

Hölldobler, B., & Wilson, E. O. (1990). *The Ants*. Springer.

Hünefeld, F. (2007). The genital morphology of *Zorotypus hubbardi* Caudell, 1918 (Insecta: Zoraptera: Zorotypidae). *Zoomorphology*, 126(3), 135–151. https://doi.org/10.1007/s00435-007-0033-5

Hünefeld, F. (2009). The evolution of the female postabdomen and genitalia in mecopterid insects (Insecta: Mecopterida). Friedrich-Schiller-Universität Jena.

Hünefeld, F., Mißbach, C., & Beutel, R. G. (2012). The morphology and evolution of the female postabdomen of Holometabola (Insecta). *Arthropod Structure & Development*, 41(4), 361–371. https://doi.org/10.1016/j.asd.2012.05.002

Hustert, R., Frisch, M., Böhm, A., & Pass, G. (2014). A new kind of auxiliary heart in insects: Functional morphology and neuronal control of the accessory pulsatile organs of the cricket ovipositor. *Frontiers in Zoology*, 11(1), 43. https://doi.org/10.1186/1742-9994-11-43

Jałoszyński, P., Luo, X., & Beutel, R. G. (2020). Profound head modifications in *Claviger testaceus* (Pselaphinae, Staphylinidae, Coleoptera) facilitate integration into communities of ants. *Journal of Morphology*, 281(9), 1072–1085. https://doi.org/10.1002/jmor.21232

Janet, C. (1893). *Études sur les fourmis, les guêpes et les abeilles*. Société entomologique de France.

Janet, C. (1894). Note 7: Sur l'anatomie du pétiole de *Myrmica rubra* L. *Mémoires de la Société Zoologique de France*, 7, 185–202.

Janet, C. (1897). *Études sur les fourmis, les guêpes et les abeilles. Note 16. Limites morphologiques des anneaux post-céphaliques et musculature des anneaux post-thoraciques chez la Myrmica rubra*. Le Bigot Frères.

Janet, C. (1898a). *Note 18. Aiguillon de laAppareil de fermeture de la glande à venin Myrmica rubra*: G. Carré et C. Naud.

Janet, C. (1898b). Note 19. Anatomie du corselet de la *Myrmica rubra* reine. *Mémoires de La Société Zoologique de France*, 11, 393–450.

Janet, C. (1898c). Sur on organe non décrit, servant à la fermeture du réservoir du venin et sur le mode de fonctionnement de l'aiguillon chez les Fourmis. *Comptes Rendus de l'Académie des Sciences*, 127, 638–341.

Janet, C. (1902). *Anatomie du gaster de la Myrmica rubra*. G. Carré et C. Naud.

Keller, R. A. (2011). A phylogenetic analysis of ant morphology (Hymenoptera: Formicidae) with special reference to the poneromorph subfamilies. *Bulletin of the American Museum of Natural History*, 355, 1–90. https://doi.org/10.1206/355.1

Khalife, A., Keller, R. A., Billen, J., Hita Garcia, F., Economo, E. P., & Peeters, C. (2018). Skeletomuscular adaptations of head and legs of *Melissotarsus* ants for tunnelling through living wood. *Frontiers in Zoology*, 15(1), 30. https://doi.org/10.1186/s12983-018-0277-6

Khila, A., & Abouheif, E. (2008). Reproductive constraint is a developmental mechanism that maintains social harmony in advanced ant societies. *Proceedings of the National Academy of Sciences*, 105(46), 17884–17889. https://doi.org/10.1073/pnas.0807351105

Khila, A., & Abouheif, E. (2010). Evaluating the role of reproductive constraints in ant social evolution. *Philosophical Transactions of the Royal Society, B: Biological Sciences*, 365(1540), 617–630. https://doi.org/10.1098/rstb.2009.0257

Kimsey, L. S. (1992). Functional morphology of the abdomen and phylogeny of the chrysidid wasps (Hymenoptera: Chrysididae). *Journal of Hymenoptera Research*, 1, 165–174.

King, R. C. (1970). *Ovarian Development in Drosophila melanogaster*. Academic Press.

Klass, K.-D. (2001). The female abdomen of the viviparous earwig *Hemimerus vosseleri* (Insecta: Dermaptera: Hemimeridae), with a discussion of the postgenital abdomen of Insecta. *Zoological Journal of the Linnean Society*, 131(3), 251–307. https://doi.org/10.1006/zjls.2001.0246

Klass, K.-D. (2008a). The female abdomen of ovipositor-bearing Odonata (Insecta: Pterygota). *Arthropod Systematics & Phylogeny*, 66(1), 45–142.

Klass, K.-D. (2008b). The pregenital abdomen of a mantid and a cockroach: Musculature and nerve topography, with comparative remarks on other Neoptera (Insecta: Dictyoptera). *Deutsche Entomologische Zeitschrift*, 46(1), 3–42. https://doi.org/10.1002/mmnd.19990460102

Klopfstein, S., Vilhelmsen, L., & Ronquist, F. (2015). A nonstationary Markov model detects directional evolution in Hymenopteran morphology. *Systematic Biology*, 64(6), 1089–1103. https://doi.org/10.1093/sysbio/syv052

Kugler, C. (1978). Comparative study of myrmicine sting apparatus (Hymenoptera, Formicidae). *Studia Entomologica*, 20, 413–548.

Kugler, C. (1979). Evolution of the sting apparatus in the myrmicine ants. *Evolution*, 33(1), 117–130.

Kugler, C. (1980). The sting apparatus in the primitive ants *Nothomyrmecia* and *Myrmecia*. *Journal of the Australian Entomological Society*, 19, 263–267. https://doi.org/10.1111/j.1440-6055.1980.tb00983.x

Kugler, C. (1992). Stings of ants of the Leptanillinae (Hymenoptera: Formicidae). *Psyche: A. Journal of Entomology*, 99(1), 103–115. https://doi.org/10.1155/1992/70194

Kugler, C. (1997). Stings of some species of *Lordomyrma* and *Mayriella* (Formicidae: Myrmicinae). *Insecta Mundi*, 11(3–4), 193–199.

Kumpanenko, A., Gladun, D., & Vilhelmsen, L. (2019). Functional morphology and evolution of the sting sheaths in Aculeata (Hymenoptera). *Arthropod Systematics & Phylogeny*, 77(2), 325–338. https://doi.org/10.26049/ASP77-2-2019-08

Kumpanenko, A. S., & Gladun, D. V. (2018). Functional morphology of the sting apparatus of the spider wasp *Cryptocheilus versicolor* (Scopoli, 1763) (Hymenoptera: Pompilidae). *Entomological Science*, 21(1), 124–132. https://doi.org/10.1111/ens.12288

Kuwasawa, K., Ai, H., & Matsushita, T. (1999). Cardiac reflexes and their neural pathways in lepidopterous insects. *Comparative Biochemistry and Physiology Part A: Molecular & Integrative Physiology*, 124(4), 581–586. https://doi.org/10.1016/S1095-6433(99)00153-1

Lighton, J. R. B., & Garrigan, D. (1995). Ant breathing: Testing regulation and mechanism hypotheses with hypoxia. *The Journal of Experimental Biology*, 198, 1613–1620.

Liu, S.-P., Richter, A., Stoessel, A., & Beutel, R. G. (2019). The mesosomal anatomy of *Myrmecia nigrocincta* workers and evolutionary transformations in Formicidae (Hymenoptera). *Arthropod Systematics & Phylogeny*, 77(1), 1–19. https://doi.org/10.26049/ASP77-1-2019-01

Loktionov, V., & Lelej, A. (2008). On the morphological differences between related species of spider wasps *Auplopus* Spinola, 1841 (Hymenoptera, Pompilidae). Чтения Памяти Алексея Ивановича Куренцова, 19, 35–41.

Markl, H. (1966). Peripheres Nervensystem und Muskulatur im Thorax der Arbeiterin von *Apis mellifica* L., *Formica polyctena* Foerster und *Vespa vulgaris* L. und der Grundplan der Innervierung des Insektenthorax. *Zoologische Jahrbücher, Abteilung Für Anatomie Und Ontogenie Der Tiere*, 83, 107–184.

Masuko, K. (2020). Colony composition, arthropod egg predation, and antennal structure of the ant *Discothyrea sauteri* (Hymenoptera: Formicidae). *Asian Myrmecology*, 12, e012002. https://doi.org/10.20362/AM.012002

Matsuda, R. (1957). Comparative morphology of the abdomen of a machilid and a rhaphidiid. *Transactions of the American Entomological Society (1890-)*, 83(1), 39–63.

Matte, A., & Billen, J. (2021). Flight muscle histolysis in *Lasius niger* queens. *Asian Myrmecology*, 13, 1–16.

Matushkina, N. (2011). Sting microsculpture in the digger wasp *Bembix rostrata* (Hymenoptera, Crabronidae). *Journal of Hymenoptera Research*, 21, 41–52. https://doi.org/10.3897/jhr.21.873

Meurville, M.-P., & LeBoeuf, A. C. (2021). Trophallaxis: The functions and evolution of social fluid exchange in ant colonies (Hymenoptera: Formicidae). *Myrmecological News*, 31, 1–30. https://doi.org/10.25849/myrmecol.news_031:001

Miller, F. W. (1933). Musculature of the lacewing (*Chrysopa plorabunda*) Neuroptera. *Journal of Morphology*, 55(1), 29–51. https://doi.org/10.1002/jmor.1050550104

Möglich, M., & Hölldobler, B. (1974). Social carrying behavior and division of labor during nest moving in ants. *Psyche: A Journal of Entomology*, 81(2), 219–236. https://doi.org/10.1155/1974/25763

Nation, J. L. (2008). Alary Muscles. In (Ed.) Capinera, J. L., *Encyclopedia of entomology* (pp. 95–95). Springer Netherlands. https://doi.org/10.1007/978-1-4020-6359-6_127

Niven, J. E., Graham, C. M., & Burrows, M. (2008). Diversity and evolution of the insect ventral nerve cord. *Annual Review of Entomology*, 53(1), 253–271. https://doi.org/10.1146/annurev.ento.52.110405.091322

Noirot, C., & Quennedey, A. (1974). Fine structure of insect epidermal glands. *Annual Review of Entomology*, 19(1), 61–80. https://doi.org/10.1146/annurev.en.19.010174.000425

Noirot, C., & Quennedey, A. (1991). Glands, gland cells, glandular units: Some comments on terminology and classification. *Annales de La Société Entomologique de France (N.S.)*, 27(2), 123–128.

Nutting, W. L. (1951). A comparative anatomical study of the heart and accessory structures of the orthopteroid insects. *Journal of Morphology*, 89(3), 501–597. https://doi.org/10.1002/jmor.1050890306

Oeser, R. (1961). Vergleichend-morphologische Untersuchungen über den Ovipositor der Hymenopteren. *Mitteilungen Aus Dem Museum Für Naturkunde in Berlin. Zoologisches Museum Und Institut Für Spezielle Zoologie (Berlin)*, 37(1), 3–119. https://doi.org/10.1002/mmnz.19610370102

Okada, Y., Miyazaki, S., Miyakawa, H., Ishikawa, A., Tsuji, K., & Miura, T. (2010). Ovarian development and insulin-signaling pathways during reproductive differentiation in the queenless ponerine ant Diacamma sp. *Journal of Insect Physiology*, 56(3), 288–295. https://doi.org/10.1016/j.jinsphys.2009.10.013

Ovtshinnikova, O. G., & Galinskaya, T. V. (2016). Musculature of the abdomen and male genitalia of a member of Celyphidae (Diptera, Cyclorrhapha). *Oriental Insects*, 50(4), 178–186. https://doi.org/10.1080/00305316.2016.1227733

Ovtshinnikova, O. G., Galinskaya, T. V., & Lukashevich, E. D. (2018). Skeleton and musculature of the male abdomen in Tanyderidae (Diptera, Nematocera) of the Southern Hemisphere. *ZooKeys*, 809, 55–77. https://doi.org/10.3897/zookeys.809.29032

Packer, L. (2003). Comparative morphology of the skeletal parts of the sting apparatus of bees (Hymenoptera: Apoidea). *Zoological Journal of the Linnean Society*, 138(1), 1–38. https://doi.org/10.1046/j.1096-3642.2003.00055.x

Paganin, D., Mayo, S. C., Gureyev, T. E., Miller, P. R., & Wilkins, S. W. (2002). Simultaneous phase and amplitude extraction from a single defocused image of a homogeneous object. *Journal of Microscopy*, 206, 33–40.

Pass, G. (2000). Accessory pulsatile organs: Evolutionary innovations in insects. *Annual Review of Entomology*, 45(1), 495–518. https://doi.org/10.1146/annurev.ento.45.1.495

Pavan, M., & Ronchetti, G. (1955). Studi sulla morfologia esterna e anatomia interna dell'operaia di Iridomyrmex humilis Mayr e ricerche chimiche e biologiche sulla iridomirmecina. *Atti della Società italiana di scienze naturali*, 94, 379–477.

Peeters, C., & De Greef, S. (2015). Predation on large millipedes and self-assembling chains in Leptogenys ants from Cambodia. *Insectes Sociaux*, 62(4), 471–477. https://doi.org/10.1007/s00040-015-0426-2

Pereanu, W., Spindler, S., Cruz, L., & Hartenstein, V. (2007). Tracheal development in the Drosophila brain is constrained by glial cells. *Developmental Biology*, 302(1), 169–180. https://doi.org/10.1016/j.ydbio.2006.09.022

Perrault, G. H. (2004). Étude morphoanatomique et biométrique du métasoma antérieur des ouvrières. Contribution à la systématique et à la phylogénie des fourmis (Hymenoptera: Formicidae). *Annales de La Société Entomologique de France (N.S.)*, 40(3–4), 291–371. https://doi.org/10.1080/00379271.2004.10697428

Piek, T. (1986). *Venoms of the Hymenoptera: Biochemical, Pharmacological and Behavioural Aspects*. Academic Press.

Poinapen, D., Konopka, J. K., Umoh, J. U., Norley, C. J. D., McNeil, J. N., & Holdsworth, D. W. (2017). Micro-CT imaging of live insects using carbon dioxide gas-induced hypoxia as anesthetic with minimal impact on certain subsequent life history traits. *BMC Zoology*, 2, 9.

Poldi, B. (1963). Alcune osservazioni sul Proceratium melinum Rog. E sulla fuzione della particolare struttura del gastro. *Atti della Accademia Nazionale Italiana di Entomologia, Rendiconti*, 11, 221–229.

Pollock, J. N. (1999). A study of the male abdomen of Gyrostigma rhinocerontis Hope (Diptera: Gasterophilidae), the stomach bot of the African rhinoceroses, with notes on the ground plan and affinities of Gasterophilidae. *Journal of Natural History*, 33(5), 777–788. https://doi.org/10.1080/002229399300173

Püffel, F., Pouget, A., Liu, X., Zuber, M., van de Kamp, T., Roces, F., & Labonte, D. (2021). Morphological determinants of bite force capacity in insects: A biomechanical analysis of polymorphic leaf-cutter ants. *Journal of the Royal Society Interface*, 18(182), 20210424. https://doi.org/10.1098/rsif.2021.0424

Quicke, D., Fitton, M. G., & Ingram, S. (1992). Phylogenetic implications of the structure and distribution of ovipositor valvilli in the Hymenoptera (Insecta). *Journal of Natural History*, 26, 587–608. https://doi.org/10.1080/00222939200770361

Ramsay, C., Lasko, P., & Abouheif, E. (2020). Evo-devo lessons from the reproductive division of labor in eusocial hymenoptera. In (Eds.) Nuno de la Rosa, L. & Müller, G., *Evolutionary Developmental Biology* (pp. 1–14). Springer International Publishing. https://doi.org/10.1007/978-3-319-33038-9_173-1

Rasnitsyn, A. P. (1988). An outline of evolution of the hymenopterous insects (Order Vespida). *Oriental Insects*, 22(1), 115–145. https://doi.org/10.1080/00305316.1988.11835485

Remane, A. (1952). *Die Grundlagen des natürlichen Systems, der vergleichenden Anatomie und der Phylogenetik*. Leipzig: Geest & Portig K.-G.

Richards, A. G. (1963). The ventral diaphragm of insects. *Journal of Morphology*, 113(1), 17–47. https://doi.org/10.1002/jmor.1051130103

Richter, A., Hita Garcia, F., Keller, R. A., Billen, J., Economo, E. P., & Beutel, R. G. (2020). Comparative analysis of worker head anatomy of Formica and Brachyponera (Hymenoptera: Formicidae). *Arthropod Systematics & Phylogeny*, 78(1), 133–170. https://doi.org/10.26049/ASP78-1-2020-06

Richter, A., Hita Garcia, F., Keller, R. A., Billen, J., Katzke, J., Boudinot, B. E., & Beutel, R. G. (2021). The head anatomy of Protanilla lini (Hymenoptera: Formicidae: Leptanillinae), with a hypothesis of their mandibular movement. *Myrmecological News*, 31, 85–114. https://doi.org/10.25849/myrmecol.news_031:085

Richter, A., Keller, R. A., Rosumek, F. B., Economo, E. P., Hita Garcia, F., & Beutel, R. G. (2019). The cephalic anatomy of workers of the ant species Wasmannia affinis (Formicidae, Hymenoptera, Insecta) and its evolutionary implications. *Arthropod Structure & Development*, 49, 26–49. https://doi.org/10.1016/j.asd.2019.02.002

Rietschel, P. (1937). Bau und Funktion des Wehrstachels der staatenbildenden Bienen und Wespen. *Zeitschrift für Morphologie und Ökologie der Tiere*, 33(3), 313–357. https://doi.org/10.1007/BF00407850

Ronquist, F., Rasnitsyn, A. P., Roy, A., Eriksson, K., & Lindgren, M. (1999). Phylogeny of the Hymenoptera: A cladistic reanalysis of Rasnitsyn's (1988) data. *Zoologica Scripta*, 28(1–2), 13–50. https://doi.org/10.1046/j.1463-6409.1999.00023.x

Rühr, P. T., van de Kamp, T., Faragó, T., Hammel, J. U., Wilde, F., Borisova, E., Edel, C., Frenzel, M., Baumbach, T., & Blanke, A. (2021). Juvenile ecology drives adult morphology in two insect orders. *Proceedings of the Royal Society B: Biological Sciences*, 288(1953), 20210616. https://doi.org/10.1098/rspb.2021.0616

Schoeters, E., & Billen, J. (1992). Morphological and ultrastructural study of the metapleural gland in Diacamma (Hymenoptera, Formicidae), *Biology and Evolution of Social Insects* (pp. 239–247). Leuven University Press.

Schoeters, E., & Billen, J. (1993). Anatomy and fine structure of the metapleural gland in Atta (Hymenoptera, Formicidae). *Belgian Journal of Zoology*, 123(1), 67–75.

Schoeters, E., & Billen, J. (1996). The control apparatus of the venom gland in formicine ants (Hymenoptera: Formicidae). *Netherlands Journal of Zoology*, 46(3–4), 281–289.

Schoeters, E., Ito, F., Miyata, H., & Billen, J. (1999). Aberrant venom glands in Amblyoponini (Formicidae, Ponerinae): Morphology, ultrastructure and

histochemistry. *Acta Zoologica*, 80(1), 3–9. https://doi.org/10.1046/j.1463-6395.1999.20001.x

Schwermann, A. H., dos Santos Rolo, T., Caterino, M. S., Bechly, G., Schmied, H., Baumbach, T., & van de Kamp, T. (2016). Preservation of three-dimensional anatomy in phosphatized fossil arthropods enriches evolutionary inference. *eLife*, 5, e12129. https://doi.org/10.7554/eLife.12129

Shankland, D. L. (1965). Nerves and muscles of the pregenital abdominal segments of the American cockroach, *Periplaneta americana* (L.). *Journal of Morphology*, 117(3), 353–385. https://doi.org/10.1002/jmor.1051170304

Short, J. R. T. (1959). On the skeleto-muscular mechanisms of the anterior abdominal segments of certain adult Hymenoptera. *Transactions of the Royal Entomological Society of London*, 111(8), 175–203. https://doi.org/10.1111/j.1365-2311.1959.tb02281.x

Silva, T. S. R., & Feitosa, R. M. (2019). Using controlled vocabularies in anatomical terminology: A case study with *Strumigenys* (Hymenoptera: Formicidae). *Arthropod Structure & Development*, 52, 100877. https://doi.org/10.1016/j.asd.2019.100877

Smith, E. L. (1969). Evolutionary morphology of external insect genitalia. 1. Origin and relationships to other appendages *Annals of the Entomological Society of America*, 62(5), 1051–1079.

Smith, E. L. (1970). Evolutionary morphology of the external insect genitalia. 2. Hymenoptera. *Annals of the Entomological Society of America*, 63(1), 1–27. https://doi.org/10.1093/aesa/63.1.1

Smith, E. L. (1972). Biosystematics and morphology of symphyta—III. External genitalia of *Euura* (Hymenoptera: Tenthredinidae): Sclerites, sensilla, musculature, development and oviposition behavior. *International Journal of Insect Morphology and Embryology*, 1(4), 321–365. https://doi.org/10.1016/0020-7322(72)90016-5

Snodgrass, R. E. (1910). Anatomy of the Honey Bee. *U.S. Department of Agriculture, Bureau of Entomology, Technical Series*, 18, 1–162.

Snodgrass, R. E. (1933). How the bee stings. *Bee World*, 14(1), 3–6. https://doi.org/10.1080/0005772X.1933.11093188

Snodgrass, R. E. (1935a). *Principles of Insect Morphology*. McGraw-Hill Book Company, Inc.

Snodgrass, R. E. (1935b). The abdominal mechanisms of a grasshopper. *Smithsonian Miscellaneous Collections*, 94(6).

Snodgrass, R. E. (1935c). The bee laboratory. *Bee World*, 16(1), 9–11. https://doi.org/10.1080/0005772X.1935.11093387

Snodgrass, R. E. (1942). The skeleto-muscular mechanisms of the honey bee. *Smithsonian Miscellaneous Collections*, 103(2), 124.

Snodgrass, R. E. (1947). The skeletal anatomy of fleas (Siphonaptera). *Smithsonian Miscellaneous Collections*, 104(18), 123.

Snodgrass, R. E. (1956). *Anatomy of the honey bee* (1st ed.). Cornell University.

Snodgrass, R. E. (1962). Suture or sulcus? *Proceedings of the Entomological Society of Washington*, 64, 222–223.

Socha, J. J., Förster, T. D., & Greenlee, K. J. (2010). Issues of convection in insect respiration: Insights from synchrotron X-ray imaging and beyond. *Respiratory Physiology & Neurobiology*, 173, S65–S73. https://doi.org/10.1016/j.resp.2010.03.013

Solis, D. R., Caetano, F. H., Yabuki, A. T., Moretti, T. C., & Bueno, O. C. (2009). Ultramorphology of the digestive tract of *Paratrechina longicornis* (Hymenoptera, Formicidae). *Sociobiology*, 53, 51–59.

Solis, D. R., Rossi, M. L., Fox, E. G. P., de Lima Nogueira, N., Tanaka, F. A. O., & Bueno, O. C. (2013). On the morphology of the digestive system of two *Monomorium* ant species. *Journal of Insect Science*, 13(1), 70. https://doi.org/10.1673/031.013.7001

Soriano, C., Archer, M., Azar, D., Creaser, P., Delclòs, X., Godthelp, H., Hand, S., Jones, A., Nel, A., Néraudeau, D., Ortega-Blanco, J., Pérez-de la Fuente, R., Perrichot, V., Saupe, E., Kraemer, M. S., & Tafforeau, P. (2010). Synchrotron X-ray imaging of inclusions in amber. *Comptes Rendus Palevol*, 9(6–7), 361–368. https://doi.org/10.1016/j.crpv.2010.07.014

Taylor, R. W. (1978). *Nothomyrmecia macrops*: A living-fossil ant rediscovered. *Science (New York, N.Y.)*, 201(4360), 979–985. https://doi.org/10.1126/science.201.4360.979

Traniello, J. F. A. (1978). Caste in a primitive ant: Absence of age polyethism in *Amblyopone*. *Science*, 202(4369), 770–772. https://doi.org/10.1126/science.202.4369.770

Traniello, J. F. A. (1982). Population structure and social organization in the primitive ant *Amblyopone pallipes* (Hymenoptera: Formicidae). *Psyche: A Journal of Entomology*, 89(1–2), 65–80. https://doi.org/10.1155/1982/79349

Trojan, E. (1935). Zur Frage der Oligomerie weiblicher Akuleaten. *Zeitschrift für Morphologie und Ökologie der Tiere*, 30(4), 597–628. https://doi.org/10.1007/BF00403139

Tulloch, G. S. (1936). The metasternal glands of the ant, *Myrmica rubra*, with special reference to the Golgi bodies and the intracellular canaliculi. *Annals of the Entomological Society of America*, 29, 81–84.

Tulloch, G. S., Shapiro, J. E., & Hershenov, B. (1963). The ultrastructure of the metasternal glands of ants. *Bulletin of the Brooklyn Entomological Society*, 57, 91–101.

van de Kamp, T., Schwermann, A. H., dos Santos Rolo, T., Lösel, P. D., Engler, T., Etter, W., Faragó, T., Göttlicher, J., Heuveline, V., Kopmann, A., Mähler, B., Mörs, T., Odar, J., Rust, J., Tan Jerome, N., Vogelgesang, M., Baumbach, T., & Krogmann, L. (2018). Parasitoid biology preserved in mineralized fossils. *Nature Communications*, 9(1), 3325. https://doi.org/10.1038/s41467-018-05654-y

van Marle, J., & Piek, T. (1986). Morphology of the venom apparatus. In T. Piek (Ed.), *Venoms of the hymenoptera: Biochemical, pharmacological and behavioural aspects* (pp. 17–44).

Vasvary, L. M. (1966). Musculature and nervous system of the thorax, of the sound mechanism, and of a typical pregenital abdominal segment of the male of the annual cicada, *Tibicen chloromera* (Walker) (Homoptera: Cicadidae). *Journal of the New York Entomological Society*, 74(1), 2–55.

Vilhelmsen, L. (2000). The ovipositor apparatus of basal Hymenoptera (Insecta): Phylogenetic implications and functional morphology. *Zoologica Scripta*, 29(4), 319–345. https://doi.org/10.1046/j.1463-6409.2000.00046.x

Vogelgesang, M., Chilingaryan, S., dos Santos Rolo, T., & Kopmann, A. (2012). UFO: A scalable GPU-based image processing framework for on-line monitoring. *Proceedings of the HPCC-ICESS*, 824–829.

Vogelgesang, M., Farago, T., Morgeneyer, T. F., Helfen, L., dos Santos Rolo, T., Myagotin, A., & Baumbach, T. (2016). Real-time image-content-based beamline control for smart 4D X-ray imaging. *Real-time image-content-based beamline control for smart 4D X-ray imaging*, 23, 1254–1263.

von Kéler, S. (1955). *Entomologisches Worterbuch*. Akademie-Verlag.

Westneat, M. W. (2003). Tracheal respiration in insects visualized with synchrotron X-ray imaging. *Science*, 299(5606), 558–560. https://doi.org/10.1126/science.1078008

Wheeler, W. M. (1927). Ants of the genus *Amblyopone* Erichson. *Proceedings of the American Academy of Arts and Sciences*, 62(1), 1–29.

Wilson, E. O. (1955). A monographic revision of the ant genus *Lasius*. *Bulletin of the Museum of Comparative. Zoology*, 113, 1–201. https://doi.org/10.5281/zenodo.25290

Wilson, E. O. (1971). *The Insect Societies*. Harvard University Press.

Wilson, E. O., Carpenter, F. M., & Brown, W. L., Jr. (1967). The first Mesozoic ants, with the description of a new subfamily. *Psyche: A Journal of Entomology*, 74, 1–19.

Wipfler, B., Letsch, H., Frandsen, P. B., Kapli, P., Mayer, C., Bartel, D., Buckley, T. R., Donath, A., Edgerly-Rooks, J. S., Fujita, M., Liu, S., Machida, R., Mashimo, Y., Misof, B., Niehuis, O., Peters, R. S., Petersen, M., Podsiadlowski, L., Schütte, K., … Simon, S. (2019). Evolutionary history of Polyneoptera and its implications for our

understanding of early winged insects. *Proceedings of the National Academy of Sciences*, 116(8), 3024–3029. https://doi.org/10.1073/pnas.1817794116

Yanai, I., & Lercher, M. (2019). Night science. *Genome Biology*, 20(1), 179. https://doi.org/10.1186/s13059-019-1800-6

Yanai, I., & Lercher, M. (2020a). A hypothesis is a liability. *Genome Biology*, 21(1), 231. https://doi.org/10.1186/s13059-020-02133-w

Yanai, I., & Lercher, M. (2020b). The two languages of science. *Genome Biology*, 21(1), 147. https://doi.org/10.1186/s13059-020-02057-5

Yek, S. H., & Mueller, U. G. (2011). The metapleural gland of ants. *Biological Reviews*, 86(4), 774–791. https://doi.org/10.1111/j.1469-185X.2010.00170.x

Yoder, M. J., Mikó, I., Seltmann, K. C., Bertone, M. A., & Deans, A. R. (2010). A gross anatomy ontology for Hymenoptera. *PLoS One*, 5(12), e15991. https://doi.org/10.1371/journal.pone.0015991

Yoshimura, M., & Fisher, B. L. (2012). A revision of male ants of the Malagasy Amblyoponinae (Hymenoptera: Formicidae) with resurrections of the genera *Stigmatomma* and*Xymmer*. *PLoS One*, 7(3), e33325. https://doi.org/10.1371/journal.pone.0033325

Youssef, N. N. (1968). Musculature, nervous system and glands of pregenital abdominal segments of the female of *Nomia melanderi* Ckll. (Hymenoptera, Apoidea). *Journal of Morphology*, 125(2), 205–217. https://doi.org/10.1002/jmor.1051250206

SUPPORTING INFORMATION

Additional supporting information can be found online in the Supporting Information section at the end of this article.